Retirement Accumulation Strategies with Real Assets and Inflation Risk*

Benjamin Bruder Amundi Retirement Solutions benjamin.bruder@amundi.com

Camille Schittly
Amundi Innovation Lab
camille.schittly@amundi.com

Thierry Roncalli
Amundi Investment Institute
thierry.roncalli@amundi.com

Jiali Xu Amundi Investment Institute jiali.xu@amundi.com

October 2025

Abstract

This article presents a comprehensive, dynamic asset allocation framework for retirement savings, extending the classical Merton model to include human capital. This framework reconciles the intuitive age-based glide path with financial theory, recognizing that total wealth consists of financial capital and the present value of future contributions. It shows that the optimal allocation of risky assets depends on the ratio of human to financial capital, risk aversion, investment horizon, and key market parameters, such as the risk premium and volatility. Under CRRA utility, closed-form solutions are derived, demonstrating that continuous contributions increase risk exposure relative to the constant-mix strategy. The article also compares glide path strategies with constant-mix approaches, revealing that glide paths generally provide better downside protection and higher probabilities of meeting retirement goals, while dynamically adjusting risk exposure over time. The analysis further examines the shape of the glide path and shows that practical constraints, such as leverage limits, time-varying risk aversion, and rising contribution patterns, transform the theoretically convex allocation path into the empirically observed concave form.

The article expands the model to include multiple asset classes, providing a deep analysis of the practical differences between single-asset and multi-asset approaches. It emphasizes how allocation constraints, such as long-only requirements, leverage limits, and maximum exposure caps, impact optimal portfolio construction. The analysis shows that incorporating multiple asset classes yields greater diversification benefits, thereby enhancing risk-adjusted returns and improving retirement savings outcomes. Including real assets, such as private equity, private debt, real estate, and infrastructure, is valuable due to their unique risk-return profiles and lower correlations with traditional public equities and bonds. The framework acknowledges the practical challenges posed by liquidity risk and transaction costs, recognizing that real assets typically operate in markets with investment frictions during ramp-up and run-off phases when capital is deployed or withdrawn. It incorporates a time-varying liquidity weight that adjusts the portfolio's exposure to illiquid assets dynamically over the investment horizon. This

^{*}The authors are very grateful to Jean-Baptiste Berthon, Claudia Bertino, Marie Brière, Dominic Byrne, Dominique Carrel-Billiard, Laura Fiorot, Karin Franceries, Viviana Gisimundo, Christophe Granjon, Paula Niall, Lionel Paquin, and Nicola Zanetti for their helpful comments. The opinions expressed in this research are those of the authors and are not meant to represent the opinions or official positions of Amundi Asset Management.

mechanism reflects the natural lifecycle of investments. Younger investors can tolerate more illiquid investments for their potentially higher returns, while those approaching retirement gradually shift toward more liquid assets to ensure accessibility when needed.

Recognizing that inflation risk is a critical concern for retirement planning since inflation erodes the real purchasing power of accumulated wealth, the framework explicitly incorporates inflation dynamics and inflation-sensitive assets. By modeling inflation as a stochastic process and introducing assets whose returns are linked to inflation, the optimal allocation naturally decomposes into two components: a growth-oriented market portfolio and a liability-hedging portfolio designed to protect against inflation risk. This decomposition aligns defined contribution strategies with liability-driven investment principles used by defined benefit plans, ensuring that portfolios grow nominal wealth and preserve real value over time. From this perspective, assets serve as performance drivers and hedges against inflation risk. This underscores the importance of including inflation-sensitive assets, such as real assets.

Keywords: Retirement planning, lifecycle investing, target date fund, dynamic asset allocation, glide path, accumulation, risk premium, real assets, inflation risk, portfolio optimization, utility function, stochastic optimal control, Hamilton-Jacobi-Bellman equation, hedging demand, liability-driven investment.

JEL Classification: C61, G11, G50.

1 Introduction

The demographic transformation occurring in developed economies poses one of the most significant challenges to retirement systems today. Global life expectancy has increased dramatically, rising from an average of 46 years in 1950 to 73 years in 2025 (United Nations, 2024). Projections suggest it will reach 77 and 82 years by 2050 and 2100, respectively. Meanwhile, fertility rates have plummeted below replacement levels in most advanced economies, resulting in an unprecedented shift in population age structure. For example, the median age of the global population was 22 and 30 years in 1950 and 2025, respectively. However, it is projected to be 36 and 42 years by 2050 and 2100, respectively. Consequently, the proportion of the world's population aged 60 and older grew from less than 8\% in 1950 to 15\% in 2025. We expect this proportion to continue to increase, reaching 22\% and 30% by 2050 and 2100, respectively. This dual demographic transition — longer lifespans combined with fewer working-age individuals supporting each retiree — fundamentally alters the mathematics of retirement planning. Longevity risk, which is traditionally defined as uncertainty about one's lifespan, now encompasses broader systemic issues¹. These issues include the risk of outliving one's savings, whether pay-as-you-go pension systems can withstand growing demographic pressures, and whether retirement income will suffice for extended post-career periods that may span three decades or more. These evolving realities demand dynamic asset allocation strategies that can adapt to the ageing process and changing macroeconomic conditions over investment horizons that regularly extend 40-50 years.

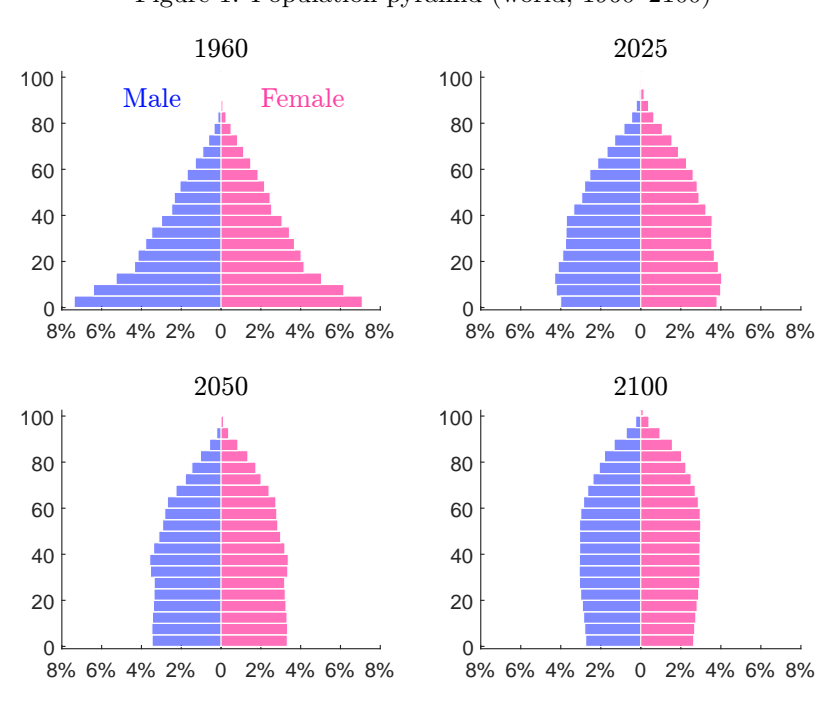


Figure 1: Population pyramid (world, 1960–2100)

Source: United Nations (2024) & Authors' calculations.

¹This challenge is illustrated by the old-age dependency ratio, defined as the number of people aged 65 and over relative to those of working age (25–64), expressed as the number of dependents per 100 workingage individuals. The ratio was 5.6 in 1950, has doubled over the past 75 years, and is projected to rise to 31.3 by the year 2100.

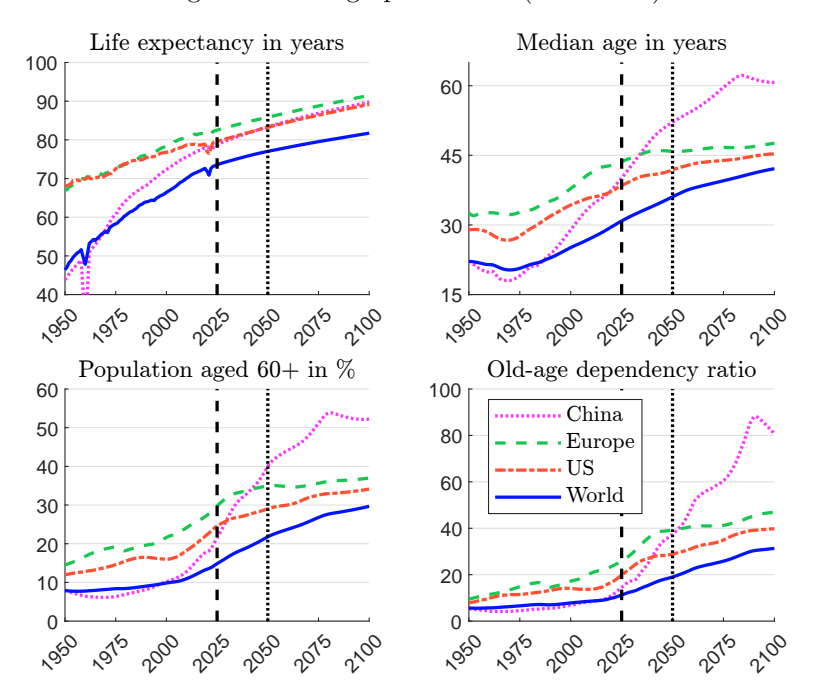


Figure 2: Demographic trends (1950–2100)

Source: United Nations (2024) & Authors' calculations.

Figure 1 illustrates the evolution of population pyramids. The global population structure no longer resembles the classic pyramid shape observed in the 20th century. The population structure has currently changed significantly, and projections indicate that it will increasingly resemble a barrel or a modern tall skyscraper such as the Gherkin, the Empire State Building or the Petronas Twin Towers. This profound transformation of the age structure applies to both developed countries and emerging economies that have experienced rapid growth over the past 50 years. Figures 53-57 on pages 113-115 compare the population pyramids of China, India, Japan, the United States, and Western Europe. China and India already have constrictive pyramids, and their bases are expected to narrow further by the year 2100. Figure 2 highlights these demographic trends, showing the rise in life expectancy and median age, the growing share of individuals aged 60 and older, and the increasing old-age dependency ratio. Currently, China lags behind Europe and the United States in these indicators, but it is projected to surpass them after 2050. Consequently, retirement planning challenges are no longer confined to developed countries. These challenges are becoming a global issue that increasingly affects emerging economies, such as China and India. In the coming decades, these countries will face problems similar to those developed countries have already experienced in recent years. Naturally, the situation remains heterogeneous across countries and regions. For example, Tables 1 and 2 present statistics for a sample of countries. Regarding the old-age dependency ratio, Hong Kong is projected to reach 144.8 by the year 2100. In contrast, the ratio will remain very low in Middle Africa, around 12.

In parallel with these demographic pressures, the retirement savings landscape has undergone a structural transformation, shifting from traditional defined benefit (DB) plans to defined contribution (DC) schemes. Additionally, most public pay-as-you-go (PAYG) pension systems² are under significant strain and pose serious long-term sustainability chal-

²A pay-as-you-go pension scheme is a retirement system in which the pensions of current retirees are financed directly from the contributions of current workers, rather than from returns on an accumulated fund. The sustainability of such schemes depends critically on the balance between contributors and beneficiaries,

Table 1: Trends in life expectancy and median age (1950–2100)

ISO]	Life exp	ectancy	7	I	Media	n age	
150	1950	2025	2050	2100	1950	2025	2050	2100
AUS	69.0	84.2	87.2	92.6	29.4	38.3	42.0	44.8
BRA	48.5	76.2	80.3	86.8	17.5	34.8	43.9	50.7
CAN	68.2	82.9	86.2	91.7	26.7	40.6	45.1	46.9
$_{\rm CHN}$	43.8	78.4	83.4	89.8	22.2	40.1	52.1	60.7
FRA	66.4	83.6	86.6	92.1	33.4	42.3	43.5	47.1
DEU	66.8	81.7	85.2	90.8	32.9	45.5	47.9	47.4
HKG	57.8	85.8	89.1	94.4	$^{1}_{1}$ 22.8	47.4	62.0	72.4
IND	41.2	72.5	77.5	85.3	20.0	28.8	38.3	47.8
ITA	65.7	84.0	87.2	92.8	27.5	48.2	52.9	53.4
$_{ m JPN}$	59.3	85.0	88.4	94.4	21.3	49.8	52.8	53.0
SAU	40.0	79.2	84.0	90.3	18.0	29.6	32.0	35.8
SGP	54.1	84.0	87.1	92.7	18.9	36.2	50.9	56.0
SWE	71.1	83.6	86.8	92.2	33.2	40.3	44.1	48.6
CHE	68.9	84.2	87.3	92.8	32.2	42.9	47.8	48.1
TWN	56.6	80.9	84.9	90.9	17.7	44.8	56.3	56.8
USA	68.1	79.6	83.2	89.2	29.0	38.5	41.9	45.3
ĒĀĀ	43.2	79.3	83.8	$90.\bar{1}$	$2\bar{1}.\bar{8}$	41.0	$5\bar{2}.\bar{2}$	59.5
LCN	48.7	76.0	80.1	86.4	18.3	31.7	40.5	49.1
MIA	36.6	62.4	66.3	72.6	18.5	16.4	20.6	32.2
WEU	67.0	82.5	85.9	91.5	32.6	43.6	45.8	47.6
WLD	46.4	73.5	77.0	81.7	22.2	30.9	36.1	42.1

Table 2: Trends in percentage of population aged 60+ and old-age dependency ratio (1950–2100)

-	% of	populat	ion age	d 60±	Old-s	Old-age dependency ratio				
ISO	1950	2025	2050	2100	1950	2025	2050	2100		
AUS	12.5	23.8	29.9	33.8	7.9	20.4	30.0	40.6		
BRA	4.0	16.6	29.3	39.9	3.0	11.0	24.8	48.6		
CAN	11.3	27.0	31.9	36.0	8.0	21.6	32.1	43.3		
$_{\rm CHN}$	8.0	21.5	40.0	52.2	5.3	14.5	37.3	80.8		
FRA	16.2	28.8	33.0	36.5	11.5	27.3	38.8	46.4		
DEU	13.6	31.7	37.0	36.7	8.3	26.5	41.1	46.3		
HKG	3.7	32.1	55.2	66.3	2.6	22.7	67.2	144.8		
IND	5.4	11.1	20.6	36.3	3.7	7.1	14.7	40.6		
ITA	12.0	32.7	42.9	43.4	8.2	28.7	55.3	59.4		
$_{ m JPN}$	7.7	36.3	43.3	43.1	5.5	40.1	57.5	60.9		
SAU	5.6	5.4	12.1	20.9	3.7	2.5	7.4	20.2		
SGP	3.7	19.7	34.8	46.7	2.8	12.7	30.1	64.0		
SWE	14.9	26.8	32.2	37.8	9.9	25.5	32.9	48.5		
CHE	13.9	27.5	36.9	37.5	9.1	22.6	40.3	48.4		
TWN	3.7	27.8	46.0	47.5	2.4	18.4	51.0	71.4		
USA	12.0	24.6	29.0	34.1	7.8	19.8	28.9	39.8		
ĒĀĀ	7.8	$\bar{2}\bar{2}.9^{-}$	-40.3	-50.7	5.2	16.4	39.0	$-77.\bar{1}$		
LCN	5.2	14.7	25.0	38.0	4.0	10.3	20.9	44.9		
MIA	5.8	4.6	6.0	16.1	4.7	3.9	4.4	11.9		
WEU	14.5	29.8	35.0	37.0	9.5	25.9	39.3	46.9		
WLD	7.9	14.9	21.8	29.7	5.6	11.2	19.0	31.3		

AUS: Australia, BRA: Brazil, CAN: Canada, CHN: China, FRA: France, DEU: Germany, HKG: Hong Kong, IND: India, ITA: Italy, JPN: Japan, SAU: Saudi Arabia, SGP: Singapore, SWE: Sweden, CHE: Switzerland, TWN: Taiwan, USA: United States of America, EAA: Eastern Asia, LCN: Latin America and the Caribbean, MIA: Middle Africa, WEU: Western Europe, WLD: World.

Source: United Nations (2024) & Authors' calculations.

Table 3: Public expenditure on old-age and survivor benefits in percentage of government spending and GDP

Country	Gov't	spending	% of	GDP	Country	Gov't s	spending	% of GDP	
Country	2000	2019	2000	2019	Country	2000	2019	2000	2019
Australia	12.8	10.3	4.7	4.3	Austria	23.9	26.8	12.2	13.0
Belgium	17.8	20.6	8.8	10.7	Canada	10.1	11.3	4.2	5.0
Denmark	12.0	16.4	6.3	8.1	Finland	15.5	22.4	7.4	11.9
France	22.2	24.3	11.5	13.4	Germany	22.8	23.1	10.9	10.4
Greece	21.9	32.7	10.2	15.7	Iceland	4.6	6.6	2.1	2.9
Ireland	10.3	13.7	3.1	3.3	Italy	29.0	32.8	13.5	15.9
Netherlands	10.9	11.8	4.6	5.0	Norway	11.1	13.8	4.7	7.1
Poland	24.3	26.2	10.5	10.9	Portugal	18.3	29.3	7.8	12.4
Spain	21.5	26.7	8.4	11.3	Sweden	12.8	14.2	6.8	7.0
Switzerland	17.8	19.6	5.9	6.4	United Kingdom	13.4	11.5	4.8	4.9
United States	16.4	18.6	5.7	7.1	OECD	16.2	18.1	6.5	7.7

Source: OECD (2023, Table 8.2, page 211).

lenges, particularly given the recent increase in public debt and deficits that have worsened since the covid-19 pandemic³. This evolution is not coincidental. It is a direct consequence of the challenges posed by increasing longevity⁴. Under DB plans, employers bore the full weight of both investment risk and longevity risk, guaranteeing a specific income for the entire duration of a retiree's life. As lifespans extended and financial markets remained volatile, the long-term cost and uncertainty of these guarantees became unsustainable for many corporations⁵ and public entities. The resulting shift to DC plans has effectively (or

because workers today fund retirees today, and the next generation of workers will fund their pensions when they retire. Most public pension systems in Europe, including those in France, Germany, and Italy, operate predominantly on a PAYG basis.

"Better recognition and mitigation of longevity risk should be undertaken now. Measures will take years to bear fruit and effectively addressing this issue will become more difficult if remedial action is delayed. Attention to population aging and the additional risk of longevity is part of the set of reforms needed to rebuild confidence in the viability of private and public sector balance sheets." (International Monetary Fund, 2012, page 123).

However, finding an effective solution has proven increasingly difficult.

⁵The financial health of DB systems is usually evaluated using funding ratios, which is the percentage of pension liabilities covered by available assets. Currently, aggregate funding ratios are relatively high, with many plans reporting values above 100%. For instance, OECD (2023, Figure 9.6, page 233) estimated the following funding ratios in 2022: 112.3% in Finland, 116.1% in Germany, 127.6% in Iceland, 126.0% in Ireland, 104.4% in Luxembourg, 66.7% in Mexico, 116.0% in the Netherlands, 115.4% in Norway, 106.0% in Switzerland, 113.1% in the United Kingdom, 63.6% in the United States, and 96.6% in Indonesia. However, these figures can be misleading. First, there is significant heterogeneity both across and within countries. Within a single jurisdiction, funding ratios can vary widely, with the interquartile range (between the 25th and 75th percentiles) often being around 20 percentage points. This means that even when the national average exceeds 100%, a significant portion of DB pension schemes remain underfunded. Second, today's relatively high funding ratios largely reflect the strong performance of the stock market since the global financial crisis of 2008. For instance, the estimated aggregate full buyout funding ratio in the United Kingdom was 55.9% in 2006, increased to 71.5% in 2019, and reached 94.4% in 2024 (Pension Protection Fund, 2025, Figure 4.3, page 12). In the United States, the funding ratio of the 100 largest corporate DB pension plans was 123% in 2000, falling to 82% in 2002, 106% in 2007, 79% in 2008, 88% in 2020, and recovered to 101% in 2024 (Wadia et al., 2025, Figure 3, page 2). These figures illustrate how equity downturns can trigger sharp declines in DB funding ratios, exposing both pension schemes and their sponsoring companies to financial

³While public expenditure on old-age and survivor benefits accounted for 16.2% of total government spending in OECD countries in 2000, this share had risen to 18.1% by 2019, just before the covid-19 crisis. In terms of GDP, these expenditures represented 7.7% of OECD GDP (OECD, 2023, page 10). There are, however, significant disparities across countries. For example, public pension spending reached 15.9% and 15.7% of total government expenditure in Italy and Greece, respectively, while it was only 2.9% and 3.3% in Iceland and Ireland (Table 3).

⁴Undoubtedly, we have reached a point where it is appropriate to speak of a retirement savings crisis (Benartzi and Thaler, 2013). The problem has long been recognized:

Table 4: Gross and net pension replacement rates from mandatory (public and private) and voluntary pension schemes (in %)

	Manda	atory	Volun	itary		Manda	atory	Volun	tary
Country	Gross	Net	Gross	Net	Country	Gross	Net	Gross	Net
Australia	26.0	33.7			Austria	74.1	87.4		
Belgium	43.5	60.9	52.4	73.8	Canada	36.8	44.2	57.0	66.0
Denmark	73.1	77.3			Estonia	28.1	34.4	47.4	54.7
Finland	58.4	65.1			France	57.6	71.9		
Germany	43.9	55.3	54.7	69.5	Greece	80.8	90.0		
Iceland	43.1	52.1			Ireland	26.2	36.1	55.7	74.3
Israel	38.0	47.3	51.7	63.2	Italy	76.1	82.6		
Japan	32.4	38.8			Lithuania	18.2	28.9	30.1	47.9
Mexico	55.5	62.4	64.7	72.7	Netherlands	74.7	93.2		
New Zealand	39.7	43.5	54.9	61.9	Norway	44.5	54.8		
Poland	29.3	40.3			Portugal	73.9	98.8		
Spain	80.4	86.5			Sweden	62.3	65.3		
Switzerland	39.9	45.3			United Kingdom	41.9	54.4		
United States	39.1	50.5	73.2	87.7	OECD	50.7	61.4	55.2	66.9

Source: OECD (2023, Table 4.5, page 159).

partially) transferred these complex risks from the institution to the individual⁶. This transfer is particularly concerning when measured by gross and net replacement rates⁷ (Table 4). In several OECD countries, gross mandatory replacement rates fall below 50%, with net rates often relying heavily on tax advantages or voluntary schemes to reach adequate levels. Across the OECD, gross mandatory replacement rates range from 18.2% in Lithuania to 80.8% in Greece, averaging 50.7%. After taxation, net replacement rates are generally higher, averaging 61.4%. However, significant adequacy gaps remain. In jurisdictions with relatively low mandatory coverage, retirees depend heavily on voluntary private pensions to maintain their standard of living. For instance, the gross replacement rate from mandatory plans in the United States is only 39.1%, but it rises to 73.2% when voluntary contributions are included. Taken together, these figures suggest that mandatory public pensions are often insufficient on their own and that supplementary savings are essential for maintaining living standards in retirement. No longer promised a predictable lifelong income, each person is now personally responsible for managing their own investment portfolio to accumulate sufficient capital and for ensuring those savings last through a retirement period of uncertain and increasing length. This profound transfer of responsibility has created an urgent need for investment strategies that can systematically manage risk over a multi-decade horizon. This need is particularly critical for individuals who lack financial expertise (Poterba et al., 2009) and the literacy needed to navigate these complex decisions independently (Lusardi and Mitchell, 2014). It is precisely this need that has fueled the rise of default investment solutions, such as target date funds, decumulation strategies, annuities, and tontines⁸.

stress (Antolín and Stewart, 2009). The risks for companies are not merely theoretical. One of the most prominent cases was the merger between British Airways and Iberia in 2009–2010. The deal was jeopardized by British Airways' substantial DB pension deficit (£3.7 billion at the end of 2009), which posed a significant financial burden and became a focal point in the negotiations.

⁶This highlights the importance of the third pillar of retirement planning. Voluntary private pension schemes are essential for individuals who wish to maintain their standard of living after retiring.

⁷According to OECD (2023, pages 150 and 156), "the gross pension replacement rate is defined as gross pension entitlement divided by gross pre-retirement earnings. The net pension replacement rate is defined as the individual net pension entitlement divided by net pre-retirement earnings, taking into account personal income taxes and social security contributions paid by workers and pensioners." Both indicators capture how effectively a pension system provides a retirement income to replace earnings, the main source of income before retirement.

⁸Annuities and tontines are mechanisms that pool longevity risk. They provide guaranteed income and distribute risk among participants, offering protection against uncertainty regarding lifespan. These products

As shown in Figure 3, a complete pension scheme consists of two phases: pre-retirement accumulation and post-retirement decumulation. The accumulation phase is the period during which a person saves and makes long-term investments to accumulate retirement funds. In contrast, the decumulation phase is the process by which investors convert their retirement savings into income to meet their needs while continuing to invest their remaining funds (Bruder et al., 2023). During this phase, there is a regular outflow of cash from the reserve. The two phases are closely interconnected. The adequacy of decumulation depends critically on the wealth accumulated beforehand, while accumulation choices depend on expectations about retirement consumption. Rising life expectancy complicates this balance by increasing the necessary resources for an adequate income and extending the period over which savings must be managed. Consequently, voluntary savings and supplementary pension plans are necessary to bridge the gap left by public and mandatory programs. This interdependence highlights the fact that retirement planning is an ongoing process in which saving, investing, and spending decisions are continuously linked. The accumulation phase is particularly important in this context. Without sufficient wealth at retirement, the choice of decumulation options, such as systematic withdrawals, annuities, and tontines, becomes largely irrelevant. This highlights the importance of sound accumulation strategies, such as target date funds and other lifecycle investment approaches, which balance growth and risk over time.

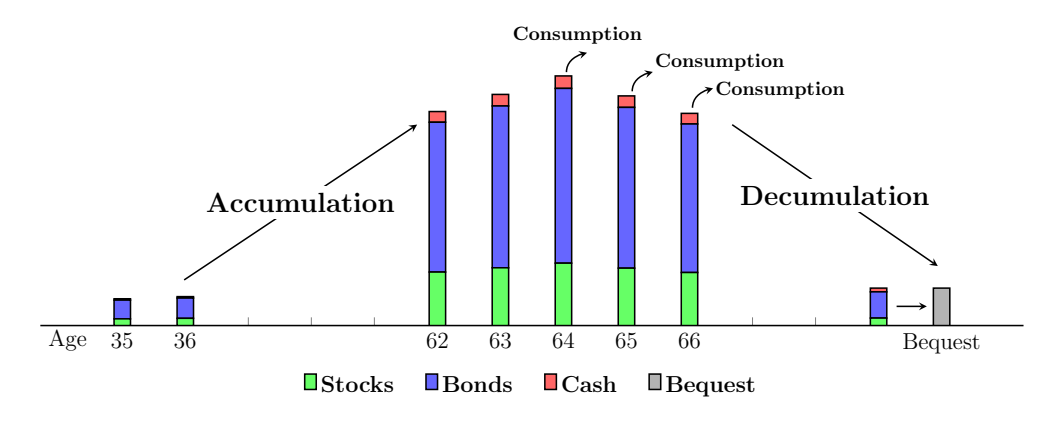


Figure 3: Accumulation and decumulation

Target date funds are typically structured as portfolios of underlying funds representing different investment styles or asset classes. As their name suggests, they are designed with a specific retirement year in mind, such as 2040 or 2050 vintage. The investment firm manages the asset allocation on behalf of investors, and it evolves over time as the target date approaches. John C. Bogle, the founder of Vanguard and proponent of simple investing, promoted the rule of thumb that investors should hold a percentage of bonds equal to their age, with the remainder in equities. This heuristic has intuitive appeal and aligns with the expectations of many investors. However, it appears inconsistent with financial theory at first glance. Academic literature on optimal portfolios generally recommends maintaining a relatively stable mix of equities and bonds throughout one's life. According to this theory, the optimal allocation is primarily determined by the equity risk premium and the investor's risk aversion. The investment horizon plays only a secondary role. Under this view, the equity-to-bond ratio should remain largely constant over time⁹. The apparent

complement or substitute traditional decumulation strategies.

⁹This is another asset allocation puzzle (Jagannathan and Kocherlakota, 1996; Canner et al., 1997).

contradiction between the glide path strategy of target date funds and the constant-mix strategy of balanced funds can be reconciled by introducing the concept of human capital (Viceira, 2001; Campbell and Viceira, 2002; Cocco et al., 2005). Human capital is defined as the sum of current financial wealth and the present value of expected future contributions ("forward wealth"). At retirement, human capital reduces to financial capital alone because there are no remaining future contributions. Earlier in life, however, human capital far exceeds current financial wealth. The theory suggests that investors should maintain a stable proportion of their total wealth in equities, including financial assets and human capital. For younger investors decades away from retirement, this principle results in a higher equity allocation within their financial portfolio. The reason is straightforward. Younger investors have substantial human capital in the form of future earning potential, which naturally hedges against financial market volatility and enables them to take on more investment risk. This framework provides a solid theoretical foundation for Bogle's famous age-based investment rule. Although equity allocation appears to decrease with age when viewed solely through the lens of financial assets, it actually remains consistent when human capital is considered. As investors age and their human capital diminishes, they naturally shift toward more conservative investments to maintain the same risk profile relative to their total wealth. This is one of the key results confirmed by the model developed in this research paper¹⁰. Another implication is that the optimal glide path should be convex in theory. Investors would de-risk relatively early in life, slowing the pace of risk reduction as they age. However, in practice, most glide paths of target-date funds are concave. Investors maintain relatively high risky exposure for much of their working life, de-risking only as they approach retirement. Our model addresses this apparent puzzle. By relaxing the assumptions of constant risk aversion and linear income contributions, we demonstrate that the glide path can be concave. This occurs when risk aversion is time-varying, a feature supported by empirical evidence showing that individuals tend to become more risk-averse as they age. Similarly, if investors accelerate their retirement savings during the accumulation phase, particularly after age 50 when education and debt-related expenses typically decline and the need to increase retirement income becomes more urgent, the resulting glide path becomes naturally concave.

Building on this foundational insight, we expand our framework to include a comprehensive multi-asset universe. Modern portfolio construction for long-term goals like retirement requires more than a simple stock-bond mix to achieve true diversification. The objective is not merely to add assets with low correlations but also to build a more resilient portfolio by tapping into fundamentally different risk and return drivers. A well-diversified portfolio should perform well in various macroeconomic environments, including periods of high inflation and slow growth. This helps to ensure a steady accumulation of wealth and provides superior downside protection, which is critical as an investor approaches retirement. In this context, real assets, such as private equity, real estate, infrastructure, and private debt, are essential components. These asset classes offer benefits that are particularly valuable for long-term investors, including unique return drivers, inflation hedging, and an illiquidity premium (Amenc et al., 2009). Their performance is often tied to long-term contractual cash flows, operational improvements, or specific economic activities, such as rental income or toll road usage, rather than the daily sentiment of public markets. This provides a powerful diversifying effect. Many real assets, particularly infrastructure and real estate, have revenue streams that are explicitly linked to inflation. This provides a natural hedge that preserves the purchasing power of the portfolio over time. Since these assets are not as easily bought or sold as public stocks, investors typically receive higher expected returns. Savers

 $^{^{10}}$ This key result has been documented repeatedly in the academic literature (Merton, 1971; Bruder et al., 2012).

with a time horizon of several decades can benefit from this illiquidity premium because they do not need immediate access to their capital. Incorporating these assets into a portfolio enhances its efficiency, leading to better risk-adjusted returns. However, including these assets introduces complexity. Our framework addresses the practical constraints that these assets impose, including leverage limits, long-only requirements, and most importantly, liquidity considerations. These considerations are critical in shaping the feasible set of allocations and influencing the optimal glide path.

Inflation risk is another factor in retirement planning because inflation erodes the real purchasing power of accumulated wealth. Over long investment horizons, even moderate inflation can significantly reduce the value of retirement savings if portfolios are not adequately protected. The seminal contribution of Brennan and Xia (2002) established the foundation for dynamic asset allocation under inflation risk. Since then, their framework has been extended to optimal investment problems in DC pension plans in several directions (Munk et al., 2004; Munk and Sørensen, 2010; Han and Hung, 2012; Yao et al., 2013; Park et al., 2023). The question of how best to manage inflation risk is also closely connected to household portfolio choices such as housing decisions — whether to buy, rent, or invest — as highlighted by Kraft and Munk (2011). Our model explicitly incorporates inflation dynamics and inflation-sensitive assets. This allows us to decompose the optimal portfolio into two components: a performance portfolio that seeks long-term returns and a liability-hedging portfolio (LHP) that protects against inflation risk. This structure aligns DC investment strategies with the liability-driven investment (LDI) principles traditionally applied in DB pension schemes. It ensures that portfolios are managed to grow not only nominal wealth, but also to preserve real purchasing power over time. A key challenge lies in calibrating the LHP. Early foundational work by Fama and Schwert (1977) documented the complex relationship between inflation and asset returns. They showed that inflation can have significant and sometimes adverse effects on real returns, particularly for nominal bonds and equities. This motivates the inclusion of alternative inflation-sensitive assets, such as treasury inflation-protected securities, as well as real assets like real estate, infrastructure, and commodities (Brière and Signori, 2012). However, reliably aligning portfolio returns with changes in the cost of living remains challenging. This highlights the importance of carefully incorporating these assets into retirement portfolios to safeguard nominal balances and real wealth over the long term.

This paper is structured as follows. Section Two provides background on the modeling of glide path strategies. We extend the classical Merton model by incorporating future contributions, introduce the concept of the human-to-financial capital ratio, and analyze the properties of the optimal dynamic allocation. We then derive analytical formulas for the glide path and wealth dynamics, discuss the convexity/concavity of the glide path, and illustrate dynamic asset allocation in a setting that combines public and private assets. Section Three extends the baseline model to multiple asset classes. We show that in the absence of allocation constraints, the analytical solution can be derived using a one-stage approach, and we compare this to the two-stage solution from the baseline model. We then derive the optimal allocation under allocation constraints and demonstrate how it can be obtained using Howard's policy-iteration algorithm. This section also includes an empirical application, where we simulate an optimal glide path for an investor in the Eurozone. Section Four addresses inflation risk. We solve a simplified model with two assets — both correlated with inflation volatility, but only one with a risk premium linked to the inflation level and derive analytical solutions for several cases. We further provide examples and empirical evidence to illustrate how the liability-hedging portfolio affects dynamic allocation. Finally, Section Five concludes with closing remarks.

2 Baseline modeling of glide path strategy

2.1 Theoretical Model

We follow the framework introduced by Merton (1969) and the extension proposed by Bruder et al. (2012), which incorporates stochastic permanent contributions. We consider a dynamic asset allocation problem in which an individual invests in a risky asset S_t and a risk-free zero-coupon bond B_t , while making regular contributions c_t to a target date strategy. The investor's wealth process X_t evolves according to the following stochastic differential equation:

$$\frac{\mathrm{d}X_t}{X_t} = \alpha_t \frac{\mathrm{d}S_t}{S_t} + (1 - \alpha_t) \frac{\mathrm{d}B_t}{B_t} + \frac{c_t}{X_t} \,\mathrm{d}t$$

where α_t is the proportion of wealth invested in the risky asset at time t and \mathbf{c}_t is the contribution flow at time t, typically originating from savings. Moreover, we have the following standard dynamics for S_t and B_t : $\mathrm{d}S_t = \mu_t S_t \, \mathrm{d}t + \sigma_t S_t \, \mathrm{d}W_t$ where μ_t is the expected return and σ_t is the volatility of the risky asset, and $\mathrm{d}B_t = r_t B_t \, \mathrm{d}t$ where r_t is the short-term interest rate. The investor aims to maximize the expected utility of terminal wealth:

$$\alpha_t^{\star} = \arg \max \mathbb{E}_t \left[\mathcal{U} \left(X_T \right) \right]$$

2.1.1 The no-contribution case

We first consider the case of no contributions: $c_t = 0$. The model reduces then to the classical framework of Merton (1969, 1971).

Optimal general solution Let $\mathcal{J}(t,x)$ be the value function associated with the investor's problem:

$$\mathcal{J}\left(t,x\right) = \sup_{\alpha} \mathbb{E}_{t} \left[\mathcal{U}\left(X_{T}\right) \mid X_{t} = x \right]$$

By defining the Hamiltonian function as follows:

$$\mathcal{H}(t,x,\alpha) = \left(\alpha\mu_t x + (1-\alpha)r_t x\right) \frac{\partial \mathcal{J}(t,x)}{\partial x} + \frac{1}{2}\alpha^2 \sigma_t^2 x^2 \frac{\partial^2 \mathcal{J}(t,x)}{\partial x^2}$$
(1)

the function $\mathcal{J}(t,x)$ satisfies the Hamilton-Jacobi-Bellman (HJB) equation:

$$\frac{\partial \mathcal{J}(t,x)}{\partial t} + \max_{\alpha_t} \mathcal{H}(t,x,\alpha_t) = 0$$
 (2)

with terminal condition:

$$\mathcal{J}\left(T,x\right) = \mathcal{U}\left(x\right) \tag{3}$$

The first-order condition of the maximization of the Hamiltonian function is:

$$\frac{\partial \mathcal{H}(t, x, \alpha)}{\partial \alpha} = 0 \quad \Leftrightarrow \quad (\mu_t x - r_t x) \, \partial_x \mathcal{J}(t, x) + \alpha \sigma_t^2 x^2 \partial_x^2 \mathcal{J}(t, x) = 0$$

$$\Leftrightarrow \quad \alpha_t^* = -\frac{\mu_t - r_t}{\sigma_t^2} \cdot \frac{\partial_x \mathcal{J}(t, x)}{x \partial_x^2 \mathcal{J}(t, x)} \tag{4}$$

The optimal allocation α_t^* can then be expressed as the Sharpe ratio $SR_t = (\mu_t - r_t)/\sigma_t$ divided by the product of the volatility σ_t and the Arrow-Pratt measure of relative risk aversion $\Re(t,x) = -x\partial_x^2 \mathcal{J}(t,x)/\partial_x \mathcal{J}(t,x)$. Solving the system of equations (1–4) yields the optimal value function and the optimal allocation strategy. While a closed-form solution exists in the CRRA case, in general we use numerical methods and a finite difference scheme.

Remark 1. When the value function is separable $-\mathcal{J}(t,x) = f(t)\mathcal{U}(x)$ with f(T) = 1, the investor's relative risk aversion is:

$$\Re\left(t,x\right) = -\frac{x\partial_{x}^{2}\mathcal{J}\left(t,x\right)}{\partial_{x}\mathcal{J}\left(t,x\right)} = -\frac{x\partial_{x}^{2}\mathcal{U}\left(x\right)}{\partial_{x}\mathcal{U}\left(x\right)}$$

The optimal exposure is an increasing function of the Sharpe ratio of the risky asset, and a decreasing function of both the asset's volatility and the investor's relative risk aversion. This result aligns with the classical findings of the Markowitz mean-variance optimization framework.

The CRRA case We now consider the case when the utility function corresponds to the CRRA form:

$$\mathcal{U}\left(x\right) = \frac{x^{\gamma}}{\gamma}$$

with $\gamma \leq 1$. In Appendix A.2 on page 88, we show that:

$$\alpha_t^{\star} = \frac{\mu_t - r_t}{(1 - \gamma)\sigma_t^2} := \bar{\alpha}_t \tag{5}$$

and:

$$\mathcal{J}(t,x) = \exp\left(\int_{t}^{T} \left(\gamma r_{s} + \frac{1}{2} \frac{\gamma (\mu_{s} - r_{s})^{2}}{(1 - \gamma) \sigma_{s}^{2}}\right) ds\right) \cdot \frac{x^{\gamma}}{\gamma}$$
 (6)

The optimal strategy corresponds to a constant-mix allocation. In particular, when the risk premium and the volatility of the risky asset are constant over time, then the optimal proportion invested in the risky asset also remains constant.

The solution $\bar{\alpha}_t$ arises from the classical Tobin-Markowitz mean-variance analysis. Considering an investment universe of n assets, we have:

$$w_t^{\star} = \arg\max \mathcal{U}(w_t) = w_t^{\top}(\mu_t - r_t) - \frac{(1 - \gamma)}{2} w_t^{\top} \Sigma_t w_t$$

where w_t is the vector of portfolio weights, $\mathcal{U}(w_t)$ is the mean-variance utility function, μ_t is the vector of expected returns and Σ_t is the covariance matrix of asset returns. Since the first-order condition is $\partial_w \mathcal{U}(w_t) = (\mu_t - r_t) - (1 - \gamma) \Sigma_t w_t = \mathbf{0}_n$, we get:

$$w_t^{\star} = \frac{1}{(1-\gamma)} \Sigma_t^{-1} \left(\mu_t - r_t \right)$$

In the special case of a single risky asset, this reduces to:

$$w_t^{\star} = \frac{\mu_t - r_t}{(1 - \gamma)\,\sigma_t^2} = \bar{\alpha}_t$$

Hence, $\bar{\alpha}_t$ represents the optimal allocation to the tangency portfolio, while $1 - \bar{\alpha}_t$ represents the optimal allocation to the risk-free asset.

Remark 2. If the Markowitz optimization problem is written in quadratic programming (QP) form:

$$w_t^{\star} = \arg\min \frac{1}{2} w_t^{\top} \Sigma_t w_t - \varphi w_t^{\top} (\mu_t - r_t)$$

 $we \ have \ the \ following \ correspondence:$

$$\varphi = \frac{1}{1 - \gamma} \in [0, \infty)$$

While γ measures the relative risk aversion, φ measures the investor's risk tolerance.

2.1.2 The case with contributions

When we have contributions $c_t \ge 0$, Equations (1–4) are exactly the same but, with the following change of variables¹¹:

$$\begin{cases} \tilde{\alpha}_{t} = \alpha_{t} \frac{X_{t}}{X_{t} + H_{t}} \\ \tilde{X}_{t} = X_{t} + H_{t} \\ H_{t} = \int_{t}^{T} e^{-\int_{t}^{s} r_{u} \, du} \boldsymbol{c}_{s} \, ds \\ \tilde{\mathcal{J}}(t, \tilde{x}) = \mathcal{J}(t, x) = \mathcal{J}(t, \tilde{x} - H_{t}) \end{cases}$$

For the CRRA utility function, the optimal allocation is:

$$\alpha_t^{\star} = \frac{\mu_t - r_t}{(1 - \gamma)\sigma_t^2} + \frac{\mu_t - r_t}{(1 - \gamma)\sigma_t^2 x} \int_t^T e^{-\int_t^s r_u \, \mathrm{d}u} \boldsymbol{c}_s \, \mathrm{d}s$$
 (7)

while the optimal value function is:

$$\mathcal{J}(t,x) = \exp\left(\int_{t}^{T} \left(r_{s}\gamma + \frac{1}{2} \frac{\gamma \left(\mu_{s} - r_{s}\right)^{2}}{\left(1 - \gamma\right) \sigma_{s}^{2}}\right) ds\right) \cdot \frac{\left(x + \int_{t}^{T} e^{-\int_{t}^{s} r_{u} du} \boldsymbol{c}_{s} ds\right)^{\gamma}}{\gamma}$$
(8)

We observe that the optimal allocation is composed of two components:

$$\alpha_t^{\star} = \bar{\alpha}_t + \frac{\bar{\alpha}_t}{x} \int_t^T B(t, s) \, \boldsymbol{c}_s \, \mathrm{d}s$$

where $B(t,s) = \exp\left(-\int_t^s r_u \,\mathrm{d}u\right)$ is the discount factor or zero-coupon bond price between times t and s. The first term corresponds to the classical Merton solution $\bar{\alpha}_t$ while the second term reflects the present value of the cumulative future contributions. Assuming that $c_t \geq 0$, we deduce that $\int_t^T B(t,s) \, c_s \, \mathrm{d}s \geq 0$. It follows that:

$$\alpha_t^{\star} \geq \bar{\alpha}_t$$

This allocation strategy is adjusted upward to account for the investor's future contributions¹². This result was already established by Merton (1971) when he introduced the concept of non-capital gain income:

"[...] one finds that, in computing the optimal decision rules, the individual capitalizes the lifetime flow of wage income as the market (risk-free) rate of interest and then treats the capitalized value of an addition to the current stock of wealth" (Merton, 1971, Section 7, page 395).

In our model, capital gain income corresponds to the wealth generated by X_t , while the non-capital gain income corresponds to the wealth generated by H_t . Let W_t^S be the nominal wealth invested in the risky asset. We have:

$$W_t^S = \alpha_t^* X_t = \bar{\alpha}_t \left(X_t + H_t \right) = \bar{\alpha}_t W_t \tag{9}$$

In Merton terminology, the interest rate is constant and $H_t = \int_t^T e^{-r(s-t)} \boldsymbol{c}_s \, \mathrm{d}s$ represents the "capitalization of the lifetime flow of contributions". This interpretation remains consistent with the constant-mix allocation solution if we generalize the investor's wealth to include not only current (spot) wealth but also the present value of future contributions. Typically, these future contributions stem from the investor's expected wage income. Hence, H_t can be interpreted as human capital, which contributes to the investor's total wealth.

 $^{^{11}\}mathrm{The}$ different proofs are given in Appendix A.3 on page 88.

¹²Note that α_t^* decreases monotonically with time t. At maturity, the optimal allocation converges to the baseline allocation: $\alpha_T^* = \bar{\alpha}_T$.

Table 5: Optimal exposure α_t^* in %

		Contr	ibution c_0)
x	0	100	1000	10000
1 000	34.6	51.1	199.2	1681.0
2000	34.6	42.8	116.9	857.8
5000	34.6	37.9	67.5	363.9
10000	34.6	36.2	51.1	199.2
50000	34.6	34.9	37.9	67.5

To illustrate the impact of human capital, let us consider an example. We assume that $r_t = 2\%$, $\mu_t = 6\%$, $\sigma_t = 17\%$, and $\gamma = -3.0$. Table 5 shows the values of α_t^* when the initial wealth X_t is equal to x, the contribution equals c_0 , and the investment horizon T-t is five years. Without a contribution, the optimal strategy is the constant-mix strategy, allocating 34.6% to the risky asset and 65.4% to the risk-free asset, regardless of the initial wealth level. However, when annual contributions are made, the value of α_t^{\star} becomes more sensitive to the initial wealth. For instance, if the contribution equals \$100 and the initial wealth is \$1000, then $\alpha_t^* = 51.1\%$. However, if the initial wealth is \$50000, then $\alpha_t^* = 34.9\%$. Therefore, the impact is more significant for lower initial wealth levels. This effect stems from the relative size of current wealth compared to the present value of future contributions. For example, if $c_0 = 100 , then the human capital H_t equals \$476. If the annual contribution increases to \$10000, H_t becomes \$47581. In this case, the investor has substantial future wealth. However, if the initial wealth is only \$1000, the optimal allocation requires an investment of 1681% in the risky asset, which is highly leveraged. The investor's total wealth is $W_t = 48581 . Applying the constant-mix strategy to this total wealth implies that the investor should allocate $34.6\% \times 48581 = 16810 to the risky asset. Since the investor only has \$1000 in current wealth, they must borrow \$15810, resulting in a leverage ratio of 16.81. Table 6 presents the values of total wealth W_t and the amount W_t^S invested in the risky asset. Regardless of the values of x and c_0 , the ratio W_t^S/W_t remains constant at 34.6%, confirming the result derived in Equation (9).

Table 6: Total wealth and amount invested in the risky asset

		Total W	ealth W_t		Nominal exposure W_t^S				
x/c_0	0	100	1000	10000	0	100	1000	10000	
1 000	1 000	1476	5758	48581	346	511	1992	16810	
2000	2000	2476	6758	49581	692	857	2338	17156	
5000	5000	5476	9758	52581	1730	1895	3377	18194	
10000	10000	10476	14758	57581	3460	3625	5107	19924	
50 000	50000	50476	54758	97581	17 301	17466	18947	33765	

Remark 3. We observe that when both initial wealth x and future contributions \mathbf{c}_t are multiplied by the same factor, the optimal exposure α_t^{\star} remains unchanged. This suggests that the results can be normalized because they depend only on the relative ratio between future contributions and current wealth. For example, Table 5 shows that the optimal exposure is the same for $x = \$1\,000$ and $\mathbf{c}_t = \$1\,00$ as it is for $x = \$10\,000$ and $\mathbf{c}_t = \$1\,000$. Therefore, without loss of generality, we can normalize x to 1.

The specification of the contribution function plays a significant role in determining risk exposure. In Appendix A.5 on page 91, we consider a quadratic convex function defined as:

$$\boldsymbol{c}_t = \boldsymbol{c}_0 + b_{\boldsymbol{c}}t + a_{\boldsymbol{c}}t^2$$

and we explain how to calibrate the parameters (c_0, b_c, a_c) . This specification allows us to represent different scenarios.

- A special case is the constant contribution function: $c_t = c_0$. In this case, the individual invests a fixed nominal amount of their salary each month into their pension plan. However, this is not very realistic since salaries typically increase with age. Young individuals tend to save less than older individuals.
- Another case is a linear contribution function: $c_t = c_0 + b_c t$. Here, contributions increase with age, which is more realistic. However, this model still omits an important stylized fact: savings do not increase indefinitely. In practice, older individuals may reduce their savings due to health issues or unemployment risks. Therefore, the maximum contribution may occur before retirement age T.
- This behavior can be captured using a quadratic contribution function $c_t = c_0 + b_c t + a_c t^2$ with a negative coefficient a_c , which ensures the function has a maximum. In this case, the maximum contribution is reached at:

$$t_{\max} = -\frac{b_{\boldsymbol{c}}}{2a_{\boldsymbol{c}}}$$

and the corresponding maximum contribution level is:

$$\boldsymbol{c}_{\text{max}} = \boldsymbol{c}_0 - \frac{b_{\boldsymbol{c}}^2}{4a_{\boldsymbol{c}}}$$

Let us illustrate the impact of the spot contribution c_t on the forward contribution H_t with an example. We assume that the initial contribution of an individual at age 20 is equal to c(20) = 1, and that the maximum contribution of 2.50 is reached at age 50. Based on these assumptions, we obtain the following calibrated functions:

Function	Expression
Constant	$c_t = 1.75$
Linear	$c_t = 0.5 \times t$
Quadratic	$c_t = -1.667 + 0.167 \times t - 1.667 \times 10^{-3} \times t^2$
$\overline{\text{Quadratic}} \ \# \overline{2}$	$\bar{c}_t = -6.875 + 0.375 \times t - 3.75 \times 10^{-3} \times t^2$

These functions are illustrated in Figure 4. The convexity of the quadratic function plays an important role. For instance, consider the same maximum contribution point (age 50) with a new initial point: c(30) = 1. This leads to the curve labeled Quadratic #2. We observe that the function is symmetric around $t_{\text{max}} = 50$ years. To achieve an asymmetric convex shape, a polynomial of degree higher than two would be required. Next, we compute the forward contribution H_t , assuming an interest rate $r_t = 2\%$, and plot the results in Figure 5. We see that H_t is decreasing in the constant case, while it is increasing and then decreasing in the other cases ¹³. At first glance, this may seem counterintuitive, especially when the spot contribution c_t is strictly positive. However, the forward contribution H_t reflects time preference, and the discount rate can have a significant impact. This explains why, in the linear case of c_t , H_t increases up to age 30 and decreases thereafter.

 $^{^{13}}$ In Appendix A.6 on page 93, we derive the time at which H_t reaches its maximum. The exact solutions are 29.94 years for the linear case, 25.63 years for the quadratic case, and 32.31 years for the quadratic #2 case.

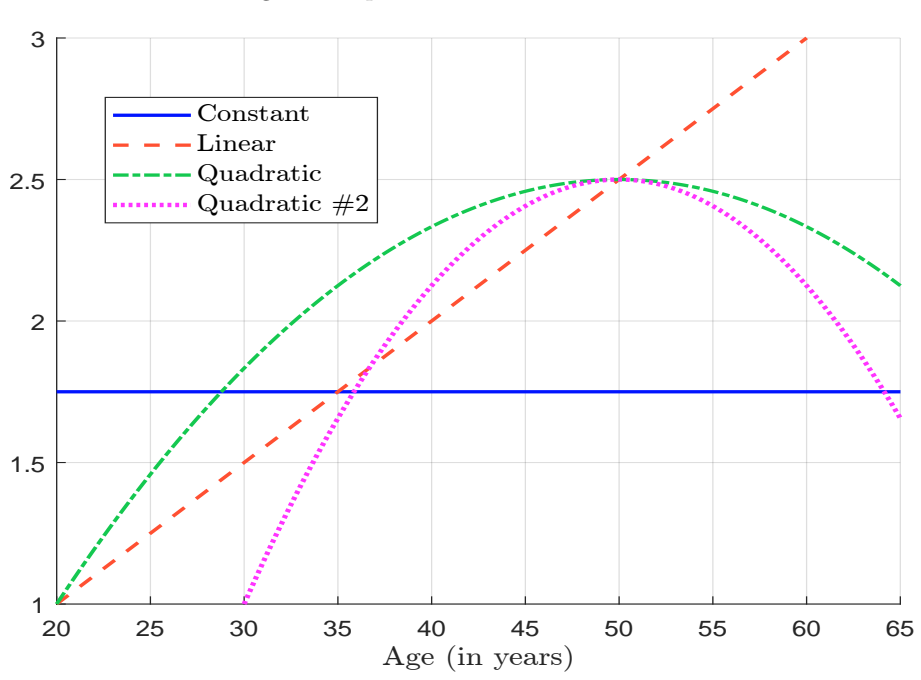
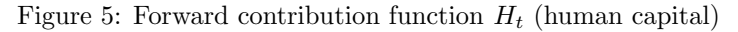
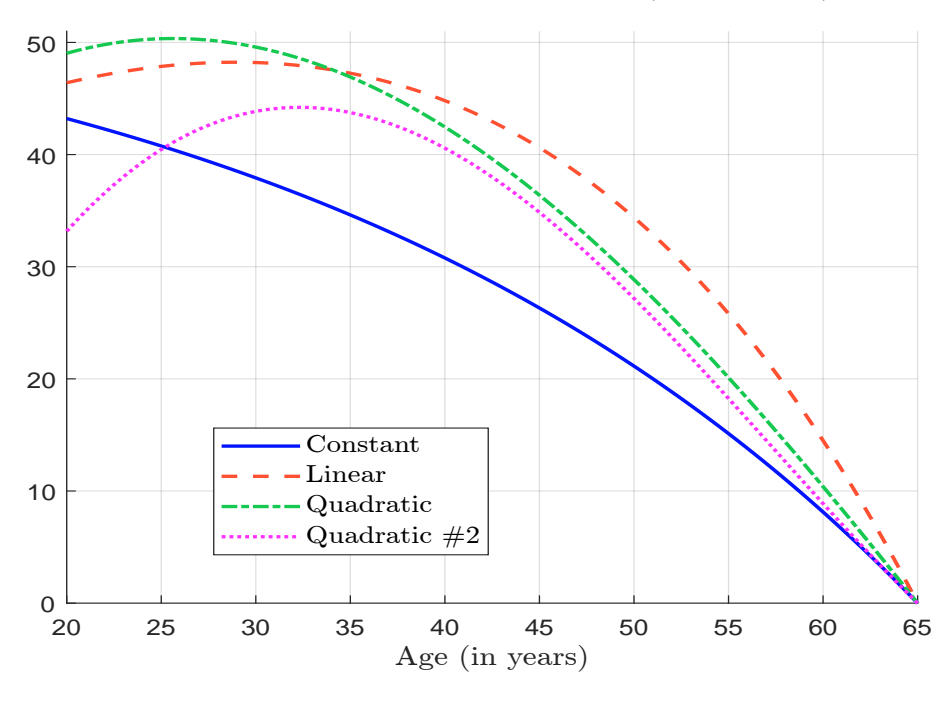


Figure 4: Spot contribution function c_t





2.1.3 Properties of the optimal exposure α_t^*

We recall that the optimal exposure is given by:

$$\alpha_t^{\star} = \frac{\mu_t - r_t}{(1 - \gamma)\sigma_t^2} \left(1 + \frac{H_t}{X_t} \right) = \frac{SR_t}{(1 - \gamma)\sigma_t} \left(1 + \frac{H_t}{X_t} \right)$$

We deduce the following properties:

- α_t^{\star} is an increasing function of the risk premium μ_t and the Sharpe ratio SR_t . In other words, an individual will allocate more to a risky asset if it offers a higher excess return relative to its risk.
- α_t^{\star} is a decreasing function of volatility σ_t . Risky assets with higher volatility are penalized in the allocation strategy.
- α_t^{\star} decreases as risk aversion increases (i.e., it increases with the coefficient γ). A more risk-tolerant individual will have a higher exposure to risky assets.
- α_t^* is inversely related to current financial wealth X_t . An individual with lower current wealth will allocate a higher proportion of their wealth to risky assets.
- α_t^* increases with expected future contributions H_t . Individuals who anticipate higher future income or contributions will have a higher exposure.

In fact, the last two properties can be unified, since the optimal exposure depends on the ratio H_t/X_t rather than the individual absolute values of H_t and X_t . Notably, H_t reflects expectations about future wealth. For example, consider an individual who has just finished school and currently earns a low salary. If he anticipates a significant increase in earnings due to his high level of education, we can expect a large future contribution relative to his current wealth. In this context, the ratio H_t/X_t can be interpreted in multiple ways:

$$\frac{H_t}{X_t} = \frac{\text{Forward wealth}}{\text{Current wealth}} = \frac{\text{Human capital}}{\text{Financial capital}} := \text{HFCR}_t$$

This ratio highlights the individual's balance between human capital (expected future earnings) and financial capital (current accumulated wealth). This ratio is generally called the human-to-financial capital ratio (HFCR).

Incorporating human capital fundamentally alters an individual's perception of risk. Since human capital serves as a buffer against financial risk, individuals can afford to take on more financial risk in the present. In this context, the optimal allocation can be rewritten in the form of the traditional Merton-Markowitz solution:

$$\alpha_t^{\star} = \frac{\mu_t - r_t}{(1 - \bar{\gamma}_t) \, \sigma_t^2}$$

where the adjusted relative risk aversion $\bar{\gamma}_t$ accounts for human capital and is defined as follows:

$$\bar{\gamma}_t = \frac{\gamma}{1 + \text{HFCR}_t} + \frac{\text{HFCR}_t}{1 + \text{HFCR}_t}$$

As the HFCR becomes large (i.e., human capital dominates financial capital), the adjusted relative risk aversion $\bar{\gamma}_t$ tends toward 1:

$$\lim_{\mathrm{HFCR}_t \to \infty} \bar{\gamma}_t = 1 \Rightarrow \varphi \to \infty$$

In practical terms, individuals with a high HFCR exhibit nearly infinite risk tolerance. This is because human capital acts as a cushion against financial losses. When future earnings are expected to be substantial relative to current financial wealth, individuals are more comfortable taking on risky investments today, knowing that future income will help compensate for potential short-term losses. In essence, the presence of significant human capital plays a role similar to a risk-free asset. It provides stability and predictability in overall wealth, even if financial assets fluctuate.

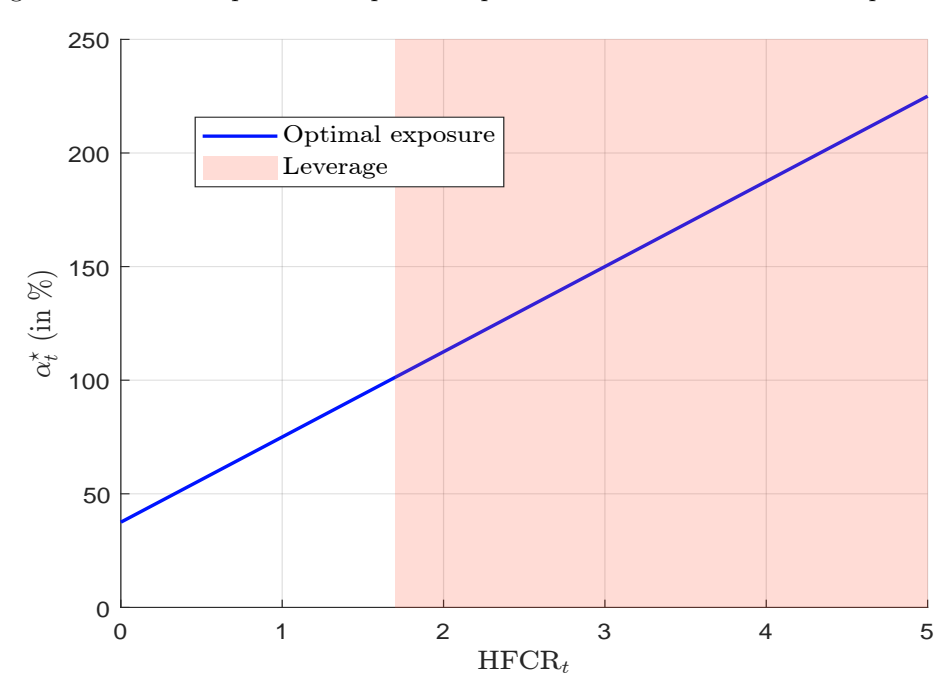


Figure 6: Relationship between optimal exposure and human-to-financial capital ratio

Remark 4. Let us consider an example with $SR_t = 0.30$, $\sigma_t = 20\%$, $r_t = 2\%$ and $\gamma = -3$. The resulting optimal allocation is illustrated in Figure 6. When HFCR_t exceeds a certain threshold HFCR_t* = $(1 - \gamma) \sigma_t / SR_t - 1$, individuals begin to use leverage. While this solution is theoretically optimal, it may not be practical due to real-world frictions such as transaction costs, borrowing constraints, and regulatory limits on leverage. Nevertheless, this example demonstrates how expectations about future wealth, as captured by forward-looking human capital, significantly influence present-day risk aversion and investment behavior.

In this context, we observe that the adjusted relative risk aversion $\bar{\gamma}_t$ becomes dynamic. Unlike in the classical Merton framework, where risk aversion remains constant over time, the inclusion of human capital introduces variability over time. As individuals progress through their life cycle, their HFCR evolves. For example, young individuals usually have more human capital than financial capital, resulting in lower effective risk aversion. Over time, as they accumulate financial wealth and their expected lifetime earnings decrease, their HFCR declines and their implied risk aversion increases. This shift leads to a natural lifecycle investment strategy where exposure to risky assets decreases with age or career progression. We illustrate this property in Figure 7. The parameters are set as follows: $\mu_t = 8\%$, $\sigma_t = 20\%$, $r_t = 2\%$, $\gamma = -3$, $t_0 = 20$, T = 60, $X_{t_0} = 1$, and $c_t = 0.05$. The first panel shows the relationship between the wealth X_t and the optimal exposure α_t^* for three different values of t. Since $H_t = 0$ when the current time t is the retirement date T, α_t^* is constant and equal

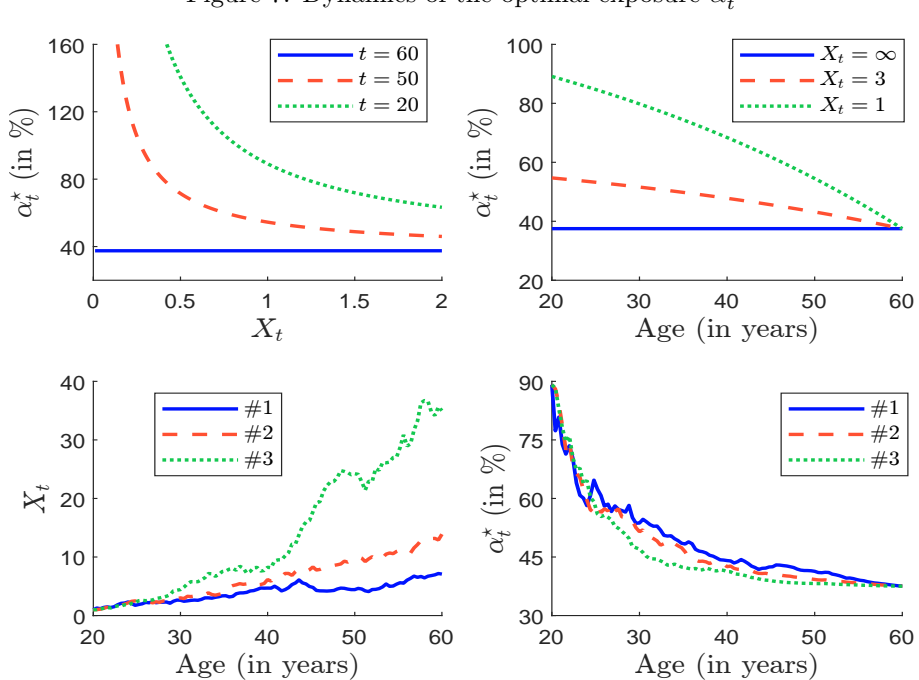
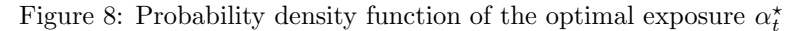
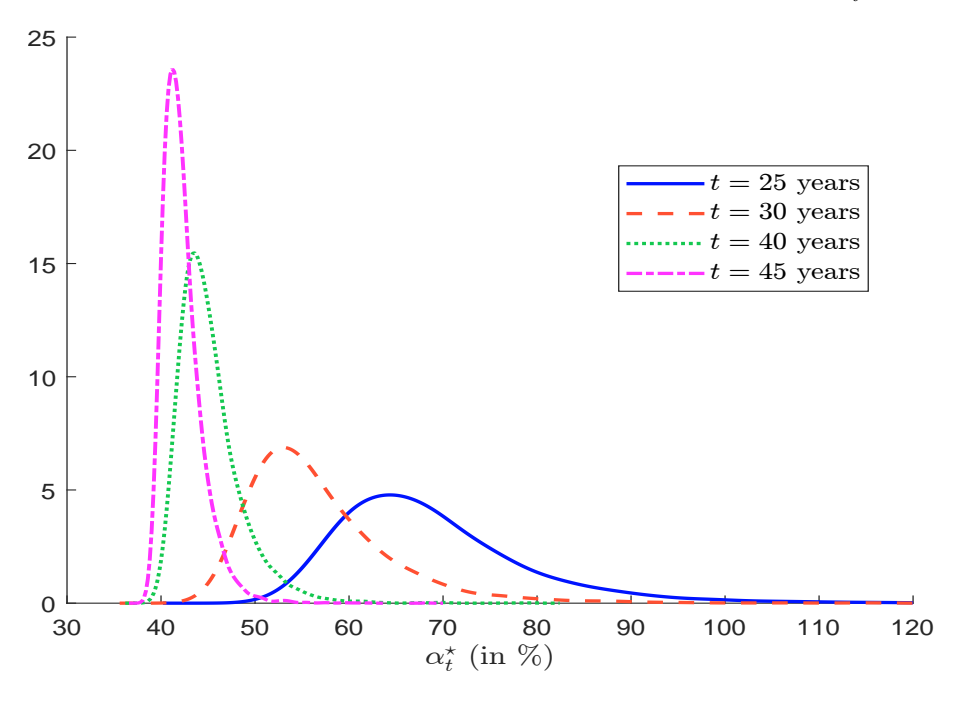


Figure 7: Dynamics of the optimal exposure α_t^{\star}





to $\bar{\alpha}_t = 37.5\%$, regardless of X_t . In contrast, when t = 20 years, the value of human capital H_t is 1.38. In this case, we observe the decreasing behavior of α_t^* with respect to X_t , as predicted by theory. The second panel shows the relationship between age t and α_t^* for three values of financial wealth X_t . Since human capital H_t decreases over time — from 1.38 to 0, we again observe a decreasing pattern in α_t^* as individuals approach retirement. Finally, the third and fourth panel show three simulated paths of the state-control system (X_t, α_t^*) . Due to the randomness introduced by the Brownian motion W_t , each simulation yields a distinct trajectory. Despite this variability, a clear trend emerges: Wealth X_t tends to increase over time, while optimal exposure α_t^* tends to decrease, reflecting the empirical lifecycle pattern in which individuals reduce their exposure to risky assets as they age. However, it is important to note that the path of α_t^* is not deterministic. Because of the uncertainty in the performance of the risky asset, which is captured by the stochastic component W_t , the optimal exposure α_t^* is a random variable for all $t \in (t_0, T)$. There are only two exceptions:

- At the initial date t_0 , when the current wealth X_{t_0} is known with certainty;
- At the retirement date T, when human capital H_T is supposed to be known with certainty and equals zero.

Between these two dates t_0 and T, α_t^* evolves stochastically. Figure 8 illustrates this by showing the probability density function of α_t^* for four selected time points t. In Figure 9, we verify that the Standard deviation of the optimal exposure α_t^* is zero at the current date, increases sharply during the first five years, and then gradually decreases until it reaches again zero at retirement. Interestingly, a higher volatility of the risky asset does not lead to an increase in $\sigma(\alpha_t^*)$. Rather, it results in a lower standard deviation. This occurs because greater volatility reduces the overall level of optimal exposure, thereby dampening its variability.

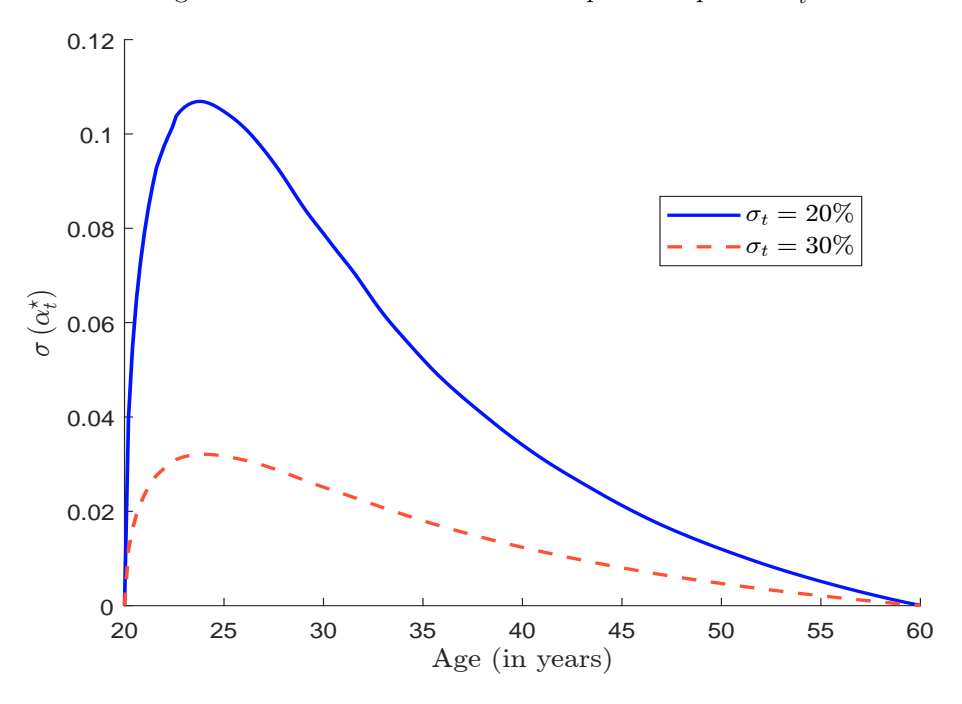


Figure 9: Standard deviation of the optimal exposure α_t^{\star}

2.1.4 Dynamics of the wealth X_t

The wealth follows a stochastic differential equation:

$$dX_t = ((r_t + \eta_t) X_t + \eta_t H_t + \mathbf{c}_t) dt + \bar{\alpha}_t \sigma_t (X_t + H_t) dW_t$$

where:

$$\eta_t = \frac{\mathrm{SR}_t^2}{(1-\gamma)}$$

 X_t can be simulated using numerical schemes such as Euler-Maruyama or Milstein¹⁴. To characterize the dynamics of X_t , we analyse its expected wealth $m_t = \mathbb{E}[X_t]$ and variance $v_t = \text{var}(X_t)$. To gain intuition, we consider the case where all parameters are constant. Under this assumption, we obtain¹⁵:

$$m_t = e^{(r+\eta)(t-t_0)} \left(x_0 + \int_{t_0}^t e^{-(r+\eta)(s-t_0)} \left(\eta H_s + \mathbf{c}_s \right) \, \mathrm{d}s \right)$$
 (10)

and:

$$v_t = \bar{\alpha}^2 \sigma^2 \int_{t_0}^t (m_s + H_s)^2 e^{(2(r+\eta) + \bar{\alpha}^2 \sigma^2)(t-s)} ds$$
 (11)

The expected wealth m_t is an increasing function of the initial wealth x_0 , the contribution policy c_t , the interest rate r_t , the Sharpe ratio SR_t and the risk aversion parameter γ . Similar monotonicity properties hold for the variance process v_t .

We consider again the same example: $\mu_t = 8\%$, $\sigma_t = 20\%$, $r_t = 2\%$, $\gamma = -3$, and $X_{t_0} = 1$. We assume that $t_0 = 20$, and T = 60. Figure 10 illustrates the evolution of expected wealth over age t for different contributions \mathbf{c}_t . Even modest contributions exhibit a multiplicative effect on expected wealth growth. For a constant contribution function, Equation (10) becomes:

$$m_t = e^{(r+\eta)(t-t_0)}x_0 + \left(\left(e^{(r+\eta)(t-t_0)} - 1\right) - e^{-r(T-t_0)}\left(e^{(r+\eta)(t-t_0)} - e^{r(t-t_0)}\right)\right)\frac{c_0}{r}$$

If we assume that $x_0 \approx 0$, we find that m_t is proportional to the constant contribution level c_0 :

$$m_t = f(t) \frac{c_0}{r}$$

This homogeneity property is particularly important, as it shows that the expected wealth scales linearly with the contribution level.

We now analyze the relationship between the Sharpe ratio SR and the expected terminal wealth $m_T = \mathbb{E}[X_T]$, which simplifies to:

$$m_T = e^{(r+\eta)(T-t_0)} x_0 + \left(e^{(r+\eta)(T-t_0)} - e^{\eta(T-t_0)} \right) \frac{\mathbf{c}_0}{r}$$

As shown in Figure 11, this relationship exhibits strong log-concavity, as shown by the following identity:

$$\ln \left(m_T \mid SR \neq 0 \right) = SR^2 \frac{(T - t_0)}{1 - \gamma} + \ln \left(m_T \mid SR = 0 \right)$$

This result is particularly significant, because it highlights that the performance of the strategy scales linearly with the investment horizon $(T - t_0)$, but quadratically with respect

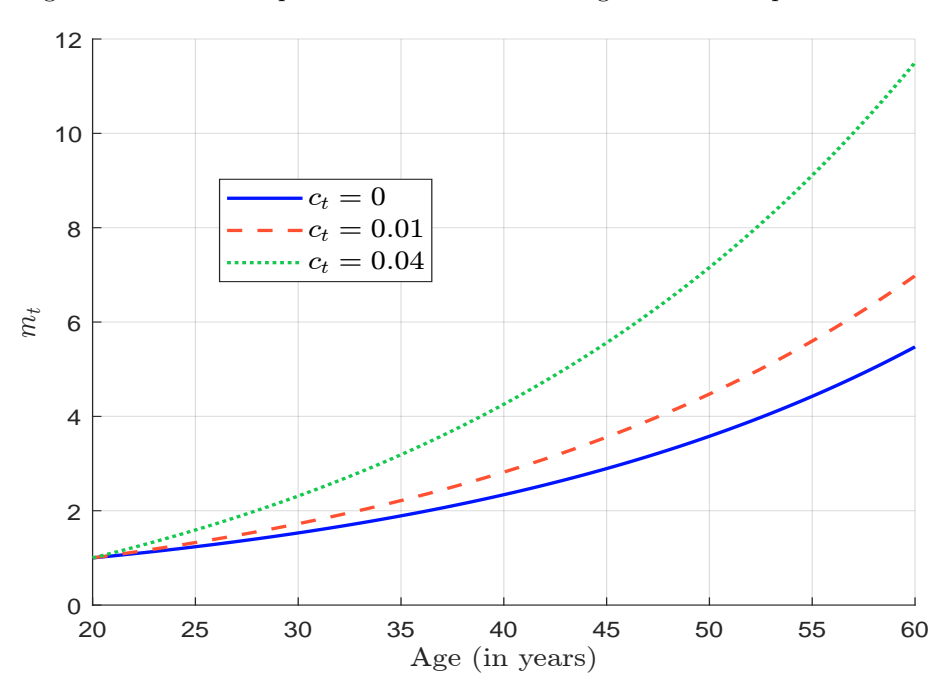
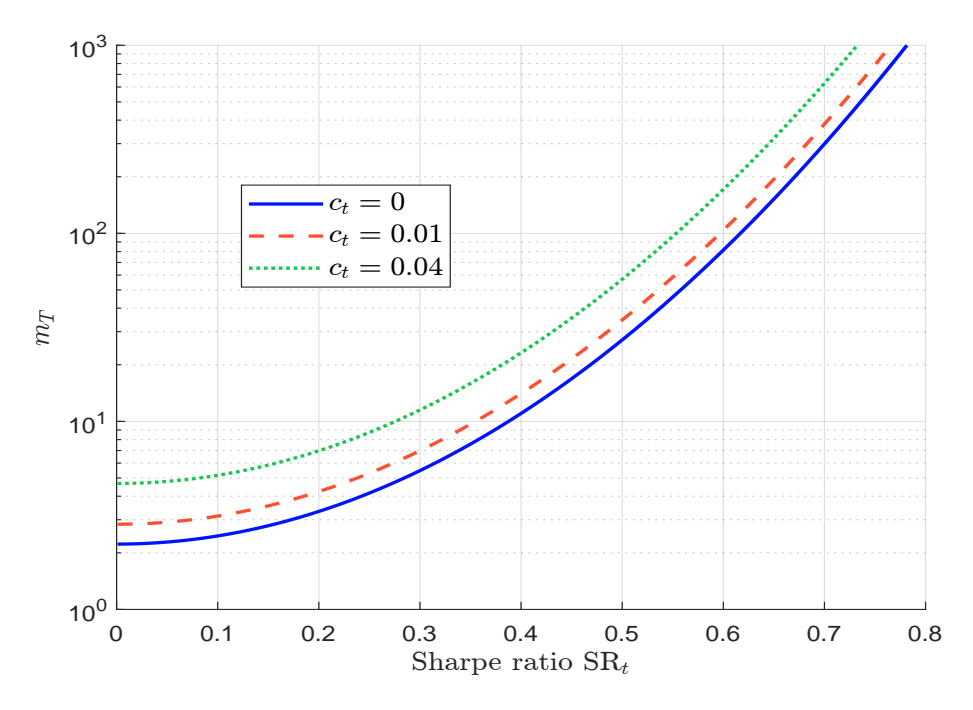


Figure 10: Relationship between an individual's age and their expected wealth

Figure 11: Relationship between the Sharpe ratio of the risky asset and expected terminal wealth

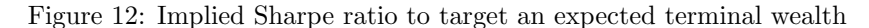


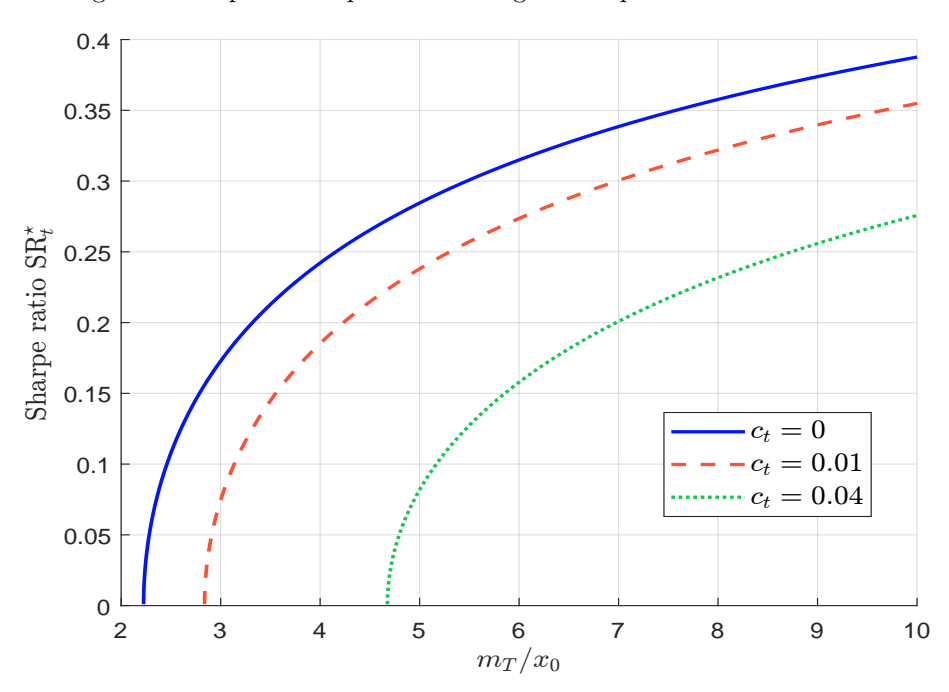
to the Sharpe ratio. In other words, any improvement in the Sharpe ratio has a squared effect on terminal wealth, as its impact is effectively doubled.

We now address the following question: What Sharpe ratio is required to achieve a terminal wealth equal to β times the initial wealth? This inverse calibration problem can be solved numerically by solving the equation $m_T = \beta x_0$. In fact, we can show that the implied Sharpe ratio is given analytically by ¹⁶:

$$SR^* = \sqrt{\frac{1-\gamma}{T-t_0} \ln\left(\frac{\beta}{\lambda}\right)}$$

Figure 12 illustrates the calibration of SR* for the example discussed earlier. These results confirm the leverage impact of the Sharpe ratio on the wealth.





Remark 5. Figure 12 shows that the variation of the implied Sharpe ratio SR^* is significantly smaller than the variation of the multiplier β . This notable property indicates that the strategy greatly benefits from even small improvements in the Sharpe ratio. The underlying reason is the convex relationship between the Sharpe ratio and terminal wealth. In fact, we can demonstrate that:

$$\Delta\,\mathrm{SR}^{\star} \approx \frac{1}{2\sqrt{\ln\beta - \ln\lambda}}\sqrt{\frac{1-\gamma}{T-t_0}}\frac{\Delta\beta}{\beta}$$

Thus, the absolute variation of the Sharpe ratio translates into the relative variation of terminal wealth. In other words, modest gains in the Sharpe ratio have an amplified effect on performance, especially in long-term strategies.

$$\lambda = e^{r(T-t_0)}x_0 + \left(e^{r(T-t_0)} - 1\right)\frac{c_0}{r}$$

 $^{^{14}\}mathrm{See}$ Appendix A.12 on page 100.

¹⁵General formulas are provided in Appendices A.7 and A.8 on pages 94 and 96, respectively.

¹⁶We have:

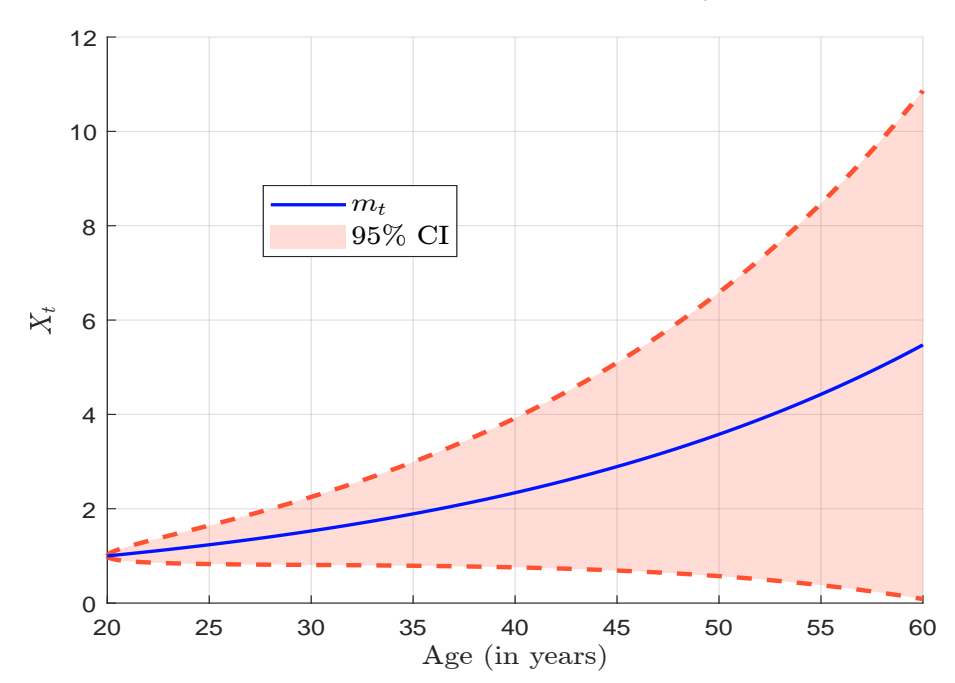


Figure 13: 95% confidence interval of the wealth when $c_t = 0$ (gaussian approximation)

The variance process v_t can be used to build a confidence interval for the wealth X_t . For instance, the Gaussian confidence interval is given by:

$$\operatorname{CI}_{\alpha}\left(X_{t}\right)=\left[m_{t}-z_{\alpha}\sqrt{v_{t}},m_{t}+z_{\alpha}\sqrt{v_{t}}\right]$$

where $z_{\alpha} = \Phi^{-1}((1+\alpha)/2)$. Figure 13 shows the 95% confidence interval of X_t when $c_t = 0$. However, the issue is that X_t is far from Gaussian. In fact, it inherits the lognormal property of the geometric Brownian motion S_t . Figure 14 represents the probability density function of X_T . If we assume that $X_t \sim \mathcal{LN}(\tilde{\mu}_t, \tilde{\sigma}_t^2)$, we must have:

$$\begin{cases} m_t = \exp\left(\tilde{\mu}_t + \frac{1}{2}\tilde{\sigma}_t^2\right) \\ v_t = \exp\left(2\tilde{\mu}_t + \tilde{\sigma}_t^2\right) \left(\exp\left(\tilde{\sigma}_t^2\right) - 1\right) \end{cases}$$

The solution is:

$$\begin{cases} \tilde{\mu}_t = 2\ln m_t - \frac{1}{2}\ln\left(\upsilon_t + m_t^2\right) \\ \tilde{\sigma}_t^2 = \ln\left(\frac{\upsilon_t + m_t^2}{m_t^2}\right) \end{cases}$$

In Figure 14, we also show the fitted log-normal distribution of X_T , verifying that the true and calibrated density functions are very close. Therefore, it is more appropriate to consider a log-normal confidence interval:

$$\operatorname{CI}_{\alpha}(X_t) = \left[\exp \left(\tilde{\mu}_t - z_{\alpha} \tilde{\sigma}_t \right), \exp \left(\tilde{\mu}_t + z_{\alpha} \tilde{\sigma}_t \right) \right]$$

Figure 15 shows the 95% log-normal confidence interval of X_t when $c_t = 0$. This interval is more realistic than the one shown in Figure 13.

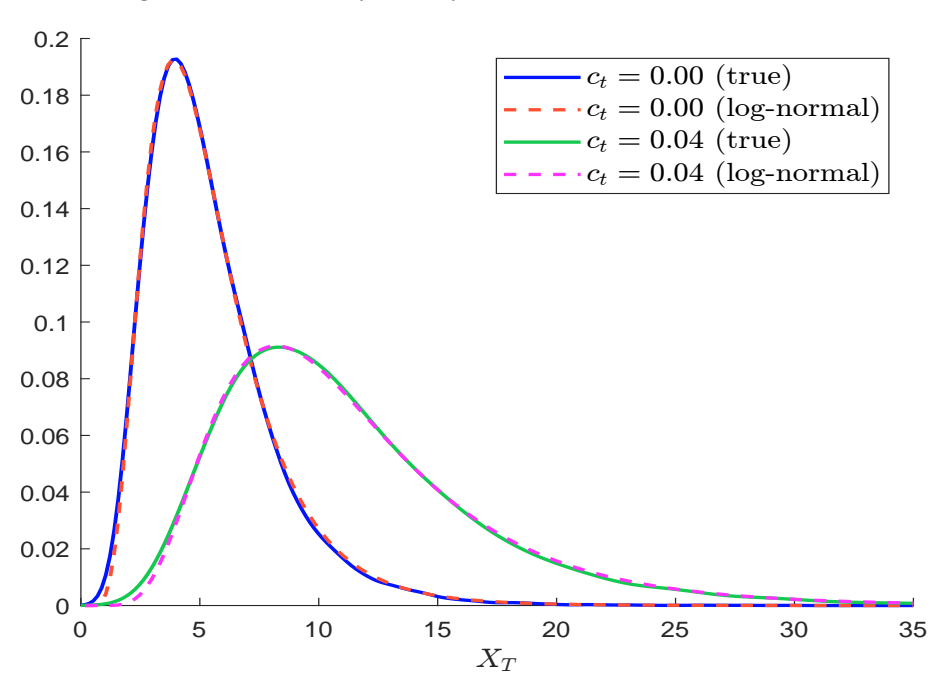
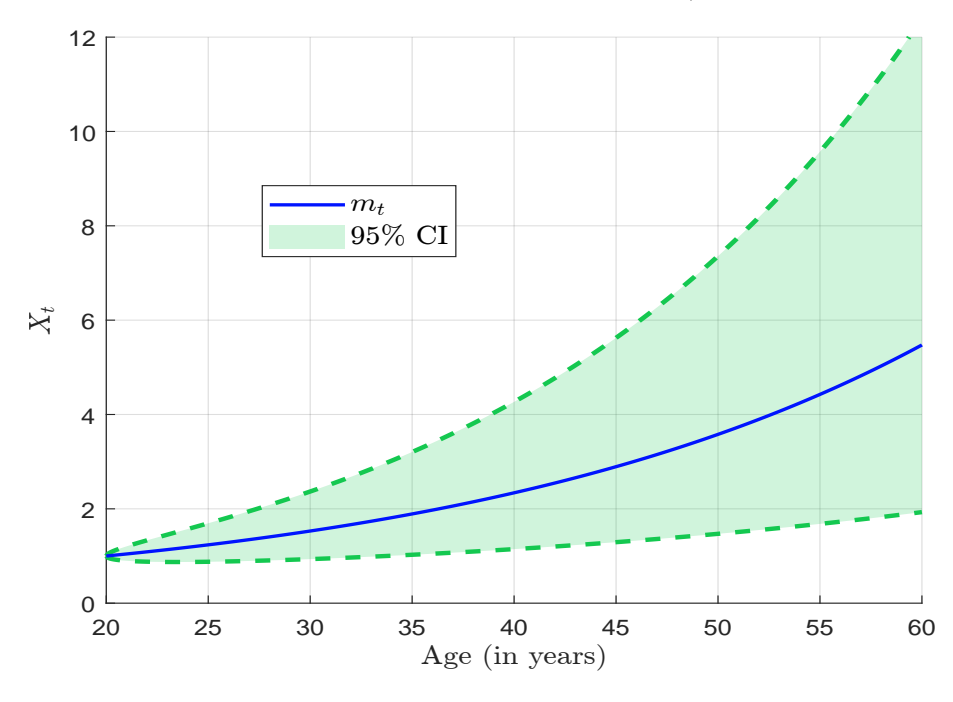


Figure 14: Probability density function of the terminal wealth





2.2 Definition of the glide path g_t

The glide path refers to the dynamic asset allocation strategy used by target date funds. In theory, the glide path aligns with the optimal dynamic exposure $\{\alpha_t^*, t \leq T\}$. However, it is important to note that the allocation at each point in time depends on the path of the investor's wealth, which is influenced by the allocation itself. This feedback loop makes both the optimal exposure and the wealth process endogenous: $X_t \longrightarrow \alpha_t^* \longrightarrow \mathrm{d} X_t \longrightarrow X_{t+\mathrm{d}t}$. As a result, there is not a single deterministic glide path, but rather a multitude of potential paths, as illustrated by the Monte Carlo simulations¹⁷ in Figure 16. From a practical standpoint, implementing such personalized, path-dependent dynamic allocations in a collective investment vehicles is infeasible. This is because the optimal exposure α_t^* varies across individuals, depending on factors such as risk preferences, contribution patterns, and investment horizons.

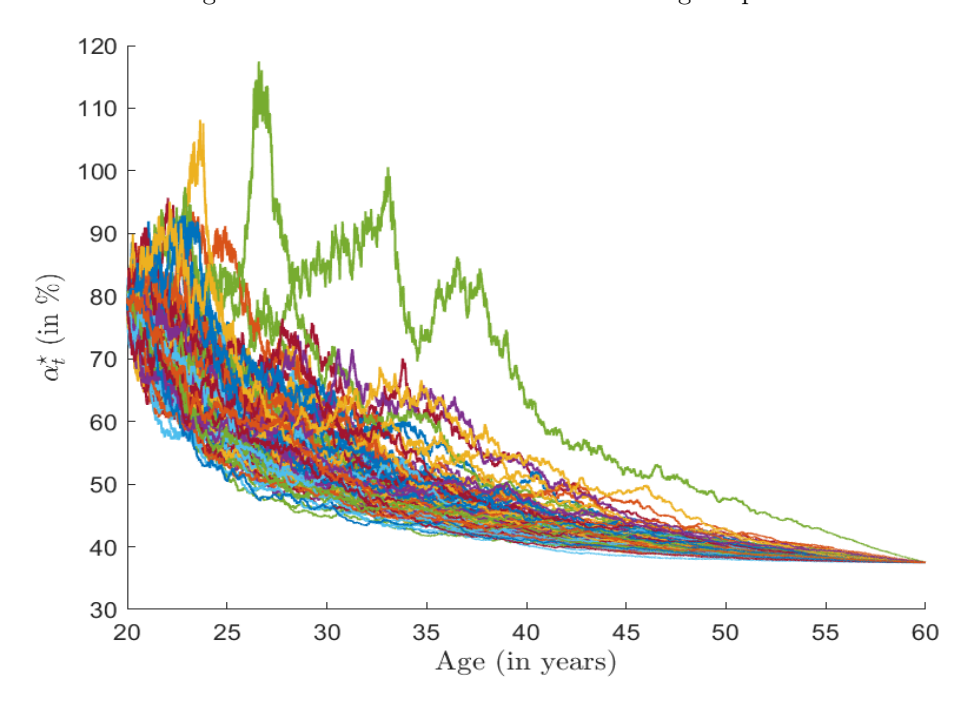


Figure 16: Monte Carlo simulations of the glide path

2.2.1 Analytical expression and main properties

The glide path g_t is the deterministic, dynamic asset allocation computed at the initial date t_0 . It corresponds to the conditional expectation of the stochastic optimal exposure α_t^* with respect to the filtration \mathcal{F}_{t_0} :

$$g_{t} = \mathbb{E}\left[\alpha_{t}^{\star} \mid \mathcal{F}_{t_{0}}\right]$$

$$= \frac{\mu_{t} - r_{t}}{(1 - \gamma)\sigma_{t}^{2}} \left(1 + H_{t}\mathbb{E}\left[\frac{1}{X_{t}}\middle|\mathcal{F}_{t_{0}}\right]\right)$$
(12)

The continue to use the same example: $\mu_t = 8\%$, $\sigma_t = 20\%$, $r_t = 2\%$, $\gamma = -3$, $X_{t_0} = 1$, $t_0 = 20$, T = 60, and $c_t = 0.04$.

In Bruder et al. (2012), the expectation of $1/X_t$ is approximated using the inverse of the expected wealth:

$$\mathbb{E}\left[\left.\frac{1}{X_t}\right|\mathcal{F}_{t_0}\right] \approx \frac{1}{\mathbb{E}\left[\left.X_t\right|\mathcal{F}_{t_0}\right]} = \frac{1}{m_t}$$

which leads to the approximate formula:

$$g_t \approx \frac{\mu_t - r_t}{(1 - \gamma)\sigma_t^2} \left(1 + \frac{H_t}{m_t} \right) \tag{13}$$

This approximation can be refined by applying Jensen's inequality. As shown in Appendix A.10 on page 98, a second-order correction gives:

$$\mathbb{E}\left[\left.\frac{1}{X_t}\right|\mathcal{F}_{t_0}\right] \approx \frac{1}{m_t} + \frac{v_t}{m_t^3}$$

We deduce that:

$$g_t \approx \frac{\mu_t - r_t}{\left(1 - \gamma\right)\sigma_t^2} \left(1 + \frac{H_t}{m_t} + \frac{H_t v_t}{m_t^3}\right) \tag{14}$$

If we assume that $X_t \sim \mathcal{LN}(\tilde{\mu}_t, \tilde{\sigma}_t^2)$, we can compute the exact conditional expectation:

$$\mathbb{E}\left[\frac{1}{X_t}\middle|\mathcal{F}_{t_0}\right] = \exp\left(-\tilde{\mu}_t + \frac{1}{2}\tilde{\sigma}_t^2\right)$$

$$= \exp\left(-2\ln m_t + \frac{1}{2}\ln\left(v_t + m_t^2\right) + \frac{1}{2}\ln\left(\frac{v_t + m_t^2}{m_t^2}\right)\right)$$

$$= \exp\left(-3\ln m_t + \ln\left(v_t + m_t^2\right)\right)$$

$$= \frac{v_t + m_t^2}{m_t^3}$$

Therefore, Equation (12) becomes:

$$g_t = \frac{\mu_t - r_t}{(1 - \gamma)\sigma_t^2} \left(1 + H_t \exp\left(-\tilde{\mu}_t + \frac{1}{2}\tilde{\sigma}_t^2\right) \right)$$

$$= \frac{\mu_t - r_t}{(1 - \gamma)\sigma_t^2} \left(1 + H_t \left(\frac{\upsilon_t + m_t^2}{m_t^3}\right) \right)$$
(15)

Thus, Equations (14) and (15) are mathematically equivalent 18 .

If we denote by g_t^- and g_t^+ the approximations of the glide path given in Equations 13 and 14, respectively, we have $g_t^- < g_t^+$ because $v_t \ge 0$. Figure 17 shows the true glide path g_t , along with the two approximations g_t^- and g_t^+ . We observe that $g_t^- \le g_t$ and $g_t \approx g_t^+$. This inequality holds because, by analyzing the Taylor expansion underlying Jensen's inequality, we can show that g_t^- provides a lower bound, due to the fact that the variance and skewness of the wealth are always positive. In practice, the second-order approximation is generally

¹⁸See Appendix A.11 on page 99 for a formal proof demonstrating the equivalence between the Jensen-corrected glide path and the exact formulation under a log-normal wealth assumption.

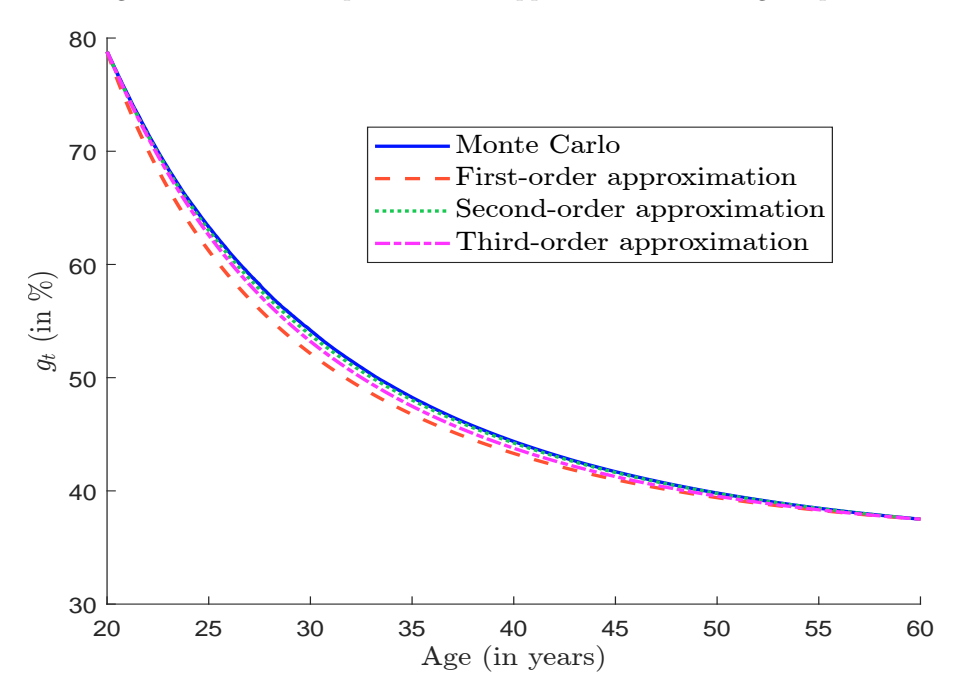


Figure 17: Exact computation and approximation of the glide path

sufficient for estimating the glide path, and incorporating skewness does not significantly improve the accuracy.

The glide path g_t inherits key properties from the optimal allocation α_t^{\star} . As discussed in Bruder *et al.* (2012), it is useful to categorize the model parameters into two main families:

- Parameters related to financial assets
- Parameters related to the individual or investor

These two types of parameters influence the design of the investment strategy in fundamentally different ways. Parameters related to financial assets, such as the expected return or volatility of the risky asset, are typically associated with the portfolio manager's decisions. In the context of a target date fund, for instance, the manager is mandated to adjust the asset allocation based on short- or long-term market views. In this sense, asset-related parameters are somewhat endogenous, as they can vary across portfolio managers and target date funds. Conversely, individual-related parameters, such as the investor's risk aversion, retirement date, age, and current or projected wealth, are more exogenous. These factors are intrinsic to the investor and do not depend on the portfolio manager. These factors help shape the target date fund market and explain why such funds are typically structured by generation and risk profile.

2.2.2 Shape of the glide path

Until now, we have assumed that the optimal exposure α_t^* is unconstrained. This results in a convex glide path, as shown in Figure 18. However, this hypothesis is not realistic since individuals cannot borrow to invest and be leveraged, implying $\alpha_t^* \in [0, 1]$. The constrained glide path is therefore defined by the conditional expectation:

$$g_t^c = \mathbb{E}\left[\alpha_t^\star \mid \alpha_t^\star \in [0, 1]\right]$$

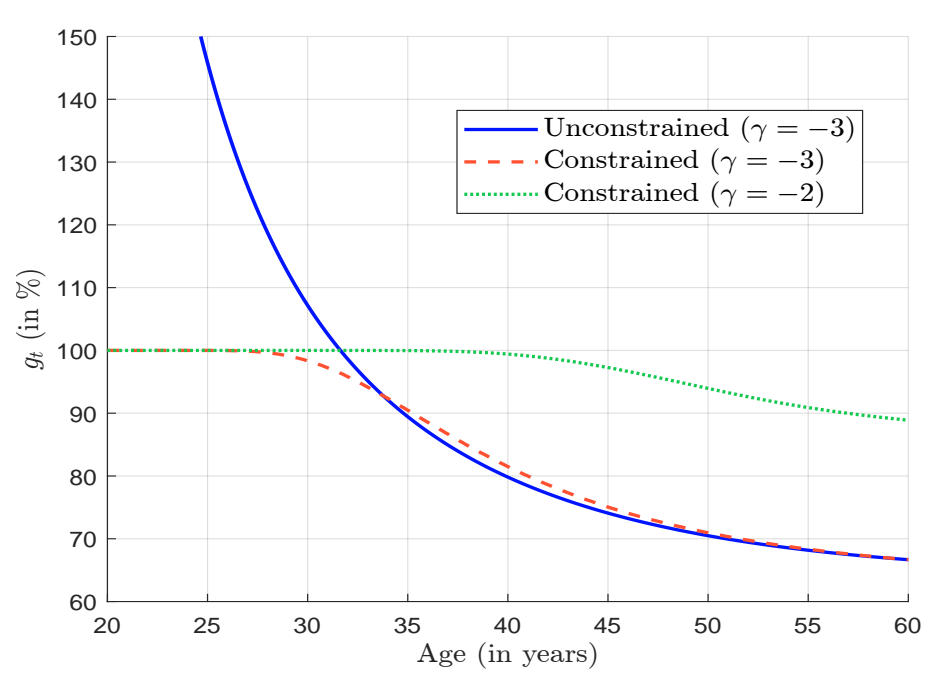
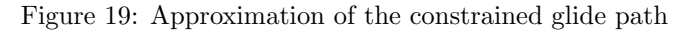
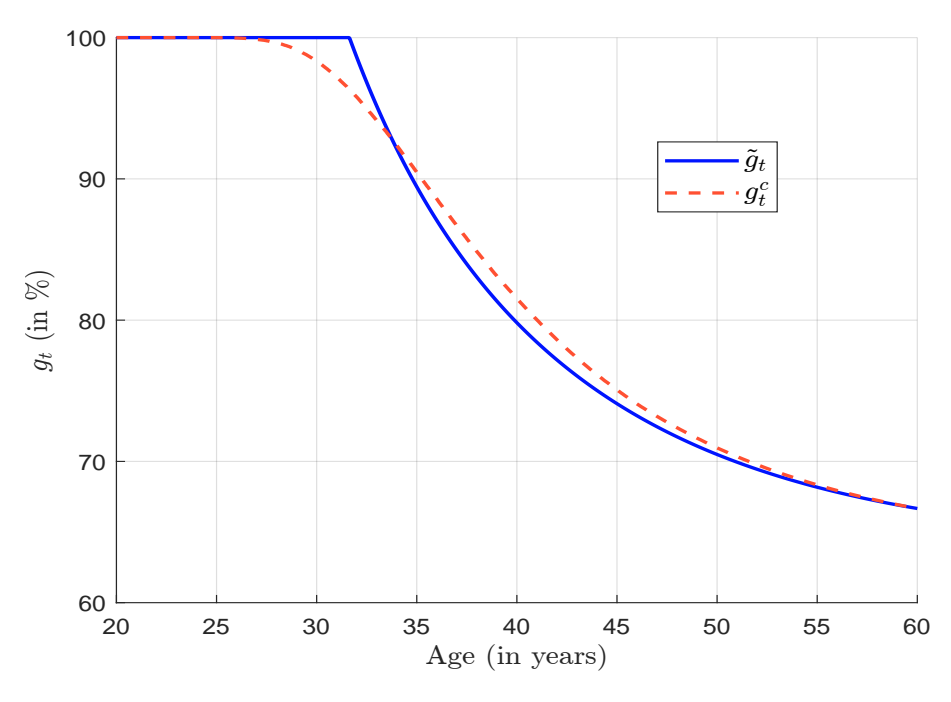


Figure 18: Constrained vs. unconstrained glide path





The value of g_t^c can be estimated using Monte Carlo simulations. In Figure 18, we compare the unconstrained glide path g_t with the constrained glide path g_t^c . As expected, the difference is more pronounced when individuals are young, due to higher forward wealth¹⁹. The shape of g_t^c is also sensitive to the relative risk aversion γ , as shown in Figure 18. A practical approximation of the constrained glide path is:

$$g_t^c \approx \tilde{g}_t := \min\left(\frac{\mu_t - r_t}{(1 - \gamma)\sigma_t^2} \left(1 + \frac{H_t}{m_t} + \frac{H_t v_t}{m_t^3}\right), 1\right)$$

The comparison between g_t^c and \tilde{g}_t is provided in Figure 19.

If all parameters in Equation (7) are held constant, the glide path g_t is convex in t. However, in practice, the glide paths implemented by asset managers are usually concave. This raises the question of what factors lead to a concave glide path. One key factor is time-varying risk preferences, specifically a changing coefficient of relative risk aversion. In reality, an individual's risk tolerance evolves over time. At the initial date t_0 , an investor may be relatively risk-tolerant, implying a small negative value for γ_t . As the retirement date T approaches, however, the same investor typically becomes more risk-averse, leading to a significant decrease of γ_t . Since the optimal portfolio exposure α_t^* is calibrated to the current value of γ_t , any change in risk aversion makes the original allocation suboptimal. This leads to a form of time inconsistency, where the optimal decision at one time is no longer optimal at a future date. These types of problems fall within the framework of time-inconsistent stochastic control. Following the foundational idea of Strotz (1955) and its continuous-time formulation by Ekeland and Lazrak (2008), we model the investor as a continuum of selves, one for each instant t, each controlling the portfolio over the infinitesimal interval [t, t + dt]. We assume a no-commitment setting, meaning the investor can revise their plan at any future time. In this framework, the appropriate solution concept is a subgame-perfect Nash equilibrium rather than the standard Bellman optimality principle. Björk et al. (2017) derive the associated equilibrium HJB equations for such time-inconsistent problems. They show that, for a CRRA utility function with a time-varying coefficient γ_t , the optimal exposure still admits a closed-form solution:

$$\alpha_t^{\star} = \frac{\mu_t - r_t}{(1 - \gamma_t) \,\sigma_t^2} \left(1 + \frac{H_t}{X_t} \right)$$

This expression mirrors the earlier solution derived under constant risk aversion. The main difference is that the constant γ has been replaced by the time-varying function γ_t .

To illustrate the impact of time-varying risk aversion, we consider the following functional form for γ_t :

$$\gamma_t = \gamma_0 + (\gamma_T - \gamma_0) \left(\frac{e^{k(t-t_0)} - 1}{e^{k(T-t_0)} - 1} \right)$$

where $\gamma_0 > \gamma_T$. This function provides a smooth interpolation between γ_0 at time t_0 and γ_T at the retirement date T, with the curvature governed by the parameter k. It exhibits the following limiting cases:

$$\gamma_t = \begin{cases} \gamma_0 & \text{if } k \to +\infty \\ \gamma_0 + (\gamma_T - \gamma_0) \left(\frac{t - t_0}{T - t_0}\right) & \text{if } k \to 0 \\ \gamma_T & \text{if } k \to -\infty \end{cases}$$

¹⁹We continue to use the same numerical example, but with a lower volatility — $\sigma_t = 15\%$ — and a higher contribution — $c_t = 0.10$.

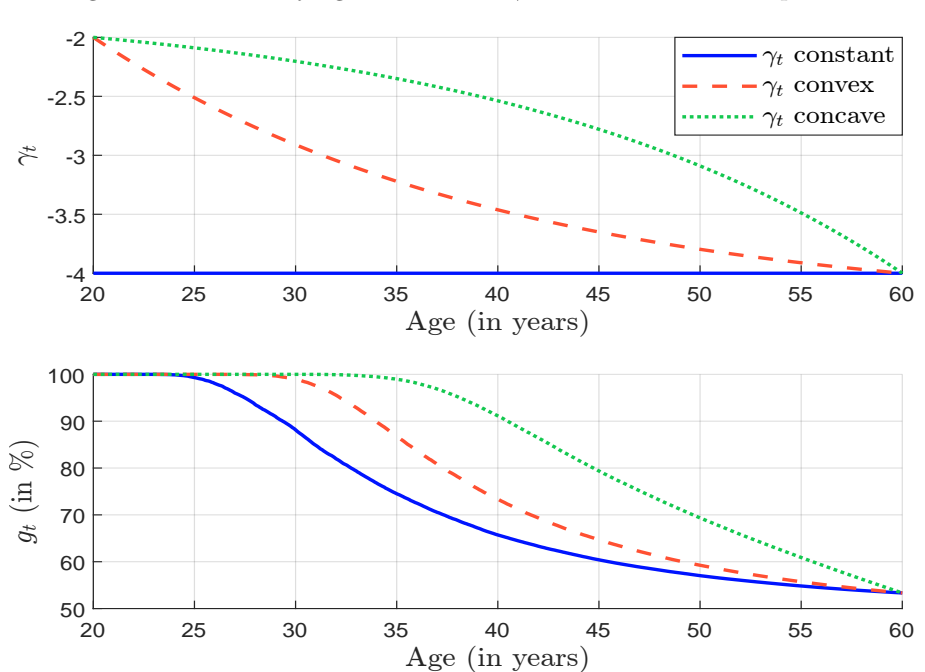
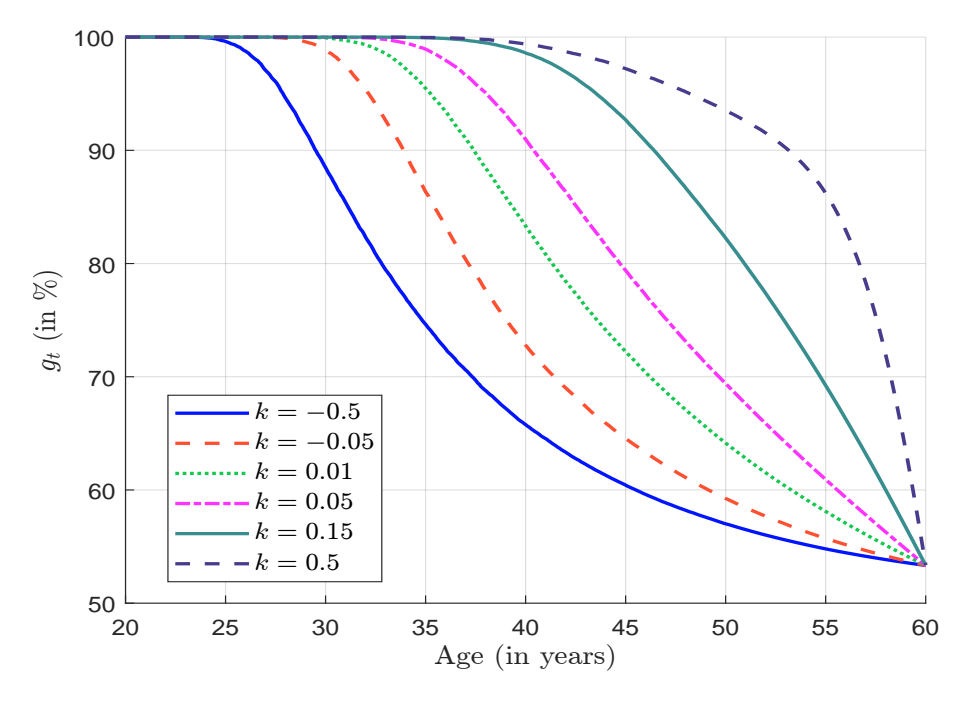


Figure 20: Time-varying risk aversion γ_t : concave vs. convex profiles

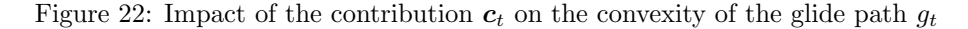


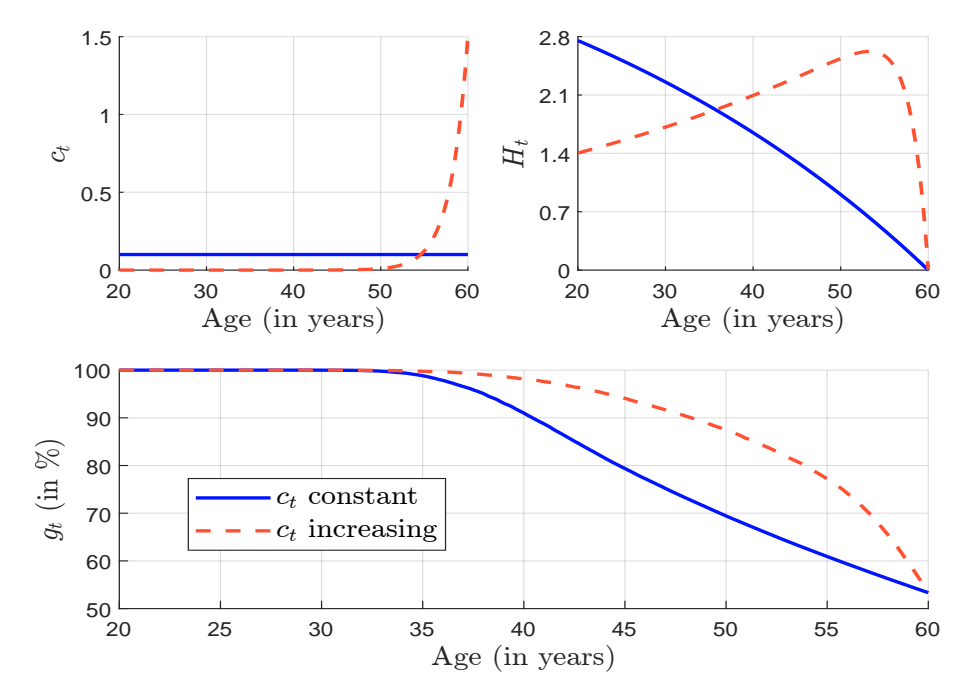


Moreover, it can be shown that γ_t is concave when k > 0 and convex when k < 0. In Figure 20, we set $\gamma_0 = -2$ and $\gamma_T = -4$, and plot the function γ_t for three values of k: 0.05, -0.05, and $-\infty$. The case k = 0.05 corresponds to a concave risk aversion profile, while k = -0.05 yields a convex profile. Using these three specifications for γ_t we compare the resulting glide paths²⁰. As expected, we observe the following ordering:

$$g_t(\gamma_t = -4) \le g_t(k = 0.05) \le g_t(k = -0.05)$$

This illustrates that, while the glide path g_t is convex in t when relative risk aversion is constant or convex, it becomes concave when γ_t itself is concave. The degree of concavity of the glide path increases with the curvature of the risk aversion profile, *i.e.*, with increasing values of k (Figure 21).





The shape of the risk aversion function is not the only factor that can result in a concave glide path. A similar effect can be achieved by assuming that the contribution c_t is an increasing function of time. This behavior reflects the psychology of real-world investors. Young people tend to have less wealth and generally don't worry much about planning for retirement. However, as retirement approaches, they become more aware of the need to save and increase their contributions. In such cases, it can be shown that the accumulated future contribution H_t becomes a concave function. The curvature of the glide path is then primarily driven by the second derivative of the ratio H_t/m_t : curvature $(g_t) \propto \partial_t^2 \left(\frac{H_t}{m_t}\right)$. Figure 22 illustrates this relationship under the assumption that the relative risk aversion γ_t is time-varying and concave, with a shape parameter k=0.05. However, it is important to note that concavity in the glide path g_t also arises when the time-varying risk aversion function γ_t is convex.

²⁰We use the following example: $\mu_t = 8\%$, $\sigma_t = 15\%$, $r_t = 2\%$, $X_{t_0} = 1$, $t_0 = 20$, T = 60, and $c_t = 0.10$.

To summarize, the glide path g_t is theoretically convex when all model parameters are held constant. In practice, however, it becomes concave due to three key factors that reflect real-world constraints and investor behavior:

- 1. Leverage constraints Individuals cannot borrow or use leverage, imposing a bound on exposure $(\alpha_t^* \in [0,1])$
 - This constraint fundamentally alters the shape of the glide path, especially for younger investors. In an unconstrained theoretical scenario, optimal exposure could exceed 100%, resulting in a convex path in which young investors would hold leveraged positions in risky assets. However, regulatory restrictions and practical limitations prevent retail investors from borrowing to invest. This constraint is most significant at the beginning of the investment horizon, when human capital is relatively high compared to financial wealth and an unconstrained optimal allocation would suggest extreme leverage. Consequently, the constrained glide path g_t^c has reduced curvature compared to the theoretical optimum, providing a more moderate and feasible allocation strategy, particularly at early stages of the life cycle.
- 2. Time-varying risk aversion Risk aversion tends to vary over time and often follows a concave profile (k > 0)
 - This may be the model's most psychologically realistic feature. Young investors typically exhibit lower risk aversion because they have longer investment horizons, more human capital, and different life priorities. However, as retirement approaches, investors naturally become more conservative, seeking to preserve their accumulated wealth rather than maximize growth. The concave profile (k > 0) realistically captures this accelerating shift in risk preferences. This behavioral evolution counteracts theoretical convexity because the denominator $(1 \gamma_t)$ in the optimal allocation formula changes more rapidly in later years, reducing equity exposure more aggressively as retirement approaches.
- 3. Increasing contribution patterns Contribution rates typically increase with age, which induces concavity in H_t
 - This factor reflects the typical career progression in which earnings and consequently retirement contributions increase over time due to promotions, salary growth, and a greater awareness of retirement needs. As contributions grow, the accumulated future contributions H_t become a concave function of time²¹. Since the glide path's curvature is proportional to $\partial_t^2(H_t/m_t)$, additional concavity is created in the allocation path. Economically, this makes sense. As future contributions grow larger relative to current wealth, the insurance value of these contributions justifies holding riskier assets early in one's career. However, this effect diminishes as retirement approaches and future contribution streams shorten.

Taken together, these factors reflect institutional constraints and behavioral tendencies. They explain why the glide paths implemented by asset managers tend to be concave. Initially, these paths prioritize high equity exposure, shifting cautiously toward safer assets as retirement approaches. The concave structure more closely aligns with observed investor behavior and the practical constraints of financial markets than the theoretically convex solution.

 $^{^{21}}$ This also challenges the simplistic interpretation of H_t as human capital, which typically increases over time. A more accurate view considers H_t as the discounted sum of future contributions, which can have a concave shape depending on the trajectory of contributions.

2.3 Empirical results

2.3.1 Comparison with constant-mix strategies

In the constant-mix strategy $\mathcal{CM}_{\alpha/1-\alpha}$, the individual allocates a fixed proportion α of their wealth to stocks and the remaining $1-\alpha$ to bonds. Therefore, the investor's wealth process X_t evolves according to the following stochastic differential equation:

$$\frac{\mathrm{d}X_t}{X_t} = \alpha \frac{\mathrm{d}S_t}{S_t} + (1 - \alpha) \frac{\mathrm{d}B_t}{B_t} + \frac{\mathbf{c}_t}{X_t} \,\mathrm{d}t$$

We assume that $\mu_t = 8\%$, $\sigma_t = 20\%$, $r_t = 2\%$, $X_{t_0} = 1$, $t_0 = 20$, T = 60, and $c_t = 0.10$. We evaluate three constant-mix strategies: $\mathcal{CM}_{0/100}$ which is fully invested in bonds (no exposure to equities), $\mathcal{CM}_{60/40}$ with 60% in stocks and 40% in bonds, and $\mathcal{CM}_{100/0}$ which is fully invested in stocks. These are compared against three glide path strategies, each defined by a different time-varying relative risk aversion profile: \mathcal{GP}_1 with $\gamma_t = -4$, \mathcal{GP}_2 with $\gamma_{t_0} = -2$, $\gamma_T = -4$, and k = 0.05, and \mathcal{GP}_3 with $\gamma_t = -1$.

Table 7: Comparison of the terminal wealth X_T ($\mu_t = 8\%$, $SR_t = 0.30$)

Strategy	TP [V]	l	C)uantile	Hit ratio				
	$\mathbb{E}\left[X_T\right]$	5%	10%	25%	50%	75%	90%	R=2%	R=4%
$\mathcal{CM}_{0/100}$	8.4	i		8					
$\mathcal{CM}_{60/40}$	24.3	7.7	9.4	13.3	19.9	30.1	44.2	93.2%	69.0%
$\mathcal{CM}_{100/0}$	53.7	6.0	8.4	15.0	29.5	60.3	117.3	90.0%	75.4%
$\bar{\mathcal{GP}}_1$	77.1	8.5	9.8	12.3	15.9	20.6	-25.9	95.4%	57.4%
\mathcal{GP}_2	21.6	8.2	9.8	13.3	18.8	26.7	36.5	94.6%	68.0%
\mathcal{GP}_3	40.8	6.8	9.1	15.3	27.4	49.8	85.4	91.8%	76.2%

Table 8: Comparison of the terminal wealth ($\mu_t = 4\%$, $SR_t = 0.10$)

Ctmatager	$\mathbb{E}\left[X_{T}\right]$	ı I	Q	uantile	Hit ratio				
Strategy		5%	10%	25%	50%	75%	90%	R=2%	R = 3%
$\mathcal{CM}_{0/100}$	8.4	l		8	l				
$\mathcal{CM}_{60/40}$	11.7	4.1	5.0	6.8	9.8	14.4	20.5	61.6%	41.5%
$\mathcal{CM}_{100/0}$	14.8	2.4	3.1	5.1	9.0	17.0	30.8	53.5%	41.2%
$\bar{\mathcal{GP}}_1$	9.0	7.3	$-\bar{7}.\bar{6}$	8.2	9.0	9.8	10.6	· 71.5%	4.9%
\mathcal{GP}_2	9.3	6.9	7.3	8.2	9.2	10.4	11.5	70.2%	14.8%
\mathcal{GP}_3	10.2	5.7	6.5	7.8	9.7	12.0	14.5	68.0%	34.2%

Results are given in Table 7. The pure equity strategy $\mathcal{CM}_{100/0}$ yields the highest expected terminal wealth (\$53.7), followed by the glide path strategy \mathcal{CP}_3 and the balanced constant-mix strategy $\mathcal{CM}_{60/40}$. \mathcal{GP}_3 notably outperforms $\mathcal{CM}_{60/40}$ in terms of average terminal wealth, highlighting the advantages of dynamically adjusting risk exposure over time. Glide path strategies offer superior downside protection. For instance, the 5% quantile of terminal wealth for \mathcal{GP}_1 is \$8.5, which is significantly higher than the \$7.7 quantile for the constant-mix strategy $\mathcal{CM}_{60/40}$. Even the conservative glide path \mathcal{GP}_1 exhibits strong performance in the lower tail of the distribution. While $\mathcal{CM}_{100/0}$ achieves the highest 90% quantile (\$117.3), it does so at the cost of much greater dispersion in outcomes. In contrast, glide path strategies deliver more stable results by reducing extreme outcomes, sacrificing some upside potential in exchange for enhanced stability and predictability. All glide path

strategies have hit ratios²² above 92%, indicating a greater likelihood of outperforming the risk-free benchmark. This makes them particularly attractive from a pension adequacy and risk management perspective. Table 8 presents results with a lower Sharpe ratio scenario ($SR_t = 0.10$), simulating a less favorable market environment. As expected, all strategies generate lower terminal wealth compared to the high Sharpe ratio case. However, the relative advantage of glide path strategies becomes more pronounced. These strategies provide better downside protection and higher hit ratios than their constant-mix counterparts. While constant-mix strategies may outperform glide paths on average during strong market conditions, they are also more vulnerable to downside risk. Glide path strategies, by gradually reducing risk exposure as retirement approaches, better align with behavioral pattern and real-world investment constraints. Consequently, they tend to deliver more consistent outcomes and increase the probability of meeting long-term retirement goals.

 Strategy
 $\mu_t = 8\%$ $\mu_t = 4\%$
 $\mathcal{CM}_{60/40}$ 60.0% 60.0%

 \mathcal{GP}_1 46.3% 16.5%

 \mathcal{GP}_2

 \mathcal{GP}_3

Table 9: Comparison of average risky exposure

60.3%

90.0%

23.9%

41.4%

Remark 6. The previous comparison is not entirely fair because the average exposure of each glide path strategy to risky assets depends on its specifications and parameter values. For example, when $\mu_t = 8\%$, the average exposure of strategy \mathcal{GP}_2 to risky assets is similar to the exposure of the 60/40 constant-mix strategy (Table 9). However, when $\mu_t = 4\%$, none of the glide path strategies have an average exposure close to the 60/40 benchmark. Therefore, direct comparisons between constant-mix and glide path strategies are difficult because their risk profiles do not align.

2.3.2 Comparison with industry solutions

In practice, the glide path is typically divided into several distinct phases that correspond to different stages of an investor's journey toward retirement. Inspired by the FTSE Lifecycle Screened Select Index, we can divide a 40-year accumulation period into four 10-year phases.

1. Stabilising phase

During the first decade of accumulation, the portfolio maintains a high equity allocation of 90%. This enables investors to benefit from long-term growth while they are still far from retirement.

2. Early gradual de-risking

Over the next 10 years, the equity allocation is reduced by 1% per year, gradually shifting into less volatile assets as investors approach mid-career milestones.

3. Mid-term gradual de-risking

During the third decade, de-risking accelerates, reducing equity exposure by 2% annually. This reflects the growing importance of capital preservation as retirement approaches.

 $^{^{22}}$ The hit ratio measures the probability that the strategy outperforms a risk-free investment with an annualized return of R. For example, if $R = r_t = 2\%$, the hit ratio represents the probability that the strategy delivers a higher return than the risk-free bond.

Figure 23: Phases of a target date fund



Accumulation time (years until retirement)

Source: FTSE Lifecycle Screened Select Index.

4. Late rapid de-risking

In the final 10 years before retirement, the equity allocation declines linearly from its level at T-10 to 0% at the target retirement date. By that time, the portfolio has fully transitioned to low-risk, income-oriented assets.

This approach balances the need for long-term growth with prudent risk management. It begins with a high equity allocation and gradually shifts toward capital protection as the target date approaches. The corresponding risky asset exposure α_t is shown in Figure 24. Based on this, we calibrate the implied relative risk aversion using the formula:

$$\gamma_t = 1 - \frac{\mu_t - r_t}{\alpha_t \sigma_t^2} \tag{16}$$

We then estimate the functional form of γ_t , yielding the approximation²³:

$$\gamma_t \approx -1 - 1.01 \times 10^{-7} \times e^{0.5(t-20)}$$
 (17)

We refer to this as the Merton solution. Figure 24 compares the industry glide path to the Merton solution in terms of both risky asset allocation α_t and aversion risk γ_t . The two approaches align closely, except between years 30 and 50, where the industry method reduces risky exposure more aggressively than the Merton-derived solution.

Table 10: Winning Probability of Merton Solutions vs. Industry Solution

	SI	$R_t = 0.$	10	SI	$R_t = 0.$	20	$SR_t = 0.30$		
						$\gamma_t^{(3)}$			
						72.7			
						70.7			
6%	32.2	62.0	63.7	70.4	37.7	58.5	89.2	84.8	83.0
7%	25.1	68.3	69.8	65.8	38.2	51.1	87.4	82.6	81.7
8%	20.2	73.9	75.2	60.7	40.8	49.9	85.5	83.6	80.3

To evaluate the performance of each approach, we simulate a competition between the industry solution and the Merton solution by computing the probability that the Merton solution yields higher terminal wealth. The simulation uses the following assumptions: $r_t = 2\%$, $X_{t_0} = 1$, $t_0 = 20$, T = 60, and $c_t = 0.10$. We explore a range of expected returns μ_t , and compute the volatility σ_t based on a given Sharpe ratio SR_t. Table 10 shows the probability that the Merton strategy outperforms the industry strategy across different Sharpe ratios. Three versions of the Merton solution are considered, which are distinguished by their specification of γ_t . $\gamma_t^{(1)}$ corresponds to the implied relative risk aversion

²³We have $\gamma_0 = -1$, $\gamma_T = -50$, and k = 0.50.

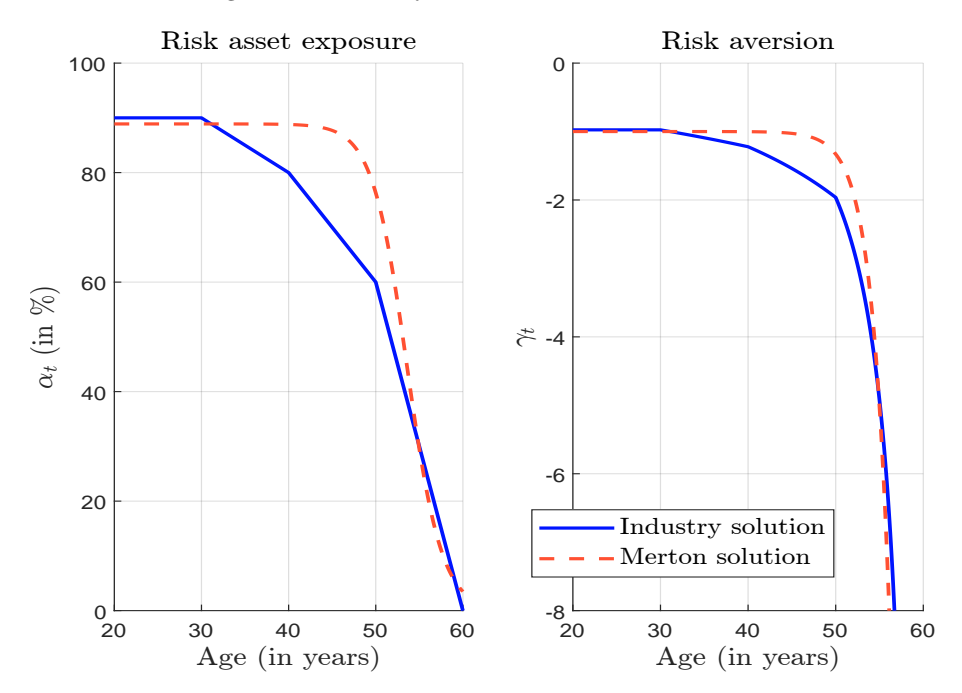


Figure 24: Industry solution vs. Merton solution

based directly on Equation (16), $\gamma_t^{(2)}$ is the functional form given by Equation (17), and $\gamma_t^{(3)}$ is a equal to -1. Several insights emerge from the results. First, the probability of the Merton solution outperforming the industry glide path increases with the Sharpe ratio because higher risk-adjusted returns enhance the effectiveness of dynamic allocation strategies. Among the three specifications, the constant risk aversion case $\gamma_t^{(3)}$ consistently performs well, particularly for moderate to high values of μ_t , suggesting that simple allocation rules can be effective in favorable market conditions. The implied aversion $\gamma_t^{(1)}$, although directly calibrated from the industry glide path, often underperforms the other two specifications — especially at higher Sharpe ratios. The functional form $\gamma_t^{(2)}$ generally delivers strong results, but it is somewhat unstable at intermediate Sharpe ratios (e.g., $\mathrm{SR}_t = 0.20$). These differences underscore the critical role of the contribution rate c_t in determining the optimal exposure α_t^{\star} . For example, when $c_t = 0$, the strategy based on $\gamma_t^{(1)}$ should, in theory, closely align with the industry solution, resulting in a performance probability approaching 50%. However, in practice, the Merton strategy using $\gamma_t^{(1)}$ tends to outperform because it results in higher effective risk exposure due to the wealth-contribution dynamics captured in the Merton formula:

$$\alpha_t^{\star} = \frac{(\mu_t - r_t)}{\left(1 - \gamma_t^{(1)}\right) \sigma_t^2} \left(1 + \frac{H_t}{X_t}\right) \ge \frac{(\mu_t - r_t)}{\left(1 - \gamma_t^{(1)}\right) \sigma_t^2}$$

Here, the term $\frac{H_t}{X_t}$ reflects the impact of future contributions relative to current wealth, amplifying the overall risk exposure compared to the industry allocation. Overall, the findings suggest that Merton-based strategies can outperform traditional glide paths significantly, provided the specification of risk aversion is well chosen. In many cases, a simple constant-aversion profile offers a robust and practical alternative to more complex, time-varying formulations.

2.3.3 Dynamic asset allocation

To illustrate asset allocation dynamics along a typical glide path, we examine a seven assetclass portfolio consisting of government bonds, investment-grade corporate bonds, public equities, private equities, private debt, real estate, and infrastructure. The first three represent traditional liquid assets commonly used in strategic asset allocation (bonds, credit, and stocks). The remaining four fall under the category of real (or private) assets, which are being considered more and more in long-term investment strategies. Table 11 and 12 show the expected returns, volatilities, and correlations for each asset class over a 30-year investment horizon. These values were simulated using the Amundi CASM model (Global calibration, USD, as of June 2025).

Table 11: Expected return (%), volatility (%) and Sharpe ratio of asset classes (Global, 30-year time horizon)

Asset class	μ_i	σ_i	SR_i	SR_i/σ_i
Govt Bonds	4.25	4.12	0.21	5.01
IG Corp Bonds	5.16	5.46	0.32	5.90
Public Equity	7.46	16.63	0.24	1.47
Private Equity	10.75	20.11	0.37	1.82
Private Debt	7.94	10.10	0.45	4.45
Real Estate	7.35	11.68	0.34	2.90
Infrastructure	8.10	14.86	0.32	2.13

Source: Simulated with the Amundi CASM model (Global model, USD, June 2025), Amundi (2021).

Asset classes can be grouped based on their return characteristics. Private equity has the highest expected return at 10.75%, followed by a group of real assets, including private debt, real estate, and infrastructure, as well as public equity, with expected returns between 7% and 8%. Government and IG corporate bonds exhibit lower expected returns. In terms of volatility, private equity is the most volatile asset class at 20.1%, followed by public equity at 16.6%. The annual return of the risk-free asset (cash) is assumed to be 3.40%. Using these figures, we calculate the Sharpe ratio, ranging from 0.21 for government bonds to 0.45 for private debt. As expected, real assets display higher Sharpe ratios due to the illiquidity premium they carry.

Table 12: Correlation matrix in % (Global, 30-year time horizon)

Govt Bonds	100.0	60.5	-15.4	-21.0	-33.8	-18.7	40.0
IG Corp Bonds	60.5	100.0	50.6 -	37.7	24.4	2.9	46.6
Public Equity	-15.4	50.6	100.0	79.8	59.6	37.5	29.2
Private Equity	-21.0	$\bar{37.7}$	79.8	$\bar{1}00.\bar{0}$	-66.6	-54.4	-26.4
Private Debt	-33.8	24.4	59.6^{+1}	66.6	100.0	45.7	10.1
Real Estate	-18.7	2.9	37.5	54.4	45.7	100.0	26.3
Infrastructure	40.0	46.6	29.2	26.4	10.1	26.3	100.0

Source: Simulated with the Amundi CASM model (Global model, USD, June 2025), Amundi (2021).

The correlation matrix reveals several well-known facts. For example, the negative correlation (-15.4%) between government bonds and public equities reflects their traditional role as diversified assets. IG corporate bonds and equities are strongly positively correlated (50.6%), indicating that credit and equity risks are partially intertwined. Private equity and private debt are highly correlated (66.6%), as are public equity and private equity (79.8%). Private debt is also highly correlated with public equities (59.6%) and investment-grade

(IG) credit (24.4%). Real estate and infrastructure show moderate correlations with other asset classes, contributing to the overall diversification potential. However, these correlations depend on geographic region, investment horizon, and macroeconomic environment, particularly prevailing monetary policy.

To determine the dynamic asset allocation along the glide path, we first compute the efficient frontier using the Markowitz optimization framework:

$$w^{\star}(\varphi) = \arg\min \frac{1}{2} w^{\top} \Sigma w - \varphi w^{\top} (\mu - r)$$

s.t.
$$\begin{cases} \mathbf{1}_{n}^{\top} w = 1 \\ w \geq \mathbf{0}_{n} \end{cases}$$

For each optimal portfolio, we calculate the expected return $\mu(w) = w^{\top}\mu$ and the volatility $\sigma(w) = \sqrt{w^{\top}\Sigma w}$. Results are shown in Figure 58 on page 116, which compares the investment universe both with and without the inclusion of real assets. We observe that incorporating real assets improves the Sharpe ratio of the mean-variance optimized portfolios. The detailed portfolio compositions are illustrated in Figures 59 and 60 on page 117. When the investor's risk tolerance φ is low, the portfolio predominantly consists of sovereign bonds. When φ is high, however, the allocation shifts toward public equities. For intermediate values of φ , the portfolio is a mix of corporate bonds and public equities. By using the relationship between risk tolerance φ and relative risk aversion $\gamma = 1 - \varphi^{-1}$, we map the optimized portfolios $w^*(\varphi)$ into the corresponding portfolios $w^*(\gamma)$, and obtain the resulting allocations in Figures 61 and 62 on page 118.

We use the function form of γ_t , which is calibrated to the industry solution²⁴, and assume that $c_t = 0$. Figure 25 illustrates the change in risk portfolio allocations when comparing strategies with and without real assets²⁵. In both cases, the allocation shifts from riskier to more conservative assets, consistent with lifecycle investment principles. However, including real assets in the investment universe results in greater portfolio diversification, particularly during the middle stages of life (ages 20–40). During this period, asset classes such as private equity, private debt, real estate, and infrastructure are utilized more heavily, replacing some exposure to traditional public equities. This expanded allocation can improve risk-adjusted returns by spreading exposure across less correlated assets. In contrast, the glide path without real assets relies more heavily on public equities and corporate bonds, resulting in a less diversified and potentially more volatile investment strategy. As retirement approaches, both strategies converge toward a conservative allocation dominated by government bonds. Figure 26 presents a mixed glide path, where the optimal portfolio at each point in time is a convex combination of the solutions with and without real assets:

$$w_{\text{mixed}}^{\star}\left(\gamma_{t}\right) = \left(1 - \omega\right) \cdot w_{\text{w/o}}^{\star}\left(\gamma_{t}\right) + \omega \cdot w_{\text{w/}}^{\star}\left(\gamma_{t}\right)$$

where $w_{\text{w/o}}^{\star}(\gamma_t)$ and $w_{\text{w/}}^{\star}(\gamma_t)$ denote the optimal portfolios without and with real assets, respectively, γ_t is the time-varying risk aversion, and $\omega \in [0,1]$ is the relative weight assigned to the real asset-enhanced solution. An important advantage of this mixed approach is that it provides a built-in mechanism to cap exposure to real assets. Specifically, the total allocation to the set of real assets satisfies $\sum_{i \in \mathcal{R}eal} \mathcal{A}_{ssets} w_{\text{mixed},i}^{\star}(\gamma_t) \leq \omega$. This constraint ensures that exposure to real assets remains controlled, offering flexibility in portfolio construction while preserving diversification benefits.

 $^{^{24}\}gamma_0$ is set to 1/3, γ_T is set to -50, and k is set to 0.05.

²⁵We show the dynamical evolution of the vector of risky asset exposures at time t, i.e., $\omega_t^{\star} = \alpha_t^{\star} w_t^{\star}$.

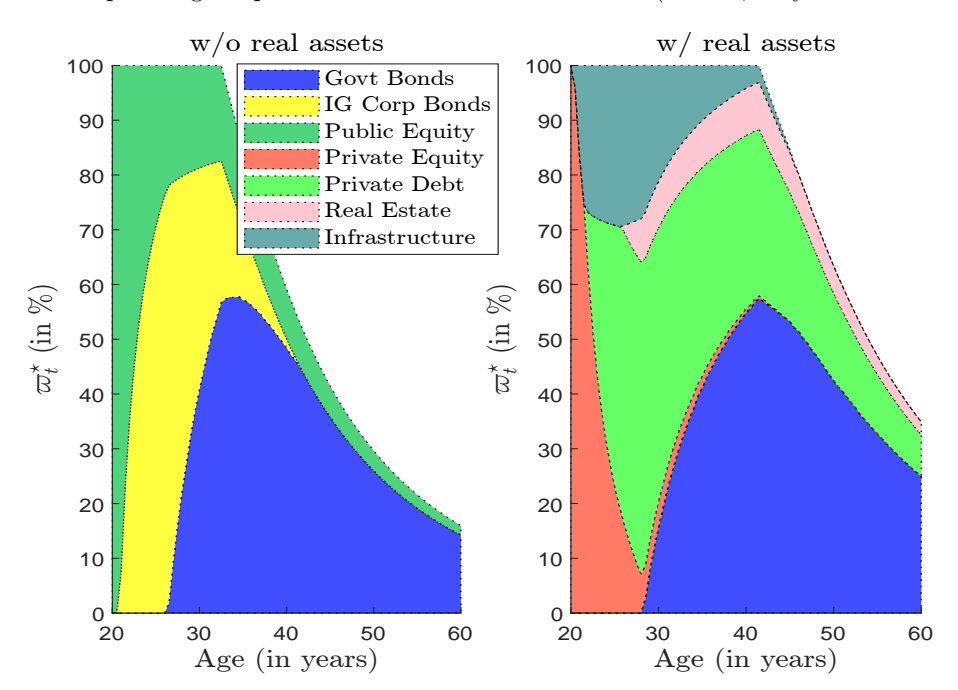
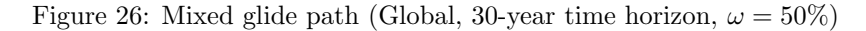
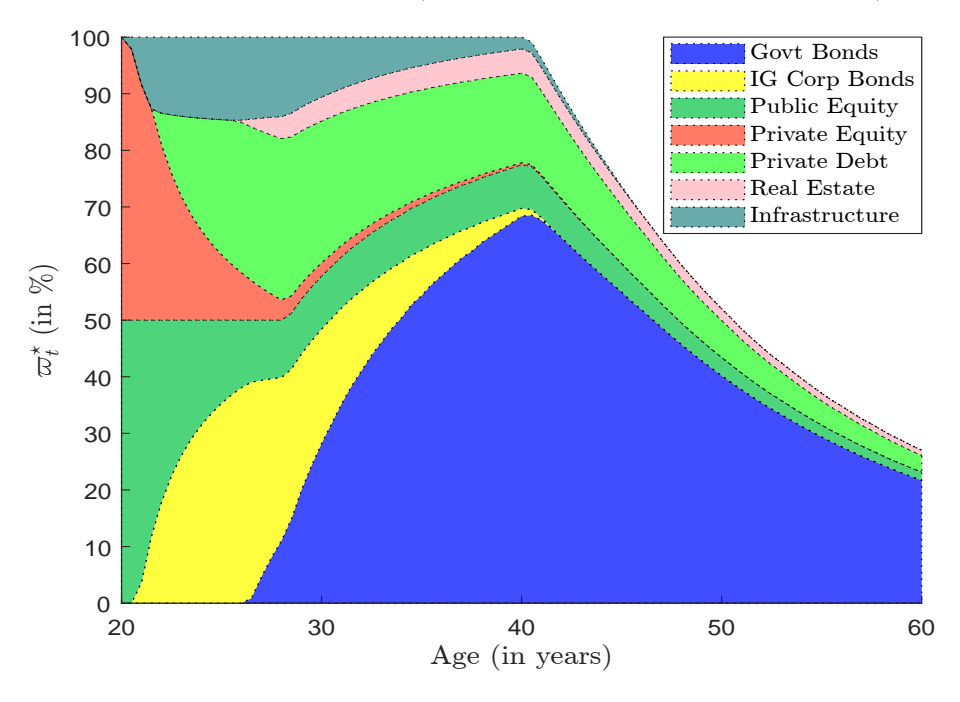
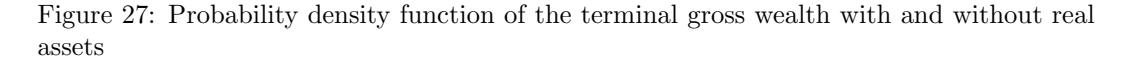
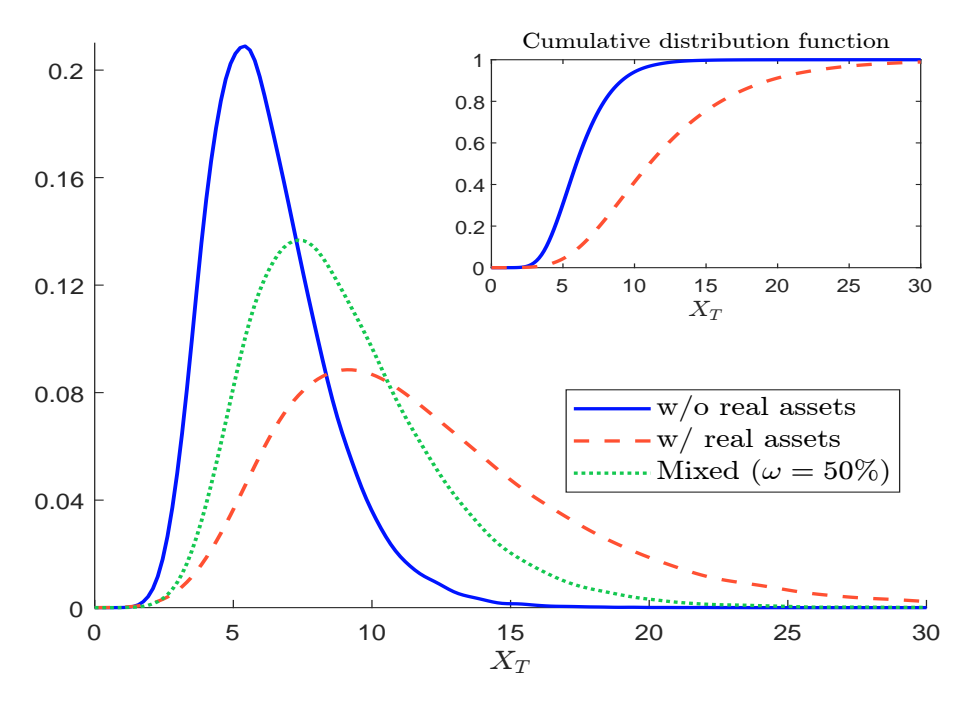


Figure 25: Optimal glide path with and without real assets (Global, 30-year time horizon)









As expected, the inclusion of real assets in the investment universe leads to superior outcomes in terms of terminal wealth. Figure 27 presents the probability density functions of terminal wealth X_T under both strategies (with and without real assets), highlighting a clear rightward shift when real assets are included²⁶. The corresponding cumulative distribution functions demonstrate second-order stochastic dominance of the real asset strategy, confirming that it not only increases expected terminal wealth but does so with lower downside risk across the distribution. Table 13 summarizes key performance statistics. Notably, the inclusion of real assets nearly doubles the expected terminal wealth compared to the strategy without them, delivering 164 bps of additional annualized performance. The mixed strategy yields an intermediate gain of 87 basis points per year. These results highlight the substantial benefits of improved diversification and the contribution of private markets in enhancing long-term retirement outcomes.

Table 13: Comparison of the terminal gross wealth with and without real assets

Ctnotomy	IF [V]	ΔR	 	Quantile $\mathbb{Q}\left(X_{T},p\right)$					Hit ratio	
Strategy	$\mathbb{E}[X_T]$ $(\text{in bps}) + 5\%$ 25%	50%	75%	90%	R=4%	R = 5%				
w/o real assets	6.3		3.4	4.7	5.9	7.4	9.1	70.3%	25.7%	
w/ real assets	12.1	164	5.4	8.2	11.0	14.8	19.3	96.7%	81.7%	
Mixed ($\omega = 50\%$)	8.9	87	4.6	6.5	8.3	10.7	13.3	92.5%	63.0%	

Remark 7. The previous application highlights that the investor holds a large exposure to the risk-free asset, which is not very realistic. Those results correspond to those of a prudent or conservative investor. By contrast, if we adopt a more aggressive risk-tolerance function, the outcomes differ significantly for moderate or aggressive investors. This naturally raises the question of what constitutes the risk-free asset in this framework. It can be interpreted as a combination of cash and a zero-coupon bond maturing at the retirement date. For young

²⁶We have also included the mixed strategy with $\omega = 50\%$.

investors, the risk-free asset primarily consists of the zero-coupon bond that matches the retirement horizon. As retirement approaches, the allocation gradually shifts toward cash, with the weight on cash increasing most strongly in the final years before retirement. Another way to increase exposure to risky assets is to exclude bonds from the investment universe altogether. Bruder et al. (2012) take this approach in their model, which is a more general version of ours. They adopt the zero-coupon bond maturing at T as the numéraire and derive formulas similar to ours. The main distinction lies in how they treat risk premia. In our framework, the risk premium is defined relative to the risk-free asset and is approximated using the risk-free rate as the numéraire. In contrast, the risk premium in the model of Bruder et al. (2012) is defined directly with respect to the bond numéraire. Their model is therefore theoretically more precise, but also more difficult to implement. Nevertheless, when comparing results, both approaches lead to very similar outcomes.

2.3.4 Introducing liquidity risk management

Liquidity risk encompasses several aspects related to the efficient trading of assets. Transaction costs are incurred each time the portfolio is rebalanced. These costs vary by asset class, time period, and market condition. Generally, transaction costs are relatively low for traditional asset classes. Sovereign bonds and public equities typically incur the lowest costs, followed by corporate bonds. In contrast, transaction costs are substantially higher for real assets. However, liquidity risk is not limited to bid-ask spreads. It also includes other factors, most notably market impact. Market impact refers to the price effect caused by executing large orders or trading in markets with limited depth. Market impact can result from the size of a trade or from a significant imbalance between supply and demand, especially during periods of market stress when liquidity dries up. Real assets are particularly vulnerable in such conditions because they are traded less frequently and often lack active secondary markets. These characteristics can amplify liquidity risk precisely when investors need flexibility the most. Thus, liquidity risk reflects the cost of trading and the potential difficulty of executing trades without significantly affecting market prices, especially in adverse conditions. Additionally, management fees can differ substantially between liquid and illiquid assets. For example, public equities accessed through exchange-traded funds or passive funds can carry management fees of less than 50 basis points (bps). In contrast, private equity typically involves much higher fees, often exceeding 150 bps, due to the complexity and illiquidity of the underlying investments. As shown in Figure 27 and Table 13, our simulations reflect terminal gross wealth, not terminal net wealth. This distinction is important, as the difference in management fees and transaction costs across asset classes can significantly impact net outcomes.

To assess the impact of liquidity costs, we calculate the expected turnover of the glide path strategy²⁷:

$$oldsymbol{ au} = \mathbb{E}\left[\sum_{t_h = t_0}^T \left\|arpi_{t_h}^\star - arpi_{t_{h-1}}^\star
ight\|_1
ight]$$

where t_h is a set of portfolio rebalancing dates, and $\varpi_{t_h}^{\star} = \alpha_{t_h}^{\star} w_{t_h}^{\star}$ is the vector of optimal risky asset exposures at rebalancing date t_h . Figure 28 shows the turnover profile²⁸ for the

²⁷This formula for turnover ignores portfolio weight drift that arises passively from asset price changes between rebalancing dates. In other words, it only captures the explicit reallocation decisions made at each rebalancing date and not the natural evolution of asset weights due to market movements. Consequently, this turnover reflects only active trading and not the total change in portfolio composition over time.

²⁸The model parameters remain unchanged. However, we set the contribution term $c_t = 0$ to isolate the impact of rebalancing activity. A non-zero contribution would introduce periodic inflows, which artificially inflate the turnover by requiring additional trades to absorb the new capital. By setting $c_t = 0$, we ensure

mixed glide path strategy as a function of $\omega \in [0,1]$. Over a 40-year horizon, the strategy that is fully invested in liquid assets yields a total turnover of 360%, which corresponds to an annual turnover of 9%. When $\omega = 1$, the turnover increases slightly to 420%, or 10.5% per year. These relatively modest turnover levels are typical of retirement strategies, where allocations change gradually and investment horizons are long term. However, turnover alone does not capture liquidity risk because it treats all assets equally regardless of their individual trading characteristics.

Table 14: Numerical values of unit trading costs

Asset	Sovereign	Corporate	Public	Private	Private	Real	Infra-
class	bonds	bonds	equity	equity	debt	estate	structure
C_i (in bps)	15	30	30	200	150	200	200

To account for this, we compute the expected trading cost:

$$\mathcal{C} = \mathbb{E}\left[\sum_{t_h=t_0}^T \sum_{i=1}^n \left|arpi_{i,t_h}^{\star} - arpi_{i,t_{h-1}}^{\star}
ight| \cdot \mathcal{C}_i
ight]$$

where n is the number of assets in the portfolio and \mathcal{C}_i denotes the unit trading cost of asset i. This formulation allows us to capture asset-specific liquidity effects, providing a more accurate measure of the true cost of rebalancing across heterogeneous assets. Using the unit costs shown in Table 14, the estimated trading cost ranges between 100 and 600 basis points, depending on the value of ω . This implies that allocating more to illiquid real assets can increase trading costs by up to six times compared to strategies invested solely in liquid assets.

There are several approaches to incorporate liquidity risk into retirement strategies. One simple and effective method is to introduce a time-varying liquidity weight ω_t , which blends two portfolio policies:

$$w_t^{\star}(\gamma_t) = (1 - \omega_t) \cdot w_{\text{w/o}}^{\star}(\gamma_t) + \omega_t \cdot w_{\text{w/}}^{\star}(\gamma_t)$$

where $w_{\text{w/o}}^{\star}(\gamma_t)$ is the optimal allocation with liquid assets, $w_{\text{w/}}^{\star}(\gamma_t)$ is the optimal allocation accounting for illiquid assets and γ_t denotes the risk aversion at time t. The function ω_t governs the transition between the regimes:

$$\omega_t = \begin{cases} \omega^+ & \text{if } t \le t_1^* \\ \text{is decreasing} & \text{if } t \in [t_1^*, t_2^*] \\ 0 & \text{if } t > t_2^* \end{cases}$$

This structure reflects a progressive shift toward liquidity as the investor approaches retirement. Before time t_1^* , the long investment horizon justifies holding illiquid assets. After t_2^* , typically five to ten years before retirement, the investor is assumed to fully transition into liquid assets to ensure flexibility and reduce liquidity-related risks. Importantly, this does not imply a complete shift out of risky assets. For instance, an investor may still hold public equities, but would avoid illiquid instruments such as private equity, private debt, or real assets, which could be difficult to sell quickly or at a low cost. This gradual transition from illiquid to liquid holdings is illustrated in Figure 29, where the liquidity weight ω_t decreases linearly between $t_1^* = 30$ years and $t_2^* = 50$ years.

that the turnover measure reflects pure reallocation effects rather than changes driven by external cash flows.

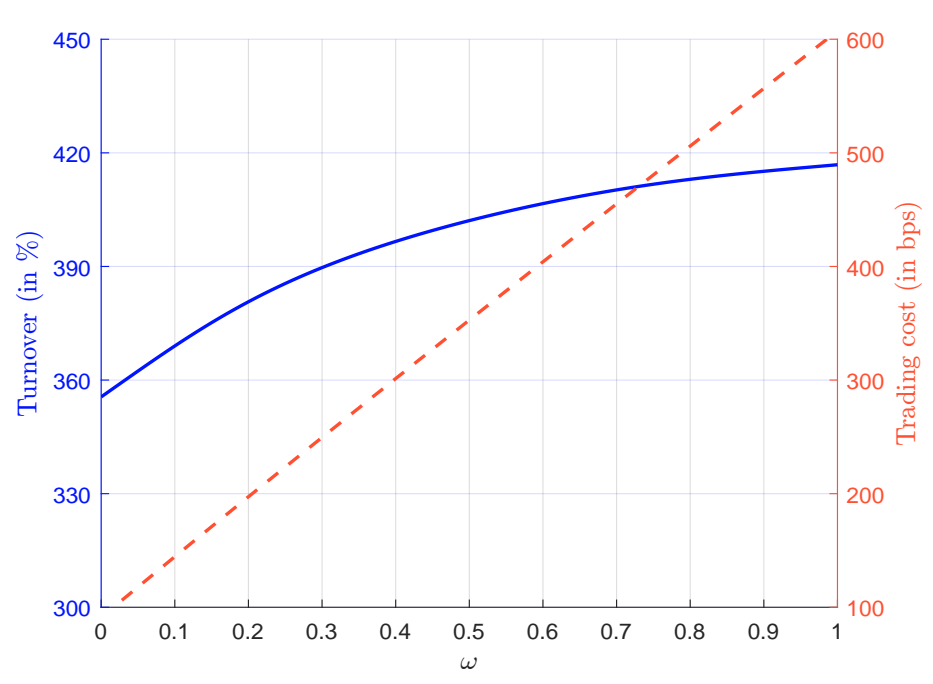


Figure 28: Turnover and liquidity cost of glide path strategy

Figure 29: Mixed glide path with liquidity constraints (Global, 30-year time horizon, $\omega^+ = 100\%$)

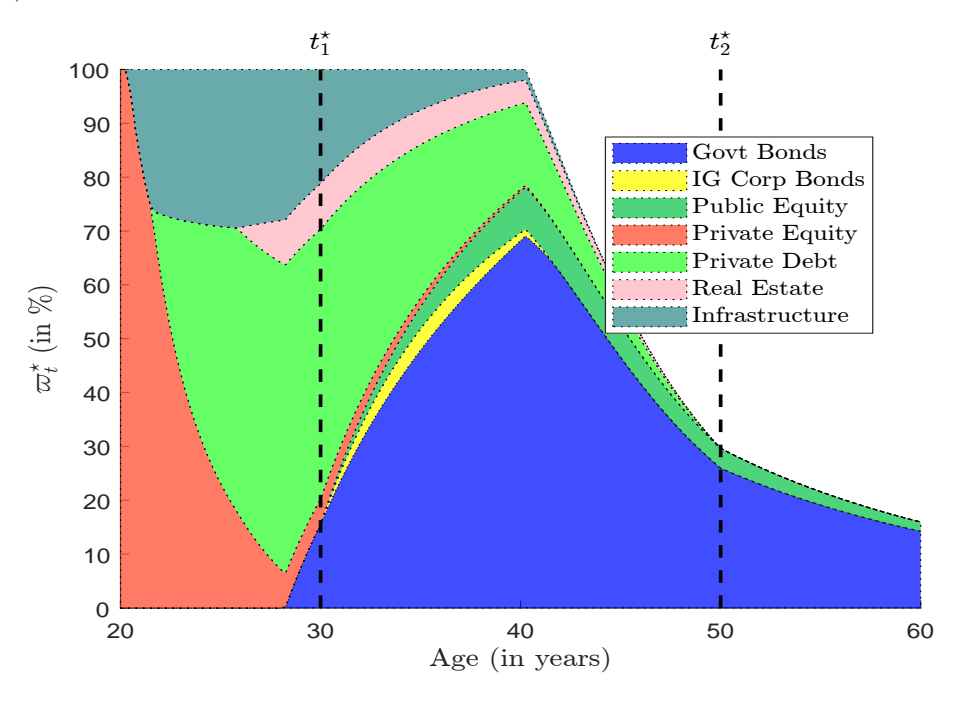


Table 15: Comparison of the terminal gross wealth with and without liquidity risk management

Churchama	$\mathbb{E}[X_T]$ ΔR		l	Quan	tile Q ($X_T, p)$		Hit ratio		
Strategy	$\mathbb{E}\left[\Lambda T\right]$	(in bps)	5%	25%	50%	75%	90%	R=4%	R = 5%	
w/o real assets	6.3		3.4	4.7	5.9	7.4	9.1	70.3%	25.7%	
w/ real assets	12.1	164	5.4	8.2	11.0	14.8	19.3	96.7%	81.7%	
Mixed ($\omega = 50\%$)	8.9	87	4.6	6.5	8.3	10.7	13.3	92.5%	63.0%	
$\bar{L}\bar{R}\bar{M} (\bar{\omega}^+ = \bar{1}0\bar{0}\bar{\%})$	-10.0		4.6	$-\bar{6}.\bar{9}$	$-\bar{9}.\bar{2}$	$1\overline{2}.\overline{2}$	15.8	92.6%	$\bar{69.1}\%$	
LRM $(\omega^+ = 50\%)$	8.0	61	4.2	5.9	7.5	9.6	11.9	87.6%	51.4%	
LRM $(\omega^+ = 20\%)$	6.9	25	3.8	5.2	6.5	8.2	10.1	79.5%	36.2%	

Remark 8. Table 15 compares terminal gross wealth with and without liquidity risk management. The results show that private assets continue to deliver superior performance relative to portfolios composed solely of public assets. For example, when $\omega^+ = 20\%$, the inclusion of private assets generates an additional annualized performance of 25 bps.

3 Extension to multi-asset classes

In this section, we extend the previous framework by incorporating multiple risky assets. First, we compare the single-asset and multi-asset solutions in the absence of allocation constraints. Then, we analyze the impact of imposing such constraints on the multi-asset setting.

3.1 Theoretical Model

We consider a dynamic asset allocation problem where an investor allocates wealth among n risky assets $S_t = (S_{1,t}, \ldots, S_{n,t})$ and a risk-free zero-coupon bond B_t , while making regular contributions according to a target date strategy. Each risky asset $S_{i,t}$ follows the following stochastic differential equation:

$$dS_{i,t} = \mu_i S_{i,t} dt + \sigma_i S_{i,t} dW_{i,t}$$

where the Brownian motions $\{W_{i,t}\}_{i=1}^n$ are correlated such that $\mathbb{E}\left[\mathrm{d}W_{i,t}\,\mathrm{d}W_{j,t}\right] = \rho_{i,j}\,\mathrm{d}t$ and $\rho_{i,i} = 1$. We denote by $\alpha_t = (\alpha_{1,t},\ldots,\alpha_{n,t})$ the vector of portfolio weights allocated to the n risky assets at time t. In particular, each weight $\alpha_{i,t}$ represents the fraction of total wealth invested in risky asset i, while the remainder $\left(1 - \mathbf{1}_n^\top \alpha_t\right)$ is allocated to the risk-free asset. The resulting wealth process X_t satisfies the stochastic differential equation:

$$dX_t = \left(\left(r_t + \alpha_t^\top \left(\mu_t - r_t \mathbf{1}_n \right) \right) X_t + \mathbf{c}_t \right) dt + \alpha_t^\top \sigma_t X_t dW_t$$

where $W_t = (W_{1,t}, \ldots, W_{n,t})$, $\mu_t = (\mu_{1,t}, \ldots, \mu_{n,t})$, $\sigma_t = \text{diag}(\sigma_{1,t}, \ldots, \sigma_{n,t})$, and r_t is the constant risk-free rate. The investor aims to maximize the expected utility of terminal wealth:

$$\alpha_t^{\star} = \arg \max \mathbb{E}_t \left[\mathcal{U} \left(X_T \right) \right]$$

We define the covariance matrix by Σ_t , so that $(\Sigma_t)_{i,j} = \rho_{i,j}\sigma_{i,t}\sigma_{j,t}$. The associated HJB equation is:

$$\frac{\partial \mathcal{J}(t,x)}{\partial t} + \max_{\alpha_t} \mathcal{H}(t,x,\alpha_t) = 0 \quad \text{s.t.} \quad \mathcal{J}(T,x) = \mathcal{U}(x)$$
(18)

where:

$$\mathcal{H}\left(t, x, \alpha\right) = \left(\left(r_{t} + \alpha_{t}^{\top} \left(\mu_{t} - r_{t} \mathbf{1}_{n}\right)\right) x + \boldsymbol{c}_{t}\right) \frac{\partial \mathcal{J}\left(t, x\right)}{\partial x} + \frac{1}{2} \left(\alpha_{t}^{\top} \Sigma_{t} \alpha_{t}\right) x^{2} \frac{\partial^{2} \mathcal{J}\left(t, x\right)}{\partial x^{2}}$$

The first-order condition of the maximization of the Hamiltonian function is:

$$\frac{\partial \mathcal{H}(t, x, \alpha)}{\partial \alpha} = \mathbf{0}_{n} \quad \Leftrightarrow \quad (\mu_{t} - r_{t} \mathbf{1}_{n}) x \partial_{x} \mathcal{J}(t, x) + \frac{1}{2} (2\Sigma_{t} \alpha_{t}) x^{2} \partial_{x}^{2} \mathcal{J}(t, x) = \mathbf{0}_{n}$$

$$\Leftrightarrow \quad \alpha_{t}^{\star} = -\frac{\partial_{x} \mathcal{J}(t, x)}{x \partial_{x}^{2} \mathcal{J}(t, x)} \Sigma_{t}^{-1} (\mu_{t} - r_{t} \mathbf{1}_{n}) \tag{19}$$

In the case of CRRA utility, the optimal weights take the form:

$$\alpha_t^{\star} = \bar{\alpha}_t \left(1 + \frac{H_t}{X_t} \right)$$

where:

$$\bar{\alpha}_t = \frac{\sum_t^{-1} \left(\mu_t - r_t \mathbf{1}_n \right)}{1 - \gamma}$$

3.2 The case without allocation constraints

We now compare the single-asset and multi-asset solutions. In the single-asset case, the optimal total exposure is:

$$\varpi_t^{\star} = \alpha_t^{\star} w_t^{\star} = \frac{\left(\mu\left(w_t^{\star}\right) - r\right)}{\left(1 - \gamma_t\right) \sigma^2\left(w_t^{\star}\right)} \left(1 + \frac{H_t}{X_t}\right) w_t^{\star}$$

where w_t^{\star} is the mean-variance optimized portfolio:

$$w_t^{\star} := w^{\star} (\varphi_t) = \arg\min \frac{1}{2} w^{\top} \Sigma_t w - \varphi_t w^{\top} (\mu_t - r \mathbf{1}_n)$$

where $\varphi_t = (1 - \gamma_t)^{-1}$. The closed-form solution is:

$$w^{\star} (\gamma_t) = \frac{1}{1 - \gamma_t} \Sigma^{-1} (\mu - r \mathbf{1}_n)$$

Assuming normalized portfolio weights, we have:

$$w^{\star} (\gamma_t) = \frac{\theta_t}{1 - \gamma_t} \Sigma^{-1} (\mu - r \mathbf{1}_n)$$

where $\theta_t = (1 - \gamma_t)^{-1} \mathbf{1}_n^{\top} \Sigma^{-1} (\mu - r \mathbf{1}_n)$. We deduce that:

$$\mu(w_t^*) - r = w^* (\gamma_t)^\top \mu - r$$

$$= w^* (\gamma_t)^\top (\mu - r \mathbf{1}_n)$$

$$= \frac{\theta_t}{1 - \gamma_t} (\mu - r \mathbf{1}_n)^\top \Sigma^{-1} (\mu - r \mathbf{1}_n)$$

and:

$$\sigma^{2}(w_{t}^{\star}) = w^{\star}(\gamma_{t})^{\top} \Sigma w^{\star}(\gamma_{t})$$

$$= \frac{\theta_{t}}{1 - \gamma_{t}} (\mu - r\mathbf{1}_{n})^{\top} \Sigma^{-1} \Sigma \frac{\theta_{t}}{1 - \gamma_{t}} \Sigma^{-1} (\mu - r\mathbf{1}_{n})$$

$$= \frac{\theta_{t}^{2}}{(1 - \gamma_{t})^{2}} (\mu - r\mathbf{1}_{n})^{\top} \Sigma^{-1} (\mu - r\mathbf{1}_{n})$$

It follows that:

$$\frac{\mu\left(w_{t}^{\star}\right) - r}{\sigma^{2}\left(w_{t}^{\star}\right)} = \frac{1 - \gamma_{t}}{\theta_{t}}$$

and:

$$\varpi_t^* := \alpha_t^* w_t^* = \frac{\left(\mu\left(w_t^*\right) - r\right)}{\left(1 - \gamma_t\right)\sigma^2\left(w_t^*\right)} \left(1 + \frac{H_t}{X_t}\right) w_t^* \\
= \frac{1}{\theta_t} \left(1 + \frac{H_t}{X_t}\right) w_t^* \\
= \frac{1}{1 - \gamma_t} \Sigma^{-1} \left(\mu - r\mathbf{1}_n\right) \left(1 + \frac{H_t}{X_t}\right) \tag{20}$$

Recall that the multi-asset solution is:

$$\alpha_t^{\star} = \bar{\alpha}_t \left(1 + \frac{H_t}{X_t} \right) = \frac{1}{1 - \gamma_t} \Sigma_t^{-1} \left(\mu - r \mathbf{1}_n \right) \left(1 + \frac{H_t}{X_t} \right) \tag{21}$$

By comparing Equations (20) and (21), we can see that both approaches lead to the same optimal exposure vector. However, the two differ in methodology:

- In the single-asset approach, the total exposure α_t^* to risky assets is first determined. Then the Markowitz model is applied to find the optimal fully-invested portfolio w_t^* . Finally, the vector of exposures ϖ_t^* is obtained by scaling the portfolio weights w_t^* by the total exposure α_t^* .
- In the multi-asset approach, the vector of exposures α_t^* is directly computed and coincides with the vector ϖ_t^* of the single-asset approach.

In the absence of allocation constraints, this leads to a dynamic two-fund separation result, where the portfolio composition is determined independently of the total exposure or leverage ratio.

3.3 The case with allocation constraints

In practice, we generally include weight constraints, meaning that the multi-asset approach can not be solved using the single-asset approach. For example, we cannot invest more than 100% of our wealth in the risky assets, implying the constraint $\mathbf{1}_n^{\top}\alpha_t \leq 1$. A common additional restriction is the long-only constraint: $\alpha_t \geq \mathbf{0}_n$. Other constraints may also apply, such as limiting the allocation to real assets to a maximum of 50%, or capping private equity exposure at 20%. Let $\alpha_t \in \Omega$ denote the admissible set of portfolio weights satisfying all such constraints. Under these constraints, there is generally no closed-form solution for the optimal allocation α_t^* . However, the problem can still be solved numerically using Howard's policy iteration algorithm applied to Equation (18):

- Initialization Begin with an initial guess for the control policy α_t , for example by using the unconstrained solution. Then repeat until convergence:
- Policy evaluation With α_t held fixed, discretize the HJB equation using a finite-difference scheme and compute an approximation of $\mathcal{J}(t,x)$ over the chosen (t,x) grid. From these values, estimate the partial derivatives $\partial_x \mathcal{J}(t,x)$ and $\partial_x^2 \mathcal{J}(t,x)$ numerically.

• Policy improvement At each grid point (t, x), update the control α_t by solving the constrained maximization program

$$\alpha_t^{\star} = \arg \max \mathcal{H}(t, x, \alpha_t)$$

s.t. $\alpha_t \in \Omega$

where the Hamiltonian is given by:

$$\mathcal{H}\left(t, x, \alpha\right) = \left(\left(r_{t} + \alpha_{t}^{\top}\left(\mu_{t} - r_{t}\mathbf{1}_{n}\right)\right)x + c_{t}\right)\frac{\partial \mathcal{J}\left(t, x\right)}{\partial x} + \frac{1}{2}\left(\alpha_{t}^{\top}\Sigma_{t}\alpha_{t}\right)x^{2}\frac{\partial^{2} \mathcal{J}\left(t, x\right)}{\partial x^{2}}$$

The previous algorithm can be simplified because the maximization step can be reformulated as a quadratic programming problem:

$$\alpha_t^{\star} = \arg\min \frac{1}{2} \alpha_t^{\top} \tilde{\Sigma}_t \alpha_t - \alpha_t^{\top} \tilde{\mu}_t$$
s.t. $\alpha_t \in \Omega$

where:

$$\begin{cases} \tilde{\mu}_t = x \left(\mu_t - r_t \mathbf{1}_n \right) \partial_x \mathcal{J} \left(t, x \right) \\ \tilde{\Sigma}_t = -x^2 \Sigma_t \partial_x^2 \mathcal{J} \left(t, x \right) \end{cases}$$

Consequently, when applying Howard's policy-iteration algorithm, we must repeatedly solve a QP program at each grid node (t,x) until convergence, which makes the computation time-consuming. Because of this, the single-stage optimization approach is not scalable in practical applications.

Remark 9. We have:

$$\mathcal{H}\left(t, x, \alpha\right) = \left(r_{t} x + \boldsymbol{c}_{t}\right) \frac{\partial \mathcal{J}\left(t, x\right)}{\partial x} - x^{2} \frac{\partial^{2} \mathcal{J}\left(t, x\right)}{\partial x^{2}} \left(-\frac{1}{2} \alpha_{t}^{\top} \Sigma_{t} \alpha_{t} - \frac{\partial_{x} \mathcal{J}\left(t, x\right)}{x \partial_{x}^{2} \mathcal{J}\left(t, x\right)} \alpha_{t}^{\top} \left(\mu_{t} - r_{t} \boldsymbol{1}_{n}\right)\right)$$

We deduce that:

$$\alpha_t^{\star} = \arg\min \frac{1}{2} \alpha_t^{\top} \Sigma_t \alpha_t - \tilde{\varphi}_t \alpha_t^{\top} (\mu_t - r_t)$$
s.t. $\alpha_t \in \Omega$

where:

$$\tilde{\varphi}_{t} = -\frac{\partial_{x} \mathcal{J}\left(t, x\right)}{x \partial_{x}^{2} \mathcal{J}\left(t, x\right)}$$

It might be tempting to conjecture that $\tilde{\varphi}_t = \frac{1}{1 - \gamma_t}$, but this is not generally correct. The constraint $\alpha_t \in \Omega$ modifies the value function $\mathcal{J}(t,x)$, which implies that:

$$-\frac{x\partial_{x}^{2}\mathcal{J}\left(t,x\right)}{\partial_{x}\mathcal{J}\left(t,x\right)}\neq-\frac{x\partial_{x}^{2}\mathcal{U}\left(x\right)}{\partial_{x}\mathcal{U}\left(x\right)}\Rightarrow-\frac{x\partial_{x}^{2}\mathcal{J}\left(t,x\right)}{\partial_{x}\mathcal{J}\left(t,x\right)}\neq1-\gamma_{t}$$

However, there are specific cases where the approximation $\tilde{\varphi}_t \approx \frac{1}{1 - \gamma_t}$ remains acceptable.

3.4 Empirical results

We consider the numerical example described on page 38, under the following set of constraints:

$$\Omega = \left\{ \alpha \in \mathbb{R}^n : \alpha \ge 0, \mathbf{1}_n^\top \alpha \le 1 \right\}$$

This formulation imposes both a long-only constraint and a no-leverage constraint. Since Ω is a standard simplex, the feasible region is convex, which simplifies the maximization step in the HJB equation. In this setting, the optimal portfolio weights can be computed using the projected gradient descent (PGD) method. We start with the unconstrained solution $\alpha_t^{(0)} = (1 - \gamma_t)^{-1} \sum_{t=1}^{t-1} (\mu_t - r_t \mathbf{1}_n)$ and we repeat the following steps until convergence:

1. At iteration k, we apply the gradient step:

$$\ddot{\alpha} = \alpha_t^{(k)} - \eta \nabla f\left(\alpha_t^{(k)}\right)$$

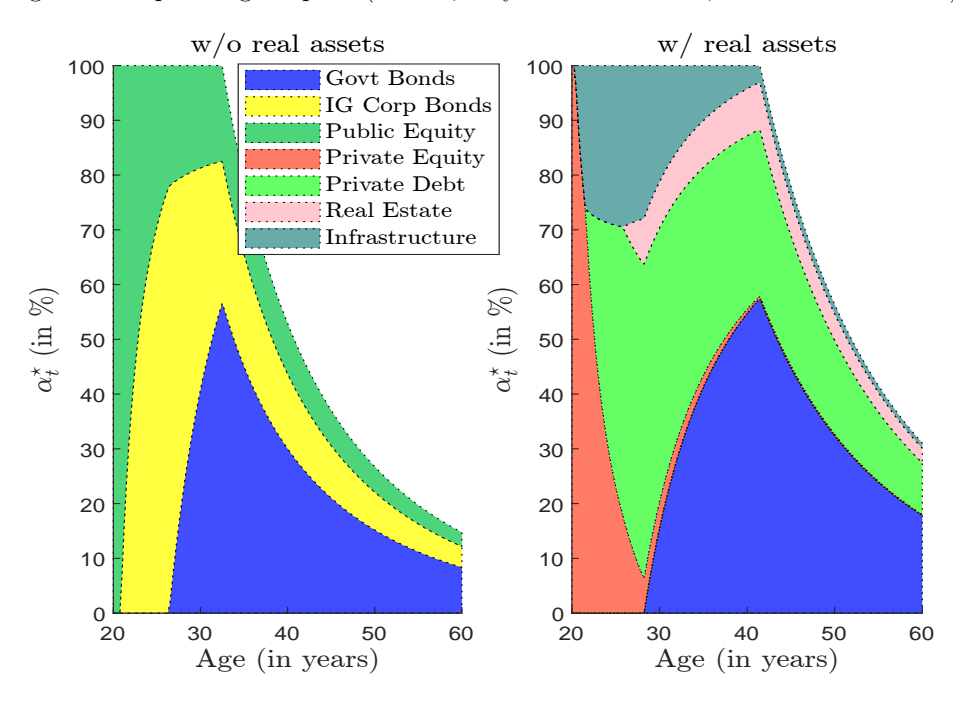
where $\eta > 0$ is the step size and $\nabla f(\alpha) = \alpha^{\top} \Sigma_t - \frac{1}{1 - \gamma_t} (\mu_t - r_t \mathbf{1}_n)$ is the gradient of the objective function.

2. We project onto the simplex:

$$\alpha_t^{(k+1)} = \Pi_{\Omega} \left(\breve{\alpha} \right)$$

where $\Pi_{\Omega}(x) = \arg\min_{y \in \Omega} \|y - x\|_2^2$ is the projection onto the simplex Ω . This projection can be efficiently computed using the method described in Appendix A.13 on page 101.





Using the same parameters as in Figure 25 (identical risk aversion γ_t and no contribution $c_t = 0$), we obtain the solutions²⁹ shown in Figure 30. These results reproduce most of the stylized facts observed in the two-stage (single-asset) approach. For instance:

- The allocation shifts from riskier to more conservative assets as the retirement date approaches;
- Introducing private assets reduces the share invested in public assets, especially public equity;
- The overall shape of the allocations is very similar between Figures 25 and 30.

However, the allocations are not identical. Although the two-stage (single-asset) and one-stage (multi-asset) formulations share the same objective function, they differ in their constraint sets:

• Two-stage (single-asset) approach:

$$\begin{cases} w_t^{\star} = \arg\min \frac{1}{2} w_t^{\top} \Sigma_t w_t - \frac{1}{1 - \gamma_t} w_t^{\top} (\mu_t - r_t) & \text{s.t.} \quad \Omega = \left\{ w_t : w_t \ge 0, \mathbf{1}_n^{\top} w_t = 1 \right\} \\ \alpha_t^{\star} = \min \left(\frac{1}{1 - \gamma_t} \left(\frac{\mu_t^{\top} w_t^{\star} - r_t}{w_t^{\star \top} \Sigma_t w_t^{\star}} \right), 1 \right) \\ \varpi_t^{\star} = \alpha_t^{\star} w_t^{\star} \end{cases}$$

• One-stage (multi-asset) approach:

$$\alpha_t^{\star} = \arg\min \frac{1}{2} \alpha_t^{\top} \Sigma_t \alpha_t - \frac{1}{1 - \gamma_t} \alpha_t^{\top} (\mu_t - r_t) \quad \text{s.t.} \quad \Omega = \left\{ \alpha_t : \alpha_t \ge 0, \mathbf{1}_n^{\top} \alpha_t \le 1 \right\}$$

The key difference lies in how leverage is handled. In the two-stage approach, leverage is adjusted in the second step, outside of the quadratic program. In contrast, the one-stage approach incorporates leverage directly into the QP constraints. This structural distinction explains the allocation differences observed between Figures 25 and 30. The two-stage approach generates smoother dynamic allocations than the one-stage method. However, the one-stage approach produces more diversified portfolios. This diversification advantage is particularly evident in the treatment of investment-grade corporate bonds. While the two-stage approach eliminates this allocation after 40 years, the one-stage approach maintains exposure to IG corporate bonds through retirement. Despite these differences in allocation, both approaches yield comparable turnover metrics.

3.5 Insights into the multi-asset optimal solution

In this section, we analyze the drivers of the dynamic optimal allocation by considering the following optimization problem:

$$w^{\star} = \arg\min \frac{1}{2} w^{\top} \Sigma w - \frac{1}{1 - \gamma} w^{\top} (\mu - r \mathbf{1}_n)$$
s.t.
$$\begin{cases} w \ge \mathbf{0}_n \\ \mathbf{1}_n^{\top} w \le 1 \text{ (or } \mathbf{1}_n^{\top} w = 1) \end{cases}$$

The inequality constraint $\mathbf{1}_n^\top w \leq 1$ corresponds to the one-stage approach, while the equality constraint $\mathbf{1}_n^\top w = 1$ relates to the two-stage approach.

²⁹We exploit the fact that the value function $\mathcal{J}(t,x)$ is separable (see Appendix A.14 on page 102).

3.5.1 Mathematical properties of the optimal weights

The associated Lagrange function is:

$$\mathcal{L}(w; \lambda_0, \lambda) = \frac{1}{2} w^{\top} \Sigma w - \frac{1}{1 - \gamma} w^{\top} (\mu - r \mathbf{1}_n) + \lambda_0 (\mathbf{1}_n^{\top} w - 1) - \lambda^{\top} w$$

where $\lambda_0 \geq 0$ and $\lambda \geq \mathbf{0}_n$ (or $\lambda \in \mathbb{R}$ if $\mathbf{1}_n^\top w = 1$). The first-order conditions are:

$$\sum w - \frac{1}{1 - \gamma} (\mu - r \mathbf{1}_n) + \lambda_0 \mathbf{1}_n - \lambda = \mathbf{0}_n$$

The optimal solution is:

$$w^* = \Sigma^{-1} \left(\frac{\mu - r \mathbf{1}_n}{1 - \gamma} + \lambda - \lambda_0 \mathbf{1}_n \right)$$

The Kuhn-Tucker complementary slackness conditions are $\lambda_0 \left(1 - \mathbf{1}_n^\top w^*\right) = 0$ if $\mathbf{1}_n^\top w \leq 1$, and $\lambda_i w_i^* = 0$ for all $i = 1 \dots, n$.

To obtain analytical solutions, we consider the two-asset case n=2. We have $\mu=(\mu_1,\mu_2)$ and:

$$\Sigma = \begin{pmatrix} \sigma_1^2 & \rho \sigma_1 \sigma_2 \\ \rho \sigma_1 \sigma_2 & \sigma_2^2 \end{pmatrix}$$

We deduce that:

$$\Sigma^{-1} = \frac{1}{(1 - \rho^2) \, \sigma_1^2 \sigma_2^2} \left(\begin{array}{cc} \sigma_2^2 & -\rho \sigma_1 \sigma_2 \\ -\rho \sigma_1 \sigma_2 & \sigma_1^2 \end{array} \right)$$

and:

$$\left\{ \begin{array}{l} w_1^\star \propto \sigma_2^2 \left(\frac{\mu_1 - r}{1 - \gamma} + \lambda_1 - \lambda_0 \right) - \rho \sigma_1 \sigma_2 \left(\frac{\mu_2 - r}{1 - \gamma} + \lambda_2 - \lambda_0 \right) \\ w_2^\star \propto \sigma_1^2 \left(\frac{\mu_2 - r}{1 - \gamma} + \lambda_2 - \lambda_0 \right) - \rho \sigma_1 \sigma_2 \left(\frac{\mu_1 - r}{1 - \gamma} + \lambda_1 - \lambda_0 \right) \end{array} \right.$$

where the proportionality constant is $(1 - \rho^2)^{-1} \sigma_1^{-2} \sigma_2^{-2}$. The optimal weights depend on risk-adjusted returns, the covariance structure, the constraint multipliers, and risk aversion. Here are some properties:

 (P_1) Let us assume that $\lambda_1 = \lambda_2 = 0$ and $\mu_1 = \mu_2$. It follows that:

$$w_1^{\star} \geq w_2^{\star} \Leftrightarrow \sigma_1 \leq \sigma_2$$

The optimal weight decreases as volatility increases.

 (P_2) Let us assume that $\lambda_1 = \lambda_2 = 0$ and $\sigma_1 = \sigma_2$. It follows that:

$$w_1^{\star} \ge w_2^{\star} \Leftrightarrow \mu_1 \ge \mu_2$$

The optimal weight increases with the expected return.

(P₃) Let us assume that $\rho = 0$. In this case, $\lambda_1 = \lambda_2 = 0$ and we get:

$$w_i^{\star} = \frac{1}{\sigma_i^2} \left(\frac{\mu_i - r}{1 - \gamma} - \lambda_0 \right)$$
 for $i \in \{1, 2\}$

Thus, the optimal weight is inversely proportional to volatility and increasing in expected return. If additionally $\lambda_0=0$ (which occurs, for example, when $\gamma\to-\infty$ under the one-stage approach), we get:

$$w_i^{\star} \propto \frac{\mu_i - r}{\sigma_i^2}$$
 for $i \in \{1, 2\}$

In this case, the optimal weight is proportional to the Sharpe ratio divided by volatility.

 (P_4) Let us assume that $\lambda_1 = \lambda_2 = 0$. It follows that:

$$w_{i}^{\star} \propto \frac{1}{1-\gamma} \left(\sigma_{\neq i}^{2} \left(\mu_{i} - r \right) - \rho \sigma_{i} \sigma_{\neq i} \left(\mu_{\neq i} - r \right) \right) - \lambda_{0} \left(\sigma_{\neq i}^{2} - \rho \sigma_{i} \sigma_{\neq i} \right) \qquad \text{for } i \in \{1, 2\}$$

The optimal weight is increasing with γ .

 (P_5) The relationship between the correlation parameter ρ and the allocation (w_1^*, w_2^*) is nontrivial. In the two-stage approach, the dependence is monotonic. As ρ increases, the weight allocated to the asset with the higher Sharpe ratio rises, while the weight in the lower Sharpe ratio asset declines. In the one-stage approach, the same qualitative pattern generally holds, but the relationship may fail to be monotonic over certain intervals $[\rho_1, \rho_2]$. Let ρ^* denote the threshold correlation such that:

$$\begin{cases} \rho < \rho^* \Leftrightarrow w_1^* w_2^* > 0 \\ \rho \ge \rho^* \Leftrightarrow w_1^* w_2^* = 0 \end{cases}$$

The value ρ^* is the highest correlation level below which both assets are included in the optimal portfolio. Once correlation reaches or exceeds ρ^* , the optimization allocates weight to only one asset. In the one-stage approach, we get:

$$\rho^{\star} = \min\left(\frac{SR_1}{SR_2}, \frac{SR_2}{SR_1}\right)$$

In the two-stage approach, the threshold becomes:

$$\rho^{\star} = \min \left(\frac{\mu_1 - \mu_2}{(1 - \gamma)\sigma_1 \sigma_2} + \frac{\sigma_2}{\sigma_1}, \frac{\mu_2 - \mu_1}{(1 - \gamma)\sigma_1 \sigma_2} + \frac{\sigma_1}{\sigma_2} \right)$$

3.5.2 Numerical examples

We consider the following parameters: $\mu_1 = 10\%$, $\mu_2 = 10\%$, $\sigma_1 = 20\%$, $\sigma_2 = 25\%$, r = 3%, and $\gamma = -1$. Figures 31–34 illustrate Properties P_1 – P_4 for different values of the correlation parameter ρ under the one-stage approach. For Property P_5 , we use the following parameter sets³⁰:

Results for the two-stage approach are reported in Figures 64–68 on pages 119–121. The behavior of the two approaches is broadly consistent. However, it is worth noting that in Set #3, the allocation to Asset 1 is monotonic in ρ under the two-stage approach, whereas this is not the case under the one-stage approach.

We now have the background to better interpret the glide path obtained previously when real assets are introduced. Remember that the allocation to public equities disappears. This is because public equities have a relatively low Sharpe ratio compared to other asset classes. Not only are they dominated by private equity, but also by the other three real asset classes: private debt, real estate and infrastructure. For example, if the Sharpe ratio of public equities increases, the optimiser will start allocating to them (Figure 36, top-left panel). Moreover, when the Sharpe ratio is set to 0.45, the allocation to private equity disappears

³⁰Results are shown in Figure 35. The dashed line is the threshold correlation ρ^* .

Figure 31: Impact of the volatility σ_1 on the optimal solution (one-stage approach, Property P_1)

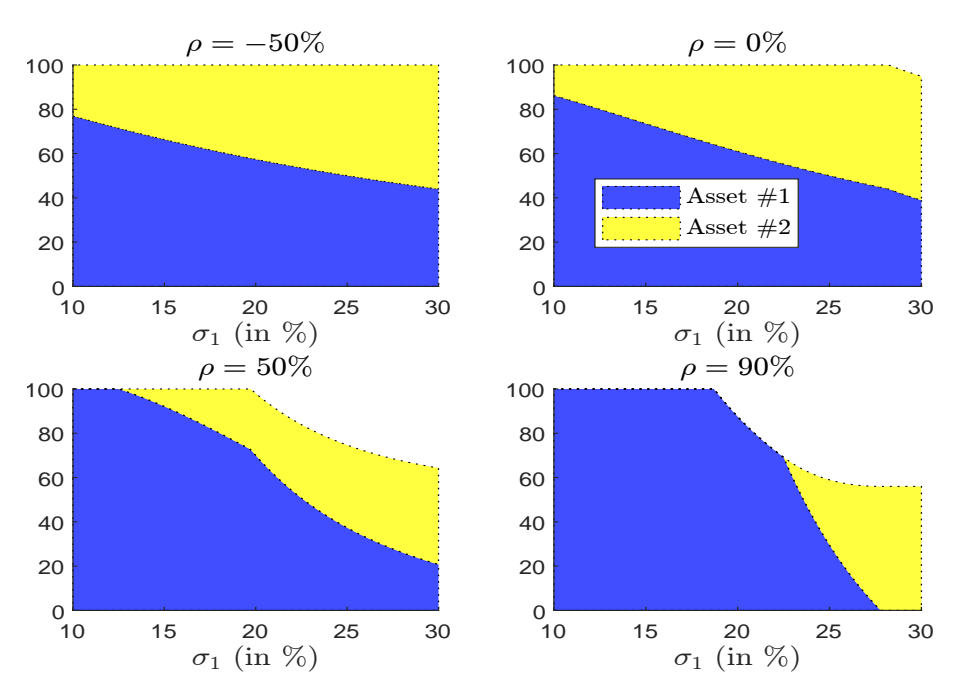


Figure 32: Impact of the expected return μ_1 on the optimal solution (one-stage approach, Property P_2)

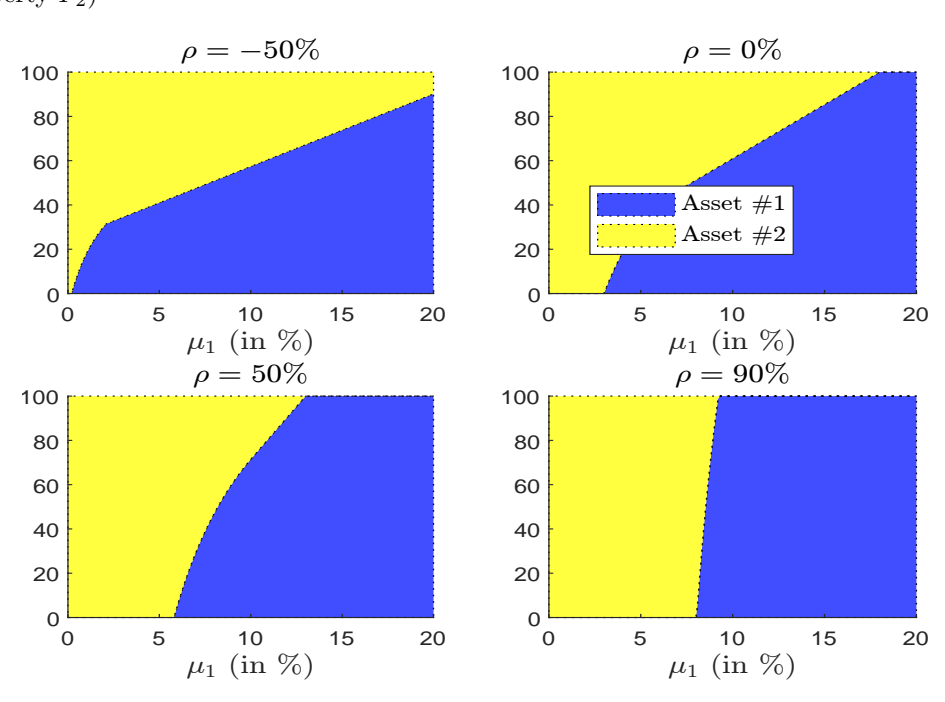


Figure 33: Impact of the parameter SR_1/σ_1 on the optimal solution (one-stage approach, Property P_3)

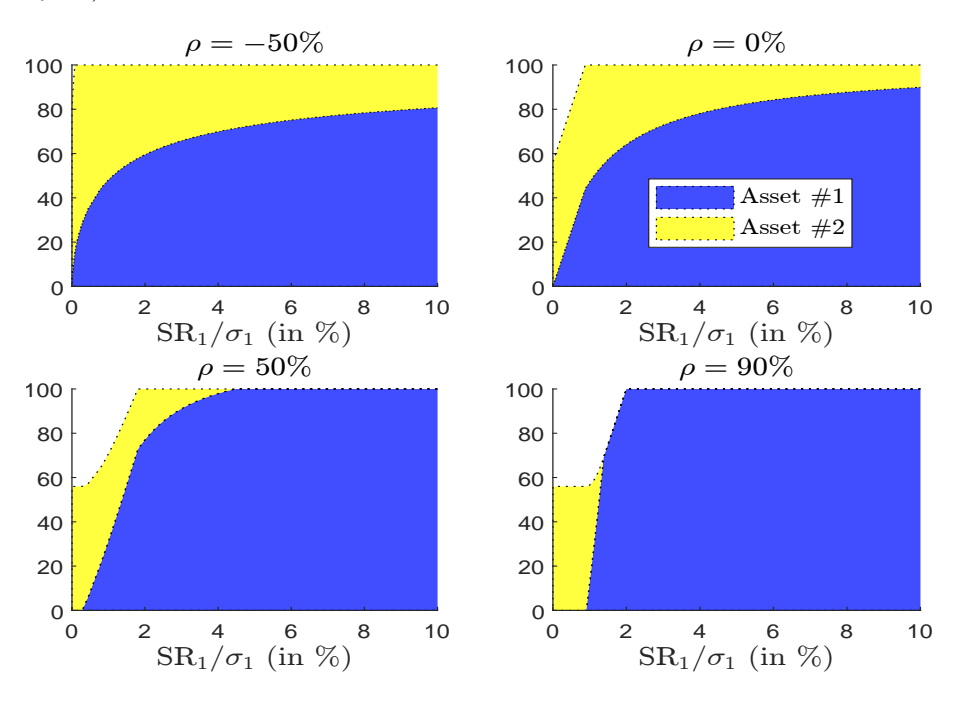


Figure 34: Impact of the risk aversion γ on the optimal solution (one-stage approach, Property P_4)

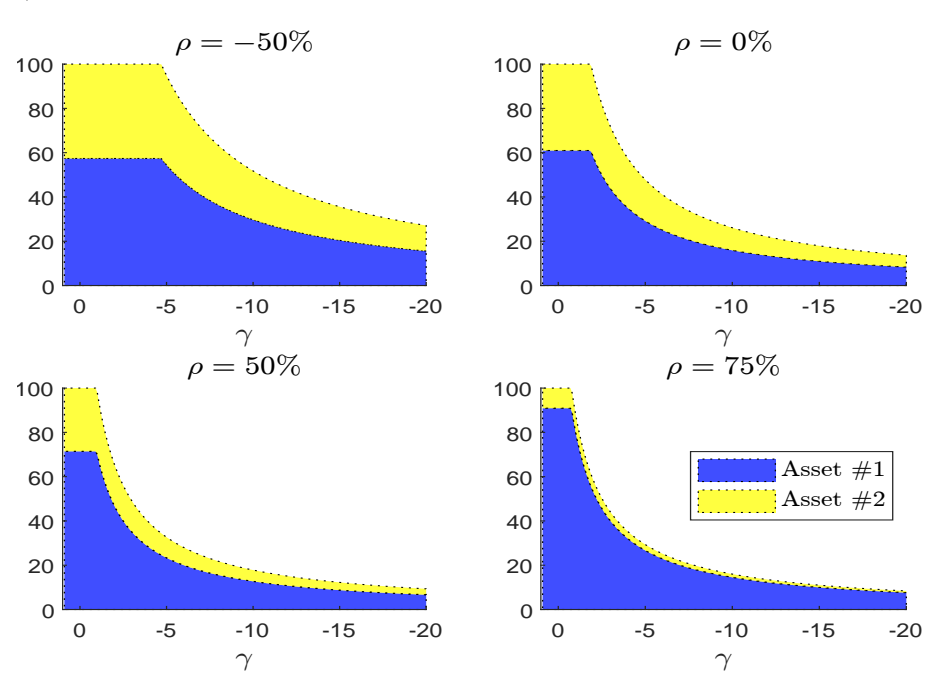


Figure 35: Impact of the correlation ρ on the optimal solution (one-stage approach, Property P_5)

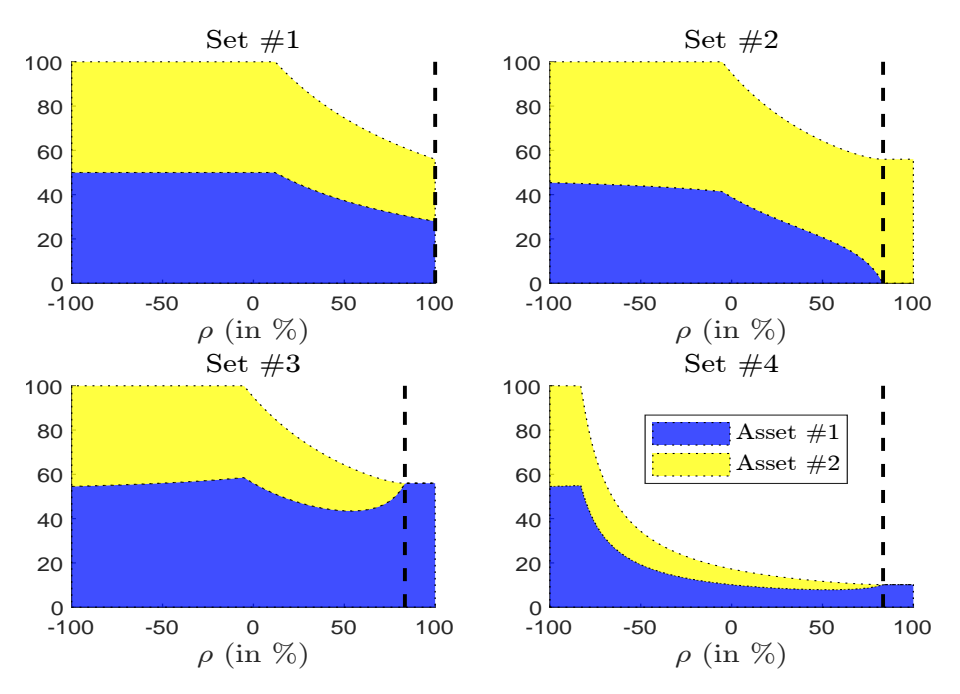
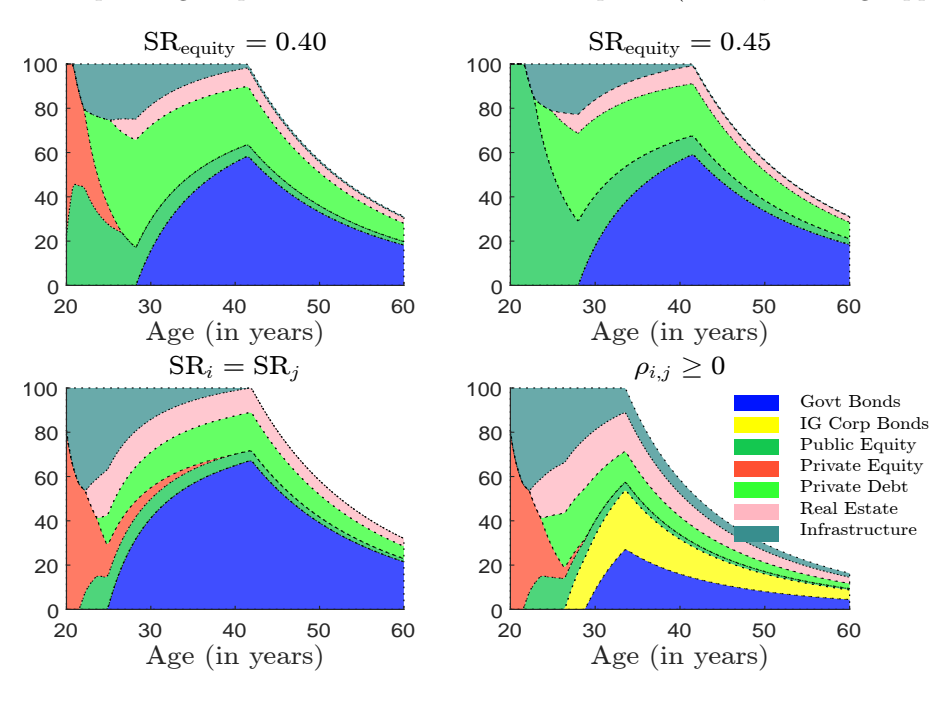


Figure 36: Optimal glide path under four different assumptions (Global, one-stage approach)



(Figure 36, top-right panel). This illustrates the strong trade-off between public and private equities (and, to a certain extent, private debt), given that these asset classes are highly correlated. The case of investment-grade corporate bonds is different. Even when Sharpe ratios are equalised across asset classes, the optimal dynamic solution assigns no weight to IG corporate bonds (Figure 36, bottom-left panel). This exclusion is not driven by Sharpe ratio considerations, but rather by their high correlation with other assets, especially government bonds. For instance, when all correlations are strictly positive, the glide path includes an allocation to IG corporate bonds (Figure 36, bottom-right panel).

3.6 The case of the investor in the Eurozone

As in our previous analysis, we conduct a dynamic asset allocation exercise, but this time we focus on an investment universe restricted to the Eurozone. Using the Amundi CASM model, we calculate the expected returns, volatilities, Sharpe ratios and correlations, which are reported in Tables 16 and 17.

Table 16: Expected return (%), volatility (%) and Sharpe ratio of asset classes (Eurozone, 30-year time horizon)

Asset class	μ_i	σ_i	SR_i	$\operatorname{SR}_i/\sigma_i$
Govt Bonds	3.39	4.90	0.22	4.46
IG Corp Bonds	3.74	4.64	0.31	6.60
Public Equity	6.77	19.53	0.23	1.17
Private Equity	11.96	19.00	0.51	2.67
Private Debt	6.77	10.10	0.44	4.36
Real Estate	5.62	10.01	0.33	3.29
Infrastructure	7.61	14.64	0.36	2.47

Source: Simulated with the Amundi CASM model (Eurozone model, EUR, June 2025), Amundi (2021).

Table 17: Correlation matrix in % (Eurozone, 30-year time horizon)

Govt Bonds	100.0	68.8	-3.1	-7.4	-20.0	-1.8	38.6
IG Corp Bonds	68.8	100.0	45.7 $^{+}$	36.7	-1.3	10.0	23.5
Public Equity	-3.1	45.7	100.0	58.6	21.9	22.8	3.8
Private Equity	-7.4	-36.7	58.6	$\bar{1}00.\bar{0}$	-19.7	22.9	-11.9
Private Debt	-20.0	-1.3	21.9^{+}	-19.7	100.0	34.8	28.3
Real Estate	-1.8	10.0	22.8	22.9	34.8	100.0	8.7
Infrastructure	38.6	23.5	3.8	-11.9	28.3	8.7	100.0

Source: Simulated with the Amundi CASM model (Eurozone model, EUR, June 2025), Amundi (2021).

A comparison with the global investment universe highlights several differences. Firstly, expected returns are generally lower in the Eurozone than at a global level, except for private equity. For example, the expected returns on government bonds, corporate bonds and public equities are 3.39%, 3.74% and 6.77% respectively, compared to 4.25%, 5.16% and 7.46% in the global investment universe. The annual cash return is assumed to be 2.32% in the Eurozone, which is 109 basis points lower than the global figure. Due to this lower risk-free rate, the Sharpe ratios of Eurozone assets are broadly comparable to those of global assets. The main exception is private equity, which exhibits a higher Sharpe ratio in the Eurozone. Correlation patterns are generally similar across the two universes, but there are some notable differences. The average cross-correlation is substantially lower in the eurozone

(17.1% versus 29.0% globally). The stock-bond correlation is also different, being close to zero in the Eurozone. This suggests that government bonds are less effective as a safe-haven asset in the Eurozone than in the global context. Additionally, real assets tend to be less correlated in the Eurozone on average³¹. Overall, these patterns suggest that the benefits of diversification are likely to be greater in the Eurozone investment universe.

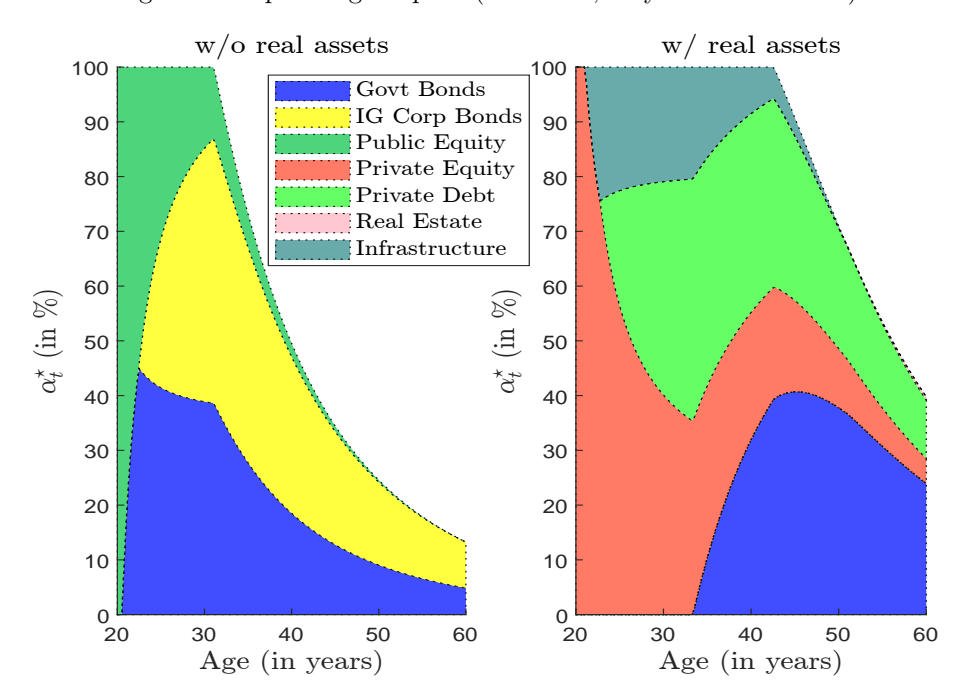


Figure 37: Optimal glide path (Eurozone, 30-year time horizon)

Figure 37 illustrates the dynamic allocation within the Eurozone investment universe with and without real assets. In both cases, the resulting portfolio is more diversified than that in the global investment universe. Notably, the allocation without real assets retains a significant exposure to corporate bonds until the retirement date. When real assets are included, private equity remains part of the allocation until the end of the investment period. Figure 38 shows the mixed glide path, which also demonstrates greater diversification. Initially, the portfolio is fully invested in public and private equities. Over time, the allocation shifts progressively towards income-generating assets, such as government and corporate bonds, private debt, and infrastructure. As with the global investment universe, we run a Monte Carlo experiment to estimate the probability density function of terminal wealth X_T . The results show that the density function shifts to the left when real assets are excluded and to the right when they are included (see Figure 39). This outcome is consistent with

 $^{^{31}}$ The average correlations are:

Asset class	Global	Eurozone
Govt Bonds	1.9	12.5
IG Corp Bonds	37.1	30.6
Public Equity	40.2	25.0
Private Equity	40.7	13.2
Private Debt	28.8	7.3
Real Estate	24.7	16.2
Infrastructure	29.8	15.2
Total	29.0	17.1

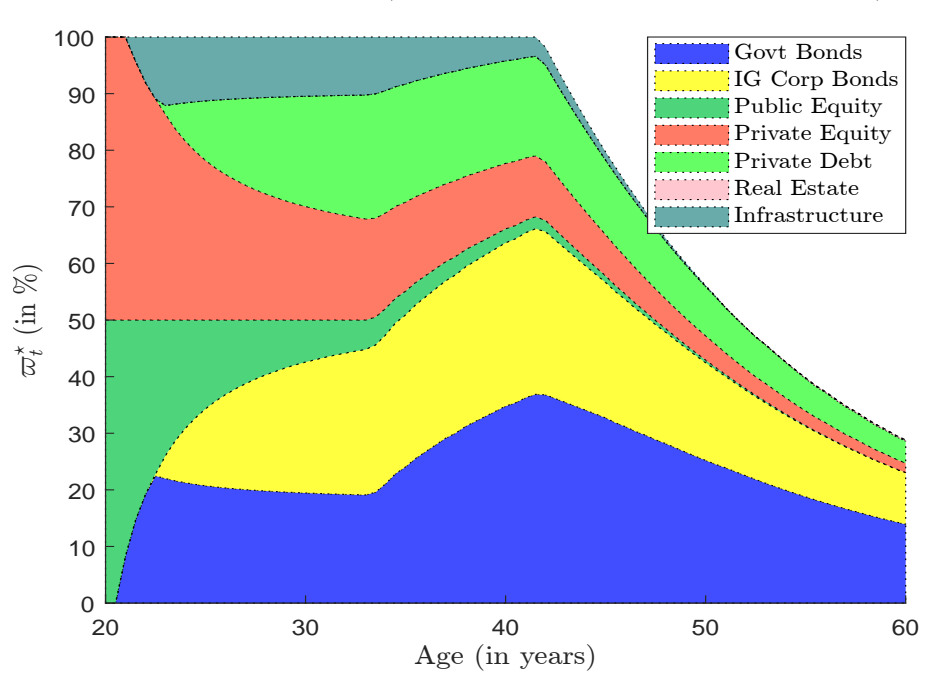
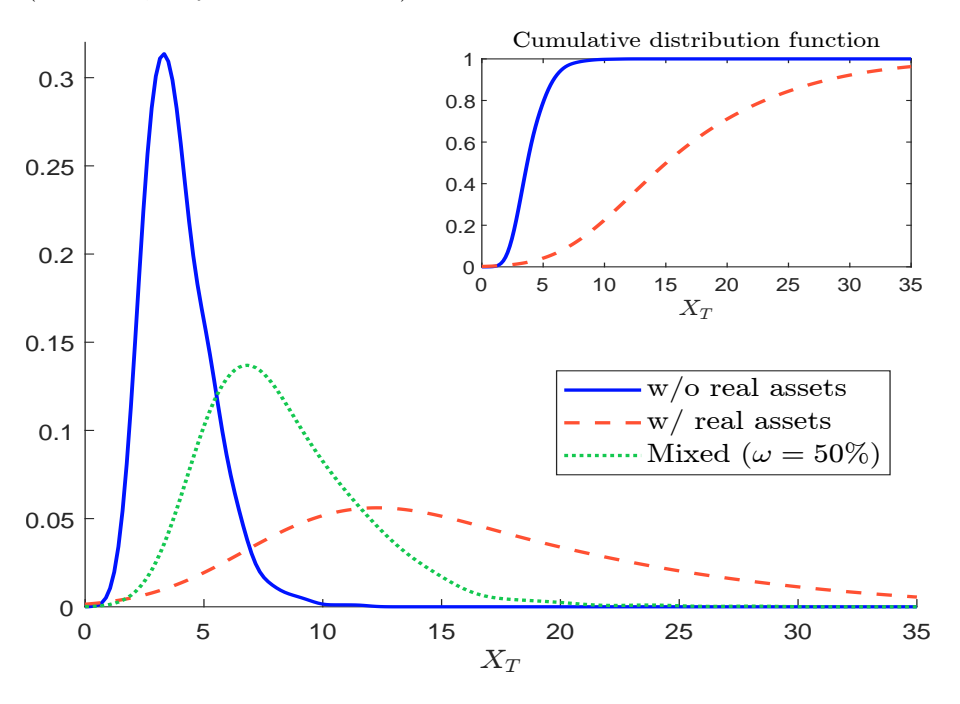


Figure 38: Mixed glide path (Eurozone, 30-year time horizon, $\omega = 50\%$)

Figure 39: Probability density function of the terminal gross wealth with and without real assets (Eurozone, 30-year time horizon)



expectations. Without real assets, the efficient frontier in the Eurozone is below that of the global universe. With real assets, however, it is above³². Consequently, the density function with real assets clearly dominates that without real assets. Table 18 reports summary statistics. These results suggest that achieving the investment objective in terms of the hit ratio is challenging when relying solely on public assets. By contrast, incorporating real assets significantly increases the probability of success. When we consider the mixed glide path, the results are very similar to those previously obtained with the global investment universe.

Table 18: Comparison of the terminal gross wealth with and without real assets, and with and without liquidity risk management (Eurozone, 30-year time horizon)

Strategy	$\mathbb{E}[X_T]$ ΔR		ı I	Quan	tile Q ((X_T,p)		Hit ratio		
Strategy	$\mathbb{E}\left[\Lambda_T\right]$	(in bps)	5%	25%	50%	75%	90%	R=4%	R = 5%	
w/o real assets	3.9		2.4	2.9	3.7	4.7	5.7	20.0%	2.2%	
w/ real assets	16.9	370	8.0	10.8	15.0	20.9	28.0	98.8%	92.6%	
Mixed ($\omega = 50\%$)	8.4	190	4.8	6.0	7.8	10.1	12.6	88.5%	55.4%	
$\bar{L}\bar{R}\bar{M}(\bar{\omega}^+=\bar{1}0\bar{0}\bar{\%})$	$-10.\bar{6}$	$-\bar{2}\bar{50}$	-4.5	7.0	$-\frac{1}{9.5}$	13.0	$\bar{1}7.1^{-}$	92.3%	-70.7%	
LRM ($\omega^+ = 50\%$)	6.5	128	3.4	4.8	6.1	7.8	9.7	71.8%	30.2%	
LRM $(\omega^+ = 20\%)$	4.8	52	2.6	3.6	4.6	5.8	7.1	40.4%	8.0%	

Remark 10. Figures 70 and 71 show the mixed glide path with liquidity risk management. Compared to the global universe, the Eurozone-only portfolio is penalized when limited to public assets. The expected terminal wealth is 3.9, versus 6.3 in the global case. However, when private assets and liquidity risk management are included, terminal wealth rises to 6.5 when $\omega^+ = 50\%$ and 4.8 when $\omega^+ = 20\%$, respectively. Performance thus converges toward that of the global investment universe. Including European private assets further improves outcomes, adding an additional annualized return of 128 and 52 bps, respectively.

4 Incorporating inflation risk

In the previous sections, we analyzed dynamic asset allocation in terms of nominal wealth. However, one of the major risks in retirement planning is inflation risk, which implies that the analysis must also be conducted in real terms rather than being limited to nominal outcomes. In what follows, we develop an approach that explicitly incorporates inflation risk into the dynamic asset allocation framework and compare the results with those obtained previously when maximizing only nominal wealth.

4.1 General framework

To account for inflation risk, we extend the model to include both financial assets and an inflation process. For simplicity, we assume the portfolio is invested in three financial instruments:

• A risk-free asset B_t , with an instantaneous rate of return r_t :

$$dB_t = r_t B_t dt$$

• A risky asset S_t , whose price follows a geometric Brownian motion with deterministic drift μ_t and volatility σ_t :

$$dS_t = \mu_t S_t dt + \sigma_t S_t dW_t$$

³²See Figures 58 on page 116 and 69 on page 122.

• An inflation-sensitive risky asset R_t , whose price follows a geometric Brownian motion with stochastic drift $\mu'_t = a + b\pi_t$ and deterministic volatility σ'_t :

$$dR_t = (a_t + b_t \pi_t) R_t dt + \sigma_t' R_t dW_t'$$

where a_t and b_t are two parameters. The parameter a_t captures the asset's inflation-independent expected return, while b_t quantifies the sensitivity of expected return to the current inflation rate π_t .

• The inflation rate is modeled as an Ornstein-Uhlenbeck process:

$$d\pi_t = \kappa \left(\pi_{\infty} - \pi_t \right) dt + \sigma_t^{(\pi)} dW_t^{(\pi)}$$

where $\kappa > 0$ is the mean-reversion rate, π_{∞} is the long-term mean inflation rate, and $\sigma_t^{(\pi)} > 0$ is the volatility of inflation.

At time t, we assume that a proportion α_t of the wealth is invested in the risky asset S_t , a proportion β_t is allocated to the inflation-sensitive asset R_t , and the remaining proportion $1 - \alpha_t - \beta_t$ is invested in the risk-free asset B_t . In the following, we define the discounted wealth as $X_t = \tilde{X}_t Y_t$ where \tilde{X}_t is the nominal wealth process, $Y_t = e^{-\int_{t_0}^t \rho \pi_s \, \mathrm{d}s}$ is the inflation discount factor, and $\rho \in \{0,1\}$ is a scaling parameter:

- If $\varrho = 0$, the analysis is conducted in nominal terms as in the previous sections.
- If $\varrho = 1$, the analysis is done in real terms.

The dynamics of the nominal wealth process \tilde{X}_t is given by:

$$\frac{\mathrm{d}X_t}{\tilde{X}_t} = \alpha_t \frac{\mathrm{d}S_t}{S_t} + \beta_t \frac{\mathrm{d}R_t}{R_t} + (1 - \alpha_t - \beta_t) \frac{\mathrm{d}B_t}{B_t} + \frac{c_t}{\tilde{X}_t} \mathrm{d}t$$

We deduce that:

$$d\tilde{X}_{t} = \left(\alpha_{t}\mu_{t}\tilde{X}_{t} + \beta_{t}\left(a_{t} + b_{t}\pi_{t}\right)\tilde{X}_{t} + \left(1 - \alpha_{t} - \beta_{t}\right)r_{t}\tilde{X}_{t} + \mathbf{c}_{t}\right)dt + \alpha_{t}\sigma_{t}\tilde{X}_{t}dW_{t} + \beta_{t}\sigma'_{t}\tilde{X}_{t}dW'_{t}$$

Since Y_t has finite variation, we have $dY_t = -\varrho \pi_t Y_t dt$ and $d\left\langle \tilde{X}, Y \right\rangle_t = 0$. We get:

$$dX_t = Y_t d\tilde{X}_t + \tilde{X}_t dY_t = \frac{X_t}{\tilde{X}_t} d\tilde{X}_t - \tilde{X}_t \varrho \pi_t Y_t dt = \left(\frac{d\tilde{X}_t}{\tilde{X}_t} - \varrho \pi_t dt\right) X_t$$

Using the dynamics for \tilde{X}_t , we deduce that:

$$dX_t = \left(\alpha_t \mu_t X_t + \beta_t \left(a_t + b_t \pi_t\right) X_t + \left(1 - \alpha_t - \beta_t\right) r_t X_t - \varrho \pi_t X_t + c_t'\right) dt + \alpha_t \sigma_t X_t dW_t + \beta_t \sigma_t' X_t dW_t'$$

where $\mathbf{c}_t' = \mathbf{c}_t e^{-\int_{t_0}^t \varrho \pi_s \, \mathrm{d}s}$ is the discounted value of the contribution. We assume that the Brownian motions W_t , W_t' , and $W_t^{(\pi)}$ are correlated with $\mathbb{E}\left[\mathrm{d}W_t \, \mathrm{d}W_t'\right] = \rho_t \, \mathrm{d}t$, $\mathbb{E}\left[\mathrm{d}W_t' \, \mathrm{d}W_t^{(\pi)}\right] = \rho_t^{(R)} \, \mathrm{d}t$ and $\mathbb{E}\left[\mathrm{d}W_t \, \mathrm{d}W_t^{(\pi)}\right] = \rho_t^{(S)} \, \mathrm{d}t$. It follows that:

$$\begin{cases} (dX_t)^2 = \left(\alpha_t^2 \sigma_t^2 + \beta_t^2 \left(\sigma_t'\right)^2 + 2\alpha_t \beta_t \rho_t \sigma_t \sigma_t'\right) X_t^2 dt \\ (d\pi_t)^2 = \left(\sigma_t^{(\pi)}\right)^2 dt \\ dX_t d\pi_t = \left(\alpha_t \rho_t^{(S)} \sigma_t + \beta_t \rho_t^{(R)} \sigma_t'\right) \sigma_t^{(\pi)} X_t dt \end{cases}$$

Let $\mathcal{J}(t, x, \pi)$ be the value function:

$$\mathcal{J}\left(t, x, \pi\right) = \sup_{(\alpha, \beta)} \mathbb{E}_{t}\left[\mathcal{U}\left(X_{T}\right) \mid X_{t} = x, \pi_{t} = \pi\right]$$

The HJB equation is:

$$\frac{\partial \mathcal{J}\left(t,x,\pi\right)}{\partial t} + \kappa \left(\pi_{\infty} - \pi_{t}\right) \frac{\partial \mathcal{J}\left(t,x,\pi\right)}{\partial \pi} + \frac{1}{2} \left(\sigma_{t}^{(\pi)}\right)^{2} \frac{\partial^{2} \mathcal{J}\left(t,x,\pi\right)}{\partial \pi^{2}} + \max_{(\alpha,\beta)} \mathcal{H}\left(t,x,\pi,\alpha,\beta\right) = 0$$

with terminal condition:

$$\mathcal{J}\left(T, x, \pi\right) = \mathcal{U}\left(x\right)$$

The expression of the Hamiltonian is:

$$\mathcal{H}(t, x, \pi, \alpha, \beta) = \left(\alpha \mu_t x + \beta \left(a_t + b_t \pi\right) x + \left(1 - \alpha - \beta\right) r_t x - \varrho \pi x + \mathbf{c}_t'\right) \frac{\partial \mathcal{J}(t, x, \pi)}{\partial x} + \frac{1}{2} \left(\alpha^2 \sigma_t^2 + \beta^2 \left(\sigma_t'\right)^2 + 2\alpha \beta \rho_t \sigma_t \sigma_t'\right) x^2 \frac{\partial^2 \mathcal{J}(t, x, \pi)}{\partial x^2} + \left(\alpha \rho_t^{(S)} \sigma_t + \beta \rho_t^{(R)} \sigma_t'\right) \sigma_t^{(\pi)} x \frac{\partial^2 \mathcal{J}(t, x, \pi)}{\partial x \partial \pi}$$

4.2 The case without allocation constraints

4.2.1 General solution

In Appendix A.16 on page 105, we show that the optimal solution is:

$$\nu_t^{\star} = \begin{pmatrix} \alpha_t^{\star} \\ \beta_t^{\star} \end{pmatrix} = -\Sigma_t^{-1} \left(\theta_t \frac{\mathcal{J}_x}{x \mathcal{J}_{x,x}} + \zeta_t \frac{\mathcal{J}_{x,\pi}}{x \mathcal{J}_{x,x}} \right)$$
 (22)

where $\mathcal{J}_{x} = \partial_{x} \mathcal{J}(t, x, \pi), \ \mathcal{J}_{x,x} = \partial_{x}^{2} \mathcal{J}(t, x, \pi), \ \mathcal{J}_{x,\pi} = \partial_{x,\pi} \mathcal{J}(t, x, \pi), \ \text{and:}$

$$\Sigma_{t} = \begin{pmatrix} \sigma_{t}^{2} & \rho_{t}\sigma_{t}\sigma_{t}' \\ \rho_{t}\sigma_{t}\sigma_{t}' & (\sigma_{t}')^{2} \end{pmatrix}, \ \theta_{t} = \begin{pmatrix} \mu_{t} - r_{t} \\ a_{t} + b_{t}\pi - r_{t} \end{pmatrix} \text{ and } \zeta_{t} = \begin{pmatrix} \rho_{t}^{(S)}\sigma_{t}\sigma_{t}^{(\pi)} \\ \rho_{t}^{(R)}\sigma_{t}'\sigma_{t}^{(\pi)} \end{pmatrix}$$

It follows that:

$$\mathcal{H}\left(t, x, \pi, \alpha_{t}^{\star}, \beta_{t}^{\star}\right) = -\frac{1}{2} \frac{\mathcal{J}_{x}^{2}}{\mathcal{J}_{x, x}} \theta_{t}^{\top} \Sigma_{t}^{-1} \theta_{t} - \frac{\mathcal{J}_{x} \mathcal{J}_{x, \pi}}{\mathcal{J}_{x, x}} \zeta_{t}^{\top} \Sigma_{t}^{-1} \theta_{t} - \frac{1}{2} \frac{\mathcal{J}_{x, \pi}^{2}}{\mathcal{J}_{x, x}} \zeta_{t}^{\top} \Sigma_{t}^{-1} \zeta_{t} + \mathcal{J}_{x} \left(r_{t} x - \varrho \pi x + \mathbf{c}_{t}^{\prime}\right)$$

$$(23)$$

Risk-premium interpretation of the optimal solution When $\zeta_t = \mathbf{0}_2$, inflation shocks are uncorrelated with asset shocks ($\rho_t^{(S)} = \rho_t^{(R)} = 0$). In this case, we recover the solution of the standard multi-asset case presented in the previous section³³:

$$\begin{pmatrix} \alpha_t^{\star} \\ \beta_t^{\star} \end{pmatrix} = -\frac{\mathcal{J}_x}{x\mathcal{J}_{x,x}} \Sigma_t^{-1} \theta_t = -\frac{\partial_x \mathcal{J}(t, x, \pi)}{x\partial_x^2 \mathcal{J}(t, x, \pi)} \begin{pmatrix} \sigma_t^2 & \rho_t \sigma_t \sigma_t' \\ \rho_t \sigma_t \sigma_t' & (\sigma_t')^2 \end{pmatrix}^{-1} \begin{pmatrix} \mu_t \\ \mu_t' \end{pmatrix} - r_t \mathbf{1}_2 \end{pmatrix}$$

When $\zeta_t \neq \mathbf{0}_2$, we obtain a similar expression, but with a correction term:

$$\begin{pmatrix} \alpha_{t}^{\star} \\ \beta_{t}^{\star} \end{pmatrix} = -\frac{\partial_{x} \mathcal{J}\left(t, x, \pi\right)}{x \partial_{x}^{2} \mathcal{J}\left(t, x, \pi\right)} \begin{pmatrix} \sigma_{t}^{2} & \rho_{t} \sigma_{t} \sigma_{t}' \\ \rho_{t} \sigma_{t} \sigma_{t}' & \left(\sigma_{t}'\right)^{2} \end{pmatrix}^{-1} \begin{pmatrix} \tilde{\mu}_{t} \\ \tilde{\mu}_{t}' \end{pmatrix} - r_{t} \mathbf{1}_{2} \end{pmatrix}$$

 $^{^{33}}$ See Equation (19) on page 46.

where:

$$\begin{pmatrix} \tilde{\mu}_{t} \\ \tilde{\mu}'_{t} \end{pmatrix} = \begin{pmatrix} \mu_{t} \\ \mu'_{t} \end{pmatrix} + \frac{\partial_{x,\pi}^{2} \mathcal{J}(t,x,\pi)}{\partial_{x} \mathcal{J}(t,x,\pi)} \begin{pmatrix} \rho_{t}^{(S)} \sigma_{t} \sigma_{t}^{(\pi)} \\ \rho_{t}^{(R)} \sigma'_{t} \sigma'_{t}^{(\pi)} \end{pmatrix}$$

In this case, the effective expected returns are adjusted to reflect the covariance risk with inflation. The direction of this adjustment depends on the signs of $\rho_t^{(S)}$, $\rho_t^{(R)}$, and the cross-derivative $\partial_{x,\pi}^2 \mathcal{J}(t,x,\pi)$:

For instance, if $\rho_t^{(S)} < 0$, $\rho_t^{(R)} > 0$ and $\partial_{x,\pi}^2 \mathcal{J}(t,x,\pi) > 0$ — a configuration that is arguably the most realistic — we get $\tilde{\mu}_t < \mu_t$ and $\tilde{\mu}_t' > \mu_t'$. Compared to the pure multi-asset solution, the optimal exposure to the standard risky asset decreases, while the exposure to the inflation-sensitive risky asset increases.

Liability-hedging interpretation of the optimal solution The optimal solution (22) can be expressed as:

$$\begin{pmatrix} \alpha_t^{\star} \\ \beta_t^{\star} \end{pmatrix} = \begin{pmatrix} -\frac{\mathcal{J}_x}{x\mathcal{J}_{x,x}} \end{pmatrix} \Sigma_t^{-1} \theta_t + \begin{pmatrix} -\frac{\mathcal{J}_{x,\pi}}{x\mathcal{J}_{x,x}} \end{pmatrix} \Sigma_t^{-1} \zeta_t$$

$$= \varpi^{(\text{msr})} \cdot \underbrace{\Sigma_t^{-1} \theta_t}_{\text{Market portfolio}} + \varpi^{(\pi)} \cdot \underbrace{\Sigma_t^{-1} \zeta_t}_{\text{Liability-hedging portfolio}}$$

$$= \varpi^{(\text{msr})} \cdot \begin{pmatrix} \alpha_t^{(\text{msr})} \\ \beta_t^{(\text{msr})} \end{pmatrix} + \varpi^{(\pi)} \cdot \begin{pmatrix} \alpha_t^{(\pi)} \\ \beta_t^{(\pi)} \end{pmatrix}$$

where $\varpi^{(\mathrm{msr})} = -\frac{\mathcal{J}_x}{x\mathcal{J}_{x,x}} > 0$ and $\varpi^{(\pi)} = -\frac{\mathcal{J}_{x,\pi}}{x\mathcal{J}_{x,x}} \lessgtr 0$. Thus, the optimal allocation has two components. The first is the market component, corresponding to the classical Markowitz

components. The first is the market component, corresponding to the classical Markowitz solution and representing the maximum Sharpe ratio (MSR) portfolio. The second is the inflation component, which depends on the covariance risk premium associated with inflation. The two component portfolios are weighted by $\varpi^{(msr)}$ and $\varpi^{(\pi)}$, which depend on the utility function, the current wealth, and the current level of inflation. Remarkably, this decomposition recovers a principle from liability-driven investment (LDI) used by defined benefit (DB) pension funds. Specifically, the inflation component can be interpreted as a liability-hedging portfolio (LHP), where the liability is the inflation risk (Roncalli, 2013). By explicitly accounting for inflation risk in retirement accumulation strategies, defined contribution (DC) solutions converge toward DB-style liability-hedging solutions, linking classical portfolio optimization with practical retirement planning. However, the dynamic allocation may take either a long or short position in the liability-hedging portfolio, depending on the sign of $\varpi^{(\pi)}$. This is a key distinction from traditional DB investment policies.

The expression of the LHP is:

$$\begin{pmatrix} \alpha_t^{(\pi)} \\ \beta_t^{(\pi)} \end{pmatrix} = \frac{\sigma_t^{(\pi)}}{(1-\gamma)\left(1-\rho_t^2\right)} \begin{pmatrix} \left(\rho_t^{(S)} - \rho_t \rho_t^{(R)}\right)/\sigma_t \\ \left(\rho_t^{(R)} - \rho_t \rho_t^{(S)}\right)/\sigma_t' \end{pmatrix}$$

The sign of each weight is fully determined by the correlations: $\operatorname{sgn} \alpha_t^{(\pi)} = \operatorname{sgn} \left(\rho_t^{(S)} - \rho_t \rho_t^{(R)} \right)$ and $\operatorname{sgn} \beta_t^{(\pi)} = \operatorname{sgn} \left(\rho_t^{(R)} - \rho_t \rho_t^{(S)} \right)$. Here are some special cases:

Special cases	$\operatorname{sgn}\left(\alpha_t^{(\pi)}\right)$	$\operatorname{sgn}\left(\beta_t^{(\pi)}\right)$
$\rho_t = 0$	$\operatorname{sgn}\left(\rho_t^{(S)}\right)$	$\operatorname{sgn}\left(ho_t^{(R)}\right)$
$\rho_t^{(S)} > \rho_t^{(R)} > 0$	+	,
$0 < \rho_t^{(S)} < \rho_t^{(R)}$		+
$\rho_t^{(S)} = 0$	$-\operatorname{sgn}\left(\rho_t\rho_t^{(R)}\right)$	$\operatorname{sgn}\left(ho_t^{(R)}\right)$
$\rho_t \longrightarrow 1$	$\operatorname{sgn}\left(\rho_t^{(S)} - \rho_t^{(R)}\right)$	$\operatorname{sgn}\left(\rho_t^{(\grave{R})} - \rho_t^{(S)}\right)$

For example, if $\rho_t = 50\%$, $\rho_t^{(S)} = -10\%$, $\rho_t^{(R)} = 25\%$, we get $\alpha_t^{(\pi)} < 0$ and $\beta_t^{(\pi)} > 0$. While the sign is governed entirely by the correlation triplet $(\rho_t, \rho_t^{(S)}, \rho_t^{(R)})$, the magnitude depends on volatilities. Each weight is:

- proportional to the inflation volatility $\sigma_t^{(\pi)}$,
- inversely proportional to its own asset volatility $(\sigma_t \text{ or } \sigma'_t)$,
- and amplified as $|\rho_t| \to 1$, since $(1 \rho_t^2)^{-1}$ becomes large.

4.2.2 CRRA solution with $c_t = 0$

In the general case, there is no closed-form solution. To obtain one, we set the contribution c_t to 0 and consider a CRRA utility function. In this case, we have:

$$\mathcal{J}\left(t, x, \pi\right) = h\left(t, \pi\right) \frac{x^{\gamma}}{\gamma}$$

where $h(t,\pi)$ is the solution³⁴ of the nonlinear partial differential equation³⁵:

$$\frac{1}{2} \left(\sigma_t^{(\pi)} \right)^2 \partial_{\pi}^2 h\left(t, \pi\right) + \left(\kappa \left(\pi_{\infty} - \pi \right) - q_t^{\theta, \zeta} \right) \partial_{\pi} h\left(t, \pi\right)
+ \left(\gamma \left(r_t - \varrho \pi \right) - \frac{1}{2} q_t^{\theta} \right) h\left(t, \pi\right) + \partial_t h\left(t, \pi\right) - \frac{1}{2} q_t^{\zeta} \frac{\left(\partial_{\pi} h\left(t, \pi\right) \right)^2}{h\left(t, \pi\right)} = 0$$
(24)

with terminal condition $h(T, \pi) = 1$ and:

$$\left\{ \begin{array}{l} q_t^{\theta} = \frac{\gamma}{\gamma - 1} \theta_t^{\top} \Sigma_t^{-1} \theta_t \\ q_t^{\theta, \zeta} = \frac{\gamma}{\gamma - 1} \zeta_t^{\top} \Sigma_t^{-1} \theta_t \\ q_t^{\zeta} = \frac{\gamma}{\gamma - 1} \zeta_t^{\top} \Sigma_t^{-1} \zeta_t \end{array} \right.$$

³⁴The proof is given in Appendix A.17 on page 106.

³⁵The PDE is not linear because of the last term.

The optimal solution is given by:

$$\begin{pmatrix} \alpha_t^{\star} \\ \beta_t^{\star} \end{pmatrix} = \frac{1}{1 - \gamma} \Sigma_t^{-1} \left(\theta_t + \zeta_t \frac{\partial_{\pi} h \left(t, \pi \right)}{h \left(t, \pi \right)} \right)$$

$$= \underbrace{\frac{1}{1 - \gamma} \Sigma_t^{-1} \theta_t}_{\text{Market portfolio}} + \underbrace{\frac{\partial_{\pi} \ln h \left(t, \pi \right)}{h \left(t, \pi \right)}}_{\text{Hedging demand}} \times \underbrace{\frac{1}{1 - \gamma} \Sigma_t^{-1} \zeta_t}_{\text{Liability-hedging portfolio}}$$

$$= \begin{pmatrix} \bar{\alpha}_t^{\star} \\ \bar{\beta}_t^{\star} \end{pmatrix} + \partial_{\pi} \ln h \left(t, \pi \right) \times \begin{pmatrix} \alpha_t^{(\pi)} \\ \beta_t^{(\pi)} \end{pmatrix}$$

This result shows that the optimal allocation consists of two portfolios:

- The market portfolio, designed to capture the performance of risky investments and achieve wealth accumulation for retirement;
- The liability-hedging portfolio, constructed to hedge inflation risk.

The hedging component corresponds to the product of the hedging demand and the LHP. Since the hedging demand, given by $\mathcal{H}_t^{(\pi)} = \partial_{\pi} \ln h (t, \pi)$, can take either positive or negative values, the resulting position in the LHP may be long or short. This allocation principle is the foundation of dynamic allocation decisions in the presence of liability risk (Martellini and Milhau, 2012).

Remark 11. The inflation component can be expressed as:

$$\begin{pmatrix} \alpha_t^{(\pi)} \\ \beta_t^{(\pi)} \end{pmatrix} = \frac{\sigma_t^{(\pi)}}{(1-\gamma)\left(1-\rho_t^2\right)} \begin{pmatrix} \left(\rho_t^{(S)} - \rho_t \rho_t^{(R)}\right)/\sigma_t \\ \left(\rho_t^{(R)} - \rho_t \rho_t^{(S)}\right)/\sigma_t' \end{pmatrix}$$

Let us assume that $\rho_t^{(S)} = 0$ and $\rho_t^{(R)} \geq 0$. Then the hedging component satisfies:

$$\alpha_t^{(\pi)} + \frac{\operatorname{cov}\left(\frac{\mathrm{d}S_t}{S_t}, \frac{\mathrm{d}R_t}{R_t}\right)}{\operatorname{var}\left(\frac{\mathrm{d}S_t}{S_t}\right)} \beta_t^{(\pi)} = 0$$

In this case, $\beta_t^{(\pi)} > 0$ while $\alpha_t^{(\pi)} < 0$. This means that the long position in the inflation-sensitive asset is partially financed by a short position in the risky asset, with the hedging ratio given by the beta of the inflation-sensitive asset relative to the risky asset.

4.2.3 Approximate closed-form solution

To solve Equation (24), we can use the finite-difference method (Roncalli, 2020). An alternative approach is to assume that:

$$h(t, \pi) = \exp\left(A(t) + B(t)\pi + C(t)\pi^{2}\right)$$

Therefore, the functions A(t), B(t) and C(t) satisfy the following system of ODEs³⁶:

$$\begin{cases}
\frac{\mathrm{d}A(t)}{\mathrm{d}t} &= -\kappa \pi_{\infty} B(t) - \frac{1}{2} \left(\sigma_{t}^{(\pi)}\right)^{2} \left(B^{2}(t) + 2C(t)\right) - \gamma r_{t} + \\
\frac{1}{2} \frac{\gamma}{\gamma - 1} \left(\bar{\theta}_{t} + B(t) \zeta_{t}\right)^{\top} \Sigma_{t}^{-1} \left(\bar{\theta}_{t} + B(t) \zeta_{t}\right) \\
\frac{\mathrm{d}B(t)}{\mathrm{d}t} &= -\kappa \left(2\pi_{\infty} C(t) - B(t)\right) - 2 \left(\sigma_{t}^{(\pi)}\right)^{2} B(t) C(t) + \gamma \varrho + \\
\frac{\gamma}{\gamma - 1} \left(\bar{\theta}_{t} + B(t) \zeta_{t}\right)^{\top} \Sigma_{t}^{-1} \left(\hat{\theta}_{t} + 2C(t) \zeta_{t}\right) \\
\frac{\mathrm{d}C(t)}{\mathrm{d}t} &= 2\kappa C(t) - 2 \left(\sigma_{t}^{(\pi)}\right)^{2} C^{2}(t) + \\
\frac{1}{2} \frac{\gamma}{\gamma - 1} \left(\hat{\theta}_{t} + 2C(t) \zeta_{t}\right)^{\top} \Sigma_{t}^{-1} \left(\hat{\theta}_{t} + 2C(t) \zeta_{t}\right)
\end{cases} (25)$$

with terminal conditions A(T) = B(T) = C(T) = 0. The numerical solution can be obtained with a Runge-Kutta scheme. Finally, the optimal weights are equal to:

$$\begin{pmatrix} \alpha_{t}^{\star} \\ \beta_{t}^{\star} \end{pmatrix} = \frac{1}{1 - \gamma} \Sigma_{t}^{-1} \theta_{t} + \frac{1}{1 - \gamma} \left(B\left(t \right) + 2C\left(t \right) \pi \right) \Sigma_{t}^{-1} \zeta_{t}$$

We now consider the case $b_t = 0$, implying $\hat{\theta}_t = \mathbf{0}_2$. Since C(T) = 0 and:

$$\frac{\mathrm{d}C\left(t\right)}{\mathrm{d}t} = 2\kappa \cdot C\left(t\right) - 2\left(\left(\sigma_{t}^{(\pi)}\right)^{2} + \frac{\gamma}{\gamma - 1}\zeta_{t}^{\top}\Sigma_{t}^{-1}\zeta_{t}\right) \cdot C^{2}\left(t\right)$$

we deduce that C(t) = 0. It follows that:

$$\frac{\mathrm{d}B\left(t\right)}{\mathrm{d}t} = \kappa B\left(t\right) + \gamma \varrho$$

Using the terminal condition B(T) = 0, we get:

$$B(t) = \varrho \gamma \left(\frac{e^{\kappa(t-T)} - 1}{\kappa} \right)$$

The optimal solution becomes 37 :

$$\begin{pmatrix} \alpha_t^{\star} \\ \beta_t^{\star} \end{pmatrix} = \frac{1}{1 - \gamma} \Sigma_t^{-1} \theta_t + \varrho \frac{\gamma}{1 - \gamma} \left(\frac{e^{\kappa(t - T)} - 1}{\kappa} \right) \Sigma_t^{-1} \zeta_t$$

If $\gamma < 0$, the hedging demand is positive and decreases over time. At the retirement date T, the inflation-hedging demand vanishes.

We consider the following numerical application: $\mu_t = 8\%$, $\sigma_t = 20\%$, $r_t = 2\%$, $a_t = 4\%$, $b_t = 0$, $\sigma_t' = 15\%$, $\rho_t = 10\%$, $\kappa = 0.5$, $\pi_\infty = 4\%$, $\sigma_t^{(\pi)} = 2\%$, $\rho_t^{(S)} = 20\%$, $\rho_t^{(R)} = 50\%$, $\varrho = 1$ and $\gamma = -1$. We solve the ODE system using the Runge-Kutta algorithm for $t \in [20, 60]$ and find the following initial values: A(20) = -0.3460, B(20) = 2, C(20) = 0. Figure 40 shows the solutions A(t), B(t), C(t) and A(t) for two values of π . If we assume that $b_t = 1$, the initial values are A(20) = -1.6145, B(20) = 0.4750, and C(20) = -10.4705, while the solutions A(t), B(t), C(t) and A(t), B(t), are shown in Figure 41.

³⁶The proof is given in Appendix A.17 on page 106.

 $^{^{37}}$ If $b_t = 0$ and $\varrho = 0$, meaning that the investor is not sensitive to their real wealth, there is no hedging demand.

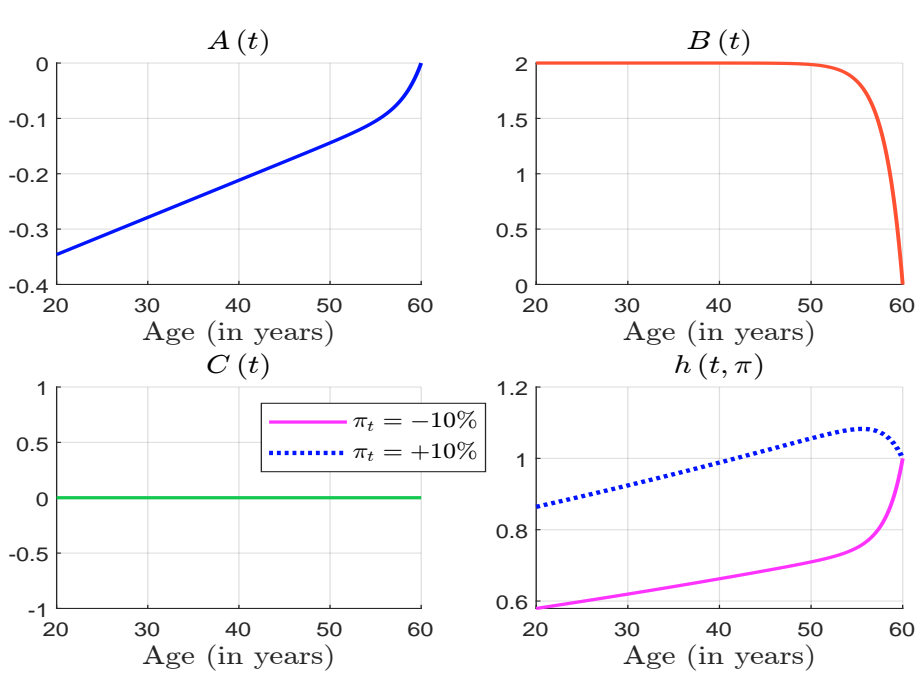
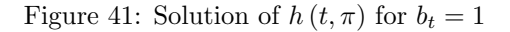
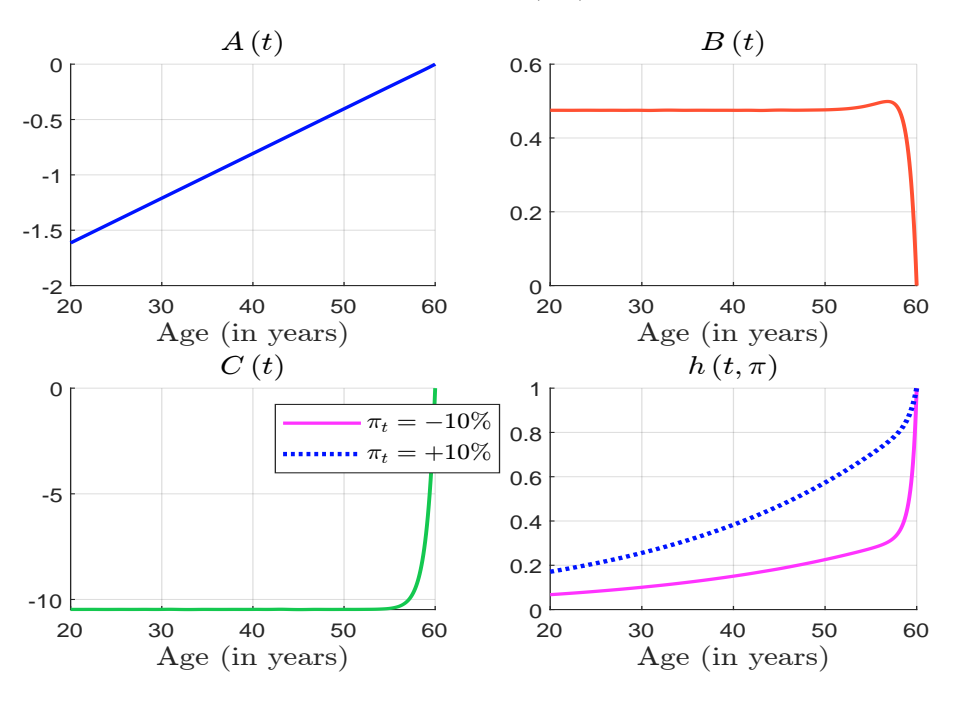


Figure 40: Solution of $h\left(t,\pi\right)$ for $b_{t}=0$





	b_t =	= 0	l	$b_t = 1$	
	$\pi_t = -10\%$	$\pi_t = +10\%$	$\pi_t = -30\%$	$\pi_t = -10\%$	$\pi_t = +10\%$
$\bar{\alpha}_t^{\star}$	72.39	72.39	122.90	89.23	55.56
$ar{lpha}_t^{\star} \ ar{eta}_t^{\star}$	34.79	34.79	-638.61	-189.67	259.26
$\alpha_t^{(\pi)}$	0.76	0.76	0.76	0.76	0.76
$\beta_{t_{-}}^{(\pi)}$	3.23	3.23	3.23	3.23	3.23
$\mathcal{H}_{t_0}^{(\pi)}$	200.00	200.00	675.73	256.91	-161.91
$\mathcal{H}_T^{(\pi)}$	0.00	0.00	0.00	0.00	0.00

Table 19: Market and liability-hedging portfolios (in %)

In Table 19, we report the market portfolio $(\bar{\alpha}_t^{\star}, \bar{\beta}_t^{\star})$, the liability-hedging portfolio $(\alpha_t^{(\pi)}, \beta_t^{(\pi)})$, and the hedging demand $\mathcal{H}_t^{(\pi)}$ at both the initial date and the retirement date. When $b_t = 0$, the market portfolio, the LHP, and the hedging demand are independent of the inflation level π_t . However, when $b_t = 1$, the hedging demand becomes sensitive to inflation. In this case, $\mathcal{H}_t^{(\pi)}$ may take negative values, indicating that the optimal allocation involves a short position in the liability-hedging portfolio.

4.3 The case with allocation constraints

When we impose constraints on α_t and β_t , a closed-form solution is generally no longer available. If the constraint set Ω is independent of wealth x, then under CRRA utility and no contributions c_t , the value function $\mathcal{J}(t, x, \pi)$ remains x-separable:

$$\mathcal{J}\left(t, x, \pi\right) = h\left(t, \pi\right) \frac{x^{\gamma}}{\gamma}$$

We deduce that $\frac{\mathcal{J}_x}{x\mathcal{J}_{x,x}} = \frac{1}{\gamma - 1}$ and $\frac{\mathcal{J}_{x,\pi}}{x\mathcal{J}_{x,x}} = \frac{1}{\gamma - 1} \frac{\partial_{\pi} h\left(t,\pi\right)}{h\left(t,\pi\right)}$. However, in this case we cannot use the method from the previous section³⁸, because the unconstrained optimizer itself depends on $B\left(t\right)$ and $C\left(t\right)$, whose functional forms are unknown. Instead, we solve the problem numerically with Howard's policy-iteration algorithm, as described in Section 3.3 on page 47. As the x-separability holds when there are no contributions, we work directly with the PDE for $h\left(t,\pi\right)$. At each time step t, we proceed in two steps:

• Policy evaluation Given a fixed control $\nu = (\alpha, \beta)$, we solve the PDE backward in time using an implicit scheme:

$$\gamma \left(\nu_t^{\top} \theta_t + r_t - \varrho \pi + \frac{1}{2} \left(\gamma - 1 \right) \left(\nu_t^{\top} \Sigma_t \nu_t \right) \right) h \left(t, \pi \right) + \partial_t h \left(t, \pi \right)$$

$$+ \left(\kappa \left(\pi_{\infty} - \pi_t \right) + \gamma \left(\nu_t^{\top} \zeta_t \right) \right) \partial_{\pi} h \left(t, \pi \right) + \frac{1}{2} \left(\sigma_t^{(\pi)} \right)^2 \partial_{\pi}^2 h \left(t, \pi \right) = 0$$
 (26)

• Policy improvement With the updated function $h(t, \pi)$, we solve the constrained maximization program:

$$\nu_{t}^{\star} = \arg\max \frac{1}{2} (\gamma - 1) h(t, \pi) \left(\nu_{t}^{\top} \Sigma_{t} \nu_{t}\right) + \left(h(t, \pi) \theta_{t}^{\top} + \partial_{\pi} h(t, \pi) \zeta_{t}^{\top}\right) \nu_{t}$$
s.t. $\nu_{t} \in \Omega$ (27)

³⁸Namely, first computing the unconstrained optimizer and then obtaining the constrained one via a projected gradient descent approach.

We iterate these two steps until convergence for each time step t. The numerical procedure used to implement Howard's policy-iteration method is detailed in Appendix A.19.

4.4 Empirical results

The optimal portfolio weights can be expressed as the sum of two components:

$$\begin{pmatrix} \alpha_t^{\star} \\ \beta_t^{\star} \end{pmatrix} = \underbrace{\frac{1}{1 - \gamma} \Sigma_t^{-1} \theta_t}_{\text{Market portfolio}} + \underbrace{\mathcal{H}_t^{(\pi)} \times \frac{1}{1 - \gamma} \Sigma_t^{-1} \zeta_t}_{\text{Hedging component}}$$

The first term represents myopic demand and corresponds to the standard mean-variance allocation based on current asset return dynamics. This component ignores potential future changes in the economic environment. The second term captures intertemporal hedging demand and reflects the investor's desire to hedge against the adverse impact of future changes in inflation π , either on asset return dynamics or on the real discounting of wealth. This hedging term is the product of the sensitivity factor $\mathcal{H}_t^{(\pi)}$ and the LHP.

In this section, we focus on the case with no contributions ($c_t = 0$). We solve the partial differential equation governing $h(t, \pi)$ numerically using Howard's policy-iteration algorithm. The parameters used in the base case are as follows:

- Risky asset S_t : $\mu_t = 5\%$, $\sigma_t = 10\%$.
- Inflation-sensitive asset R_t : $a_t = 5\%$, $\sigma'_t = 10\%$.
- Risk-free asset: $r_t = 2\%$.
- Inflation process: the parameters are long-term mean $\pi_{\infty}=2\%$, volatility $\sigma_t^{(\pi)}=3\%$, and mean-reversion rate³⁹ $\kappa=0.25$.

First, we examine the impact of the discount factor on the hedging demand $\mathcal{H}_t^{(\pi)}$. Next, we fix the scaling parameter at $\varrho=1$ and analyze the relationship between the hedging demand and the parameters of the inflation process. Finally, we introduce a decreasing risk-aversion coefficient γ and impose portfolio constraints to obtain more realistic results. We also vary the correlation ρ_t between the two risky assets, and the correlations $\rho_t^{(S)}$ and $\rho_t^{(R)}$ between asset returns and inflation shocks to assess their respective effects on portfolio behavior.

4.4.1 Understanding the hedging demand

In this section, we examine how the discounting factor affects the hedging demand. To this end, we consider two cases: (i) maximizing the utility of nominal terminal wealth ($\varrho=0$), and (ii) maximizing the utility of discounted terminal wealth ($\varrho=1$). To gain additional insights, we combine these cases with two specifications for the parameter b:

- 1. b = 0The expected returns of the two risky assets are independent of inflation.
- 2. b = 0.5The expected return of asset R_t increases with inflation.

We set the remaining parameters as follows: $\rho_t = 0$, $\rho_t^{(S)} = 0.5$, $\rho_t^{(R)} = 0.5$, and $\gamma = -3$.

 $^{^{-39}}$ A mean-reversion speed of $\kappa = 0.25$ corresponds to a half-life of approximately 2.77 years.

We begin with $b_t=0$ and $\varrho=0$, implying that the expected returns of the two risky assets are independent of inflation. Thus, the market portfolio $\frac{1}{1-\gamma}\Sigma_t^{-1}\theta_t$ equals (75%, 75%) for any value of π , and the liability-hedging portfolio $\frac{1}{1-\gamma}\Sigma_t^{-1}\zeta_t$ equals (3.75%, 3.75%). The hedging component depends on the hedging demand $\mathcal{H}_t^{(\pi)}=\partial_\pi \ln h(t,\pi)$. As shown in Section 4.2.3 on page 64, when $b_t=0$ and $\varrho=0$, we have $\mathcal{H}_t^{(\pi)}=0$. Therefore, regardless of the values of π , ρ_t , $\rho_t^{(S)}$, or $\rho_t^{(R)}$, there is no hedging demand, and the optimal portfolio reduces to:

$$\begin{pmatrix} \alpha_t^{\star} \\ \beta_t^{\star} \end{pmatrix} = \frac{1}{1 - \gamma} \Sigma_t^{-1} \theta_t = \begin{pmatrix} 75\% \\ 75\% \end{pmatrix}$$

However, when $\varrho \neq 0$, the hedging demand becomes non-zero and can be expressed as follows:

$$\mathcal{H}_t^{(\pi)} = \varrho \gamma \left(\frac{e^{\kappa(t-T)} - 1}{\kappa} \right)$$

This expression shows that the hedging demand decreases over time:

- as $t \longrightarrow T$, $\mathcal{H}_t^{(\pi)} \longrightarrow 0$;
- as $t \longrightarrow t_0$ and T becomes large, $\mathcal{H}_t^{(\pi)} \longrightarrow -\varrho \kappa^{-1} \gamma$.

Setting $\varrho=1$ yields $-\varrho\kappa^{-1}\gamma=12$, so the hedging component $\mathcal{H}_t^{(\pi)}$ converges to $12\times (3.75\%, 3.75\%)=(45\%, 45\%)$, as reported in Table 20. Importantly, this value is independent of π .

Table 20: Behavior of the hedging component over time

Asset	Market			I	Hedging c	omponen	ıt		
Asset	portfolio	t = 30	t = 40	t = 50	t = 55	t = 57	t = 58	t = 59	t = 60
S_t	75.0%	45.0%	44.7%	41.3%	32.1%	23.7%	17.7%	10.0%	0.0%
R_t	75.0%	45.0%	44.7%	41.3%	32.1%	23.7%	17.7%	10.0%	0.0%

From an economic standpoint, the intuition is straightforward. The hedging component provides protection against adverse future changes where "adverse" depends on the context. In this case, even though the expected returns of both assets are independent of inflation (b=0), the investor maximizes real terminal wealth, which is directly affected by the inflation path through the discounting factor. An unexpected rise in inflation constitutes a negative shock, because it erodes real purchasing power via the discounting term $-\varrho\pi$ and reduces the growth rate of real wealth. To hedge against this risk, the investor optimally tilts the portfolio toward assets whose returns are positively correlated with inflation. These assets increase in value when inflation rises unexpectedly, thereby offsetting some of the loss caused by higher real discounting. This mechanism explains why the optimal policy recommends increased exposure to assets that co-move positively with inflation shocks.

Now consider the case $b_t=0.5$. The market portfolio $\frac{1}{1-\gamma}\Sigma_t^{-1}\theta_t$ changes with π , while the liability-hedging portfolio $\frac{1}{1-\gamma}\Sigma_t^{-1}\zeta_t$ remains constant at (3.75%, 3.75%). When $\varrho=0$, the investor maximizes the utility of nominal terminal wealth. In this case, hedging demand arises solely from the effect of inflation on the investment opportunity set (i.e., the dynamics of asset returns), rather than from real discounting. When $b_t>0$, a higher inflation rate

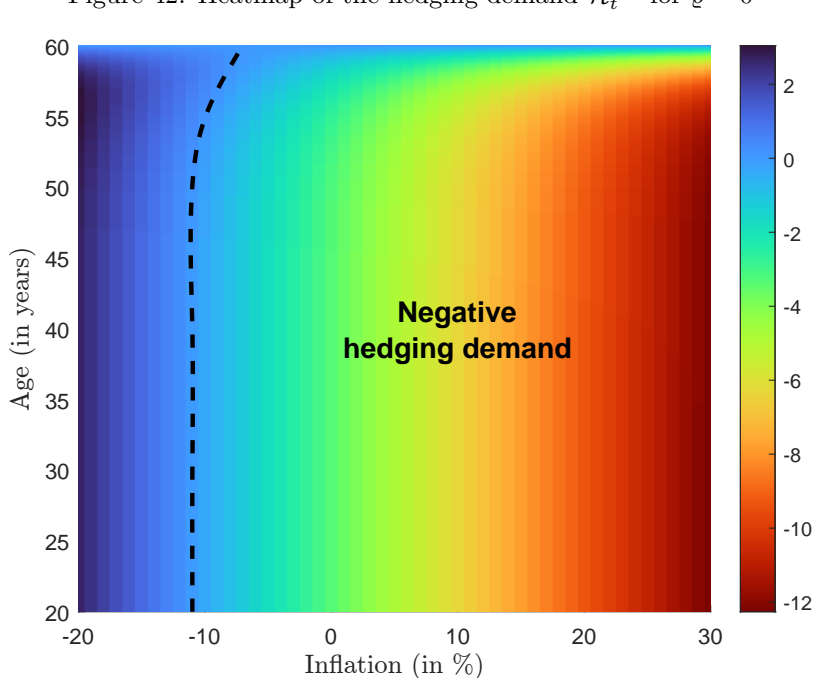
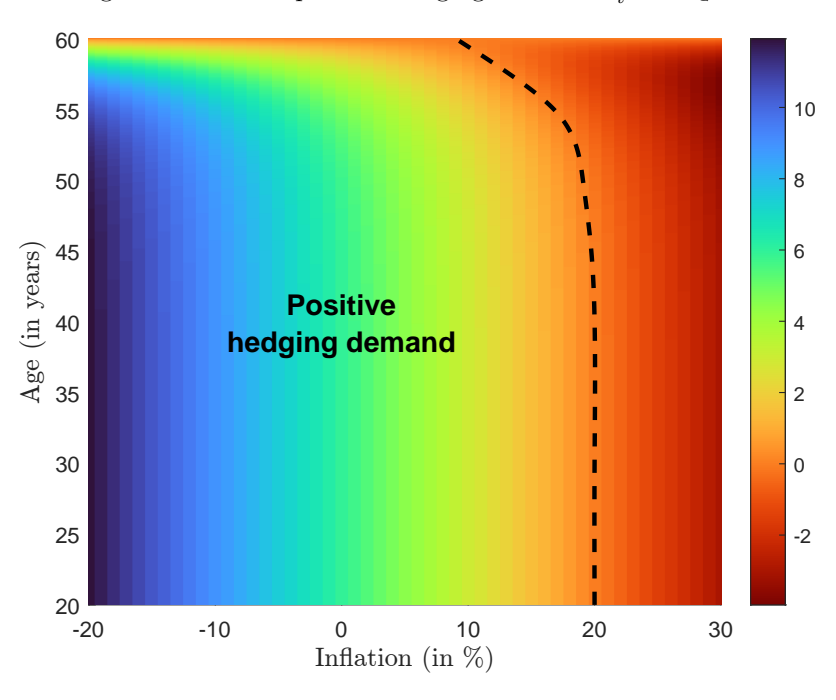


Figure 42: Heatmap of the hedging demand $\mathcal{H}_t^{(\pi)}$ for $\varrho=0$





 π increases the expected return of asset R_t . Consequently, the market portfolio increases its allocation to R_t . The main intertemporal risk then becomes an unexpected decline in π , which lowers the future expected excess return of R_t . To hedge against this risk, the hedging component should take positions that profit when π falls. Since risky assets are positively correlated with inflation shocks ($\rho_t^{(S)} = \rho_t^{(R)} = 0.5$), negative inflation shocks tend to depress their returns. As a result, the intertemporal hedging component adopts a short exposure along $\frac{1}{1-\gamma}\Sigma_t^{-1}\zeta_t$, which makes $\partial_\pi \ln h(t,\pi)$ markedly negative across most values of π (see Figures 42 and Table 21). However, when π becomes very negative, the expected return of R_t turns negative. In this situation, the market portfolio already shorts the asset R_t . In particular, when $\pi \leq -12\%$ and $\mu_t' \leq -\mu_t$, the short position in R_t can exceed the long position in S_t , leaving the aggregate portfolio net short to inflation shocks. In this case, the adverse future change is an unexpected increase in π . To hedge this risk, the intertemporal hedging demand reverses sign. $\partial_\pi \ln h(t,\pi)$ becomes positive when $\pi \leq -12\%$, adding a long position in the hedging component that benefits from an unexpected rebound in inflation.

	$\rho = 0$					$\rho = 1$				
π	-10%		_	5%	10%	-10%	_	-10%	5%	10%
t = 30	-0.3	-1.8	-3.3	-4.8	-6.3	8.9	7.5	6.0	4.5	3.0
t = 40	-0.3	-1.8	-3.3	-4.8	-6.3	8.9	7.4	6.0	4.5	3.0
t = 50	-0.2	-1.7	-3.2	-4.7	-6.2	8.7	7.2	5.7	4.2	2.8
t = 55	0.2	-1.3	-2.7	-4.1	-5.6	7.6	6.2	4.8	3.3	1.9
t = 57	0.4	-0.8	-2.1	-3.4	-4.7	6.2	5.0	3.7	2.4	1.1
t = 58	0.5	-0.6	-1.6	-2.7	-3.8	5.0	3.9	2.8	1.7	0.7
t = 59	0.4	-0.3	-1.0	-1.7	-2.4	$\frac{1}{1}$ 3.0	2.3	1.6	0.9	0.2
t = 60	0.0	0.0	0.0	0.0	0.0	0.0	0.0	0.0	0.0	0.0

Table 21: Values of the hedging demand $\mathcal{H}_{t}^{(\pi)}$ ($\varrho = 0$ vs. $\varrho = 1$)

When $\varrho=1$, the current hedging demand reflects the impact of inflation on both real discounting and its impact on the investment opportunity set. As previously shown, the discounting channel makes an unexpected rise in inflation detrimental to real wealth, pushing $\partial_{\pi} \ln h \left(t, \pi \right)$ positive. Conversely, when $b_t > 0$ and π is not too negative, an unexpected decline in π lowers the future expected return of R_t , which pushes $\partial_{\pi} \ln h \left(t, \pi \right)$ negative. Therefore, the overall hedging demand depends on the balance between these two effects and the current level of inflation. It also varies with the time remaining until the target date, since $\partial_{\pi} \ln h \left(t, \pi \right)$ gradually converges to zero as the retirement date approaches. In this case, $\partial_{\pi} \ln h \left(t, \pi \right)$ is predominantly positive across most inflation levels (see Figures 43 and Table 21). However, it can turn negative when π becomes very high, because the effect of the opportunity set dominates. In that regime, since the market portfolio tilts strongly toward R_t , the hedging component partially offsets this exposure.

4.4.2 Sensitivity analysis of the hedging demand

In the following analysis, we set $b_t = 0.5$ and $\varrho = 1$. We then examine how the hedging demand $\mathcal{H}_t^{(\pi)}$ depends on the key inflation parameters: the mean-reversion rate κ , the long-term inflation rate π_{∞} , the inflation volatility $\sigma_t^{(\pi)}$, and the inflation correlation $\rho_t^{(\pi)} = \rho_t^{(S)} = \rho_t^{(R)}$. Two distinct cases must be considered. The drift parameters κ and π_{∞} affect only the hedging demand, while the risk parameters $\sigma_t^{(\pi)}$ and $\rho_t^{(\pi)}$ influence both the hedging demand and the liability-hedging portfolio.

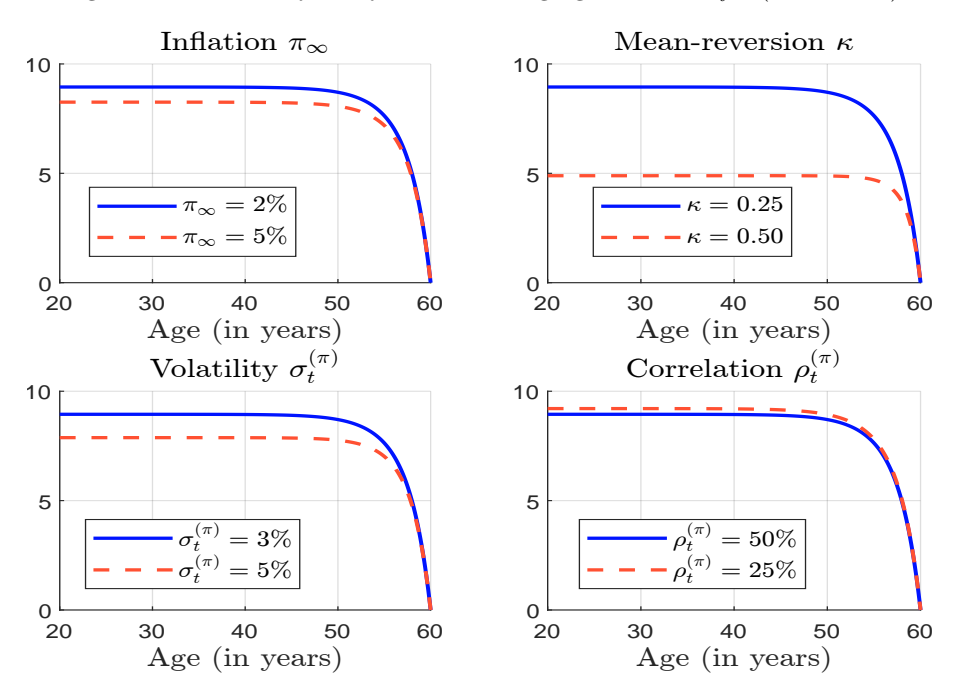
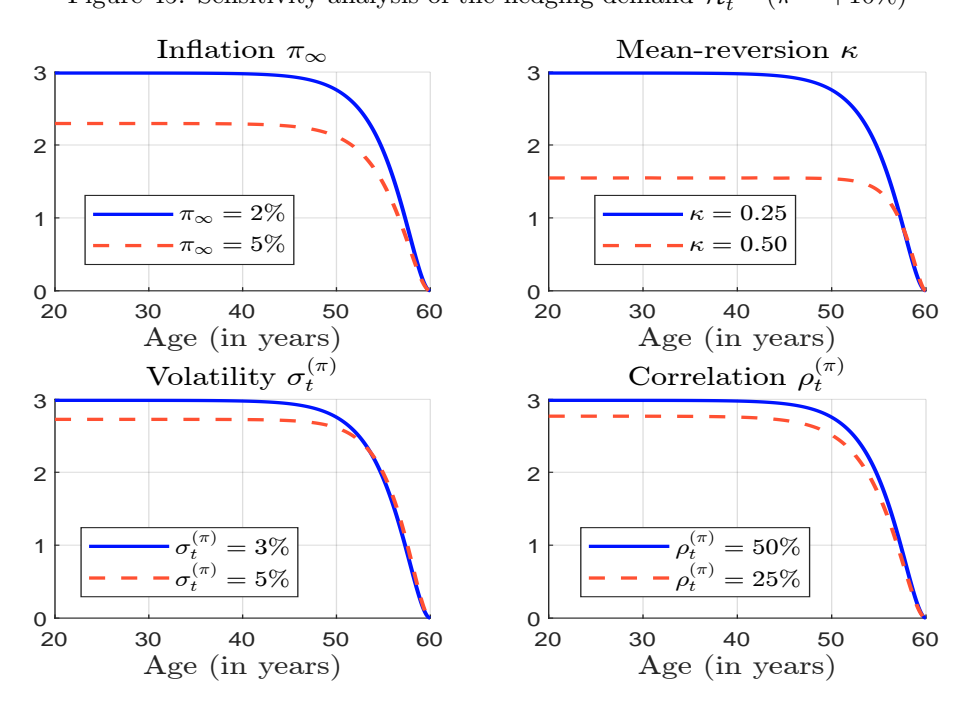


Figure 44: Sensitivity analysis of the hedging demand $\mathcal{H}_t^{(\pi)}$ $(\pi=-10\%)$





As discussed earlier, the sign and magnitude of $\mathcal{H}_t^{(\pi)}$ are determined by the interplay between the real-discounting effect and the opportunity-set effect. When κ increases, inflation shocks become less persistent, causing inflation to more rapidly revert to its long-term mean π_{∞} . As a result, both effects are dampened and the absolute value $\|\mathcal{H}_t^{(\pi)}\|$ decreases, as illustrated in Figures 44 and 45. However, the influence of π_{∞} on the hedging demand differs. When $b_t > 0$ and asset returns are positively correlated with inflation shocks, a higher π_{∞} increases the expected return of R_t . Consequently, an unexpected decline in inflation becomes more costly, making inflation risk more important to hedge. This drives $\mathcal{H}_t^{(\pi)}$ downward. Taken together, these effects imply that total hedging demand declines as π_{∞} rises, as shown in Figures 44 and 45.

The impact of the inflation volatility $\sigma_t^{(\pi)}$ is qualitatively similar to that of π_{∞} . As $\sigma_t^{(\pi)}$ increases, the opportunity-set component of the hedging demand dominates the real-discounting component, leading to a lower total hedging demand $\mathcal{H}_t^{(\pi)}$ under our calibration. However, we note that the actual hedging weights in the portfolio equal the product of the hedging demand and the LHP. Since the LHP is proportional to ζ_t , the hedging weights increase with $\sigma_t^{(\pi)}$. Therefore, even though $\mathcal{H}_t^{(\pi)}$ declines, the overall hedge in portfolio weights can still increase as $\sigma_t^{(\pi)}$ rises. Changes in the inflation correlation $\rho_t^{(\pi)}$ have only a minor direct effect on the hedging demand $\mathcal{H}_t^{(\pi)}$. However, as with $\sigma_t^{(\pi)}$, variations in $\rho_t^{(\pi)}$ strongly affect the LHP because the weights are proportional to $\rho_t^{(\pi)}$. Consequently, an increase in $\rho_t^{(\pi)}$ generally leads to a higher overall hedging component.

4.4.3 Shape of the glide path

In the following analysis, we consider a realistic, time-varying risk-aversion parameter γ_t which decreases over time⁴⁰ as in the previous section. The asset parameters are specified as follows. For the risky asset S_t , we have $\mu_t = 5\%$ and $\sigma_t = 10\%$. For the inflation-sensitive asset R_t , we use $a_t = 5\%$, $b_t = 0.5$, and $\sigma_t' = 10\%$. The risk-free rate is fixed at $r_t = 2\%$. Inflation follows a mean-reverting process with a long-term mean of $\pi_\infty = 2\%$, a volatility of $\sigma_t^{(\pi)} = 1\%$, and a mean-reversion rate of $\kappa = 0.25$. The investor's objective is to maximize real terminal wealth with $\varrho = 1$. To ensure a feasible portfolio, we impose long-only and no-leverage constraints:

$$\Omega = \left\{ \alpha, \beta \in \mathbb{R}^2 : \alpha \ge 0, \beta \ge 0, \alpha + \beta \le 1 \right\}$$

In this example, the optimal dynamic allocation $\nu_t^* = (\alpha_t^*, \beta_t^*)$ is influenced not only by expected returns, the covariance structure, and correlations with inflation, but also by the discount factor, portfolio constraints, time-varying risk aversion, and the evolution of the hedging demand. Consequently, optimal allocations may differ substantially across scenarios.

First, we consider a benchmark case in which both assets are uncorrelated with inflation (i.e., $\rho_t = 0$, $\rho_t^{(S)} = 0$, and $\rho_t^{(R)} = 0$). In this case, since the liability-hedging portfolio is (0%, 0%), the hedging component is null. Figure 46 illustrates the optimal allocations to the two assets for different values of π . When π is highly negative, the expected return of R_t is also negative, and the portfolio is allocated almost entirely to the risky asset S_t . As π approaches 0%, assets R_t and S_t exhibit similar expected returns, resulting in roughly equal allocations. When π continues to increase, the weight on R_t rises and the overall portfolio becomes more aggressive as both S_t and R_t become more attractive than the risk-free asset.

 $^{^{40}\}gamma_0 = 1/3$, $\gamma_T = -50$, and k = 0.05 (see Footnote 24 on page 39).

Figure 46: Dynamic asset allocation ν_t^{\star} including the inflation hedging ($\rho_t = 0$, $\rho_t^{(S)} = 0$, and $\rho_t^{(R)} = 0$)

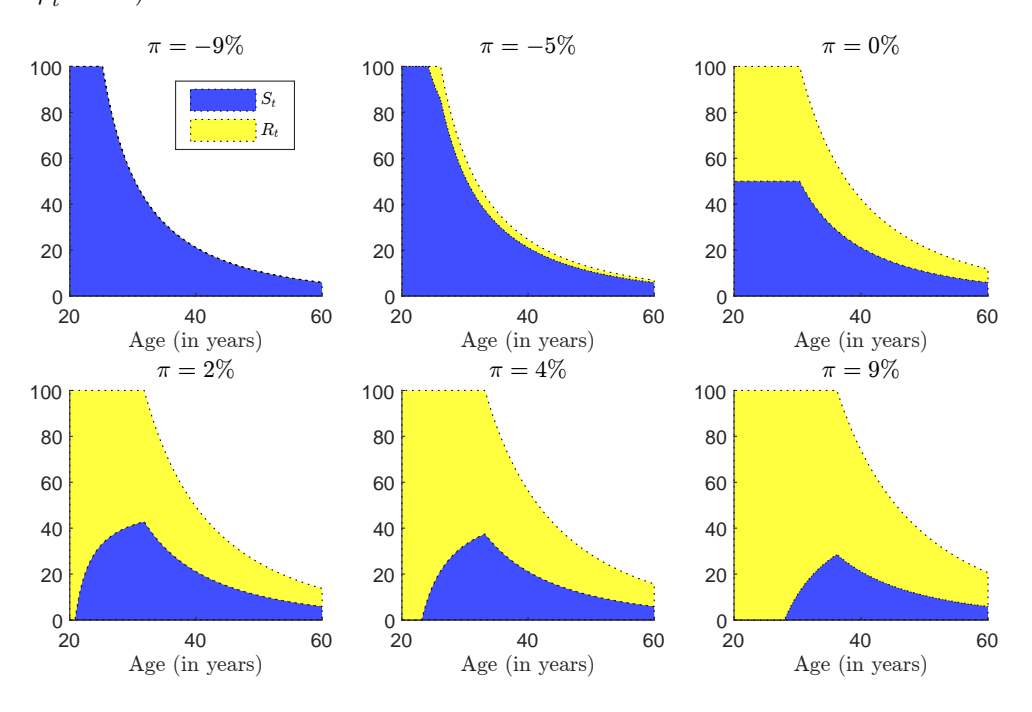


Figure 47: Dynamic asset allocation ν_t^{\star} including the inflation hedging ($\rho_t=0,\,\rho_t^{(S)}=0.5,$ and $\rho_t^{(R)}=0.5$)

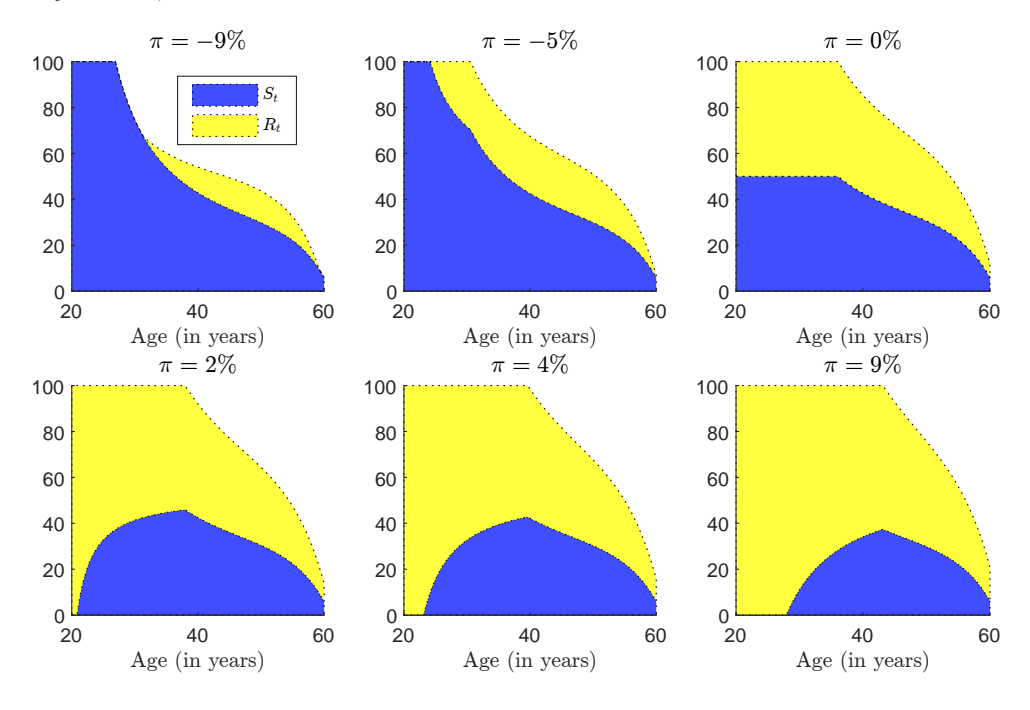


Figure 48: Dynamic asset allocation ν_t^{\star} including the inflation hedging ($\rho_t = 0.5$, $\rho_t^{(S)} = 0.5$, and $\rho_t^{(R)} = 0.5$)

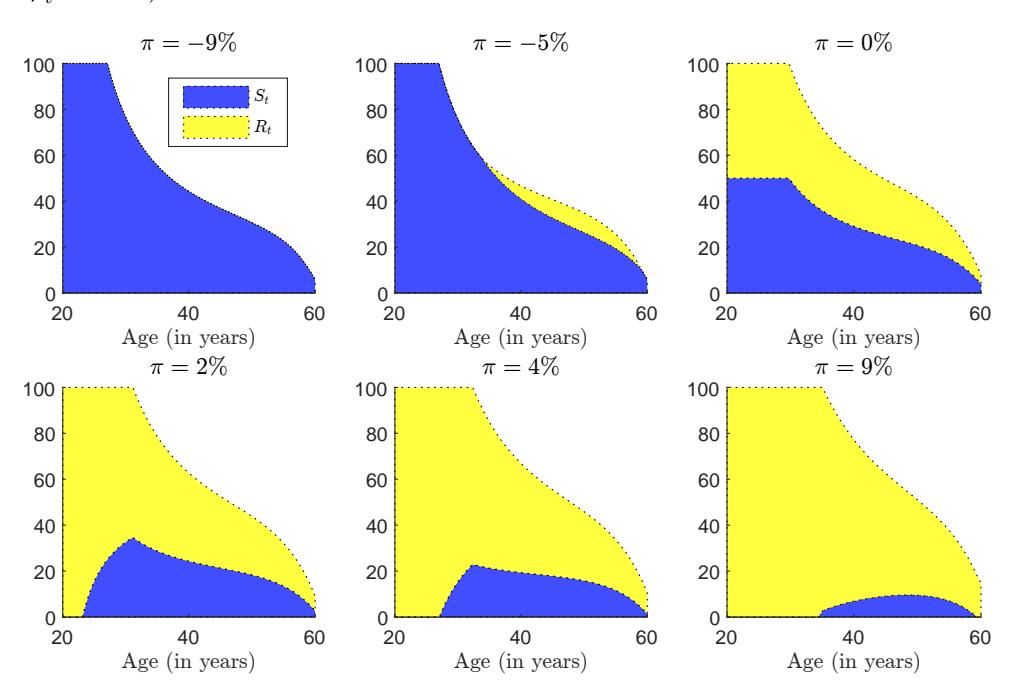


Figure 49: Dynamic asset allocation ν_t^{\star} including the inflation hedging ($\rho_t=0,\,\rho_t^{(S)}=-0.5,\,$ and $\rho_t^{(R)}=0.5)$

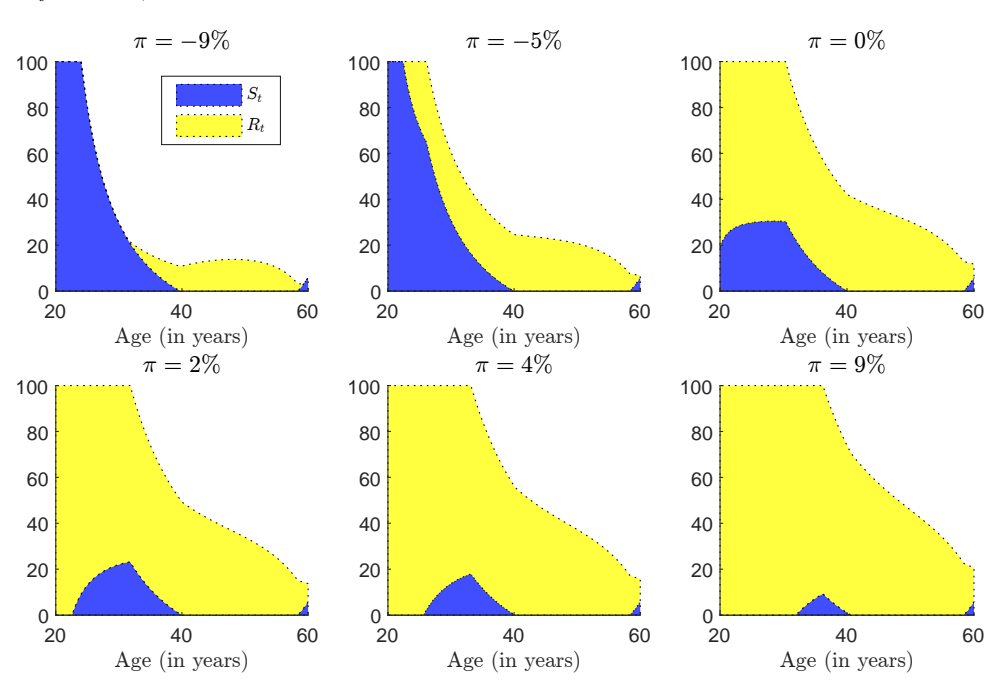


Figure 47 presents the case $\rho_t^{(S)} = 0.5$ and $\rho_t^{(R)} = 0.5$. Unlike the benchmark, the liability-hedging portfolio is now strictly positive. As discussed earlier, the hedging component offsets both real-discounting risk and opportunity-set risk. In this case, the discountingdriven component dominates, resulting in a more aggressive portfolio than in the benchmark case. A larger allocation to risky assets helps hedge inflation risk to real wealth. Notably, the glide path becomes concave as the target date approaches, reflecting the evolution of the hedging component over time. In the case of strongly negative inflation, the expected return of R_t remains low, and S_t continues to dominate the allocation. However, a non-zero position in R_t is maintained for hedging purposes, and the magnitude is also shaped by the time-varying risk-aversion parameter γ_t . When π approaches 0%, assets R_t and S_t have similar expected returns and identical hedging demands, leading to roughly equal allocations between the two assets. When the two assets are positively correlated with each other and with inflation, the benefits of diversification diminish. Figure 48 considers the case in which all three correlations are positive: $\rho_t = 0.5$, $\rho_t^{(S)} = 0.5$ and $\rho_t^{(R)} = 0.5$. Compared to Figure 47, portfolio allocations become more concentrated in the asset with the higher expected performance at a given inflation level: the risky asset S_t when π falls, and the inflation-sensitive asset R_t when π rises. Figure 49 examines the case in which the two assets have opposite correlations with inflation shocks: $\rho_t^{(S)} = -0.5$ and $\rho_t^{(R)} = 0.5$. In this configuration, the liability-hedging portfolio has opposite signs for the two assets. The hedging component strongly favors the inflation-sensitive asset R_t , while penalizing the risky asset S_t . Compared to Figure 47, Figure 49 exhibits a higher allocation to R_t and a lower allocation to S_t across all values of π . Under long-only, no-leverage constraints, the preference to short S_t manifests as a corner solution, with a frequently bounded weight at zero. Meanwhile, R_t often absorbs most of the portfolio allocation. When inflation is strongly negative, the expected return of R_t becomes very low, prompting a temporary shift toward S_t , despite its negative discounting-driven hedge component. Nevertheless, a positive position in R_t is maintained for hedging purposes, and its size is determined by the time-varying risk-aversion parameter γ_t . Around $\pi = 0\%$, the expected returns of assets R_t and S_t are similar, but the hedging component are opposite: negative for S_t and positive for R_t . This causes R_t to dominate the allocation, while the weight on S_t remains small. At higher inflation levels, the market portfolio and hedging components favor R_t , causing the portfolio to concentrate on R_t for most of the time horizon and constraining S_t near zero. As the target date approaches, intertemporal hedging demand converges to zero. Consequently, the weight on S_t increases, and the dynamic allocation aligns with the market portfolio at retirement.

4.5 Inflation, risk premium, and correlation

We previously identified three primary channels through which inflation influences portfolio construction:

- Market portfolio Inflation affects asset risk premia, which depend themselves on the prevailing inflation level, thereby influencing expected returns on the market portfolio.
- Liability-hedging portfolio

 The volatility of inflation and its correlations with various assets shape the composition
 and effectiveness of the liability-hedging portfolio.
- Hedging demand
 The discounting factor and all inflation-related parameters jointly drive the investor's intertemporal hedging demand, which adjusts portfolio exposures dynamically over time.

The relationship between inflation, asset returns, and their correlations has been extensively studied in the financial literature⁴¹. However, drawing consensus conclusions remains challenging, particularly when attempting to disentangle the three effects listed above.

Inflation risk plays a pivotal role in shaping expected returns, especially for asset classes that are sensitive to changes in the price level. This issue emerged as a central topic during the 1970s, a period of high inflation, when a growing literature sought to understand how asset prices incorporate inflation expectations and the effectiveness of different assets as inflation hedges (Roll, 1973). One key contribution came from Hagerman and Kim (1976), who developed a model showing how inflation uncertainty introduces an additional risk dimension for which investors require compensation. These papers paved the way for considering inflation as a systematic risk factor and influenced subsequent developments in multi-factor models that incorporate macroeconomic variables. A crucial step forward was taken by Fama and Schwert (1977), who distinguished between expected and unexpected inflation:

"We estimate the extent to which various assets were hedges against the expected and unexpected components of the inflation rate during the 1953–1971 period. We find that U.S. government bonds and bills were a complete hedge against expected inflation, and private residential real estate was a complete hedge against both expected and unexpected inflation. [...] The most anomalous result is that common stock returns were negatively related to the expected component of the inflation rate, and probably also to the unexpected component." (Fama and Schwert, 1977, page 115).

Following this seminal work, inflation hedging and covariance risk became central questions during the 1980s. For instance, Bodie (1982) concluded that an increase in inflation uncertainty lowers the risk premia on real assets. Simultaneously, considerable attention was paid to equity behavior and inflation-hedging properties. By the early 1980s, a consensus emerged that a negative relationship exists between stock returns and inflation components expected inflation, changes in expected inflation, and unexpected inflation (Fama, 1981; Geske and Roll, 1983; Stulz, 1986). However, Kaul (1987) challenged this view by demonstrating that nominal assets, such as equities and bonds, have complex and time-varying correlations with inflation, impacting the associated risk premia. Following this contribution, researchers increasingly recognized that the relationship between asset returns and inflation is not stable but instead depends on various factors, for instance the macroeconomic regime 42 (Brière and Signori, 2012; Campbell et al., 2020; Leombroni et al., 2020). Moreover, much of the subsequent literature concluded that conventional financial assets, particularly publicly traded equities, provide poor hedges against inflation⁴³ (Bekaert and Wang, 2010: Ang et al., 2012). In this context, the search for effective inflation hedges has expanded toward alternative assets such as real estate, gold, and commodities. Among these, Amenc et al. (2009) find that real estate and commodities display particularly favorable inflation-hedging properties. Alsati-Morad et al. (2016) confirm these findings and identify infrastructure as another promising candidate for constructing inflation-hedging portfolios. However, these results should be interpreted with caution, as inflation-hedging effectiveness often depends on the investment horizon and is mainly valid over very long time horizons (Brown et al., 2025).

⁴¹See for example Roll (1973); Hagerman and Kim (1976); Fama and Schwert (1977); Bodie (1982); Stulz (1986); Kaul (1987); Bekaert and Wang (2010); Leombroni et al. (2020); Cieslak and Pflueger (2023).

⁴²This issue is closely related to the broader question of asset correlations, especially the stock-bond correlation (Li, 2002; Burkhardt and Hasseltoft, 2012; Portelli and Roncalli, 2024).

⁴³According to Sathyanarayana and Gargesa (2018), this result is region-dependent, with certain markets exhibiting stronger inflation-hedging capacities than others.

5 Conclusion

This paper develops a comprehensive framework for retirement accumulation strategies, bridging the gap between financial theory and practical implementation. By extending the classical Merton model to include human capital, multiple asset classes, inflation risk, and real-world constraints, we provide a solid theoretical foundation and empirical evidence for optimal lifecycle investing. Although this research does not prescribe a fully implementable real-life accumulation strategy, its key findings provide valuable guidelines for understanding and improving current practices in the asset management industry. The contribution of this work is primarily analytical. We develop the theoretical infrastructure necessary to evaluate and improve existing retirement investment approaches. Rather than advocating a one-size-fits-all solution, we show that effective retirement strategies must be context-specific while remaining grounded in sound theoretical principles.

Our model is a simplified yet robust version of the framework proposed by Bruder et al. (2012). These authors assumed that individual investor contributions are stochastic and used the zero-coupon bond maturing at retirement age as the numéraire. In contrast, our model treats continuous individual contributions as deterministic and uses the risk-free asset as the numéraire⁴⁴. We determine the optimal exposure to risky assets and provide a precise definition of the glide path as the expected dynamic allocation over time. Our analysis demonstrates that optimal risky asset allocation depends on four critical factors: the human-to-financial capital ratio, risk aversion, investment horizon, and prevailing market parameters. Our framework also shows that continuous contributions systematically increase the allocation to risky assets compared with the original constant-mix strategy of Merton (1969, 1971). These findings reconcile the intuitive age-based glide path with rigorous financial theory by recognizing that total wealth encompasses both financial capital and the present value of future contributions. Thus, the concept of human capital is fundamental to designing effective accumulation retirement strategies. Despite its simplified structure, our model successfully reproduces most of the key findings from the existing literature on this subject, particularly the principles established by Bruder et al. (2012). The following summarizes how different factors influence the optimal share of risky assets in the portfolio⁴⁵. The intuition behind these effects can be explained as follows:

#1 Retirement horizon

Young investors should hold a larger percentage of risky assets. This principle underlies the design of target date funds, though our interpretation differs. Younger individuals typically anticipate substantial non-financial income, such as labor income, in the future, which acts as a buffer. Therefore, they can take on more financial risk because potential losses may be offset by future contributions before retirement.

#2 Risk aversion

The allocation is fundamentally driven by individual risk preferences. Risk-averse individuals allocate a smaller percentage of their expected total wealth to risky assets, whereas risk-tolerant individuals allocate a larger percentage.

#3 Current wealth & expected future income

The optimal allocation to risky assets increases when current wealth is low relative to expected future income. Since total expected retirement wealth includes current savings and future contributions, a high expected income justifies taking on more risk

⁴⁴This risk-free asset is a combination of cash and the zero-coupon bond. For computational simplicity, we approximate it using cash alone. This approximation means that contributions become implicitly stochastic when expressed in terms of the bond numéraire.

 $^{^{45}\}mathrm{With}$ our model, we retrieve Principles #1 to #5.

Table 22: Main principles of retirement accumulation strategies

Rule	More risky assets		Fewer risky assets
#1	Young	>	Old
#2	Risk taker	>	Risk averse
#3	Low current wealth	>	High current wealth
#4	High expected future income	>	Low expected future income
#4'	High human capital	>	Low human capital
#5	High risk premium	>	Low risk premium
#6	Low risky-asset volatility	>	High risky-asset volatility
#7	Positive stock/bond correlation	>	Negative stock/bond correlation
#8	Certain income	>	Uncertain income
#9	Income uncorrelated with equities	>	Income correlated with equities

Source: Adapted from Bruder et al. (2012).

today. However, many professional allocation models surprisingly ignore this effect, treating current wealth and future income as irrelevant. Our analysis highlights an important distinction. In the retirement context, human capital should be viewed not as the present value of future income (or a fraction thereof), but rather as the present value of future contributions. In other words, human capital reflects not only the investor's earning potential but also their willingness to channel part of that income to retirement savings. This is a key departure from the framework of Bruder et al. (2012).

#4 Risk premium & volatility

A higher risk premium raises the expected return on risky assets, increasing their attractiveness and optimal allocation. Conversely, for a given Sharpe ratio, the risky allocation is inversely related to volatility.

#5 Correlation between equities and bonds

In the context of pensions, bonds are essentially risk-free because they guarantee a fixed payout upon retirement. When equities and bonds are positively correlated, the volatility of their forward value decreases. This allows for a higher equity allocation while maintaining the same overall risk level.

#6 Income uncertainty

Greater uncertainty in future income reduces the optimal equity share because variability in income introduces additional risk to total retirement wealth. Therefore, a more conservative portfolio is necessary.

#7 Correlation between future income and equities

If future income is highly correlated with stock market performance (e.g., wages in the financial sector), it is advisable to reduce exposure to the stock market. A downturn in equities could simultaneously erode capital and labor income, amplifying losses.

Our analysis solves a fundamental puzzle in retirement planning. Why do practitioners implement concave glide paths when theory predicts convex allocation patterns? We demonstrate that three critical factors⁴⁶ transform the theoretically optimal convex path into the concave path observed in practice⁴⁷. First, leverage constraints prevent retail investors from achieving the extreme allocations that would be optimal for young investors with high human-to-financial capital ratios. Unable to access optimal leveraged positions, these investors must increase their exposure to risky assets over a longer time horizon to achieve similar risk-adjusted outcomes. Second, time-varying risk aversion, especially when following a concave profile, causes an accelerating shift toward conservative investments as retirement approaches. This behavioral pattern reflects the empirical observation that risk aversion increases with age. Younger investors typically have a higher risk tolerance than older investors, who prioritize capital preservation as retirement approaches⁴⁸. Third, the increasing contribution patterns typical of real-world careers induce additional concavity in the human capital component. This factor is readily observable. As investors approach retirement, they become concerned about retirement adequacy and substantially increase their savings rates to improve their future pension prospects. In other words, a 50-year-old investor is generally far more focused on retirement planning than a 30-year-old investor, resulting in accelerating contribution patterns that create the observed concave glide path structure. By incorporating these factors, our framework reconciles theoretical predictions with observed practice. It provides portfolio managers with a rigorous foundation for designing glide paths that align optimal allocation principles with behavioral and institutional realities.

This study extends the framework beyond a single-asset setting to provide a detailed comparison of single- and multi-asset approaches. It highlights how allocation constraints shape optimal portfolio construction and underscores the diversification benefits of broader investment universes. In the single-asset framework, the allocation problem is divided into two steps: a mean-variance optimization subproblem and a leverage calibration subproblem. In contrast, the multi-asset framework unifies these two steps into one optimization problem. We demonstrate that, under specific assumptions, the two approaches converge. However, in general, the multi-asset framework yields a more diversified solution than the two-step approach of the single-asset framework⁴⁹. To evaluate performance, we perform three empirical analyses. First, we compare glide path strategies with constant-mix approaches and find that dynamic strategies informed by lifecycle considerations offer stronger downside protection and higher probabilities of meeting retirement goals. Second, we examine global and Eurozone investment universes and find compelling evidence for including real assets (private equity, private debt, real estate, and infrastructure) in retirement portfolios. These assets add value through exposure to distinct risk-return drivers, natural inflation hedging, and illiquidity premium that long-term investors are uniquely positioned to capture. In the global universe, including these assets in a 50/50 mixed strategy enhances annualized

⁴⁶In the case of the model with inflation risk, a fourth factor can explain the concavity of the glide path. It corresponds to the impact of the hedging demand.

⁴⁷In addition to identifying the key principles of retirement accumulation strategies and solving this puzzle, our baseline model provides analytical solutions for important variables, such as the human-to-financial capital ratio, risky exposure, the glide path, and wealth dynamics. For instance, we show that the constant-mix strategy is a special case of the retirement accumulation strategy when the human-to-financial capital ratio is set to zero. We also derive closed-form formulas for the glide path that are more robust than those obtained in Bruder et al. (2012). Specifically, we use a third-order Taylor expansion of Jensen's inequality and demonstrate that the solution corresponds to log-normal wealth dynamics.

 $^{^{48}}$ This effect differs from the pattern of decreasing human-to-financial capital ratios.

⁴⁹Our analysis examines the role of cross-correlation in both the one- and two-step approaches. We show that the leverage constraint alters the treatment of cross-correlation, leading to different impacts across the two frameworks.

performance by 87 basis points. In the Eurozone, the improvement is 190 basis points⁵⁰, transforming success rates from approximately 20% to nearly 90% for reasonable return targets. Third, we propose a dynamic liquidity risk management framework that addresses the integration of illiquid assets into lifecycle strategies. We demonstrate that the benefits of real asset inclusion persist even after accounting for transaction costs and liquidity constraints by applying time-varying liquidity weights that gradually shift allocations from illiquid to liquid assets as retirement approaches. For the 80/20 mixed strategy, this approach delivers approximately 15 and 45 basis points of additional annualized performance⁵¹ in the global and Eurozone universes, respectively⁵². This lifecycle consistent evolution reflects changing investor priorities. Younger individuals can sacrifice liquidity for growth, while older investors prioritize flexibility and capital preservation. The resulting dynamic allocation patterns demonstrate sophisticated portfolio management by concentrating on growth-oriented private assets early on before transitioning to income-generating liquid alternatives while maintaining diversification throughout the accumulation phase. Together, these results show that real assets should play a much larger role in retirement accumulation strategies than they currently do in most target-date funds.

Finally, inflation risk emerges as a central concern for retirement savings. By modeling inflation as a stochastic process and incorporating inflation-sensitive assets, we show that portfolios can be divided into two components: a growth-oriented performance portfolio and a liability-hedging portfolio (LHP) designed to preserve purchasing power. This liability-driven investment (LDI) approach, which has long been used in defined benefit plans, is equally relevant for defined contribution systems. However, our analytical solution reveals that the optimal hedging component is not simply the liability-hedging portfolio itself, but rather the product of the LHP and a hedging demand coefficient. While the liability-hedging portfolio depends on conventional risk metrics (risk aversion, asset covariance matrix, inflation volatility, and covariance risk between inflation and asset returns), the hedging demand is more nuanced. It depends critically on two factors: first, the relationship between expected inflation levels and asset risk premia; and second, the investor's objective function, particularly whether they prioritize terminal nominal wealth or real purchasing power. These two forces, the opportunity-set component and the real-discounting component, jointly determine the sign and magnitude of hedging demand. Consequently, the optimal dynamic allocation may entail either a long or short position in the liability-hedging portfolio, depending on which inflation scenario poses the greatest threat to the investment strategy. For instance, high inflation presents a dual challenge. It increases risk premia on certain assets while simultaneously eroding real purchasing power. The opportunity-set effect may generate negative hedging demand if the primary risk is that inflation will revert to its long-term mean, reducing future expected returns. Conversely, the real-discounting effect unambiguously favors positive hedging demand to protect real wealth, implying long exposure to the liability-hedging portfolio. The optimal hedging demand thus reflects the balance between these competing forces, echoing the classical distinction between expected inflation risk and unexpected inflation risk. While constructing the optimal liability-hedging portfolio and precisely estimating hedging demand extends beyond the scope of this study, our framework underscores that understanding asset-inflation relationships must be a cornerstone of defined contribution solutions. In particular, this finding supports the inclusion of alternative assets that can partially hedge adverse inflation scenarios⁵³.

⁵⁰This sharp increase is also driven by the lower expected returns of Eurozone public equities relative to the global universe.

⁵¹These figures do not account for the friction involved in investing during the ramp-up and run-off phases when capital is deployed or withdrawn.

⁵²Conservative transactions costs are estimated at 7.5 and 15 bps for w/o and w/ strategies, respectively.

 $^{^{53}}$ It is illusory to think that inflation can be perfectly hedged by a static exposure on some financial assets.

Maintaining living standards after retirement remains a central challenge. Evidence shows that mandatory public pensions are often insufficient on their own, making supplementary savings essential for securing adequate retirement income. In this context, our findings suggest that the next generation of retirement investment solutions must go beyond simple equity-bond splits and static glide paths. A unified lifecycle framework integrating human capital considerations, real asset allocations, and inflation protection would provide a more comprehensive foundation for modern retirement planning. Evidence indicates the necessity of shifting investment thinking from traditional stock-bond allocations to sophisticated multi-asset strategies that reflect the complexity of lifetime wealth accumulation. For practitioners, the implication is clear: although implementing multi-asset glide paths that incorporate real assets is operationally complex, the substantial gains in risk-adjusted returns and retirement security make this evolution indispensable. For policymakers, the results underscore the importance of regulatory frameworks that facilitate access to diversified investment opportunities within retirement plans rather than restrict them.

Inflation hedging can only be partial and approximate as noticed by Bekaert and Wang (2010): "This article starts by discussing the concept of inflation hedging and provides estimates of inflation betas for standard bond and well-diversified equity indices for over 45 countries. We show that such standard securities are poor inflation hedges. Expanding the menu of assets to Treasury bills, foreign bonds, real estate and gold improves matters but inflation risk remains difficult to hedge.".

References

- ACHARYA, V. V., and PEDERSEN, L. H. (2005). Asset Pricing with Liquidity Risk. *Journal of Financial Economics*, 77(2), pp. 375-410.
- Alsati-Morad, M., Gunzberg, J., Soe, A. M., and Tsui, P. K. (2016). Exploring the Road to Inflation Protection When Energy Fails. S&P Dow Jones Indices, Education Series, 22 pages.
- AMENC, N., MARTELLINI, L., and ZIEMANN, V. (2009). Inflation-hedging Properties of Real Assets and Implications for Asset-liability Management Decisions. *Journal of Portfolio Management*, 35(4), pp. 94-110.
- Amundi Asset Management (2021). Allocating to Real and Alternative Assets: A Framework for Institutional Investors. *Investment Insights Blue Paper*, Avril, 28 pages.
- Ang, A., Brière, M., and Signori, O. (2012). Inflation and Individual Equities. *Financial Analysts Journal*, 68(4), pp. 36-55.
- Antolín, P., and Stewart, F. (2009). Private Pensions and Policy Responses to the Financial and Economic Crisis. *OECD Working Papers on Insurance and Private Pensions*, 36, 39 pages.
- Baltas, I., Dopierala, L., Kolodziejczyk, K., Szczepański, M., Weber, G. W., and Yannacopoulos, A. N. (2022). Optimal Management of Defined Contribution Pension Funds under the Effect of Inflation, Mortality and Uncertainty. *European Journal of Operational Research*, 298(3), pp. 1162-1174.
- BARBERIS, N. (2000). Investing for the Long Run When Returns Are Predictable. *Journal of Finance*, 55(1), pp. 225-264.
- Bekaert, G., and Wang, X. (2010). Inflation Risk and the Inflation Risk Premium. *Economic Policy*, 25(64), pp. 755-806.
- Benartzi, S., and Thaler, R. H. (2013). Behavioral Economics and the Retirement Savings Crisis. *Science*, 339(6124), pp. 1152-1153.
- BJÖRK, T., KHAPKO, M., and MURGOCI, A. (2017). On Time-inconsistent Stochastic Control in Continuous Time. *Finance and Stochastics*, 21(2), pp. 331-360.
- Bodie, Z. (1976). Common Stocks as a Hedge Against Inflation. *Journal of Finance*, 31(2), pp. 459-470.
- Bodie, Z. (1982). Inflation Risk and Capital Market Equilibrium. *Financial Review*, 17(1), pp. 1-25.
- Brière, M., and Signori, O. (2012). Inflation-hedging Portfolios: Economic Regimes Matter. *Journal of Portfolio Management*, 38(4), pp. 43-58.
- Brennan, M. J., and Xia, Y. (2002). Dynamic Asset Allocation under Inflation. *Journal of Finance*, 57(3), pp. 1201-1238.
- Brown, G., Lundblad, C., and Volckmann, W. (2025). Inflation Hedging and Real Assets: Are Public and Private Investments the Same?. *Institute for Private Capital, Working Paper*, 44 pages.

- BRUDER, B., CAUDAMINE, L., DO, H., GISIMUNDO, V., GRANJON, C., and Xu, J. (2023). Optimal Decumulation Strategies for Retirement Solutions, *Amundi Working Paper*, 149, available at *SSRN*, 4652428, 57 pages.
- BRUDER, B., CULERIER, L., and RONCALLI, T. (2012). How to Design Target-Date Funds?. Amundi/Lyxor White Paper, Issue #9, available at SSRN, 2289099, 32 pages.
- Burkhardt, D., and Hasseltoft, H. (2012). Understanding Asset Correlations. SSRN, 1879855, 61 pages.
- Campbell, J. Y. (2000). Asset Pricing at the Millennium. *Journal of Finance*, 55(4), pp. 1515-1567.
- CAMPBELL, J. Y., COCCO, J., GOMES, F., MAENHOUT, P. J., and VICEIRA, L. M. (2001). Stock Market Mean Reversion and the Optimal Equity Allocation of a Long-Lived Investor. *Review of Finance*, 5(3), pp. 269-292.
- Campbell, J. Y., Pflueger, C., and Viceira, L. M. (2020). Macroeconomic Drivers of Bond and Equity Risks. *Journal of Political Economy*, 128(8), pp. 3148-3185.
- Campbell, J. Y., and Viceira, L. M. (2002). Strategic Asset Allocation. Oxford University Press.
- CANNER N., MANKIW, N. G., and WEIL, D. N. (1997). An Asset Allocation Puzzle. American Economic Review, 87(1), pp. 181-191.
- CIESLAK, A., and PFLUEGER, C. (2023). Inflation and Asset Returns. *Annual Review of Financial Economics*, 15(1), pp. 433-448.
- Cocco, J. F., and Gomes, F. J. (2012). Longevity Risk, Retirement Savings, and Financial Innovation. *Journal of Financial Economics*, 103(3), pp. 507-529.
- Cocco, J. F., Gomes, F. J., and Maenhout, P. J. (2005). Consumption and Portfolio Choice over the Life Cycle. *Review of Financial Studies*, 18(2), pp. 491-533.
- CONDAT, L. (2016). Fast Projection onto the Simplex and the ℓ_1 Ball. Mathematical Programming, 158(1), pp. 575-585.
- Duchi, J., Shalev-Shwartz, S., Singer, Y., and Chandra, T. (2008). Efficient Projections onto the ℓ_1 Ball for Learning in High Dimensions. *ICML '08: Proceedings of the 25th International Conference on Machine Learning*, pp. 272-279.
- EKELAND, I., and LAZRAK, A. (2017). Equilibrium Policies When Preferences are Time Inconsistent. arXiv, 0808.3790, 45 pages.
- FAMA, E. F., and SCHWERT, G. W. (1977). Asset Returns and Inflation. *Journal of Financial Economics*, 5(2), pp. 115-146.
- Fama, E. F. (1981). Stock Returns, Real Activity, Inflation, and Money. *American Economic Review*, 71(4), pp. 545-565.
- GESKE, R., and ROLL, R. (1983). The Fiscal and Monetary Linkage between Stock Returns and Inflation. *Journal of Finance*, 38(1), pp. 1-33.
- HAGERMAN, R. L., and Kim, E. H. (1976). Capital Asset Pricing with Price Level Changes. Journal of Financial and Quantitative Analysis, 11(3), pp. 381-391.

- HAN, N. W., and HUNG, M. W. (2012). Optimal Asset Allocation for DC Pension Plans under Inflation. *Insurance: Mathematics and Economics*, 51(1), pp. 172-181.
- International Monetary Fund (2012). The Financial Impact of Longevity Risk. Global Financial Stability Report The Quest for Lasting Stability, Chapter 4, pp. 123-153.
- JAGANNATHAN, R., and KOCHERLAKOTA, N. R. (1996). Why Should Older People Invest Less in Stocks Than Younger People?. Federal Reserve Bank of Minneapols Quarterly Review, 20(3), pp. 11-23.
- KAUL, G. (1987). Stock Returns and Inflation: The Role of the Monetary Sector. *Journal of Financial Economics*, 18(2), pp. 253-276.
- KRAFT, H., and MUNK, C. (2011). Optimal Housing, Consumption, and Investment Decisions over the Life Cycle. *Management Science*, 57(6), pp. 1025-1041.
- LEOMBRONI, M., PIAZZESI, M., SCHNEIDER, M., and ROGERS, C. (2020). Inflation and the Price of Real Assets. *NBER*, 26740, 51 pages.
- Li, L. (2002). Macroeconomic Factors and the Correlation of Stock and Bond Returns. SSRN, 363641, 50 pages.
- LUSARDI, A., and MITCHELL, O. S. (2014). The Economic Importance of Financial Literacy: Theory and Evidence. *Journal of Economic Literature*, 52(1), pp. 5-44.
- MARTELLINI, L., and MILHAU, V. (2012). Dynamic Allocation Decisions in the Presence of Funding Ratio Constraints. *Journal of Pension Economics and Finance*, 11(4), pp. 549-580.
- MERTON, R. C. (1969). Lifetime Portfolio Selection under Uncertainty: The Continuous-Time Case. *Review of Economics and Statistics*, 51(3), pp. 247-257.
- MERTON, R. C. (1971). Optimum Consumption and Portfolio Rules in a Continuous-Time Model. *Journal of Economic Theory*, 3(4), pp. 373-413.
- Munk, C., and Sørensen, C. (2010). Dynamic Asset Allocation with Stochastic Income and Interest Rates. *Journal of Financial Economics*, 96(3), pp. 433-462.
- Munk, C., Sørensen, C., and Vinther, T. N. (2004). Dynamic Asset Allocation under Mean-reverting Returns, Stochastic Interest Rates, and Inflation Uncertainty: Are Popular Recommendations Consistent with Rational Behavior?. *International Review of Economics & Finance*, 13(2), pp. 141-166.
- PARK, K., Wong, H. Y., and Yan, T. (2023). Robust Retirement and Life Insurance with Inflation Risk and Model Ambiguity. *Insurance: Mathematics and Economics*, 110, pp. 1-30.
- OECD (2023). Pensions at a Glance 2023: OECD and G20 Indicators. OECD Publishing, Paris, 13 December 2023, 236 pages.
- Pension Protection Fund (2025). The Purple Book 2024 DB Pensions Universe Risk Profile. Report, 46 pages.
- PORTELLI, L., and Roncalli, T. (2024). Stock-Bond Correlation: Theory & Empirical Results. SSRN, 4823094, 139 pages.

- POTERBA, J., RAUH, J., VENTI, S., and WISE, D. (2009). Lifecycle Asset Allocation Strategies and the Distribution of 401(k) Retirement Wealth. In Wise, D. (Ed.), *Developments in the Economics of Aging*, University of Chicago Press, pp. 15-50.
- ROLL, R. (1973). Assets, Money, and Commodity Price Inflation under Uncertainty. *Journal of Money, Credit and Banking*, 5(4), pp. 903-923.
- RONCALLI, T. (2013). Introduction to Risk Parity and Budgeting. CRC Financial Mathematics Series, Chapman & Hall, 410 pages.
- RONCALLI, T. (2020). Handbook of Financial Risk Management. CRC Financial Mathematics Series, Chapman & Hall, 1142 pages.
- SATHYANARAYANA, S., and GARGESA, S. (2018). An Analytical Study of the Effect of Inflation on Stock Market Returns. *IRA-International Journal of Management & Social Sciences*, 13(2), pp. 48-64.
- STROTZ, R. H. (1955). Myopia and Inconsistency in Dynamic Utility Maximization. *Review of Economic Studies*, 23(3), pp. 165-180.
- STULZ, R. M. (1986). Asset Pricing and Expected Inflation. *Journal of Finance*, 41(1), pp. 209-223.
- United Nations (2024). World Population Prospects: The 2024 Revision. Department of Economic and Social Affairs, Population Division, July.
- VICEIRA, L. M. (2001). Optimal Portfolio Choice for Long-Horizon Investors with Nontradable Labor Income. *Journal of Finance*, 56(2), pp. 433-470.
- Wachter, J. A. (2002). Portfolio and Consumption Decisions under Mean-Reverting Returns: An Exact Solution for Complete Markets. *Journal of Financial and Quantitative Analysis*, 37(1), pp. 63-91.
- Wadia, Z., Perry, A., and Cook, R. (2025). 2025 Corporate Pension Funding Study. *Milliman White Paper*, April, 16 pages.
- YAO, H., YANG, Z., and CHEN, P. (2013). Markowitz's Mean-variance Defined Contribution Pension Fund Management Under Inflation: A Continuous-time Model. *Insurance: Mathematics and Economics*, 53(3), pp. 851-863.

A Technical appendix

A.1 Notations

- $\mathbf{0}_n$ is the vector of zeros.
- $\mathbf{1}_n$ is the vector of ones.
- α_t is the proportion of total wealth invested in the risky asset.
- β_t is the proportion of total wealth invested in the inflation-sensitive risky asset.
- B_t is the price of the bond at time t (risk-free asset).
- $B(t,T) = \exp\left(-\int_t^T r_s \, ds\right)$ is the discount factor between times t and T.
- c_t is the direct contribution of the investor to the target date fund.
- e_i is the unit vector, i.e. $[e_i]_i = 1$ and $[e_i]_i = 0$ for all $j \neq i$.
- $H_t = \int_t^T e^{-\int_t^s r_u \, du} c_s \, ds$ is the capitalization of the lifetime flow of contribution.
- HFCR_t = H_t/X_t is the human-tofinancial capital ratio.
- $\mathcal{J}(t,x) = \sup_{\alpha} \mathbb{E}_t \left[\mathcal{U}(X_T) \mid X_t = x \right]$ is the value function of the investor.
- κ is the mean-reversion rate of the inflation.
- $m_t = \mathbb{E}[X_t]$ is the mathematical expectation of the wealth.
- μ_t is the expected return of the risky asset.
 - $\mu'_t = a_t + b_t \pi_t$ is the expected return of the inflation-sensitive asset.
- $\mu(x)$ is the expected return of portfolio w
- π_t is the inflation rate at time t.
- π_{∞} is long-term mean inflation rate.

- r_t is the nominal interest rate.
- R_t is the price of the inflation-sensitive risky asset at time t.
- $\varrho \in \{0,1\}$ is the discounting binary function.
- ρ_t , $\rho_t^{(S)}$, and $\rho_t^{(R)}$ are the correlation coefficients between S_t and R_t , S_t and π_t , and R_t and π_t , respectively.
- S_t is the price of the risky asset at time t.
- $SR_t = (\mu_t r_t) / \sigma_t$ is the Sharpe ratio of the risky asset.
- Σ_t is the covariance matrix risky assets
- σ_t is the volatility of the risky asset.
- $\sigma_t^{(\pi)}$ is the inflation volatility
- $\sigma'_t = 10\%$ is the volatility of the inflation-sensitive asset.
- $\sigma(w) = \sqrt{x^{\top} \Sigma x}$ is the volatility of Portfolio w.
- $v_t = \text{var}(X_t)$ is the variance of the wealth.
- $W_t = X_t + H_t$ is the total wealth, i.e., the sum of the spot wealth and the forward wealth.
- w_t is the vector of portfolio weights in risky assets at time t.
- $\varpi_t = \alpha_t \cdot w_t$ is the vector of risky asset exposure at time t.
- W_t^S is the nominal wealth invested in the risky asset.
- X_t is the financial wealth of the investor at time t.

A.2 Proof of Equations (5) and (6)

We postulate a solution of the form:

$$\mathcal{J}(t,x) = h(t) \frac{x^{\gamma}}{\gamma}$$

Since we have $\partial_t \mathcal{J}(t,x) = h'(t) x^{\gamma}/\gamma$, $\partial_x \mathcal{J}(t,x) = h(t) x^{\gamma-1}$, and $\partial_x^2 \mathcal{J}(t,x) = (\gamma - 1) h(t) x^{\gamma-2}$, we deduce the optimal allocation strategy:

$$\alpha_t^{\star} = -\frac{(\mu_t - r_t)}{\sigma_t^2} \cdot \frac{\partial_x \mathcal{J}(t, x)}{x \partial_x^2 \mathcal{J}(t, x)}$$

$$= -\frac{(\mu_t - r_t)}{\sigma_t^2} \cdot \frac{h(t) x^{\gamma - 1}}{x (\gamma - 1) h(t) x^{\gamma - 2}}$$

$$= \frac{\mu_t - r_t}{(1 - \gamma) \sigma_t^2}$$

It follows that:

$$\max_{\alpha} \mathcal{H}(t, x, \alpha) = \left(r_t + \frac{(\mu_t - r_t)^2}{(1 - \gamma)\sigma_t^2}\right) h(t) x^{\gamma} - \frac{1}{2} \frac{(\mu_t - r_t)^2}{(1 - \gamma)\sigma_t^2} h(t) x^{\gamma}$$
$$= \beta_t h(t) \frac{x^{\gamma}}{\gamma}$$

where:

$$\beta_t = r_t \gamma + \frac{1}{2} \frac{\gamma (\mu_t - r_t)^2}{(1 - \gamma) \sigma_t^2}$$

The HJB equation with the terminal condition becomes⁵⁴:

$$\begin{cases} h'(t) + \beta h(t) = 0 \\ h(T) = 1 \end{cases}$$

The solution to the differential equation is then $h(t) = \exp\left(\int_t^T \beta_s \, ds\right)$. Finally, we obtain the value function:

$$\mathcal{J}(t,x) = \exp\left(\int_{t}^{T} \left(r_{s}\gamma + \frac{1}{2} \frac{\gamma (\mu_{s} - r_{s})^{2}}{(1 - \gamma) \sigma_{s}^{2}}\right) ds\right) \cdot \frac{x^{\gamma}}{\gamma}$$

A.3 Proof of Equations (7) and (8)

We consider the following Hamilton-Jacobi-Bellman equation:

$$\frac{\partial \mathcal{J}(t,x)}{\partial t} + \sup_{\alpha_t} \left\{ \left(r_t X_t + \alpha_t \left(\mu_t - r_t \right) X_t + \mathbf{c}_t \right) \frac{\partial \mathcal{J}(t,x)}{\partial x} + \frac{1}{2} \alpha_t^2 \sigma_t^2 X_t^2 \frac{\partial^2 \mathcal{J}(t,x)}{\partial x^2} \right\} = 0$$

with terminal condition $\mathcal{J}(T,x) = \mathcal{U}(x)$. Since the solution is not explicit in the presence of contributions, we perform the following change of variable:

$$\tilde{X}_t = X_t + H_t$$

$$= X_t + \int_t^T e^{-\int_t^s r_u \, \mathrm{d}u} c_s \, \mathrm{d}s$$

⁵⁴Since the terminal condition is $\mathcal{J}(T,x) = h(T) x^{\gamma}/\gamma = \mathcal{U}(x)$, this implies h(T) = 1.

The modified dynamics of \tilde{X}_t are:

$$d\tilde{X}_{t} = dX_{t} + dH_{t}$$

$$= (r_{t}X_{t} + \alpha_{t} (\mu_{t} - r_{t}) X_{t} + \mathbf{c}_{t}) dt + \alpha_{t}\sigma_{t}X_{t} dW_{t} + (r_{t}H_{t} - \mathbf{c}_{t}) dt$$

$$= (r_{t}\tilde{X}_{t} + \alpha_{t} (\mu_{t} - r_{t}) (\tilde{X}_{t} - H_{t})) dt + \alpha_{t}\sigma_{t} (\tilde{X}_{t} - H_{t}) dW_{t}$$

This transformation reduces the problem to the classical Merton case without contributions but with a shifted wealth process \tilde{X}_t , a transformed value function $\tilde{\mathcal{J}}(t,\tilde{x}) = \mathcal{J}(t,\tilde{x}-H_t)$ and a new control variable $\tilde{\alpha}_t$ such as $\tilde{\alpha}_t\tilde{X}_t = \alpha_tX_t$. We deduce that $\alpha_tX_t = \alpha_t\left(\tilde{X}_t - H_t\right) = \tilde{\alpha}_t\tilde{X}_t$ and:

$$\tilde{\alpha}_t = \alpha_t \frac{X_t}{\tilde{X}_t} = \frac{\alpha_t X_t}{X_t + H_t}$$

It follows that the dynamics of \tilde{X}_t under the new control $\tilde{\alpha}_t$ are:

$$d\tilde{X}_t = (r_t + \tilde{\alpha}_t (\mu_t - r_t)) \tilde{X}_t dt + \tilde{\alpha}_t \sigma_t \tilde{X}_t dW_t$$

This is exactly the classical Merton problem, now expressed in terms of $\tilde{\alpha}_t$ and \tilde{X}_t . We deduce that:

$$\tilde{\alpha}_{t}^{\star} = -\frac{(\mu_{t} - r_{t})}{\sigma_{t}^{2}} \cdot \frac{\partial_{\tilde{x}} \tilde{\mathcal{J}}(t, \tilde{x})}{\tilde{x} \partial_{\tilde{x}}^{2} \tilde{\mathcal{J}}(t, \tilde{x})}$$

In the case of the CRRA utility function, we have:

$$\tilde{\alpha}_t^{\star} = \frac{\mu_t - r_t}{(1 - \gamma)\,\sigma_t^2}$$

Finally, we get:

$$\begin{split} \alpha_t^{\star} &= \tilde{\alpha}_t^{\star} \frac{\tilde{X}_t}{X_t} \\ &= \frac{\mu_t - r_t}{(1 - \gamma)\sigma_t^2} \left(1 + \frac{H_t}{X_t} \right) \\ &= \frac{\mu_t - r_t}{(1 - \gamma)\sigma_t^2} \left(1 + \frac{1}{X_t} \int_t^T e^{-\int_t^s r_u \, \mathrm{d}u} \boldsymbol{c}_s \, \mathrm{d}s \right) \end{split}$$

A.4 Special cases of H_t

We recall that:

$$H_{t} = \int_{t}^{T} e^{-\int_{t}^{s} r_{u} du} \boldsymbol{c}_{s} ds = \int_{t}^{T} B(t, s) \boldsymbol{c}_{s} ds$$

where B(t, s) is the discount factor between times t and s. We consider several cases:

• $c_t = c_0$ When the contribution is constant, we get:

$$H_t = \mathbf{c}_0 \int_t^T B(t, s) \, \mathrm{d}s$$

Moreover, if the interest rate is constant — $r_t = r$, the previous formula becomes:

$$H_t = c_0 \left(\frac{1 - e^{-r(T-t)}}{r} \right)$$

because we have:

$$\int_{t}^{T} B(t,s) \, ds = \int_{t}^{T} e^{-r(s-t)} \, ds = \left[-\frac{e^{-r(s-t)}}{r} \right]_{t}^{T} = \frac{1 - e^{-r(T-t)}}{r}$$

• $c_t = c_0 + b_c t$ When the contribution is a linear function, we have:

$$H_{t} = \int_{t}^{T} B\left(t,s\right) \left(\boldsymbol{c}_{0} + b_{\boldsymbol{c}}s\right) \, \mathrm{d}s = \boldsymbol{c}_{0} \int_{t}^{T} B\left(t,s\right) \, \mathrm{d}s + b_{\boldsymbol{c}} \int_{t}^{T} s B\left(t,s\right) \, \mathrm{d}s$$

If the interest rate is constant, we have:

$$\begin{split} \int_{t}^{T} sB\left(t,s\right) \, \mathrm{d}s &= \int_{t}^{T} se^{-r(s-t)} \, \mathrm{d}s \\ &= \int_{0}^{T-t} \left(u+t\right) e^{-ru} \, \mathrm{d}u \\ &= \int_{0}^{T-t} ue^{-ru} \, \mathrm{d}u + t \int_{0}^{T-t} e^{-ru} \, \mathrm{d}u \\ &= \left[-\frac{ue^{-ru}}{r} \right]_{0}^{T-t} - \int_{0}^{T-t} -\frac{e^{-ru}}{r} \, \mathrm{d}u + t \left[-\frac{e^{-ru}}{r} \right]_{0}^{T-t} \\ &= \left[-\frac{ue^{-ru}}{r} \right]_{0}^{T-t} + \left[-\frac{e^{-ru}}{r^{2}} \right]_{0}^{T-t} + t \left[-\frac{e^{-ru}}{r} \right]_{0}^{T-t} \\ &= -\frac{(T-t) e^{-r(T-t)}}{r} + \frac{1-e^{-r(T-t)}}{r^{2}} + t \left(\frac{1-e^{-r(T-t)}}{r} \right) \\ &= \frac{1}{r^{2}} \left(1 + rt - (1 + rT) e^{-r(T-t)} \right) \end{split}$$

It follows that:

$$H_t = c_0 \left(\frac{1 - e^{-r(T-t)}}{r} \right) + b_c \left(\frac{1 + rt - (1 + rT)e^{-r(T-t)}}{r^2} \right)$$

• $c_t = c_0 + b_c t + a_c t^2$ When the contribution is a second degree polynomial, we have:

$$H_{t} = \int_{t}^{T} B(t, s) \left(\mathbf{c}_{0} + b_{c}s + a_{c}s^{2} \right) ds$$
$$= \int_{t}^{T} B(t, s) \left(\mathbf{c}_{0} + b_{c}s \right) ds + a_{c} \int_{t}^{T} s^{2}B(t, s) ds$$

If the interest rate is constant, we obtain:

$$H_{t} = c_{0} \left(\frac{1 - e^{-r(T-t)}}{r} \right) + b_{c} \left(\frac{1 + rt - (1 + rT)e^{-r(T-t)}}{r^{2}} \right) + a_{c} \left(\frac{2(1 + rt) + r^{2}t^{2} - (2(1 + rT) + r^{2}T^{2})e^{-r(T-t)}}{r^{3}} \right)$$

because:

$$\begin{split} \int_t^T s^2 B\left(t,s\right) \, \mathrm{d}s &= \int_t^T s^2 e^{-r(s-t)} \, \mathrm{d}s \\ &= \int_0^{T-t} (u+t)^2 \, e^{-ru} \, \mathrm{d}u \\ &= \int_0^{T-t} u^2 e^{-ru} \, \mathrm{d}u + 2t \int_0^{T-t} u e^{-ru} \, \mathrm{d}u + t^2 \int_0^{T-t} e^{-ru} \, \mathrm{d}u \\ &= \left[-\frac{2+2ru+r^2u^2}{r^3} e^{-ru} \right]_0^{T-t} + 2t \left[-\frac{1+ru}{r^2} e^{-ru} \right]_0^{T-t} + \\ &\quad t^2 \left[-\frac{e^{-ru}}{r} \right]_0^{T-t} \\ &= \frac{1}{r^3} \left(2\left(1+rt\right) + r^2t^2 - \left(2\left(1+rT\right) + r^2T^2\right) e^{-r(T-t)} \right) \end{split}$$

A.5 Calibration of c_t

We assume that we are given an empirical curve $\hat{\boldsymbol{c}}(t)$ of contributions observed at a set of regular time points t_j $(j=0,\ldots,m)$. For instance, in France, we can use data from the French savings report published by INSEE to estimate monthly contributions based on the investor's age and group. A first approach consists of using a smoothing spline to fit a non-parametric function $\boldsymbol{c}(t)$ over the interval $t \in [t_0, t_m]$. A second approach relies on analytical cases detailed in Appendix A.4. For example, if we assume the contribution function is constant — $\boldsymbol{c}_t = \boldsymbol{c}_0$, we can calibrate \boldsymbol{c}_0 as the mean value:

$$\boldsymbol{c}_{0} = \frac{1}{t_{m} - t_{0}} \int_{t_{0}}^{t_{m}} \hat{\boldsymbol{c}}\left(t\right) dt \approx \frac{1}{m+1} \sum_{j=0}^{m} \hat{\boldsymbol{c}}\left(t_{j}\right)$$

Alternatively, if we assume a linear contribution function — $c_t = c_0 + b_c t$, we can fit the parameters using the values of contribution at times t_0 and t_m . We obtain the following solution:

$$\begin{cases} c_0 = \frac{\hat{c}(t_0) t_m - \hat{c}(t_m) t_0}{t_m - t_0} \\ b_c = \frac{\hat{c}(t_m) - \hat{c}(t_0)}{t_m - t_0} \end{cases}$$

In the case of a second degree polynomial contribution function — $c_t = c_0 + b_c t + a_c t^2$, we assume that we know the initial value $\hat{c}(t_0)$ at age t_0 and the maximum contribution $\hat{c}(t_{\text{max}}) = \sup \hat{c}(t_j)$, which occurs at age t_{max} . Using the standard properties of quadratic functions⁵⁵, we obtain the following solution:

$$\begin{cases} c_0 = \frac{\hat{\boldsymbol{c}}\left(t_0\right)t_{\max}^2 + \hat{\boldsymbol{c}}\left(t_{\max}\right)t_0\left(t_0 - 2t_{\max}\right)}{\left(t_{\max} - t_0\right)^2} \\ b_{\boldsymbol{c}} = -2\frac{\boldsymbol{c}_0 - \hat{\boldsymbol{c}}\left(t_{\max}\right)}{t_{\max}} \\ a_{\boldsymbol{c}} = \frac{\boldsymbol{c}_0 - \hat{\boldsymbol{c}}\left(t_{\max}\right)}{t_{\max}^2} \end{cases}$$

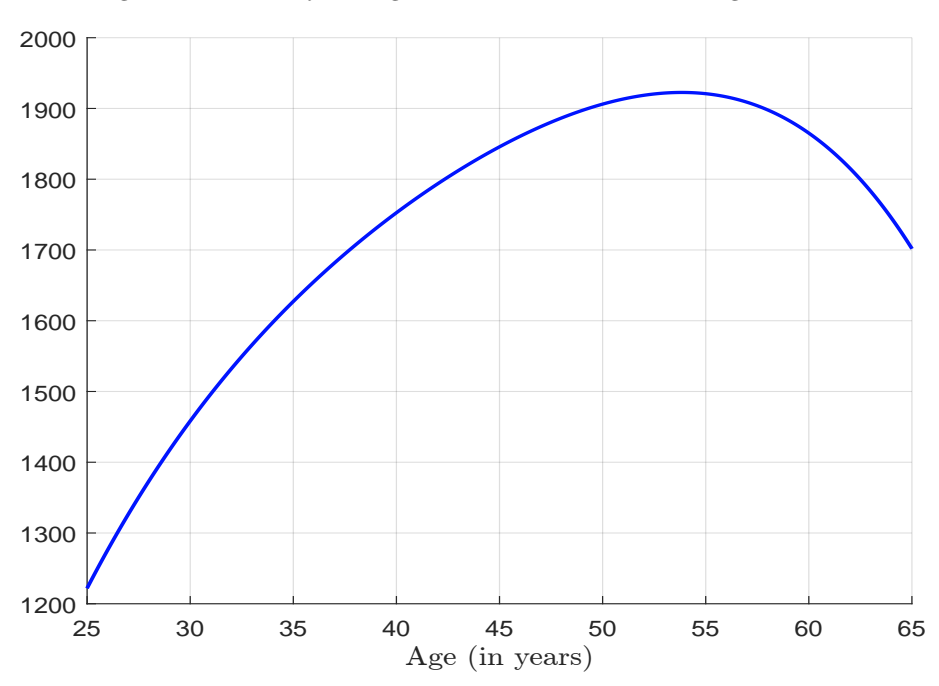


Figure 50: Monthly savings estimates in 2006 according to INSEE

Source: Bruder et al. (2012, Figure 7, page 12).

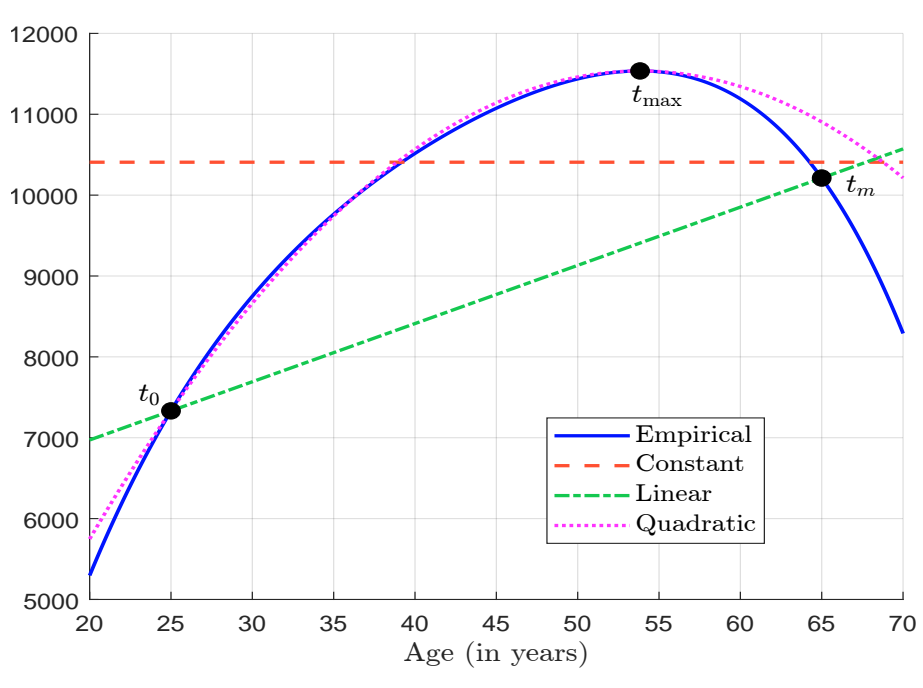


Figure 51: Calibration of the contribution function (in \$)

We consider the monthly saving amounts used by Bruder et al. (2012) to calibrate the glide path. This savings function is shown in Figure 50. We transform this estimated savings function $\hat{\boldsymbol{s}}(t)$ into a contribution function $\hat{\boldsymbol{c}}(t)$, assuming that 50% of the savings are allocated to retirement contributions⁵⁶. We obtain the following values: $\hat{\boldsymbol{c}}(t_0) = \hat{\boldsymbol{c}}(25) = \7332 , $\hat{\boldsymbol{c}}(t_m) = \hat{\boldsymbol{c}}(65) = \10212 , and $\hat{\boldsymbol{c}}(t_{\text{max}}) = \hat{\boldsymbol{c}}(53.83) = \11536 . Using the methods described above, we calibrate the analytical contribution functions⁵⁷ and report them in Figure 51.

A.6 Maximum of H_t when c_t is a quadratic function and the interest rate is constant

To find the maximum of H_t , we rewrite it as:

$$H_{t} = \frac{A + Bt + Ct^{2} - De^{-r(T-t)}}{r^{3}}$$

where:

$$\begin{cases}
A = c_0 r^2 + b_c r + 2a_c \\
B = b_c r^2 + 2a_c r \\
C = a_c r^2 \\
D = c_0 r^2 + b_c (r + r^2 T) + a_c (2 + 2rT + r^2 T^2)
\end{cases}$$

The first-order condition for a maximum is:

$$\begin{split} \frac{\partial H_t}{\partial t} &= 0 \quad \Leftrightarrow \quad B + 2Ct - rDe^{-r(T-t)} = 0 \\ & \Leftrightarrow \quad 2Ct = -B + rDe^{-rT}e^{rt} \\ & \Leftrightarrow \quad rt = \frac{-rB + r^2De^{-rT}e^{rt}}{2C} \\ & \Leftrightarrow \quad rt + \frac{rB}{2C} = \underbrace{\frac{r^2De^{-rT}e^{-\frac{rB}{2C}}}{2C}}_{K} \underbrace{e^{rt + \frac{rB}{2C}}}_{e^w} \end{split}$$

It follows that:

$$\begin{split} w &= Ke^w &\Leftrightarrow -we^{-w} = -K \\ &\Leftrightarrow -w = W\left(-K\right) \\ &\Leftrightarrow t^* = -\frac{1}{r} \left(W\left(-\frac{r^2 D e^{-rT} e^{-\frac{rB}{2C}}}{2C}\right) + \frac{rB}{2C} \right) \end{split}$$

where W(x) is the Lambert W function. Thus, the optimal time t^* is given by:

$$t^* = \max\left(-\frac{1}{r}\left(W\left(-K_1e^{-rT}e^{-K_2}\right) + K_2\right), t_0\right)$$

where:

$$K_1 = \frac{r^2 D}{2C} = \frac{\boldsymbol{c_0} r^2 + b_{\boldsymbol{c}} \left(r + r^2 T\right) + a_{\boldsymbol{c}} \left(2 + 2rT + r^2 T^2\right)}{2a_{\boldsymbol{c}}} \quad \text{and} \quad K_2 = \frac{rB}{2C} = 1 + \frac{b_{\boldsymbol{c}} r}{2a_{\boldsymbol{c}}}$$

⁵⁵The maximum occurs at $t_{\text{max}} = -b_c/(2a_c)$ and the value of the function at the maximum is $c_{t_{\text{max}}} = c_0 + b_c t_{\text{max}} + a_c t_{\text{max}}^2 = c_0 - b_c^2/(4a_c)$. We also use the vertex form $c_t = c_{t_{\text{max}}} + a_c (t - t_{\text{max}})^2$.

⁵⁶This means that $\hat{c}(t) = 50\% \times 12 \times \hat{s}(t)$.

⁵⁷We obtain the following results: $c_t = 10\,407.105$ for the constant function, $c_t = 5\,532.406 + 71.986t$ for the linear function, and $c_t = -3\,117.869 + 544.408t - 5.056t^2$ for the quadratic function.

Remark 12. If $a_c = 0$, the maximum is reached at:

$$t^{\star} = T + \frac{1}{r} \ln b_{c} - \frac{1}{r} \ln \left(c_{0}r + b_{c} \left(1 + rT \right) \right)$$

A.7 Computation of the expected wealth $\mathbb{E}[X_t]$

When the utility function is CRRA, we have $\alpha_t^* X_t = \bar{\alpha}_t (X_t + H_t)$. Substituting α_t^* into the stochastic differential equation of the wealth yields:

$$dX_t = (r_t X_t + \alpha_t^* (\mu_t - r_t) X_t + \mathbf{c}_t) dt + \alpha_t^* \sigma_t X_t dW_t$$

= $((r_t + \eta_t) X_t + \eta_t H_t + \mathbf{c}_t) dt + \bar{\alpha}_t \sigma_t (X_t + H_t) dW_t$

where:

$$\eta_t = \bar{\alpha}_t (\mu_t - r_t) = \frac{(\mu_t - r_t)^2}{(1 - \gamma) \sigma_t^2} = \frac{SR_t^2}{(1 - \gamma)}$$

Let $m_t = \mathbb{E}[X_t]$ be the mean process of X_t . We deduce that:

$$dm_t = ((r_t + \eta_t) m_t + \eta_t H_t + \mathbf{c}_t) dt$$

The function m_t satisfies the following linear ODE:

$$\begin{cases} \frac{\mathrm{d}m_t}{\mathrm{d}t} = (r_t + \eta_t) m_t + \eta_t H_t + \mathbf{c}_t \\ m_{t_0} = x_0 \end{cases}$$

Let $\lambda_t = \exp\left(-\int_{t_0}^t (r_s + \eta_s) ds\right)$ be the integrating factor. We have:

$$\frac{\mathrm{d}}{\mathrm{d}t} \left[\lambda_t m_t \right] = \frac{\mathrm{d}\lambda_t}{\mathrm{d}t} m_t + \lambda_t \frac{\mathrm{d}m_t}{\mathrm{d}t}
= -(r_t + \eta_t) \lambda_t m_t + \lambda_t \left((r_t + \eta_t) m_t + \eta_t H_t + \mathbf{c}_t \right)
= \lambda_t \left(\eta_t H_t + \mathbf{c}_t \right)$$

We deduce that:

$$\lambda_t m_t - m_0 = \int_{t_0}^t e^{-\int_{t_0}^s (r_u + \eta_u) \, du} \left(\eta_s H_s + c_s \right) \, ds$$

Therefore, the solution is:

$$m_t = e^{\int_{t_0}^t (r_s + \eta_s) \, ds} \left(x_0 + \int_{t_0}^t e^{-\int_{t_0}^s (r_u + \eta_u) \, du} \left(\eta_s H_s + \mathbf{c}_s \right) \, ds \right)$$
(28)

This is the general closed-form formula for the expectation of wealth. When the parameters are constant — $r_t = r$, $\mu_t = \mu$, $\sigma_t = \sigma$, we get:

$$m_t = e^{(r+\eta)(t-t_0)} \left(x_0 + \int_{t_0}^t e^{-(r+\eta)(s-t_0)} \left(\eta H_s + \mathbf{c}_s \right) \, \mathrm{d}s \right)$$
 (29)

We assume that $c_t = c_0 + b_c t + a_c t^2$. Using the expression of H_t in Appendix A.4, we deduce that:

$$\eta H_s + c_s = A + Bs + Cs^2 - De^{-r(T-s)}$$

where:

$$A = c_0 \frac{r + \eta}{r} + b_c \frac{\eta}{r^2} + a_c \frac{2\eta}{r^3}$$

$$B = b_c \frac{r + \eta}{r} + a_c \frac{2\eta}{r^2}$$

$$C = a_c \frac{r + \eta}{r}$$

$$D = c_0 \frac{\eta}{r} + b_c \frac{\eta (1 + rT)}{r^2} + a_c \frac{\eta (2 (1 + rT) + r^2 T^2)}{r^3}$$

It follows that:

$$\int_{t_0}^t e^{-(r+\eta)(s-t_0)} \left(\eta H_s + \mathbf{c}_s \right) ds = A \int_{t_0}^t e^{-(r+\eta)(s-t_0)} ds + B \int_{t_0}^t s e^{-(r+\eta)(s-t_0)} ds + C \int_{t_0}^t s^2 e^{-(r+\eta)(s-t_0)} ds - D e^{-r(T-t_0)} \int_{t_0}^t e^{-\eta(s-t_0)} ds$$

Since we have:

$$\int_{t_0}^t e^{-(r+\eta)(s-t_0)} ds = \frac{1 - e^{-(r+\eta)(t-t_0)}}{r+\eta}$$

$$\int_{t_0}^t s e^{-(r+\eta)(s-t_0)} ds = \left(\frac{t_0}{r+\eta} + \frac{1}{(r+\eta)^2}\right) - \left(\frac{t}{r+\eta} + \frac{1}{(r+\eta)^2}\right) e^{-(r+\eta)(t-t_0)}$$

$$\int_{t_0}^t s^2 e^{-(r+\eta)(s-t_0)} ds = \left(\frac{t_0^2}{r+\eta} + \frac{2t_0}{(r+\eta)^2} + \frac{2}{(r+\eta)^3}\right) - \left(\frac{t^2}{r+\eta} + \frac{2t}{(r+\eta)^2} + \frac{2}{(r+\eta)^3}\right) e^{-(r+\eta)(t-t_0)}$$

$$\int_{t_0}^t e^{-\eta(s-t_0)} ds = \frac{1 - e^{-\eta(t-t_0)}}{\eta}$$

we conclude that:

$$\begin{split} m_t &= e^{(r+\eta)(t-t_0)}x_0 + \frac{A}{r+\eta}\left(e^{(r+\eta)(t-t_0)} - 1\right) + \\ & B\left(\frac{t_0}{r+\eta} + \frac{1}{(r+\eta)^2}\right)e^{(r+\eta)(t-t_0)} - B\left(\frac{t}{r+\eta} + \frac{1}{(r+\eta)^2}\right) + \\ & C\left(\frac{t_0^2}{r+\eta} + \frac{2t_0}{(r+\eta)^2} + \frac{2}{(r+\eta)^3}\right)e^{(r+\eta)(t-t_0)} - C\left(\frac{t^2}{r+\eta} + \frac{2t}{(r+\eta)^2} + \frac{2}{(r+\eta)^3}\right) - \\ & \frac{D}{\eta}e^{-r(T-t_0)}\left(e^{(r+\eta)(t-t_0)} - e^{r(t-t_0)}\right) \end{split}$$

In the case of a constant contribution function, the expression for m_t simplifies to:

$$m_t = e^{(r+\eta)(t-t_0)} x_0 + \left(\left(e^{(r+\eta)(t-t_0)} - 1 \right) - e^{-r(T-t_0)} \left(e^{(r+\eta)(t-t_0)} - e^{r(t-t_0)} \right) \right) \frac{c_0}{r}$$

A.8 Computation of the variance of the wealth

We recall that:

$$dX_t = ((r_t + \eta_t) X_t + \eta_t H_t + c_t) dt + \bar{\alpha}_t \sigma_t (X_t + H_t) dW_t$$

By Itô's lemma, we have $dX_t^2 = 2X_t dX_t + (dX_t)^2$. Since $(dX_t)^2 = \bar{\alpha}_t^2 \sigma_t^2 (X_t + H_t)^2 dt$, we deduce that:

$$dX_t^2 = \left(2\left(\left(r_t + \eta_t\right)X_t + \eta_t H_t + \boldsymbol{c}_t\right)X_t + \bar{\alpha}_t^2 \sigma_t^2 \left(X_t + H_t\right)^2\right) dt + 2\bar{\alpha}_t \sigma_t \left(X_t + H_t\right)X_t dW_t$$

and:

$$\frac{\mathrm{d}}{\mathrm{d}t}\mathbb{E}\left[X_{t}^{2}\right] = \mathbb{E}\left[2\left(\left(r_{t}+\eta_{t}\right)X_{t}+\eta_{t}H_{t}+c_{t}\right)X_{t}+\bar{\alpha}_{t}^{2}\sigma_{t}^{2}\left(X_{t}+H_{t}\right)^{2}\right]$$

$$= \bar{\alpha}_{t}^{2}\sigma_{t}^{2}H_{t}^{2}+2\left(\eta_{t}H_{t}+c_{t}+\bar{\alpha}_{t}^{2}\sigma_{t}^{2}H_{t}\right)\mathbb{E}\left[X_{t}\right]+$$

$$\left(2\left(r_{t}+\eta_{t}\right)+\bar{\alpha}_{t}^{2}\sigma_{t}^{2}\right)\mathbb{E}\left[X_{t}^{2}\right]$$

We denote $m_t = \mathbb{E}[X_t]$ and $v_t = \text{var}(X_t) = \mathbb{E}[X_t^2] - m_t^2$ with $m_{t_0} = x_0$ and $v_0 = 0$. It follows that:

$$\frac{\mathrm{d}v_t}{\mathrm{d}t} = \frac{\mathrm{d}}{\mathrm{d}t} \mathbb{E}\left[X_t^2\right] - 2m_t \frac{\mathrm{d}m_t}{\mathrm{d}t}$$

$$= \bar{\alpha}_t^2 \sigma_t^2 H_t^2 + 2\left(\eta_t H_t + c_t + \bar{\alpha}_t^2 \sigma_t^2 H_t\right) m_t + \left(2\left(r_t + \eta_t\right) + \bar{\alpha}_t^2 \sigma_t^2\right) \left(v_t + m_t^2\right) - 2\left(\left(r_t + \eta_t\right) m_t + \eta_t H_t + c_t\right) m_t$$

$$= \left(2\left(r_t + \eta_t\right) + \bar{\alpha}_t^2 \sigma_t^2\right) v_t + \bar{\alpha}_t^2 \sigma_t^2 \left(m_t + H_t\right)^2$$

We know that the solution of the ODE:

$$\frac{\mathrm{d}y_t}{\mathrm{d}t} = a_t y_t + b_t$$

is:

$$y_t = e^{\int_{t_0}^t a_s \, \mathrm{d}s} \left(y_0 + \int_{t_0}^t e^{-\int_{t_0}^s a_u \, \mathrm{d}u} b_s \, \mathrm{d}s \right)$$

Finally, we get:

$$v_{t} = \exp\left(\int_{t_{0}}^{t} \left(2\left(r_{s} + \eta_{s}\right) + \bar{\alpha}_{s}^{2} \sigma_{s}^{2}\right) ds\right) \cdot$$

$$\int_{t_{0}}^{t} \bar{\alpha}_{s}^{2} \sigma_{s}^{2} \left(m_{s} + H_{s}\right)^{2} \exp\left(-\int_{t_{0}}^{s} \left(2\left(r_{u} + \eta_{u}\right) + \bar{\alpha}_{u}^{2} \sigma_{u}^{2}\right) du\right) ds$$

$$= \int_{t_{0}}^{t} \bar{\alpha}_{s}^{2} \sigma_{s}^{2} \left(m_{s} + H_{s}\right)^{2} \exp\left(\int_{s}^{t} \left(2\left(r_{u} + \eta_{u}\right) + \bar{\alpha}_{u}^{2} \sigma_{u}^{2}\right) du\right) ds$$

When the parameters are constant, the previous expression becomes:

$$v_t = \bar{\alpha}^2 \sigma^2 \int_{t_0}^t (m_s + H_s)^2 e^{(2(r+\eta) + \bar{\alpha}^2 \sigma^2)(t-s)} ds$$

Let us now also assume that the contribution is constant. We deduce that:

$$m_s + H_s = e^{(r+\eta)s} e^{-(r+\eta)t_0} \left(x_0 + \frac{\mathbf{c}_0}{r} (1 - e^{-r(T-t_0)}) \right) +$$

$$e^{-rs} \left(\frac{\mathbf{c}_0}{r} e^{-rT + 2rt_0} \right) - e^{rs} \left(\frac{\mathbf{c}_0}{r} e^{-rT} \right)$$

$$= Ae^{(r+\eta)s} + Be^{-rs} - Ce^{rs}$$

and:

$$(m_s + H_s)^2 = \left(Ae^{(r+\eta)s} + Be^{-rs} - Ce^{rs}\right)^2$$
$$= A^2e^{2(r+\eta)s} + B^2e^{-2rs} + C^2e^{2rs} + 2ABe^{\eta s} - 2ACe^{(2r+\eta)s} - 2BC$$

Let $\kappa = 2(r + \eta) + \bar{\alpha}^2 \sigma^2$. It follows that:

$$\begin{split} v_t &= \bar{\alpha}^2 \sigma^2 \int_{t_0}^t (m_s + H_s)^2 e^{\kappa(t-s)} \, \mathrm{d}s \\ &= \bar{\alpha}^2 \sigma^2 e^{\kappa t} \left[A^2 \int_{t_0}^t e^{(2(r+\eta)-\kappa)s} \, \mathrm{d}s + B^2 \int_{t_0}^t e^{(-2r-\kappa)s} \, \mathrm{d}s + C^2 \int_{t_0}^t e^{(2r-\kappa)s} \, \mathrm{d}s \right] + \\ &2 \bar{\alpha}^2 \sigma^2 e^{\kappa t} \left[AB \int_{t_0}^t e^{(\eta-\kappa)s} \, \mathrm{d}s - AC \int_{t_0}^t e^{(2r+\eta-\kappa)s} \, \mathrm{d}s - BC \int_{t_0}^t e^{-\kappa s} \, \mathrm{d}s \right] \\ &= \bar{\alpha}^2 \sigma^2 e^{\kappa t} A^2 \left(\frac{e^{(2r+2\eta-\kappa)t} - e^{(2r+2\eta-\kappa)t_0}}{2r+2\eta-\kappa} \right) - \bar{\alpha}^2 \sigma^2 e^{\kappa t} B^2 \left(\frac{e^{(-2r-\kappa)t} - e^{(-2r-\kappa)t_0}}{2r+\kappa} \right) + \\ &\bar{\alpha}^2 \sigma^2 e^{\kappa t} C^2 \left(\frac{e^{(2r-\kappa)t} - e^{(2r-\kappa)t_0}}{2r-\kappa} \right) + 2\bar{\alpha}^2 \sigma^2 e^{\kappa t} AB \left(\frac{e^{(\eta-\kappa)t} - e^{(\eta-\kappa)t_0}}{\eta-\kappa} \right) - \\ &2\bar{\alpha}^2 \sigma^2 e^{\kappa t} AC \left(\frac{e^{(2r+\eta-\kappa)t} - e^{(2r+\eta-\kappa)t_0}}{2r+\eta-\kappa} \right) + 2\bar{\alpha}^2 \sigma^2 e^{\kappa t} BC \left(\frac{e^{-\kappa t} - e^{-\kappa t_0}}{\kappa} \right) \end{split}$$

where:

$$\begin{cases}
A = e^{-(r+\eta)t_0} \left(x_0 + \frac{\mathbf{c}_0}{r} (1 - e^{-r(T-t_0)}) \right) \\
B = \frac{\mathbf{c}_0}{r} e^{-rT + 2rt_0} \\
C = e^{-rT} \frac{\mathbf{c}_0}{r} \\
\kappa = 2 (r + \eta) + \bar{\alpha}^2 \sigma^2
\end{cases}$$

A.9 Computation of the skewness of the wealth

By Itô's lemma, we have $dX_t^3 = 3X_t^2 dX_t + 3X_t (dX_t)^2$. We deduce that:

$$dX_{t}^{3} = 3\left((r_{t} + \eta_{t}) X_{t}^{3} + \eta_{t} H_{t} X_{t}^{2} + c_{t} X_{t}^{2} + \bar{\alpha}_{t}^{2} \sigma_{t}^{2} (X_{t} + H_{t})^{2} X_{t} \right) dt + 3\bar{\alpha}_{t} \sigma_{t} (X_{t} + H_{t}) X_{t}^{2} dW_{t}$$

and:

$$\frac{\mathrm{d}}{\mathrm{d}t} \mathbb{E} \left[X_t^3 \right] = 3\mathbb{E} \left[(r_t + \eta_t) X_t^3 + \eta_t H_t X_t^2 + c_t X_t^2 + \bar{\alpha}_t^2 \sigma_t^2 \left(X_t^3 + 2H_t X_t^2 + H_t^2 X_t \right) \right] \\
= 3 \left(r_t + \eta_t + \bar{\alpha}_t^2 \sigma_t^2 \right) \mathbb{E} \left[X_t^3 \right] + 3 \left(\left(\eta_t + 2\bar{\alpha}_t^2 \sigma_t^2 \right) H_t + c_t \right) \mathbb{E} \left[X_t^2 \right] + \\
3 \bar{\alpha}_t^2 \sigma_t^2 H_t^2 \mathbb{E} \left[X_t \right] \\
= a_t \mathbb{E} \left[X_t^3 \right] + b_t$$

where:

$$\begin{cases} a_t = 3\left(r_t + \eta_t + \bar{\alpha}_t^2 \sigma_t^2\right) \\ b_t = 3\left(\left(\eta_t + 2\bar{\alpha}_t^2 \sigma_t^2\right) H_t + \mathbf{c}_t\right) \left(\upsilon_t + m_t^2\right) + 3\bar{\alpha}_t^2 \sigma_t^2 H_t^2 m_t \end{cases}$$

It follows that:

$$\mathbb{E}\left[X_t^3\right] = e^{\int_{t_0}^t a_s \, \mathrm{d}s} \left(x_0^3 + \int_{t_0}^t e^{-\int_{t_0}^s a_u \, \mathrm{d}u} b_s \, \mathrm{d}s\right)$$

Finally, we get the formula of the skewness:

$$sk_{t} = \frac{\mathbb{E}\left[\left(X_{t} - \mathbb{E}\left[X_{t}\right]\right)^{3}\right]}{\mathbb{E}^{3/2}\left[\left(X_{t} - \mathbb{E}\left[X_{t}\right]\right)^{2}\right]} = \frac{\mathbb{E}\left[X_{t}^{3}\right] - 3\left(v_{t} + m_{t}^{2}\right)m_{t} + 2m_{t}^{3}}{v_{t}^{3/2}}$$

Remark 13. When the parameters are constant, the previous formula reduces to:

$$\mathbb{E}\left[X_t^3\right] = e^{a(t-t_0)}x_0^3 + \int_{t_0}^t e^{a(t-s)}b_s \,\mathrm{d}s$$

where $a=3\left(r+\eta+\bar{\alpha}^2\sigma^2\right)$ and $b_t=3\left(\left(\eta+2\bar{\alpha}^2\sigma^2\right)H_t+\mathbf{c}_t\right)\left(\upsilon_t+m_t^2\right)+3\bar{\alpha}^2\sigma^2H_t^2m_t$.

A.10 Jensen's inequality and analytics of the glide path

The glide path g_t is defined as the expected dynamic asset allocation:

$$g_{t} = \mathbb{E}\left[\alpha_{t}^{*} \mid \mathcal{F}_{t_{0}}\right]$$

$$= \mathbb{E}\left[\frac{\mu_{t} - r_{t}}{(1 - \gamma)\sigma_{t}^{2}}\left(1 + \frac{H_{t}}{X_{t}}\right) \mid \mathcal{F}_{t_{0}}\right]$$

$$= \frac{\mu_{t} - r_{t}}{(1 - \gamma)\sigma_{t}^{2}}\left(1 + \mathbb{E}\left[\frac{1}{X_{t}} \mid \mathcal{F}_{t_{0}}\right] H_{t}\right)$$

Let f(x) be a convex function. Jensen's inequality states that $\mathbb{E}\left[f(X_t)\right] \geq f\left(\mathbb{E}\left[X_t\right]\right)$. Applying this to the function $f(x) = x^{-1}$ for x > 0 gives:

$$\mathbb{E}\left[\frac{1}{X_{t}} \mid \mathcal{F}_{t_{0}}\right] \geq \frac{1}{\mathbb{E}\left[X_{t} \mid \mathcal{F}_{t_{0}}\right]}$$

Let $m_t = \mathbb{E}[X_t]$, $v_t = \text{var}(X_t) = \mathbb{E}[(X_t - m_t)^2]$ and $\varsigma_t = \mathbb{E}[(X_t - m_t)^3]$ denote the mean, variance, and skewness moment of X_t , respectively. The Taylor expansion of $f(X_t)$ around m_t gives:

$$f(X_t) = f(m_t) + f'(m_t)(X_t - m_t) + \frac{1}{2}f''(m_t)(X_t - m_t)^2 + \frac{1}{6}f'''(\varepsilon_t)(X_t - m_t)^3$$

where $\varepsilon_t \in [X_t, m_t]$. We deduce that ⁵⁸:

$$\mathbb{E}\left[\frac{1}{X_t}\right] = \frac{1}{m_t} + \frac{v_t}{m_t^3} - \frac{\varsigma_t}{\varepsilon_t^4}$$

By assuming that $|\varsigma_t| \ll \varepsilon_t^4$, we get the second-order approximation:

$$g_t \approx \frac{\mu_t - r_t}{\left(1 - \gamma\right)\sigma_t^2} \left(1 + \frac{H_t}{m_t} + \frac{H_t v_t}{m_t^3}\right)$$

Using the same approach, the third-order approximation is:

$$g_t \approx \frac{\mu_t - r_t}{(1 - \gamma)\sigma_t^2} \left(1 + \frac{H_t}{m_t} + \frac{H_t v_t}{m_t^3} - \frac{H_t v_t^{3/2}}{m_t^4} \operatorname{sk}_t \right)$$

where $v_t^{3/2}$ is the standardized third central moment (the numerator of skewness), and sk_t denotes the skewness.

A.11 Glide path formula when the wealth is log-normal distributed

If we assume that $X_t \sim \mathcal{LN}(\tilde{\mu}_t, \tilde{\sigma}_t^2)$, we know that, for any exponent $p \neq 0$, the power X_t^p also follows a log-normal distribution:

$$X_t^p \sim \mathcal{LN}\left(p\tilde{\mu}_t, p^2\tilde{\sigma}_t^2\right)$$

We deduce that:

$$\begin{cases}
\mathbb{E}\left[X_t^p\right] = \exp\left(p\tilde{\mu}_t + \frac{1}{2}p^2\tilde{\sigma}_t^2\right) \\
\operatorname{var}\left(X_t^p\right) = \exp\left(2p\tilde{\mu}_t + p^2\tilde{\sigma}_t^2\right) \left(\exp\left(p^2\tilde{\sigma}_t^2\right) - 1\right)
\end{cases}$$

In particular, for p = -1, we get:

$$\mathbb{E}\left[\frac{1}{X_t}\right] = \exp\left(-\tilde{\mu}_t + \frac{1}{2}\tilde{\sigma}_t^2\right)$$

and:

$$\operatorname{var}\left(\frac{1}{X_t}\right) = \exp\left(-2\tilde{\mu}_t + \tilde{\sigma}_t^2\right) \left(\exp\left(\tilde{\sigma}_t^2\right) - 1\right)$$

We also note the following identity:

$$\mathbb{E}\left[\frac{1}{X_t}\right] = \frac{\exp\left(\tilde{\sigma}_t^2\right)}{\mathbb{E}\left[X_t\right]}$$

Using the expression:

$$\exp\left(\tilde{\sigma}_{t}^{2}\right) = 1 + \frac{\operatorname{var}\left(X_{t}\right)}{\mathbb{E}^{2}\left[X_{t}\right]}$$

we conclude that:

$$\mathbb{E}\left[\frac{1}{X_{t}}\right] = \frac{1}{\mathbb{E}\left[X_{t}\right]} \left(1 + \frac{\operatorname{var}\left(X_{t}\right)}{\mathbb{E}^{2}\left[X_{t}\right]}\right) = \frac{1}{\mathbb{E}\left[X_{t}\right]} + \frac{\operatorname{var}\left(X_{t}\right)}{\mathbb{E}^{3}\left[X_{t}\right]}$$

 $[\]overline{{}^{58}\text{We have } f(x) = x^{-1}, \ f'(x) = -x^{-2}, \ f''(x) = 2x^{-3}, \ \text{and} \ f'''(x) = -6x^{-4}.}$

Applying this result to the glide path formula gives:

$$g_{t} = \frac{\mu_{t} - r_{t}}{\left(1 - \gamma\right) \sigma_{t}^{2}} \left(1 + H_{t} \left(\frac{1}{\mathbb{E}\left[X_{t}\right]} + \frac{\operatorname{var}\left(X_{t}\right)}{\mathbb{E}^{3}\left[X_{t}\right]}\right)\right)$$

This expression corresponds to the approximate version of the glide path obtained using Jensen's inequality.

A.12 Simulation of the state-control dynamics

A.12.1 The unconstrained case

We recall the following equations:

$$\begin{cases} \bar{\alpha}_t = \frac{\mu_t - r_t}{(1 - \gamma)\sigma_t^2} \\ \alpha_t = \bar{\alpha}_t \left(1 + \frac{H_t}{X_t}\right) \\ \eta_t = \bar{\alpha}_t \left(\mu_t - r_t\right) \\ \mathrm{d}X_t = \left((r_t + \eta_t)X_t + \eta_t H_t + \boldsymbol{c}_t\right) \mathrm{d}t + \bar{\alpha}_t \sigma_t \left(X_t + H_t\right) \mathrm{d}W_t \end{cases}$$

We discretize the process over a time grid $t \in \{t_0, t_1, \dots, t_m = T\}$, and denote by X_m the numerical solution of X_{t_m} . Using the Euler-Maruyama scheme, we obtain:

$$\begin{cases} \bar{\alpha}_{m} = \frac{\mu_{m} - r_{m}}{\left(1 - \gamma\right)\sigma_{m}^{2}} \\ \alpha_{m} = \bar{\alpha}_{m} \left(1 + \frac{H_{m}}{X_{m}}\right) \\ \eta_{m} = \bar{\alpha}_{m} \left(\mu_{m} - r_{m}\right) \\ \varepsilon_{m} \sim \mathcal{N}\left(0, t_{m+1} - t_{m}\right) \\ X_{m+1} = X_{m} + \left(\left(r_{m} + \eta_{m}\right)X_{m} + \eta_{m}H_{m} + \mathbf{c}_{m}\right)\left(t_{m+1} - t_{m}\right) + \bar{\alpha}_{m}\sigma_{m}\left(X_{m} + H_{m}\right)\varepsilon_{m} \end{cases}$$

An alternative approach is to use the Milstein scheme with fixed time steps. In this case, the update equation becomes:

$$X_{m+1} = X_m + \left((r_m + \eta_m) X_m + \eta_m H_m + \mathbf{c}_m \right) h + \bar{\alpha}_m \sigma_m \left(X_m + H_m \right) \varepsilon_m + \frac{1}{2} \bar{\alpha}_m^2 \sigma_m^2 \left(X_m + H_m \right) \left(\varepsilon_m^2 - h \right)$$

where $\varepsilon_m \sim \mathcal{N}(0, h)$ and $h = t_{m+1} - t_m$ is the time step.

A.12.2 The constrained case

The previous equations become:

$$\begin{cases} \bar{\alpha}_t = \frac{\mu_t - r_t}{(1 - \gamma)\sigma_t^2} \\ \alpha_t = \max\left(0, \min\left(\bar{\alpha}_t\left(1 + \frac{H_t}{X_t}\right), 1\right)\right) \\ dX_t = \left(\left(r_t + \alpha_t\left(\mu_t - r_t\right)\right)X_t + c_t\right) dt + \alpha_t \sigma_t X_t dW_t \end{cases}$$

and:

$$\begin{cases} \bar{\alpha}_{m} = \frac{\mu_{m} - r_{m}}{\left(1 - \gamma\right)\sigma_{m}^{2}} \\ \alpha_{m} = \max\left(0, \min\left(\bar{\alpha}_{m}\left(1 + \frac{H_{m}}{X_{m}}\right), 1\right)\right) \\ \varepsilon_{m} \sim \mathcal{N}\left(0, t_{m+1} - t_{m}\right) \\ X_{m+1} = X_{m} + \left(\left(r_{m} + \alpha_{m}\left(\mu_{m} - r_{m}\right)\right)X_{m} + c_{m}\right)\left(t_{m+1} - t_{m}\right) + \alpha_{m}\sigma_{m}X_{m}\varepsilon_{m} \end{cases}$$
The Milstein scheme, the undate equation is:

For the Milstein scheme, the update equation is:

$$X_{m+1} = X_m + \left(\left(r_m + \alpha_m \left(\mu_m - r_m \right) \right) X_m + \mathbf{c}_m \right) h + \alpha_m \sigma_m X_m \varepsilon_m + \frac{1}{2} \alpha_m^2 \sigma_m^2 X_m \left(\varepsilon_m^2 - h \right)$$

A.13 Simplex projection methods

Duchi et al. (2008) propose the sort-and-shift (water-filling) method for projecting a vector onto the simplex Ω . Given the unconstrained weight $\check{\alpha}$, the procedure is as follows:

- Sort $\check{\alpha}$ in descending order to obtain $u_1 \geq u_2 \geq \cdots \geq u_n$;
- Compute the partial sum $S_k = \sum_{i=1}^k u_i$ and the threshold $\theta_k = \frac{S_k 1}{k}$;
- Select $k_{\text{max}} = \max\{k = 1, ..., n : u_k > \theta_k\}$ and set $\theta = \theta_{k_{\text{max}}}$;
- Shift the unconstrained weights to constrained weights:

$$\alpha_t^{\star} = \max\left(\breve{\alpha} - \theta, 0\right)$$

This method has complexity $O(n \log n)$ due to the sorting step.

Condat (2016) proposes an improved variant that replaces full sorting with a QuickSelectstyle partition, reducing the complexity to O(n) on average. Given the unconstrained solution $\check{\alpha}$, the algorithm proceeds as follows:

- If $\sum_{i=1}^{n} \check{\alpha}_i = 1$ and $\check{\alpha}_i \geq 0$, then $\alpha_t^* = \check{\alpha}$ and stop;
- Otherwise, find the threshold θ such that:

$$\sum_{i=1}^{n} \max \left(\breve{\alpha}_i - \theta, 0 \right) = 1$$

This can be achieved using a QuickSelect-based routine⁵⁹. The algorithm iteratively partitions around candidate pivots, narrowing the interval until the correct threshold is found;

• Finally, shift the unconstrained weights to constrained weights:

$$\alpha_t^{\star} = \max{(\breve{\alpha} - \theta, 0)}$$

⁵⁹QuickSelect is a selection algorithm similar to QuickSort. It partitions the array around a pivot and recursively processes only the side containing the desired element, achieving an average time complexity of O(n) and finding the k-th smallest element without fully sorting.

A.14 Separability property under the constraints $c_t = 0$, $\alpha_t \ge 0$ and $\mathbf{1}^{\top} \alpha_t < 1$

The HJB equation for a CRRA utility function is given by:

$$\frac{\partial \mathcal{J}\left(t,x\right)}{\partial t} + \max_{\alpha_{t} \in \Omega} \mathcal{H}\left(t,x,\alpha_{t}\right) = 0 \qquad \text{s.t.} \qquad \mathcal{J}\left(T,x\right) = \mathcal{\boldsymbol{U}}\left(x\right) = \frac{x^{\gamma}}{\gamma}$$

where the Hamiltonian takes the form:

$$\mathcal{H}\left(t, x, \alpha\right) = \left(\left(r_{t} + \alpha_{t}^{\top} \left(\mu_{t} - r_{t} \mathbf{1}_{n}\right)\right) x + \boldsymbol{c}_{t}\right) \frac{\partial \mathcal{J}\left(t, x\right)}{\partial x} + \frac{1}{2} \left(\alpha_{t}^{\top} \Sigma_{t} \alpha_{t}\right) x^{2} \frac{\partial^{2} \mathcal{J}\left(t, x\right)}{\partial x^{2}}$$

Generally, we guess the form of the value function is separable: $\mathcal{J}(t,x) = f(t)\mathcal{U}(x)$ with f(T) = 1. Then, we have:

$$\begin{cases} \partial_t \mathcal{J}(t, x) = \partial_t f(t) \gamma^{-1} x^{\gamma} \\ \partial_x \mathcal{J}(t, x) = f(t) x^{\gamma - 1} \\ \partial_x^2 \mathcal{J}(t, x) = f(t) (\gamma - 1) x^{\gamma - 2} \end{cases}$$

Substituting these into the HJB equation yields:

$$\partial_{t} f\left(t\right) \frac{x^{\gamma}}{\gamma} + \max_{\alpha_{t} \in \Omega} \left\{ \left(\left(r_{t} + \alpha_{t}^{\top} \left(\mu_{t} - r_{t} \mathbf{1}_{n}\right)\right) x + \boldsymbol{c}_{t} \right) f\left(t\right) x^{\gamma - 1} + \frac{\gamma - 1}{2} \left(\alpha_{t}^{\top} \Sigma_{t} \alpha_{t}\right) f\left(t\right) x^{\gamma} \right\} = 0$$

When the contribution c_t is zero, then the HJB equation simplifies to:

$$\partial_{t} f\left(t\right) \frac{x^{\gamma}}{\gamma} + \max_{\alpha_{t} \in \Omega} \left\{ \left(r_{t} + \alpha_{t}^{\top} \left(\mu_{t} - r_{t} \mathbf{1}_{n}\right)\right) f\left(t\right) x^{\gamma} + \frac{\gamma - 1}{2} \left(\alpha_{t}^{\top} \Sigma_{t} \alpha_{t}\right) f\left(t\right) x^{\gamma} \right\} = 0$$

When the constraint set Ω is independent of x, this is an ODE in f(t):

$$\frac{\partial_{t} f\left(t\right)}{\gamma} + \max_{\alpha_{t} \in \Omega} \left\{ \left(r_{t} + \alpha_{t}^{\top} \left(\mu_{t} - r_{t} \mathbf{1}_{n}\right)\right) f\left(t\right) + \frac{\gamma - 1}{2} \left(\alpha_{t}^{\top} \Sigma_{t} \alpha_{t}\right) f\left(t\right) \right\} = 0$$

The optimal solution α_t^* is also independent of x. Thus, the separability assumption holds, and we obtain:

$$-\frac{x\partial_x^2 \mathcal{J}(t,x)}{\partial_x \mathcal{J}(t,x)} = 1 - \gamma \tag{30}$$

This is the case when the constraint set Ω is defined as:

$$\Omega = \left\{ \alpha \in \mathbb{R}^n : \alpha \ge 0, \mathbf{1}^\top \alpha \le 1 \right\}$$

because it is independent of x.

Remark 14. When the contribution c_t is not zero, the HJB equation becomes:

$$\frac{\partial_{t} f\left(t\right)}{\gamma} + \max_{\alpha_{t} \in \Omega} \left\{ \left(r_{t} + \alpha_{t}^{\top} \left(\mu_{t} - r_{t} \mathbf{1}_{n}\right) + \frac{\boldsymbol{c}_{t}}{x}\right) f\left(t\right) + \frac{\gamma - 1}{2} \left(\alpha_{t}^{\top} \boldsymbol{\Sigma}_{t} \alpha_{t}\right) f\left(t\right) \right\} = 0$$

In this case, the equation explicitly depends on x, and the separability hypothesis for $\mathcal{J}(t,x)$ no longer holds.

A.15 Computation of the threshold correlation

We consider the two-asset case and note:

$$\pi_i = \frac{\mu_i - r}{1 - \gamma}$$

In the two-stage approach, the equality constraint implies $w_2 = 1 - w_1$. Therefore, the optimization problem reduces to:

$$w_{1}^{\star} = \arg\min \frac{1}{2} \left(\sigma_{1}^{2} w_{1}^{2} + 2\rho \sigma_{1} \sigma_{2} w_{1} \left(1 - w_{1} \right) + \sigma_{2}^{2} \left(1 - w_{1} \right)^{2} \right) - \pi_{1} w_{1} - \pi_{2} \left(1 - w_{1} \right)$$
s.t. $0 \le w_{1} \le 1$

The optimal solution w_1^{\star} is the clipped version of the unconstrained solution:

$$w_1^* = \text{clip}_{[0,1]} \left(\frac{\pi_1 - \pi_2 + \sigma_2^2 - \rho \sigma_1 \sigma_2}{\sigma_1^2 - 2\rho \sigma_1 \sigma_2 + \sigma_2^2} \right)$$

Hence, the necessary and sufficient conditions for the existence of an interior solution $(0 < w_1 < 1)$ are:

$$\sigma_2 \left(\rho \sigma_1 - \sigma_2 \right) < \pi_1 - \pi_2 < \sigma_1 \left(\sigma_1 - \rho \sigma_2 \right)$$

Otherwise, the condition fails and w_1^* is clipped to either 0 or 1, corresponding to full investment in a single asset. For example, in our setting, as we approach the target date, γ becomes more negative and thus $\pi_1 - \pi_2 \to 0$:

$$\sigma_2 (\rho \sigma_1 - \sigma_2) < 0 < \sigma_1 (\sigma_1 - \rho \sigma_2)$$

In this case, increasing ρ can break the interior-solution condition, leading to a corner solution with full investment in one asset. This phenomenon is illustrated in Figure 52 (right panel).

In the one-stage problem, the feasible region is the triangle $\{w_1 \geq 0, w_2 \geq 0, w_1 + w_2 \leq 1\}$. Since the objective function is a convex quadratic, the optimum must lie either in the interior of the triangle or on one of its three edges. The unconstrained solution is:

$$\check{\alpha} = \Sigma^{-1} \pi = \frac{1}{\sigma_1^2 \sigma_2^2 (1 - \rho^2)} \begin{pmatrix} \sigma_2^2 \pi_1 - \rho \sigma_1 \sigma_2 \pi_2 \\ \sigma_1^2 \pi_2 - \rho \sigma_1 \sigma_2 \pi_1 \end{pmatrix}$$

Therefore, the necessary and sufficient conditions for the existence of an interior solution are:

$$\begin{cases} \sigma_2 \pi_1 - \rho \sigma_1 \pi_2 > 0 \\ \sigma_1 \pi_2 - \rho \sigma_2 \pi_1 > 0 \\ \frac{\sigma_2^2 \pi_1 - \rho \sigma_1 \sigma_2 (\pi_1 + \pi_2) + \sigma_1^2 \pi_2}{\sigma_1^2 \sigma_2^2 (1 - \rho^2)} < 1 \end{cases}$$

These conditions can be simplified by expressing them in terms of the Sharpe ratio:

$$\begin{cases} SR_{1} - \rho SR_{2} > 0 \\ SR_{2} - \rho SR_{1} > 0 \\ \frac{\sigma_{2} SR_{1} - \rho (\sigma_{1} SR_{1} + \sigma_{2} SR_{2}) + \sigma_{1} SR_{2}}{(1 - \gamma) \sigma_{1} \sigma_{2} (1 - \rho^{2})} < 1 \end{cases}$$

For example, in our setting, as we approach the target date, γ becomes more negative, so the third condition is automatically satisfied. Moreover, if $SR_1 = SR_2 > 0$, the first

two conditions also hold. In this case, increasing ρ does not violate the interior-solution condition, and the solution remains interior, with strictly positive allocations to both assets. This is illustrated in Figure 52 (left panel).

We now compute the threshold correlation ρ^* :

• Two-stage approach When the condition $\sigma_2 (\rho \sigma_1 - \sigma_2) < \pi_1 - \pi_2 < \sigma_1 (\sigma_1 - \rho \sigma_2)$ is violated, the interior solution disappears, and the allocation collapses to a corner solution (weights (0,1) or (1,0)). Under the general assumptions $\mu_i > r$, we obtain:

$$\rho_{\text{two-stage}}^{\star} = \rho^{\star} = \min \left\{ \frac{\mu_1 - \mu_2}{(1 - \gamma)\,\sigma_1 \sigma_2} + \frac{\sigma_2}{\sigma_1}, \frac{\mu_2 - \mu_1}{(1 - \gamma)\,\sigma_1 \sigma_2} + \frac{\sigma_1}{\sigma_2} \right\}$$

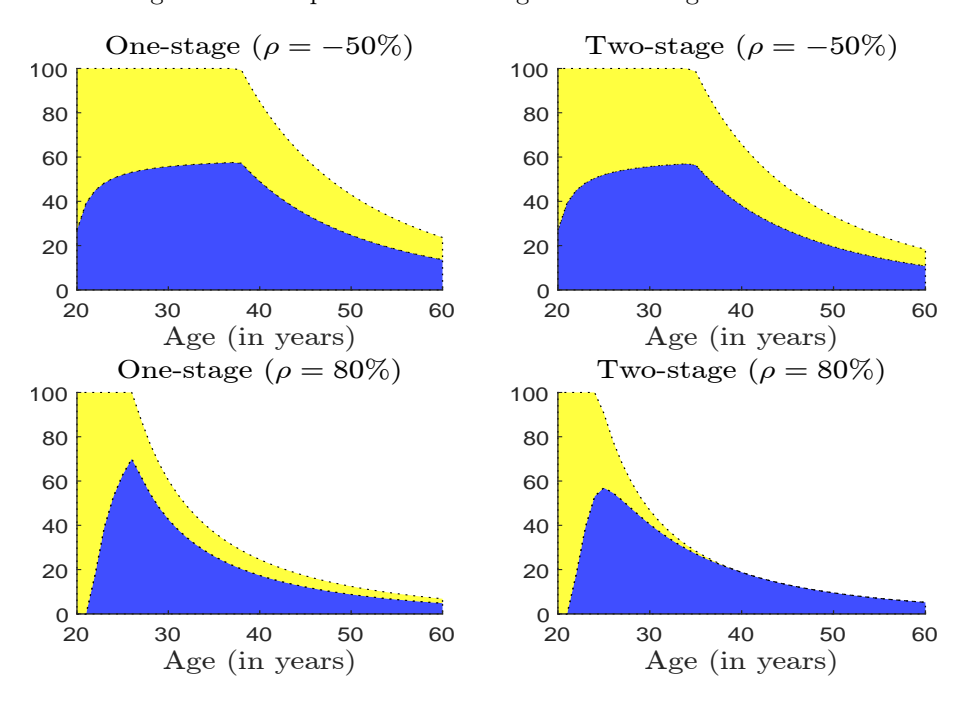
• One-stage approach Using the KKT conditions with $\lambda_0 = \lambda_1 = \lambda_2 = 0$, we obtain:

$$\rho_{\text{one-stage}}^{\star} = \rho^{\star} = \min \left\{ \frac{\sigma_{2} \left(\mu_{1} - r\right)}{\sigma_{1} \left(\mu_{2} - r\right)}, \frac{\sigma_{1} \left(\mu_{2} - r\right)}{\sigma_{2} \left(\mu_{1} - r\right)} \right\} = \min \left\{ \frac{\text{SR}_{1}}{\text{SR}_{2}}, \frac{\text{SR}_{2}}{\text{SR}_{1}} \right\}$$

The key difference is that $\rho_{\text{one-stage}}^{\star}$ is independent of the risk-aversion parameter γ , whereas $\rho_{\text{two-stage}}^{\star}$ is independent of the risk-free rate r. In particular, when $\mu_1 = \mu_2$, both formulations coincide:

$$\rho_{\text{one-stage}}^{\star} = \rho_{\text{two-stage}}^{\star} = \min \left\{ \frac{\sigma_2}{\sigma_1}, \frac{\sigma_1}{\sigma_2} \right\}$$

Figure 52: Comparison of one-stage and two-stage allocations



Remark 15. The distinction between one-stage and two-stage allocation arises from the difference between the inequality constraint, $\mathbf{1}_n^{\top} \alpha_t \leq 1$, and the equality constraint, $\mathbf{1}_n^{\top} w_t =$

1. In two-stage allocation, the allocation constraint always applies, forcing all wealth into risky assets and typically resulting in corner solutions, particularly when assets are highly correlated. Small changes in expected returns or covariances can cause significant shifts in allocation, often resulting in all investments being concentrated in a single asset. In contrast, the one-stage formulation allows the budget constraint to be slack, meaning that some wealth can remain in the risk-free asset. This flexibility reduces instability. When assets are very similar or highly correlated, the optimal solution is to invest in multiple assets with positive weights while reducing overall exposure to risky assets. These differences are illustrated in Figure 52, where the allocation to the second asset vanishes in the two-stage setting as the correlation increases, even though both assets have the same Sharpe ratio but different levels of risk⁵⁰.

A.16 Proof of Equations (22) and (23)

We remind that the Hamiltonian is:

$$\mathcal{H}(t, x, \pi, \alpha, \beta) = \left(\alpha \mu_t x + \beta \left(a_t + b_t \pi\right) x + \left(1 - \alpha - \beta\right) r_t x - \varrho \pi x + \mathbf{c}_t'\right) \frac{\partial \mathcal{J}(t, x, \pi)}{\partial x} + \frac{1}{2} \left(\alpha^2 \sigma_t^2 + \beta^2 \left(\sigma_t'\right)^2 + 2\alpha \beta \rho_t \sigma_t \sigma_t'\right) x^2 \frac{\partial^2 \mathcal{J}(t, x, \pi)}{\partial x^2} + \left(\alpha \rho_t^{(S)} \sigma_t + \beta \rho_t^{(R)} \sigma_t'\right) \sigma_t^{(\pi)} x \frac{\partial^2 \mathcal{J}(t, x, \pi)}{\partial x \partial \pi}$$

We deduce that:

$$\frac{\partial \mathcal{H}\left(t,x,\pi,\alpha,\beta\right)}{\partial \alpha} = \left(\mu_{t} - r_{t}\right) x \frac{\partial \mathcal{J}\left(t,x,\pi\right)}{\partial x} + \left(\alpha\sigma_{t}^{2} + \beta\rho_{t}\sigma_{t}\sigma_{t}'\right) x^{2} \frac{\partial^{2} \mathcal{J}\left(t,x,\pi\right)}{\partial x^{2}} + \rho_{t}^{(S)}\sigma_{t}\sigma_{t}^{(\pi)} x \frac{\partial^{2} \mathcal{J}\left(t,x,\pi\right)}{\partial x \partial \pi}$$

and:

$$\frac{\partial \mathcal{H}(t, x, \pi, \alpha, \beta)}{\partial \beta} = (a_t + b_t \pi - r_t) x \frac{\partial \mathcal{J}(t, x, \pi)}{\partial x} + \left(\beta \left(\sigma_t'\right)^2 + \alpha \rho_t \sigma_t \sigma_t'\right) x^2 \frac{\partial^2 \mathcal{J}(t, x, \pi)}{\partial x^2} + \rho_t^{(R)} \sigma_t' \sigma_t^{(\pi)} x \frac{\partial^2 \mathcal{J}(t, x, \pi)}{\partial x \partial \pi}$$

In a matrix form, the first-order conditions are:

$$\begin{pmatrix} \sigma_t^2 & \rho_t \sigma_t \sigma_t' \\ \rho_t \sigma_t \sigma_t' & \left(\sigma_t'\right)^2 \end{pmatrix} \begin{pmatrix} \alpha \\ \beta \end{pmatrix} x^2 \mathcal{J}_{x,x} + \begin{pmatrix} \mu_t - r_t \\ a_t + b_t \pi - r_t \end{pmatrix} x \mathcal{J}_x + \begin{pmatrix} \rho_t^{(S)} \sigma_t \sigma_t^{(\pi)} \\ \rho_t^{(R)} \sigma_t' \sigma_t^{(\pi)} \end{pmatrix} x \mathcal{J}_{x,\pi} = \begin{pmatrix} 0 \\ 0 \end{pmatrix}$$

where $\mathcal{J}_x = \partial_x \mathcal{J}(t, x, \pi)$, $\mathcal{J}_{x,x} = \partial_x^2 \mathcal{J}(t, x, \pi)$ and $\mathcal{J}_{x,\pi} = \partial_{x,\pi} \mathcal{J}(t, x, \pi)$. Using the notations $\theta_t = (\mu_t - r_t, a_t + b_t \pi - r_t)$ and $\zeta_t = \left(\rho_t^{(S)} \sigma_t \sigma_t^{(\pi)}, \rho_t^{(R)} \sigma_t' \sigma_t^{(\pi)}\right)$, we get:

$$x\mathcal{J}_{x,x}\Sigma_t\nu + \theta_t\mathcal{J}_x + \zeta_t\mathcal{J}_{x,\pi} = \mathbf{0}_2$$

The optimal solution is then:

$$\nu^{\star} = \begin{pmatrix} \alpha^{\star} \\ \beta^{\star} \end{pmatrix} = -\Sigma_{t}^{-1} \left(\theta_{t} \frac{\mathcal{J}_{x}}{x \mathcal{J}_{x,x}} + \zeta_{t} \frac{\mathcal{J}_{x,\pi}}{x \mathcal{J}_{x,x}} \right)$$

⁶⁰The solutions are obtained with the following parameters: $\mu_1 = 8\%$, $\mu_2 = 10\%$, $\sigma_1 = 15\%$, $\sigma_2 = 20\%$, and $\sigma_2 = 20\%$.

The matrix form of the Hamiltonian is:

$$\mathcal{H}\left(t, x, \pi, \nu\right) = \frac{1}{2} \left(x^{2} \mathcal{J}_{x, x}\right) \left(\nu^{\top} \Sigma_{t} \nu\right) + \left(x \mathcal{J}_{x}\right) \left(\nu^{\top} \theta_{t} + r_{t} - \varrho \pi\right) + \left(\mathbf{c}_{t}^{\prime} \mathcal{J}_{x}\right) + \left(x \mathcal{J}_{x, \pi}\right) \left(\nu^{\top} \zeta_{t}\right)$$

We have:

$$\begin{cases} \nu^{\star\top} \Sigma_t \nu^{\star} = \left(\frac{\mathcal{J}_x}{x \mathcal{J}_{x,x}}\right)^2 \theta_t^{\top} \Sigma_t^{-1} \theta_t + 2 \frac{\mathcal{J}_x \mathcal{J}_{x,\pi}}{\left(x \mathcal{J}_{x,x}\right)^2} \zeta_t^{\top} \Sigma_t^{-1} \theta_t + \left(\frac{\mathcal{J}_{x,\pi}}{x \mathcal{J}_{x,x}}\right)^2 \zeta_t^{\top} \Sigma_t^{-1} \zeta_t \\ \nu^{\star\top} \theta_t = -\frac{\mathcal{J}_x}{x \mathcal{J}_{x,x}} \theta_t^{\top} \Sigma_t^{-1} \theta_t - \frac{\mathcal{J}_{x,\pi}}{x \mathcal{J}_{x,x}} \zeta_t^{\top} \Sigma_t^{-1} \theta_t \\ \nu^{\star\top} \zeta_t = -\frac{\mathcal{J}_x}{x \mathcal{J}_{x,x}} \theta_t^{\top} \Sigma_t^{-1} \zeta_t - \frac{\mathcal{J}_{x,\pi}}{x \mathcal{J}_{x,x}} \zeta_t^{\top} \Sigma_t^{-1} \zeta_t \end{cases}$$

At the optimum, we deduce that:

$$\mathcal{H}(t, x, \pi, \nu_t^{\star}) = \frac{1}{2} \frac{\mathcal{J}_x^2}{\mathcal{J}_{x,x}} \theta_t^{\top} \Sigma_t^{-1} \theta_t + \frac{\mathcal{J}_x \mathcal{J}_{x,\pi}}{\mathcal{J}_{x,x}} \zeta_t^{\top} \Sigma_t^{-1} \theta_t + \frac{1}{2} \frac{\mathcal{J}_{x,\pi}^2}{\mathcal{J}_{x,x}} \zeta_t^{\top} \Sigma_t^{-1} \zeta_t - \frac{\mathcal{J}_x^2}{\mathcal{J}_{x,x}} \theta_t^{\top} \Sigma_t^{-1} \theta_t - \frac{\mathcal{J}_x \mathcal{J}_{x,\pi}}{\mathcal{J}_{x,x}} \zeta_t^{\top} \Sigma_t^{-1} \theta_t + x \mathcal{J}_x r_t - x \mathcal{J}_x \varrho \pi + \mathbf{c}_t' \mathcal{J}_x - \frac{\mathcal{J}_x \mathcal{J}_{x,\pi}}{\mathcal{J}_{x,x}} \theta_t^{\top} \Sigma_t^{-1} \zeta_t - \frac{\mathcal{J}_{x,\pi}^2}{\mathcal{J}_{x,x}} \zeta_t^{\top} \Sigma_t^{-1} \zeta_t$$

$$= -\frac{1}{2} \frac{\mathcal{J}_x^2}{\mathcal{J}_{x,x}} \theta_t^{\top} \Sigma_t^{-1} \theta_t - \frac{\mathcal{J}_x \mathcal{J}_{x,\pi}}{\mathcal{J}_{x,x}} \zeta_t^{\top} \Sigma_t^{-1} \theta_t - \frac{1}{2} \frac{\mathcal{J}_{x,\pi}^2}{\mathcal{J}_{x,x}} \zeta_t^{\top} \Sigma_t^{-1} \zeta_t + \mathcal{J}_x (r_t x - \rho \pi x + \mathbf{c}_t')$$

A.17 Proof of Equations (24) and (25)

We set the contribution c_t to 0 and consider a CRRA utility function. A common approach is to assume that the value function is separable in wealth and the state variable:

$$\mathcal{J}(t, x, \pi) = h(t, \pi) \frac{x^{\gamma}}{\gamma}$$

with terminal condition $h(T,\pi)=1$. The optimal Hamiltonian is therefore⁶¹:

$$\begin{split} \mathcal{H} \left(t, x, \pi, \nu_t^{\star} \right) & = & -\frac{1}{2} \frac{\mathcal{J}_x^2}{\mathcal{J}_{x,x}} \theta_t^{\top} \Sigma_t^{-1} \theta_t - \frac{\mathcal{J}_x \mathcal{J}_{x,\pi}}{\mathcal{J}_{x,x}} \zeta_t^{\top} \Sigma_t^{-1} \theta_t - \frac{1}{2} \frac{\mathcal{J}_{x,\pi}^2}{\mathcal{J}_{x,x}} \zeta_t^{\top} \Sigma_t^{-1} \zeta_t + \mathcal{J}_x \left(r_t x - \varrho \pi x \right) \\ & = & -\frac{1}{2} \frac{\left(h \left(t, \pi \right) x^{\gamma - 1} \right)^2}{\left(\gamma - 1 \right) h \left(t, \pi \right) x^{\gamma - 2}} \theta_t^{\top} \Sigma_t^{-1} \theta_t - \frac{h \left(t, \pi \right) x^{\gamma - 1} \partial_{\pi} h \left(t, \pi \right) x^{\gamma - 1}}{\left(\gamma - 1 \right) h \left(t, \pi \right) x^{\gamma - 2}} \zeta_t^{\top} \Sigma_t^{-1} \theta_t - \frac{1}{2} \frac{\left(\partial_{\pi} h \left(t, \pi \right) x^{\gamma - 1} \right)^2}{\left(\gamma - 1 \right) h \left(t, \pi \right) x^{\gamma - 2}} \zeta_t^{\top} \Sigma_t^{-1} \zeta_t + h \left(t, \pi \right) x^{\gamma - 1} \left(r_t - \varrho \pi \right) x \\ & = & -\frac{1}{2} \frac{h \left(t, \pi \right) x^{\gamma}}{\left(\gamma - 1 \right)} \theta_t^{\top} \Sigma_t^{-1} \theta_t - \frac{\partial_{\pi} h \left(t, \pi \right) x^{\gamma}}{\left(\gamma - 1 \right)} \zeta_t^{\top} \Sigma_t^{-1} \theta_t - \frac{1}{2} \frac{\left(\partial_{\pi} h \left(t, \pi \right) \right)^2 x^{\gamma}}{\left(\gamma - 1 \right) h \left(t, \pi \right)} \zeta_t^{\top} \Sigma_t^{-1} \zeta_t + h \left(t, \pi \right) x^{\gamma} \left(r_t - \varrho \pi \right) \end{split}$$

We obtain the following HJB equation:

$$0 = \partial_{t}h(t,\pi)\gamma^{-1} + \kappa(\pi_{\infty} - \pi)\partial_{\pi}h(t,\pi)\gamma^{-1} + \frac{1}{2}\left(\sigma_{t}^{(\pi)}\right)^{2}\partial_{\pi}^{2}h(t,\pi)\gamma^{-1} + h(t,\pi)(r_{t} - \varrho\pi) - \frac{1}{2}\frac{h(t,\pi)}{(\gamma-1)}\theta_{t}^{\top}\Sigma_{t}^{-1}\theta_{t} - \frac{\partial_{\pi}h(t,\pi)}{(\gamma-1)}\zeta_{t}^{\top}\Sigma_{t}^{-1}\theta_{t} - \frac{1}{2}\frac{\left(\partial_{\pi}h(t,\pi)\right)^{2}}{(\gamma-1)h(t,\pi)}\zeta_{t}^{\top}\Sigma_{t}^{-1}\zeta_{t}$$

Since $\theta_t = \begin{pmatrix} \mu_t - r_t \\ a_t + b_t \pi - r_t \end{pmatrix}$ depends on π , we set:

$$\theta_t = \bar{\theta}_t + \hat{\theta}_t \pi = \begin{pmatrix} \mu_t - r_t \\ a_t - r_t \end{pmatrix} + \begin{pmatrix} 0 \\ b_t \end{pmatrix} \pi$$

It follows that:

$$\begin{cases} \theta_t^\top \Sigma_t^{-1} \theta_t = \bar{\theta}_t^\top \Sigma_t^{-1} \bar{\theta}_t + 2 \bar{\theta}_t^\top \Sigma_t^{-1} \hat{\theta}_t \pi + \hat{\theta}_t^\top \Sigma_t^{-1} \hat{\theta}_t \pi^2 \\ \zeta_t^\top \Sigma_t^{-1} \theta_t = \zeta_t^\top \Sigma_t^{-1} \bar{\theta}_t + \zeta_t^\top \Sigma_t^{-1} \hat{\theta}_t \pi \end{cases}$$

We deduce that:

$$0 = \partial_{t}h(t,\pi)\gamma^{-1} + \kappa(\pi_{\infty} - \pi)\partial_{\pi}h(t,\pi)\gamma^{-1} + \frac{1}{2}\left(\sigma_{t}^{(\pi)}\right)^{2}\partial_{\pi}^{2}h(t,\pi)\gamma^{-1} + h(t,\pi)(r_{t} - \varrho\pi) - \frac{1}{2}\frac{h(t,\pi)}{(\gamma-1)}\bar{\theta}_{t}^{\top}\Sigma_{t}^{-1}\bar{\theta}_{t} - \frac{h(t,\pi)}{(\gamma-1)}\bar{\theta}_{t}^{\top}\Sigma_{t}^{-1}\hat{\theta}_{t}\pi - \frac{1}{2}\frac{h(t,\pi)}{(\gamma-1)}\hat{\theta}_{t}^{\top}\Sigma_{t}^{-1}\hat{\theta}_{t}\pi^{2} - \frac{\partial_{\pi}h(t,\pi)}{(\gamma-1)}\zeta_{t}^{\top}\Sigma_{t}^{-1}\bar{\theta}_{t} - \frac{\partial_{\pi}h(t,\pi)}{(\gamma-1)}\zeta_{t}^{\top}\Sigma_{t}^{-1}\hat{\theta}_{t}\pi - \frac{1}{2}\frac{\left(\partial_{\pi}h(t,\pi)\right)^{2}}{(\gamma-1)h(t,\pi)}\zeta_{t}^{\top}\Sigma_{t}^{-1}\zeta_{t}$$

When the constraint set Ω is independent of x, this is a non-linear partial differential equation in $h(t, \pi)$.

We assume a guess solution of $h(t, \pi)$:

$$h\left(t,\pi\right) = \exp\left(A\left(t\right) + B\left(t\right)\pi + C\left(t\right)\pi^{2}\right)$$

with terminal condition A(T) = B(T) = C(T) = 0. We have:

$$\begin{cases} \partial_{t}h(t,\pi) = (A'(t) + B'(t)\pi + C'(t)\pi^{2})h(t,\pi) \\ \partial_{\pi}h(t,\pi) = (B(t) + 2C(t)\pi)h(t,\pi) \\ \partial_{\pi}^{2}h(t,\pi) = (2C(t) + (B(t) + 2C(t)\pi)^{2})h(t,\pi) \end{cases}$$

The HJB equation becomes:

$$\begin{array}{ll} 0 & = & \left(A'\left(t\right) + B'\left(t\right)\pi + C'\left(t\right)\pi^{2}\right) + \kappa\left(\pi_{\infty} - \pi\right)\left(B\left(t\right) + 2C\left(t\right)\pi\right) + \\ & \frac{1}{2}\left(\sigma_{t}^{(\pi)}\right)^{2}\left(2C\left(t\right) + \left(B\left(t\right) + 2C\left(t\right)\pi\right)^{2}\right) + \gamma\left(r_{t} - \varrho\pi\right) - \\ & \frac{1}{2}\frac{\gamma}{\gamma - 1}\bar{\theta}_{t}^{\intercal}\Sigma_{t}^{-1}\bar{\theta}_{t} - \frac{\gamma}{\gamma - 1}\bar{\theta}_{t}^{\intercal}\Sigma_{t}^{-1}\hat{\theta}_{t}\pi - \frac{1}{2}\frac{\gamma}{\gamma - 1}\hat{\theta}_{t}^{\intercal}\Sigma_{t}^{-1}\hat{\theta}_{t}\pi^{2} - \\ & \frac{\gamma\left(B\left(t\right) + 2C\left(t\right)\pi\right)}{\gamma - 1}\zeta_{t}^{\intercal}\Sigma_{t}^{-1}\bar{\theta}_{t} - \frac{\gamma\left(B\left(t\right) + 2C\left(t\right)\pi\right)}{\gamma - 1}\zeta_{t}^{\intercal}\Sigma_{t}^{-1}\hat{\theta}_{t}\pi - \\ & \frac{1}{2}\frac{\gamma\left(B\left(t\right) + 2C\left(t\right)\pi\right)^{2}}{\gamma - 1}\zeta_{t}^{\intercal}\Sigma_{t}^{-1}\zeta_{t} \end{array}$$

or:

$$a_{\pi}(t) \pi^{2} + b_{\pi}(t) \pi + c_{\pi}(t) = 0$$
 (31)

where:

$$\begin{cases} a_{\pi}\left(t\right) &= C'\left(t\right) - 2\kappa C\left(t\right) + 2\left(\sigma_{t}^{(\pi)}\right)^{2}C^{2}\left(t\right) - \frac{1}{2}\frac{\gamma}{\gamma - 1}\hat{\theta}_{t}^{\top}\Sigma_{t}^{-1}\hat{\theta}_{t} - 2\frac{\gamma}{\gamma - 1}C\left(t\right)\zeta_{t}^{\top}\Sigma_{t}^{-1}\hat{\theta}_{t} - 2\frac{\gamma}{\gamma - 1}C^{2}\left(t\right)\zeta_{t}^{\top}\Sigma_{t}^{-1}\zeta_{t} \\ b_{\pi}\left(t\right) &= B'\left(t\right) + \kappa\left(2\pi_{\infty}C\left(t\right) - B\left(t\right)\right) + 2\left(\sigma_{t}^{(\pi)}\right)^{2}B\left(t\right)C\left(t\right) - \gamma\varrho - \frac{\gamma}{\gamma - 1}\bar{\theta}_{t}^{\top}\Sigma_{t}^{-1}\hat{\theta}_{t} - 2\frac{\gamma}{\gamma - 1}C\left(t\right)\zeta_{t}^{\top}\Sigma_{t}^{-1}\bar{\theta}_{t} - \frac{\gamma}{\gamma - 1}B\left(t\right)\zeta_{t}^{\top}\Sigma_{t}^{-1}\hat{\theta}_{t} - 2\frac{\gamma}{\gamma - 1}B\left(t\right)\zeta_{t}^{\top}\Sigma_{t}^{-1}\bar{\theta}_{t} - \frac{\gamma}{\gamma - 1}B\left(t\right)\zeta_{t}^{\top}\Sigma_{t}^{-1}\hat{\theta}_{t} - \frac{1}{2}\frac{\gamma}{\gamma - 1}B\left(t\right)\zeta_{t}^{\top}\Sigma_{t}^{-1}\hat{\theta}_{t} - \frac{1}{2}\frac{\gamma}{\gamma - 1}B\left(t\right)\zeta_{t}^{\top}\Sigma_{t}^{-1}\zeta_{t} \end{cases}$$

$$c_{\pi}\left(t\right) &= A'\left(t\right) + \kappa\pi_{\infty}B\left(t\right) + \frac{1}{2}\left(\sigma_{t}^{(\pi)}\right)^{2}\left(B^{2}\left(t\right) + 2C\left(t\right)\right) + \gamma r_{t} - \frac{1}{2}\frac{\gamma}{\gamma - 1}\bar{\theta}_{t}^{\top}\Sigma_{t}^{-1}\bar{\theta}_{t} - \frac{\gamma}{\gamma - 1}B\left(t\right)\zeta_{t}^{\top}\Sigma_{t}^{-1}\bar{\theta}_{t} - \frac{1}{2}\frac{\gamma}{\gamma - 1}B^{2}\left(t\right)\zeta_{t}^{\top}\Sigma_{t}^{-1}\zeta_{t} \end{cases}$$

Since Equation (31) must be satisfied for all values of π , we deduce that:

$$\begin{pmatrix} a_{\pi}(t) \\ b_{\pi}(t) \\ c_{\pi}(t) \end{pmatrix} = \mathbf{0}_{3}$$

It follows that ⁶²:

$$\begin{cases} \frac{\mathrm{d}A(t)}{\mathrm{d}t} &= -\kappa \pi_{\infty} B(t) - \frac{1}{2} \left(\sigma_{t}^{(\pi)}\right)^{2} \left(B^{2}(t) + 2C(t)\right) - \gamma r_{t} + \\ & \frac{\gamma}{\gamma - 1} \left(\frac{1}{2} \bar{\theta}_{t}^{\top} \Sigma_{t}^{-1} \bar{\theta}_{t} + B(t) \zeta_{t}^{\top} \Sigma_{t}^{-1} \bar{\theta}_{t} + \frac{1}{2} B^{2}(t) \zeta_{t}^{\top} \Sigma_{t}^{-1} \zeta_{t}\right) \\ \frac{\mathrm{d}B(t)}{\mathrm{d}t} &= -\kappa \left(2\pi_{\infty} C(t) - B(t)\right) - 2 \left(\sigma_{t}^{(\pi)}\right)^{2} B(t) C(t) + \gamma \varrho + \\ & \frac{\gamma}{\gamma - 1} \left(\bar{\theta}_{t} + B(t) \zeta_{t}\right)^{\top} \Sigma_{t}^{-1} \left(\hat{\theta}_{t} + 2C(t) \zeta_{t}\right) \\ \frac{\mathrm{d}C(t)}{\mathrm{d}t} &= 2\kappa C(t) - 2 \left(\sigma_{t}^{(\pi)}\right)^{2} C^{2}(t) + \\ & \frac{1}{2} \frac{\gamma}{\gamma - 1} \left(\hat{\theta}_{t} + 2C(t) \zeta_{t}\right)^{\top} \Sigma_{t}^{-1} \left(\hat{\theta}_{t} + 2C(t) \zeta_{t}\right) \end{cases}$$

where A(T) = B(T) = C(T) = 0. This is a standard ordinary differential equation with terminal value, that can be solved with Runge-Kutta algorithm and the change of variable $\tau = T - t$.

A.18 Proof of Equations (26) and (27)

We remind that the HJB equation is:

$$\frac{\partial \mathcal{J}\left(t,x,\pi\right)}{\partial t} + \kappa\left(\pi_{\infty} - \pi_{t}\right) \frac{\partial \mathcal{J}\left(t,x,\pi\right)}{\partial \pi} + \frac{1}{2} \left(\sigma_{t}^{(\pi)}\right)^{2} \frac{\partial^{2} \mathcal{J}\left(t,x,\pi\right)}{\partial \pi^{2}} + \max \mathcal{H}\left(t,x,\pi,\nu_{t}\right) = 0$$

$$\frac{\partial^{2} \mathcal{W}e \text{ use the simplifications } \hat{\theta}_{t}^{\top} \Sigma_{t}^{-1} \hat{\theta}_{t}^{\top} + 4C\left(t\right) \hat{\theta}_{t}^{\top} \Sigma_{t}^{-1} \zeta_{t} + 4C^{2}\left(t\right) \zeta_{t}^{\top} \Sigma_{t}^{-1} \zeta_{t} = \left(\hat{\theta}_{t} + 2C\left(t\right) \zeta_{t}\right)^{\top} \Sigma_{t}^{-1} \left(\hat{\theta}_{t} + 2C\left(t\right) \zeta_{t}\right) \text{ and } \hat{\theta}_{t}^{\top} \Sigma_{t}^{-1} \hat{\theta}_{t} + 2C\left(t\right) \hat{\theta}_{t}^{\top} \Sigma_{t}^{-1} \zeta_{t} + B\left(t\right) \zeta_{t}^{\top} \Sigma_{t}^{-1} \hat{\theta}_{t} + 2B\left(t\right) C\left(t\right) \zeta_{t}^{\top} \Sigma_{t}^{-1} \zeta_{t} = \left(\bar{\theta}_{t} + B\left(t\right) \zeta_{t}\right)^{\top} \Sigma_{t}^{-1} \left(\hat{\theta}_{t} + 2C\left(t\right) \zeta_{t}\right).$$

where:

$$\mathcal{H}\left(t, x, \pi, \nu_{t}\right) = \frac{1}{2} \left(x^{2} \mathcal{J}_{x, x}\right) \left(\nu_{t}^{\top} \Sigma_{t} \nu_{t}\right) + \left(x \mathcal{J}_{x}\right) \left(\nu_{t}^{\top} \theta_{t} + r_{t} - \varrho \pi\right) + \left(x \mathcal{J}_{x, \pi}\right) \left(\nu_{t}^{\top} \zeta_{t}\right)$$

By assuming that $\mathcal{J}(t, x, \pi) = h(t, \pi) \frac{x^{\gamma}}{\gamma}$ and ν_t is fixed, we get:

$$\partial_{t}h\left(t,\pi\right) + \kappa\left(\pi_{\infty} - \pi_{t}\right)\partial_{\pi}h\left(t,\pi\right) + \frac{1}{2}\left(\sigma_{t}^{(\pi)}\right)^{2}\partial_{\pi}^{2}h\left(t,\pi\right) + \frac{1}{2}\gamma\left(\gamma - 1\right)\left(\nu_{t}^{\top}\Sigma_{t}\nu_{t}\right)h\left(t,\pi\right) + \gamma\left(\nu_{t}^{\top}\theta_{t} + r_{t} - \varrho\pi\right)h\left(t,\pi\right) + \gamma\left(\nu_{t}^{\top}\zeta_{t}\right)\partial_{\pi}h\left(t,\pi\right) = 0$$

or:

$$\partial_{t}h\left(t,\pi\right) + \left(\kappa\left(\pi_{\infty} - \pi_{t}\right) + \gamma\left(\nu_{t}^{\top}\zeta_{t}\right)\right)\partial_{\pi}h\left(t,\pi\right) + \frac{1}{2}\left(\sigma_{t}^{(\pi)}\right)^{2}\partial_{\pi}^{2}h\left(t,\pi\right) +$$

$$\gamma\left(\nu_{t}^{\top}\theta_{t} + r_{t} - \varrho\pi + \frac{1}{2}\left(\gamma - 1\right)\left(\nu_{t}^{\top}\Sigma_{t}\nu_{t}\right)\right)h\left(t,\pi\right) = 0$$

Knowing $h(t, \pi)$, the maximization of the Hamiltonian implies that:

$$\max \mathcal{H}(t, x, \pi, \nu_t) = \max \frac{1}{2} \left(x^2 \mathcal{J}_{x,x} \right) \left(\nu_t^{\top} \Sigma_t \nu_t \right) + \left(x \mathcal{J}_x \right) \left(\nu_t^{\top} \theta_t + r_t - \varrho \pi \right) + \left(x \mathcal{J}_{x,\pi} \right) \left(\nu_t^{\top} \zeta_t \right)$$

$$= \max \frac{1}{2} \left(\gamma - 1 \right) \left(\nu_t^{\top} \Sigma_t \nu_t \right) h\left(t, \pi\right) + \left(\nu_t^{\top} \theta_t + r_t - \varrho \pi \right) h\left(t, \pi\right) + \left(\nu_t^{\top} \zeta_t \right) \partial_{\pi} h\left(t, \pi\right)$$

$$= \max \frac{1}{2} \left(\gamma - 1 \right) h\left(t, \pi\right) \left(\nu_t^{\top} \Sigma_t \nu_t \right) + \left(h\left(t, \pi\right) \theta_t^{\top} + \partial_{\pi} h\left(t, \pi\right) \zeta_t^{\top} \right) \nu_t$$

A.19 Numerical solution of the Howard's policy-iteration algorithm (Equations 26 and 27)

We remind that the HJB equation is given by:

$$\frac{\partial \mathcal{J}\left(t,x,\pi\right)}{\partial t} + \kappa \left(\pi_{\infty} - \pi\right) \frac{\partial \mathcal{J}\left(t,x,\pi\right)}{\partial \pi} + \frac{1}{2} \left(\sigma_{t}^{(\pi)}\right)^{2} \frac{\partial^{2} \mathcal{J}\left(t,x,\pi\right)}{\partial \pi^{2}} + \max_{\nu \in \Omega} \mathcal{H}\left(t,x,\pi,\nu\right) = 0$$

with the terminal condition $\mathcal{J}(T, x, \pi) = \mathcal{U}(x) = \gamma^{-1} x^{\gamma}$. Since the CRRA utility function is homogeneous, we use the standard separation $\mathcal{J}(t, x, \pi) = \gamma^{-1} x^{\gamma} h(t, \pi)$, where $h(t, \pi)$ is a function that depends only on time and inflation. The corresponding terminal condition is $h(T, \pi) = 1$. The HJB equation can be rewritten as:

$$\gamma^{-1}\partial_{t}h\left(t,\pi\right) + \kappa\left(\pi_{\infty} - \pi\right)\gamma^{-1}\partial_{\pi}h\left(t,\pi\right) + \frac{1}{2}\left(\sigma_{t}^{(\pi)}\right)^{2}\gamma^{-1}\partial_{\pi}^{2}h\left(t,\pi\right) + \max_{\nu \in \Omega}\mathcal{G}\left(t,\pi,\nu\right) = 0$$

where:

$$\mathcal{G}\left(t,\pi,\nu\right) = \left(r_{t} - \varrho\pi\right)h\left(t,\pi\right) + h\left(t,\pi\right)\theta_{t}^{\top}\nu + \frac{1}{2}\left(\gamma - 1\right)h\left(t,\pi\right)\nu^{\top}\Sigma_{t}\nu + \partial_{\pi}h\left(t,\pi\right)\zeta_{t}^{\top}\nu$$

and $\Omega = \{ \nu \in \mathbb{R}^2 \mid \nu \geq \mathbf{0}_n, \mathbf{1}_n^\top \nu \leq 1 \}$. Therefore, we obtain:

$$\partial_{t}h\left(t,\pi\right) + \kappa\left(\pi_{\infty} - \pi\right)\partial_{\pi}h\left(t,\pi\right) + \frac{1}{2}\left(\sigma_{t}^{(\pi)}\right)^{2}\partial_{\pi}^{2}h\left(t,\pi\right) + \gamma \cdot \max_{\nu \in \Omega} \left\{\frac{1}{2}\left(\gamma - 1\right)h\left(t,\pi\right)\nu^{\top}\Sigma_{t}\nu + \left(h\left(t,\pi\right)\theta_{t} + \partial_{\pi}h\left(t,\pi\right)\zeta_{t}\right)^{\top}\nu + \left(r_{t} - \varrho\pi\right)h\left(t,\pi\right)\right\} = 0$$

To implement the Howard's policy-iteration algorithm, we use the finite difference method for $t \in [t_0, T]$ and $\pi \in [\pi^-, \pi^+]$. Let N_t and N_π denote the number of discretization points for t and π , respectively. We define Δt and $\Delta \pi$ as the mesh spacings. Let $h_i^m \approx h\left(t_m, \pi_i\right)$ be the approximate solution of $h\left(t, \pi\right)$ at the grid point (t_m, π_i) , where $t_m = t_0 + m \cdot \Delta t$ and $\pi_i = \pi^- + i \cdot \Delta \pi$.

A.19.1 Policy evaluation

Given a fixed control ν , we have:

$$\partial_{t}h + \underbrace{\frac{1}{2} \left(\sigma_{t}^{(\pi)}\right)^{2}}_{a} \partial_{\pi}^{2}h + \underbrace{\left(\kappa \left(\pi_{\infty} - \pi\right) + \gamma \zeta_{t}^{\top} \nu\right)}_{b(\pi)} \partial_{\pi}h + \underbrace{\left(\frac{1}{2}\gamma \left(\gamma - 1\right) \nu^{\top} \Sigma_{t}\nu + \gamma \theta_{t}^{\top} \nu + \gamma \left(r_{t} - \varrho \pi\right)\right)}_{c(\pi)} h = 0$$

To solve this PDE, we use a fully implicit backward-in-time finite difference scheme with Neumann boundary conditions. The backward step of the PDE from t_{m+1} to $t_m = t_{m+1} - \Delta t$ is $\partial_t h + a \partial_{\pi}^2 h + b(\pi) \partial_{\pi} h + c(\pi) h = 0$. This gives:

$$\frac{h_i^m - h_i^{m+1}}{\Delta t} - \left(a\partial_{\pi}^2 + b\left(\pi_i\right)\partial_{\pi} + c\left(\pi_i\right)\right)h_i^m = 0$$

where $a = \frac{1}{2} \left(\sigma_t^{(\pi)} \right)^2$, $b\left(\pi_i \right) = \kappa \left(\pi_\infty - \pi_i \right) + \gamma \zeta_t^\top \nu_i^m$, and $c\left(\pi_i \right) = \frac{1}{2} \gamma \left(\gamma - 1 \right) \left(\nu_i^m \right)^\top \Sigma_t \nu_i^m + \gamma \theta_t^\top \nu_i^m + \gamma \left(r_t - \varrho \pi_i \right)$. This can be written in matrix form as $\left(I - \Delta t \mathcal{L}^m \right) h^m = h^{m+1}$ where $h^m = \left(h_0^m, h_1^m, \ldots, h_{N_\pi}^m \right)$ and $\mathcal{L}^m = a \partial_\pi^2 + b\left(\pi \right) \partial_\pi + c\left(\pi \right)$ with all coefficients evaluated at time t_m . The spatial derivatives are approximated by:

$$\partial_{\pi}^2 h_i^m \approx \frac{h_{i+1}^m - 2h_i^m + h_{i-1}^m}{\Delta \pi^2}$$

and:

$$\partial_{\pi} h_{i}^{m} \approx \begin{cases} \frac{h_{i+1}^{m} - h_{i}^{m}}{\Delta \pi} & \text{if } b\left(\pi_{i}\right) \geq 0\\ \frac{h_{i}^{m} - h_{i-1}^{m}}{\Delta \pi} & \text{if } b\left(\pi_{i}\right) < 0 \end{cases}$$

We then build the tridiagonal matrix A such that $Ah^m = h^{m+1}$, where:

$$A = I - \Delta t \mathcal{L}^m = \begin{bmatrix} d_0 & u_0 & 0 & \cdots & 0 \\ \ell_1 & d_1 & u_1 & \ddots & \vdots \\ 0 & \ddots & \ddots & \ddots & 0 \\ \vdots & \ddots & \ell_{N-1} & d_{N-1} & u_{N-1} \\ 0 & \cdots & 0 & \ell_N & d_N \end{bmatrix}$$

Let $s = a\Delta t/\Delta \pi^2$ be a constant scalar. At an interior node $i = 1, ..., N_{\pi} - 1$, the discrete equation for row i is:

• when $b(\pi_i) \geq 0$:

$$h_{i}^{m} - h_{i}^{m+1} - \left(a\frac{h_{i+1}^{m} - 2h_{i}^{m} + h_{i-1}^{m}}{\Delta \pi^{2}} + b\left(\pi_{i}\right)\frac{h_{i+1}^{m} - h_{i}^{m}}{\Delta \pi} + c\left(\pi_{i}\right)h_{i}^{m}\right)\Delta t = 0$$

which gives $\ell_i = -s$, $d_i = 1 + 2s + b(\pi_i) \Delta t / \Delta \pi - c(\pi_i) \Delta t$, and $u_i = -s - b(\pi_i) \Delta t / \Delta \pi$.

• when $b(\pi_i) < 0$:

$$h_i^m - h_i^{m+1} - \left(a\frac{h_{i+1}^m - 2h_i^m + h_{i-1}^m}{\Delta \pi^2} + b\left(\pi_i\right)\frac{h_i^m - h_{i-1}^m}{\Delta \pi} + c\left(\pi_i\right)h_i^m\right)\Delta t = 0$$

which gives
$$\ell_i = -s + b(\pi_i) \Delta t / \Delta \pi$$
, $d_i = 1 + 2s - b(\pi_i) \Delta t / \Delta \pi - c(\pi_i) \Delta t$, and $u_i = -s$.

At the left boundary (i=0), we impose the Neumann condition $\partial_{\pi}h_0^m=0$. Using central differences, it follows that $\partial_{\pi}^2 h_0^m \approx 2 \left(h_1^m - h_0^m\right)/\Delta \pi^2$ and we have:

- when $b(\pi_i) \geq 0$, $\ell_0 = 0$, $d_0 = 1 + 2s + b(\pi_0) \Delta t / \Delta \pi c(\pi_0) \Delta t$, and $u_0 = -2s b(\pi_0) \Delta t / \Delta \pi$.
- when $b(\pi_i) < 0$, $\ell_0 = 0$, $d_0 = 1 + 2s b(\pi_0) \Delta t / \Delta \pi c(\pi_0) \Delta t$, and $u_0 = -2s + b(\pi_0) \Delta t / \Delta \pi$.

At the right boundary $(i=N_{\pi})$, we impose the Neumann condition $\partial_{\pi}h_{N_{\pi}}^{m}=0$. It follows that $\partial_{\pi}^{2}h_{N_{\pi}}^{m}\approx 2\left(h_{N_{\pi}-1}^{m}-h_{N_{\pi}}^{m}\right)/\Delta\pi^{2}$, and we have:

- when $b(\pi_i) \geq 0$, $\ell_{N_{\pi}} = -2s + b(\pi_{N_{\pi}}) \Delta t / \Delta \pi$, $d_{N_{\pi}} = 1 + 2s + b(\pi_{N_{\pi}}) \Delta t / \Delta \pi c(\pi_{N_{\pi}}) \Delta t$, and $u_{N_{\pi}} = 0$.
- when $b(\pi_i) < 0$, $\ell_{N_{\pi}} = -2s + b(\pi_{N_{\pi}}) \Delta t / \Delta \pi$, $d_{N_{\pi}} = 1 + 2s b(\pi_{N_{\pi}}) \Delta t / \Delta \pi c(\pi_{N_{\pi}}) \Delta t$, and $u_{N_{\pi}} = 0$.

Finally, the linear system $Ah^m = h^{m+1}$ can be efficiently solved using a tridiagonal matrix algorithm.

A.19.2 Policy improvement

Given the updated value function h_i^m , we update the control variable ν_i^m by solving the following constrained optimization problem:

$$\nu^{\star} = \arg\max\left\{\frac{1}{2}\left(\gamma - 1\right)h_i^m \nu^{\top} \Sigma_t \nu + \left(h_i^m \theta_t^{\top} + \partial_{\pi} h_i^m \zeta_t^{\top}\right) \nu + \left(r_t - \varrho \pi\right) h_i^m\right\}$$
s.t. $\nu \in \Omega$

Equivalently, this problem can be written as a minimization:

$$\nu^{\star} = \arg\min \left\{ \frac{1}{2} (1 - \gamma) \nu^{\top} \Sigma_{t} \nu - \left(\theta_{t}^{\top} + \frac{\partial_{\pi} h_{i}^{m}}{h_{i}^{m}} \zeta_{t}^{\top} \right) \nu \right\}$$
s.t. $\nu \in \Omega$

Thus, for each time step t_m and grid point π_i , we must solve a quadratic programming problem. For the sake of simplicity, we define $Q = (1 - \gamma) \Sigma_t$ and $q_i^m = -\left(\theta + \left(\partial_\pi \ln h_i^m\right) \zeta\right)$. We approximate the derivative $\partial_\pi \ln h_i^m$ using a central difference scheme: $\partial_\pi \ln h_i^m \approx$

 $(\ln h_{i+1}^m - \ln h_{i-1}^m) / (2\Delta\pi)$. Hence, the optimization problem takes the compact quadratic form:

$$\min_{\nu \in \Omega} \frac{1}{2} \nu^{\top} Q \nu + (q_i^m)^{\top} \nu$$

This step yields the optimal control ν_i^m at each grid point, completing the policy improvement phase of Howard's algorithm.

A.19.3 Two-asset case

In dimension two, the optimization problem described above can be solved explicitly by enumerating the KKT-consistent active sets. The feasible set $\Omega = \{\nu : \nu \geq \mathbf{0}_2, \mathbf{1}_2^{\top} \nu \leq 1\}$ is a triangle, so the unique minimizer lies either in the interior, on one of the three edges, or at a corner of this triangle. To formulate the KKT conditions, we write the inequality constraints as $g_1(\nu) = -\nu_1 \leq 0$, $g_2(\nu) = -\nu_2 \leq 0$, $g_3(\nu) = \nu_1 + \nu_2 - 1 \leq 0$, and introduce the Lagrange multipliers λ_1 , λ_2 , and λ_3 . The KKT conditions are listed below:

- Stationarity: $Q\nu + q_i^m \lambda_1 e_1 \lambda_2 e_2 + \lambda_3 \mathbf{1}_2 = \mathbf{0}_2$ where $e_1 = (1,0)$ and $e_2 = (0,1)$.
- Complementary slackness: $\lambda_1\nu_1=0, \ \lambda_2\nu_2=0, \ \text{and} \ \lambda_3\left(\nu_1+\nu_2-1\right)=0.$
- Primal feasibility: $\nu_1 \geq 0$, $\nu_2 \geq 0$, and $\nu_1 + \nu_2 \leq 1$.

We now enumerate the possible active sets and derive the corresponding candidate solutions:

- 1. Interior solution If $\nu_1 > 0$, $\nu_2 > 0$, $\nu_1 + \nu_2 < 1$, then all inequality constraints are inactive: $\lambda_1 = \lambda_2 = \lambda_3 = 0$. The optimal solution is $\nu^* = -Q^{-1}q_i^m$.
- 2. Edge $\nu_1 + \nu_2 = 1$ with $\nu_1 > 0$ and $\nu_2 > 0$ In this case, we have $\lambda_1 = \lambda_2 = 0$ and $\lambda_3 \geq 0$. Stationarity gives $Q\nu + q_i^m + \lambda_3 \mathbf{1}_2 = \mathbf{0}_2$, hence $\nu = -Q^{-1} \left(q_i^m + \lambda_3 \mathbf{1}_2 \right)$. Imposing the equality $\mathbf{1}_2^\top \nu = 1$ yields $\mathbf{1}_2^\top \left(-Q^{-1} \left(q_i^m + \lambda_3 \mathbf{1}_2 \right) \right) = 1$. We deduce that $\lambda_3 = -\frac{1 + \mathbf{1}_2^\top Q^{-1} q_i^m}{\mathbf{1}_2^\top Q^{-1} \mathbf{1}_2}$ and $\nu^* = -Q^{-1} \left(q_i^m + \lambda_3 \mathbf{1}_2 \right)$.
- 3. Edge $\nu_1=0$ with $\nu_2\in[0,1]$ Assume $v_1=0$ and $0\leq v_2\leq 1$, and the sum constraint is not active. Then $\lambda_1\geq 0$, $\lambda_2=0$, and $\lambda_3=0$. The stationarity conditions become $(Q)_{1,1}\cdot 0+(Q)_{1,2}v_2+(q_i^m)_1-\lambda_1=0$ and $(Q)_{1,2}\cdot 0+(Q)_{2,2}v_2+(q_i^m)_2=0$. We get $v_2^\star=-(q_i^m)_2/(Q)_{2,2}$. If $v_2^\star\notin[0,1]$, the one-dimensional convex problem's solution is its projection onto [0,1]: $v_2^\star=\Pi_{[0,1]}\left(-\left(q_i^m\right)_2/(Q)_{2,2}\right)$.
- 4. Edge $\nu_{2} = 0$ with $\nu_{1} \in [0, 1]$ By symmetry, we get $v_{1}^{\star} = \Pi_{[0,1]} \left(-\left(q_{i}^{m}\right)_{1}/\left(Q\right)_{1,1}\right)$.
- 5. Corners
 The remaining corners are (0,0), (1,0), and (0,1).

Therefore, in the two-asset case, seven candidate solutions must be tested in total (interior, three edges, and three corners). This explicit active-set enumeration approach is computationally faster and more stable than using a general-purpose QP solver for this low-dimensional case.

A.19.4 Convergence

We iterate the two steps (policy evaluation and policy improvement) until convergence for each time step t_m . This iterative procedure yields the function solution h_i^m and the optimal constrained policy ν_i^m . The corresponding value function is then given by:

$$\mathcal{J}\left(t_{m}, x, \pi_{i}\right) = \frac{x^{\gamma}}{\gamma} h_{i}^{m}$$

B Additional results

Figure 53: Population pyramid (China, 1960–2100)



Source: United Nations (2024) & Authors' calculations.

Male Female 8% 6% 4% 2% 0 2% 4% 6% 8% 8% 6% 4% 2% 0 2% 4% 6% 8% 8% 6% 4% 2% 0 2% 4% 6% 8% 8% 6% 4% 2% 0 2% 4% 6% 8%

Figure 54: Population pyramid (India, 1960–2100)

Source: United Nations (2024) & Authors' calculations.

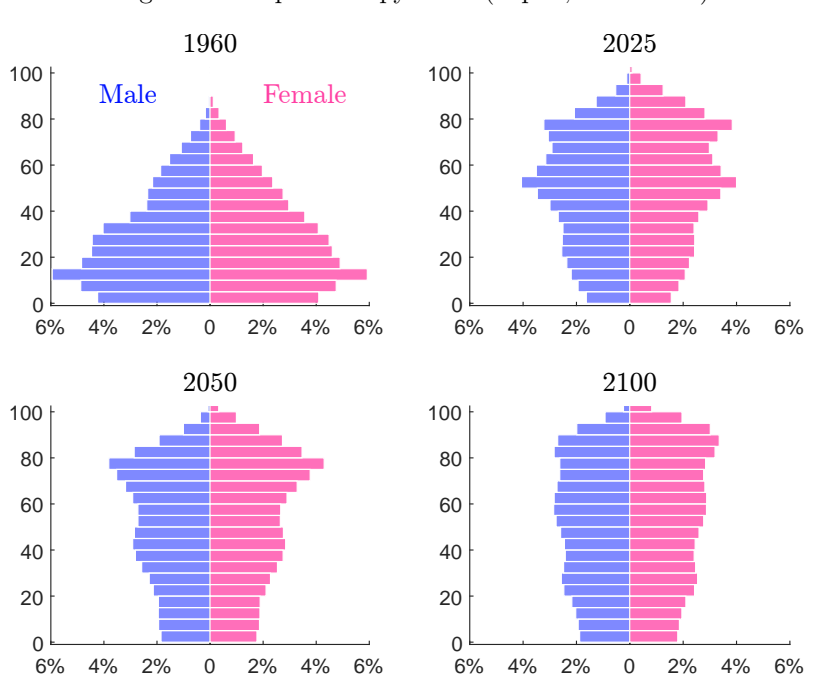


Figure 55: Population pyramid (Japan, 1960–2100)

Source: United Nations (2024) & Authors' calculations.

1960 2025100 100 Male Female 80 80 60 60 40 40 20 20 0 2% 0 2% 4% 2% 2% 6% 6% 4% 4% 6% 0 4% 2050 2100 100 100 80 80 60 60 40 40 20 20 0 6% 4% 2% 2% 4% 6% 4% 2% 2% 4% 6%

Figure 56: Population pyramid (US, 1960–2100)

Source: United Nations (2024) & Authors' calculations.



Figure 57: Population pyramid (Western Europe, 1960–2100)

Source: United Nations (2024) & Authors' calculations.

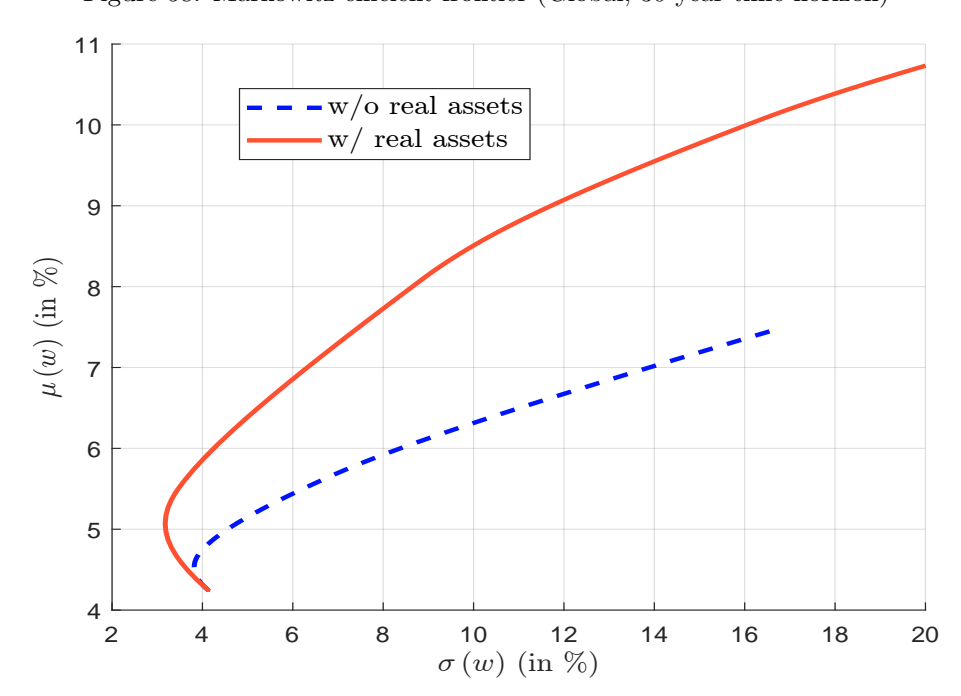


Figure 58: Markowitz efficient frontier (Global, 30-year time horizon)

Figure 59: Composition of mean-variance optimized portfolios excluding real assets (Global, 30-year time horizon)

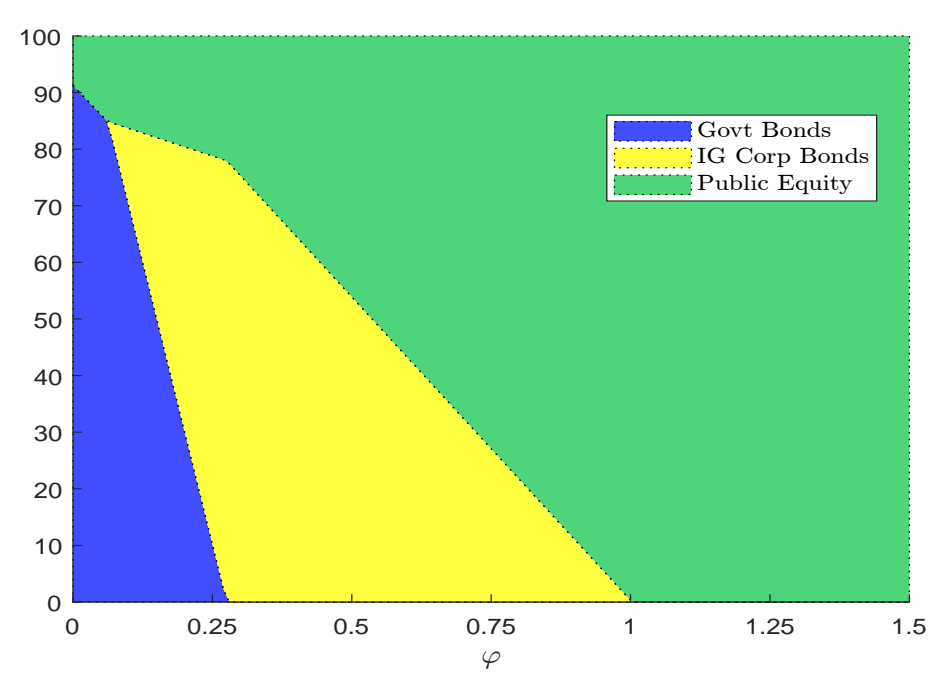


Figure 60: Composition of mean-variance optimized portfolios with real assets (Global, 30-year time horizon)

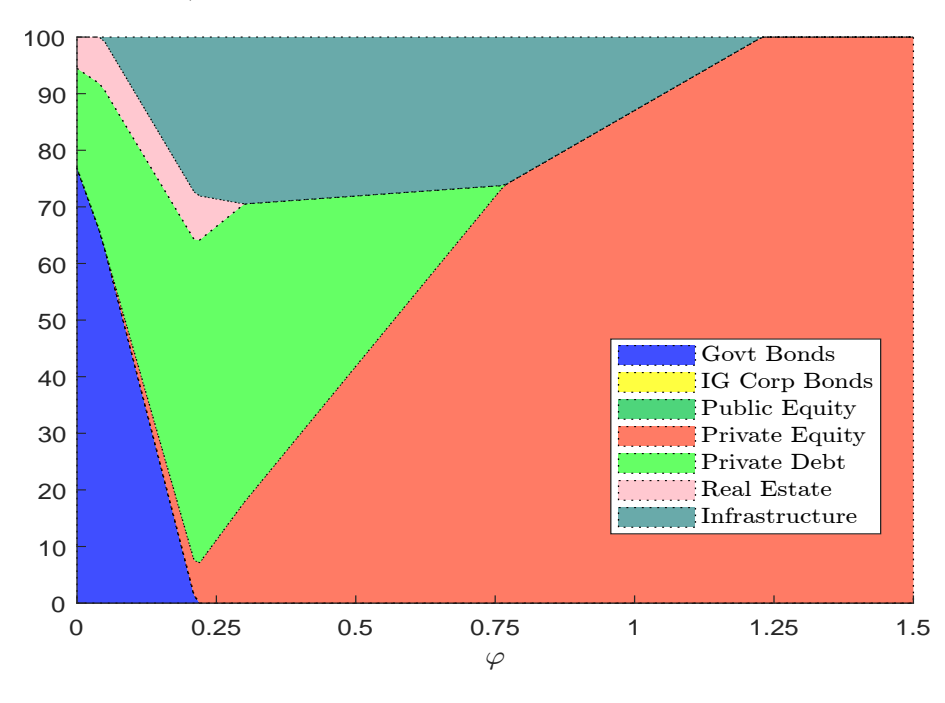


Figure 61: Optimal risky portfolio without real assets as a function of risk aversion γ (Global, 30-year time horizon)

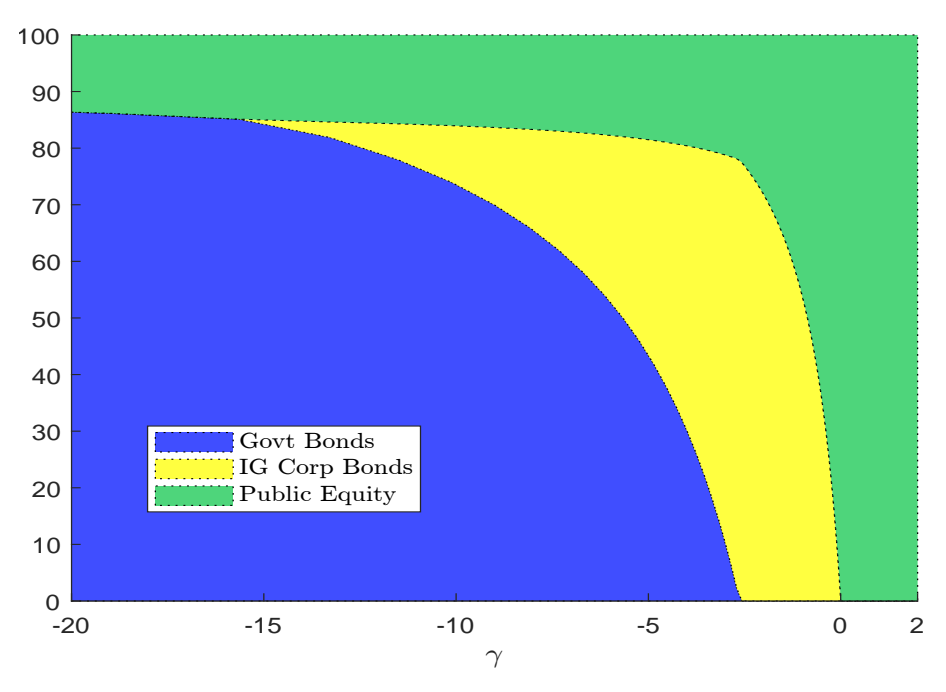


Figure 62: Optimal risky portfolio with real assets as a function of risk aversion γ (Global, 30-year time horizon)

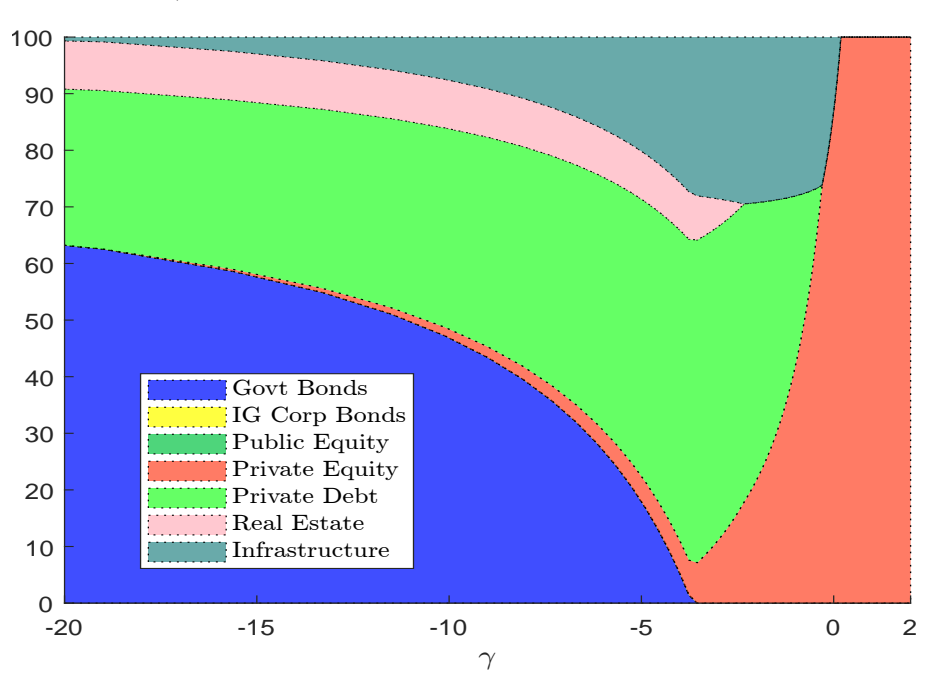


Figure 63: Mixed glide path with liquidity constraints (Global, 30-year time horizon, $\omega^+ = 50\%$)

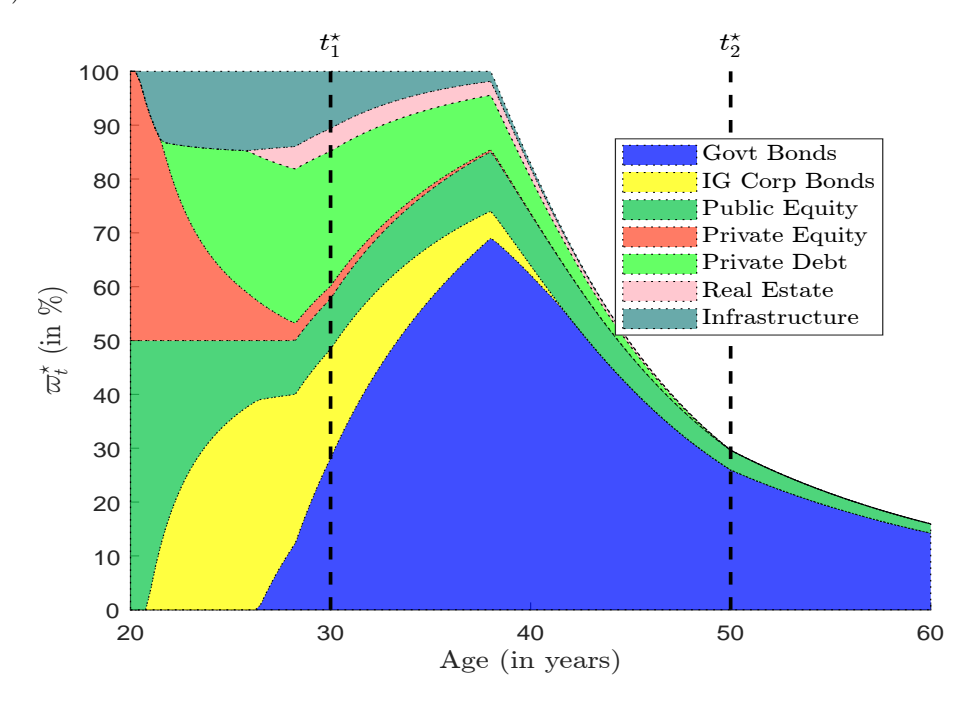


Figure 64: Impact of the volatility σ_1 on the optimal solution (two-stage approach, Property P_1)

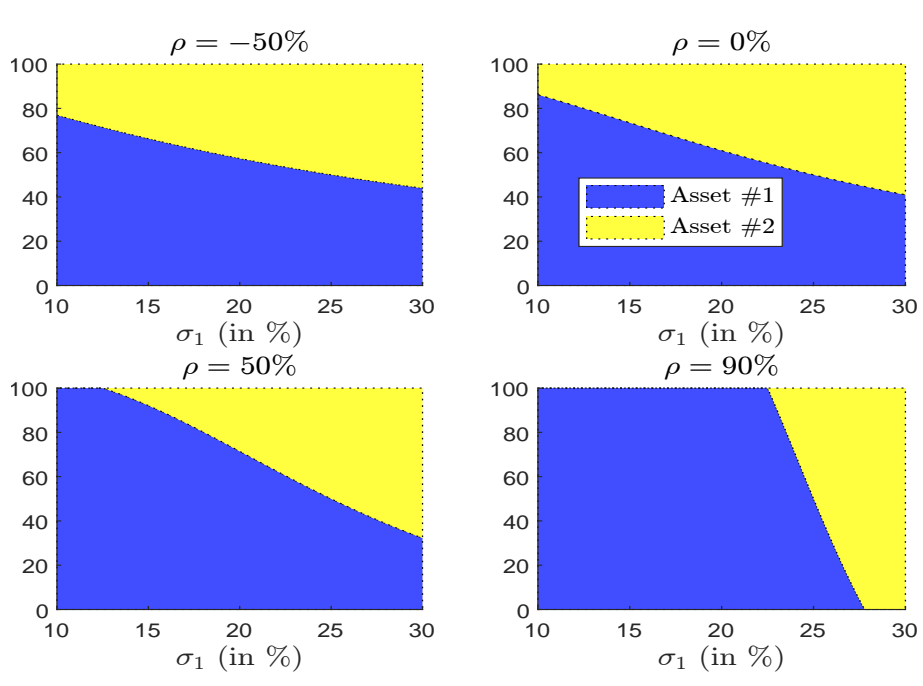


Figure 65: Impact of the expected return μ_1 on the optimal solution (two-stage approach, Property P_2)

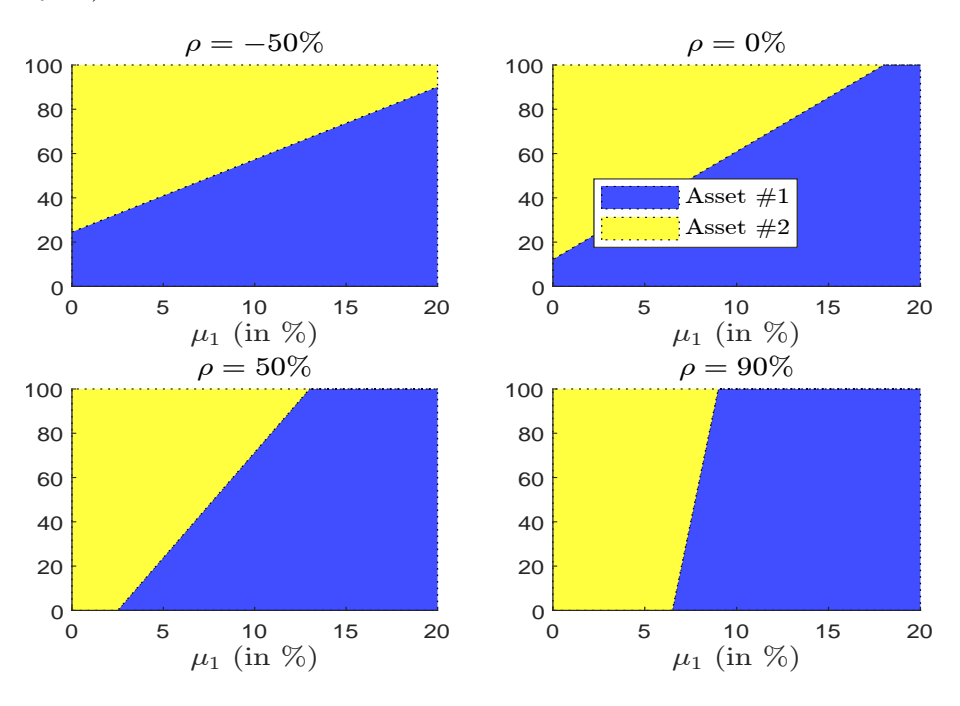


Figure 66: Impact of the parameter SR_1/σ_1 on the optimal solution (two-stage approach, Property P_3)

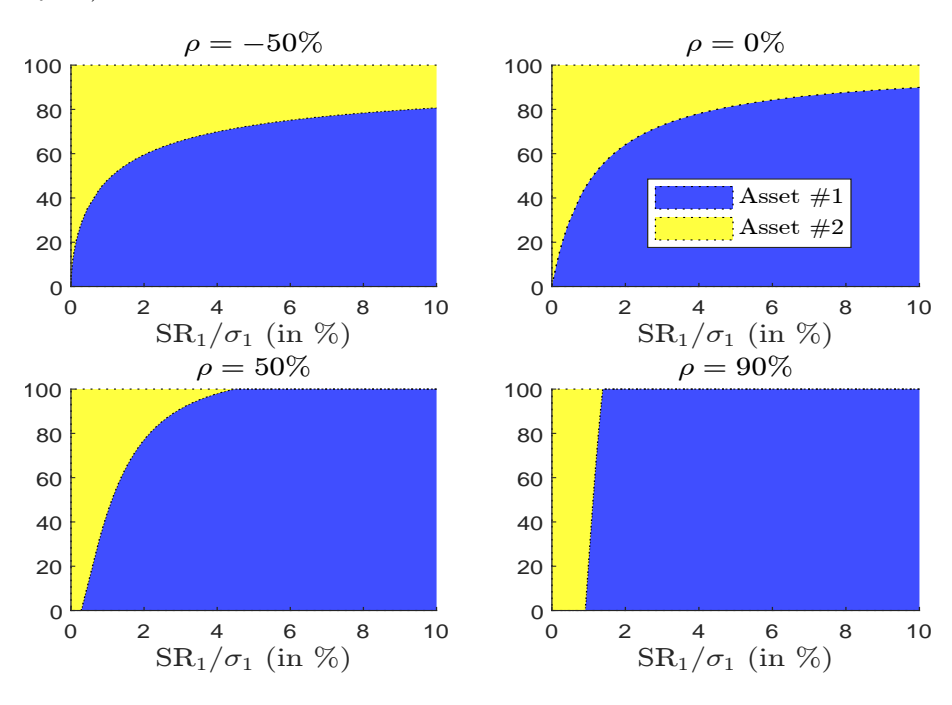


Figure 67: Impact of the risk aversion γ on the optimal solution (two-stage approach, Property P_4)

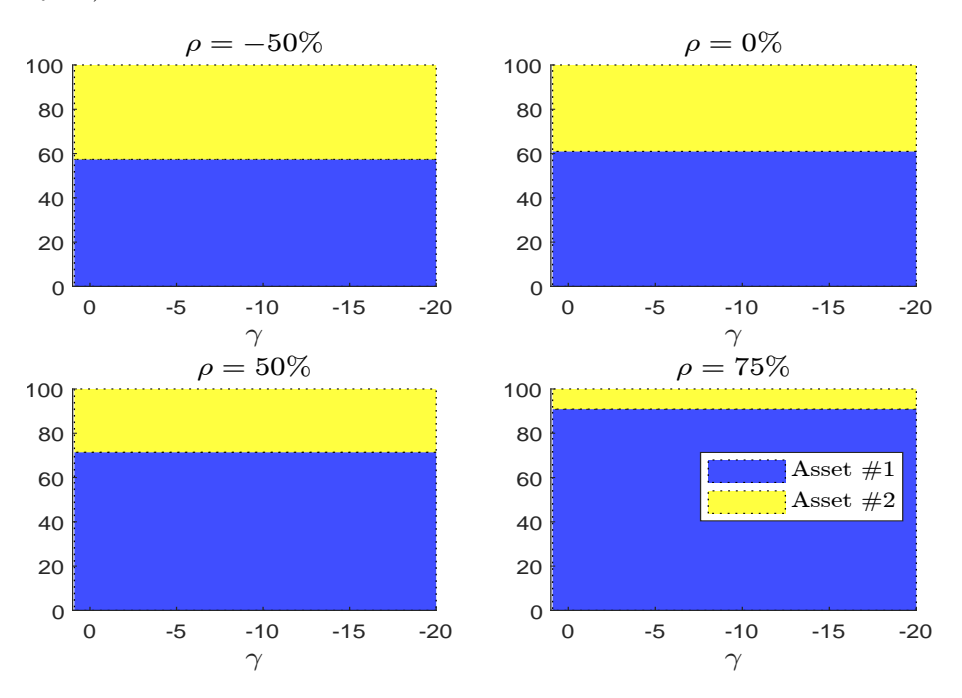
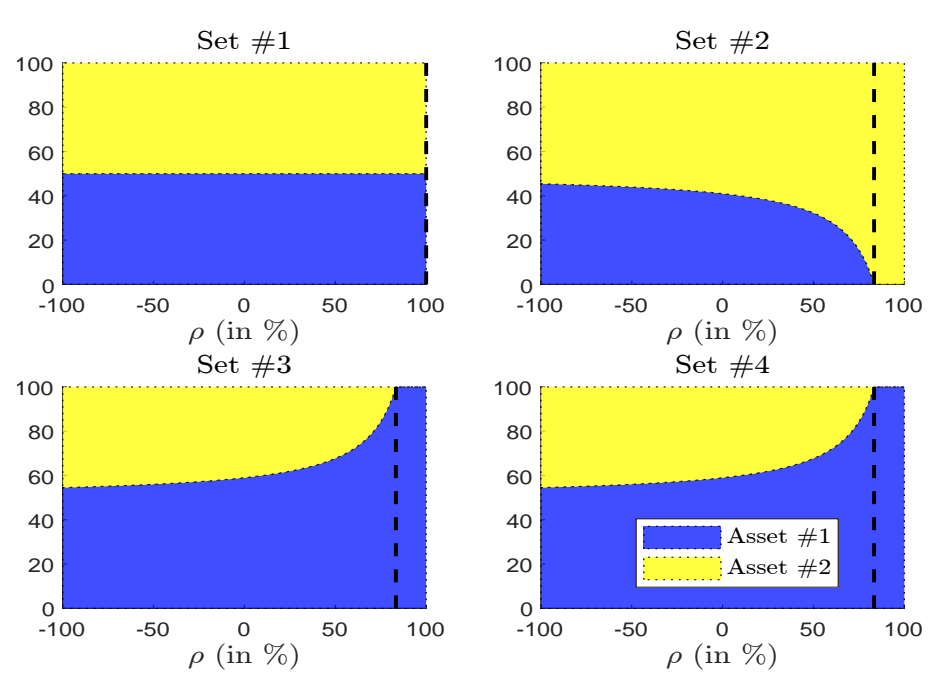


Figure 68: Impact of the correlation ρ on the optimal solution (two-stage approach, Property P_5)



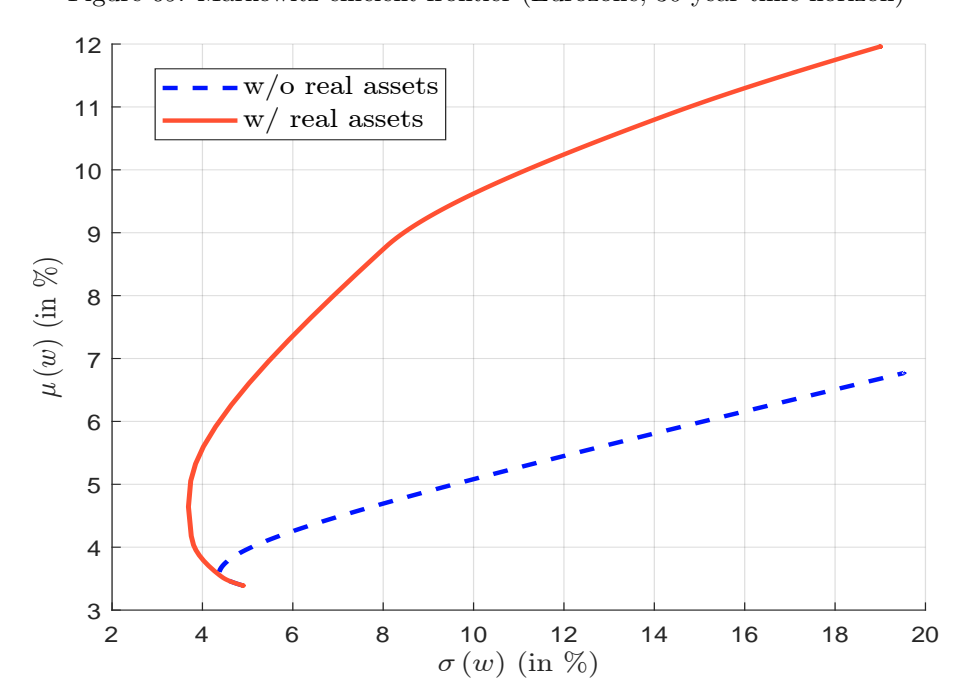
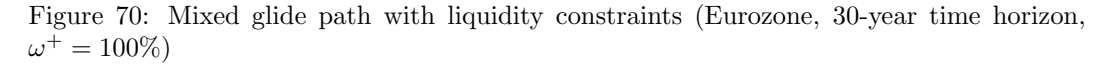


Figure 69: Markowitz efficient frontier (Eurozone, 30-year time horizon)



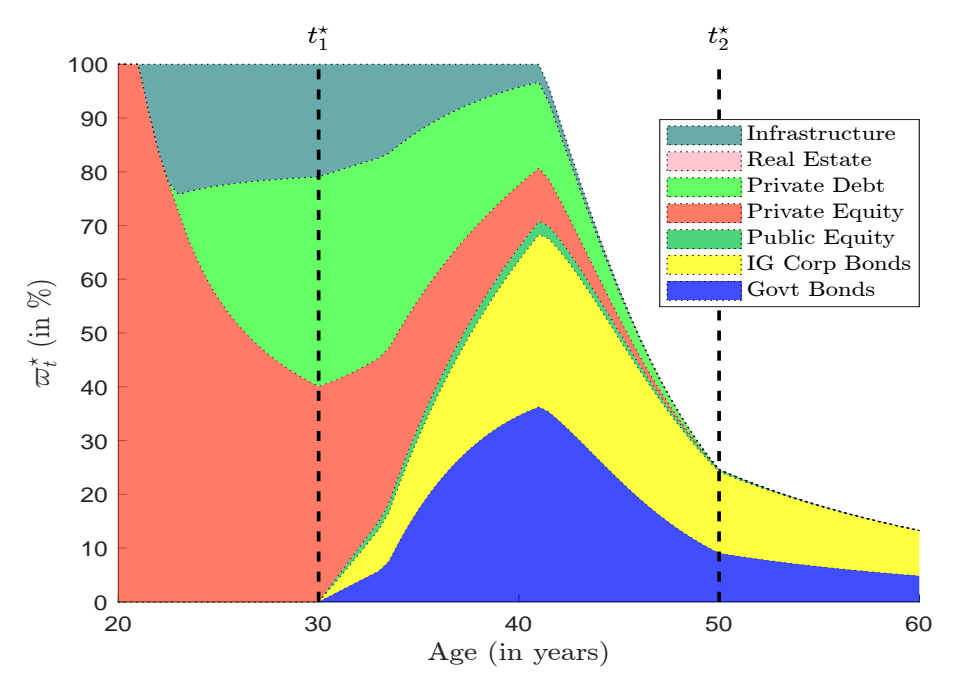


Figure 71: Mixed glide path with liquidity constraints (Eurozone, 30-year time horizon, $\omega^+ = 50\%$)

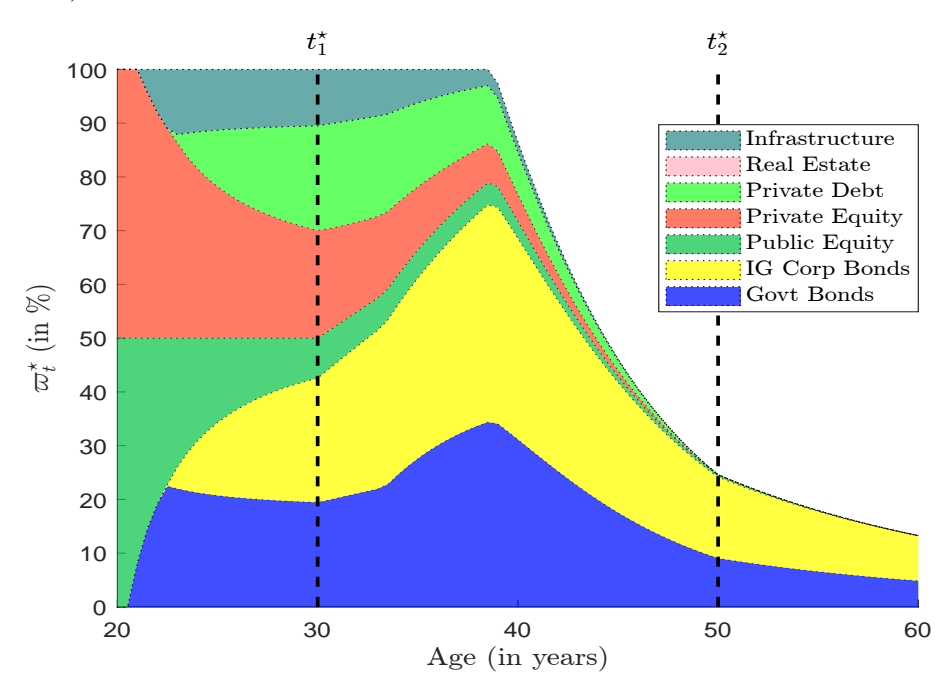


Table of Contents

1	Intr	roduction	3
2	Bas	eline modeling of glide path strategy	11
	2.1	Theoretical Model	11
		2.1.1 The no-contribution case	11
		2.1.2 The case with contributions	13
		2.1.3 Properties of the optimal exposure α_t^{\star}	17
		2.1.4 Dynamics of the wealth X_t	21
	2.2	Definition of the glide path g_t	26
		2.2.1 Analytical expression and main properties	26
			28
	2.3	Empirical results	34
		•	34
			35
			38
			42
3	\mathbf{Ext}	ension to multi-asset classes	45
	3.1	Theoretical Model	45
	3.2	The case without allocation constraints	46
	3.3	The case with allocation constraints	47
	3.4	Empirical results	49
	3.5	Insights into the multi-asset optimal solution	50
		3.5.1 Mathematical properties of the optimal weights	51
		3.5.2 Numerical examples	52
	3.6	The case of the investor in the Eurozone	56
	_		
4			59
	4.1		59
	4.2		61
			61
		· ·	63
		11	64
	4.3		67
	4.4	1	68
			68
			71
			73
	4.5	Inflation, risk premium, and correlation	76
5	Cor	nclusion	78
A	Too	hnical appondix	37
A	A.1	T. C.	87
	A.2		88
	400		88 80
	A.4		89
	A.5	Calibration of c_t	91

	A.6 Maximum of H_t when c_t is a quadratic function and the interest rate is constan	t 93
	A.7 Computation of the expected wealth $\mathbb{E}[X_t]$	94
	A.8 Computation of the variance of the wealth	96
	A.9 Computation of the skewness of the wealth	97
	A.10 Jensen's inequality and analytics of the glide path	98
	A.11 Glide path formula when the wealth is log-normal distributed	99
	A.12 Simulation of the state-control dynamics	100
	A.12.1 The unconstrained case	100
	A.12.2 The constrained case	100
	A.13 Simplex projection methods	101
	A.14 Separability property under the constraints $c_t = 0$, $\alpha_t \geq 0$ and $1^{\top} \alpha_t \leq 1$	102
	A.15 Computation of the threshold correlation	103
	A.16 Proof of Equations (22) and (23)	105
	A.17 Proof of Equations (24) and (25)	106
	A.18 Proof of Equations (26) and (27)	
	A.19 Numerical solution of the Howard's policy-iteration algorithm (Equations 26	
	and 27)	109
	A.19.1 Policy evaluation	110
	A.19.2 Policy improvement	111
	A.19.3 Two-asset case	112
	A.19.4 Convergence	113
В	Additional results	113